SEQUENTIAL FAILURE OF GRANULAR SLOPES

Thesis submitted by

Michael DUNBAVAN, BE(Hons)

in August, 1979

as partial fulfilment of the requirements for
the Degree of Doctor of Philosophy in
the Department of Civil and Systems Engineering
at the James Cook University of North Queensland

ABSTRACT

A review of some field records showed that a two-wedge mechanism formed when failure occurred in a slope underlain by a thin weak layer. A physical model which promoted plane strain conditions was designed for the study of the sequence of failure. The model consisted of a simple granular slope resting at its angle of repose on a cohesive layer. At low confining pressures, the failure of the sand in plane strain was described by a deformational failure criterion.

The sequence of failure of the model slope was determined from measurements of photographic records of experiments. The slope was analysed using numerical models and stability methods, with emphasis on the discontinuous nature of the material. A method based on the principle of virtual work and using an energy dissipation function for the definition of the critical failure mechanism was proposed by the author, who found its predictions concurred with the experimental observations. The use of an energy based analysis led to the replacement of the factor of safety by an energy quotient, Q. The virtual work analysis was applied to a prototype example and was found to give good agreement with field measurements.

CONTENTS

LIST OF FIGURES

LIST OF PLATES

LIST OF TABLES

LIST OF SYMBOLS

a, b, c	Virtual displacements for two-wedge mechanism
d_{50}	Particle diameter for 50% passing
de_1	Incremental major principal strain
ds	Incremental distance along base
dv	Incremental volume
E	Horizontal force
F	Factor of safety
$f(x)$	Thrust distribution
H	Slope crest height
h	Vertical elevation of effective wall;
	Height of prismatic sample
h_1	Vertical component of slip plane length
i	Angle of slope face
k	Arching factor
M	Critical state constant
m	Mass of representative unit
$\frac{1}{m}$	Power law index
p	Spherical pressure
Q	Energy quotient
q	Deviatoric component of octahedral stress
R, S	Reactions on crest block in two-wedge mechanism
s	Spring stiffness between representative units;
	Total displacement of toe region
T	Thrust on toe region
t	Thickness of bentonite layer
Δt	Finite difference time step
v	Specific volume
Δv	Volume change
W	Weight of crest region
X	Vertical force
x	Distance along slope base from toe
α	Angle of slip plane between toe and crest regions;
	Angle of octahedral shear stress;
	Inclination of potential slip surface to major
	principal plane
α, β	Student t-distribution values

β	Angle of slip plane between crest region and body of slope;
	Angle of Freudenthal generator on $\sigma_1\sigma_3$ plane
γ	Unit weight of slope material
$\dot{\gamma}$	Rate of shear strain
Δ	Virtual displacement along base
η	Apparent viscosity
θ	Average inclination of tangent at particle contact to potential slip surface
λ	Multiplier for force distribution f(x)
λ, Γ	Critical state constants
μ	Interparticle friction coefficient
ν	Dilatant angle
ρ	Angle between Freudenthal generator and space diagonal
$\sigma_1, \sigma_2, \sigma_3$	Principal stresses
$\sigma_1', \sigma_2', \sigma_3'$	Effective principal stresses
σ_n	Normal stress on a plane
τ	Shear stress on a plane
τ_0	Estimated initiation stress for two-wedge mechanism
τ_y	Yield stress in bentonite
ϕ	Angle of internal friction
ϕ'	Effective angle of internal friction
ϕ_{cv}	Angle of internal friction at critical voids ratio
ϕ_f	Empirical effective interparticle friction angle
ϕ_μ	Interparticle frictional angle
ψ	Angle of backfill

Note: Where a symbol has more than one meaning in the text, the relevant definition is given when the symbol is used.

DECLARATION

I declare that this thesis is my own work and has not been submitted in any form for another degree or diploma at any university or other institute of tertiary education. Information derived from the published or unpublished work of others has been acknowledged in the text and a list of references is given.

Michael Dunbavan
10 August, 1979

ACKNOWLEDGEMENTS

This research was carried out within the Department of Civil and Systems Engineering of the James Cook University of North Queensland under the supervision of Professor D.H. Trollope and Dr. K. Wallace. The author is particularly indebted to Professor Trollope for his discussion and criticism of the work in the latter half of the study; and also expresses his gratitude to the staff with the Department for their encouragement, especially Dr. H. Bock. During the study, the author was supported by a Postgraduate Research Award from the Australian Government.

The experimental portion of this study was performed with the assistance of Messrs. W. Golding and N. Hines. The excellent quality of apparatus was made possible by the craftsmanship of Messrs. R. Lee and R. Matheson, and members of the Engineering Workshop. The majority of the photography was carried out by the university's Photography Section under the direction of Mr. H. Lamont (since retired). Particular thanks goes to Mr. L. Brady for his invaluable assistance with other photographic work.

The author is grateful for the assistance of and discussions with Mr. M. Fulton concerning the numerical models and computer techniques, and Mr. J. Eckersley who was investigating a similar topic during the first half of this study. Dr. I. Harley, Head of the Department of Surveying, University of Queensland, and Mr. S. Bervoets, Chairman of the Department of Surveying, University of Melbourne, graciously permitted the author's use of photogrammetric equipment within their respective departments. The thesis was proficiently typed by Mrs. L. Derbyshire and Mrs. A. Pohlmann.

Finally, the author acknowledges the indispensable support given by his wife, Jennifer, during the term of this study, while his wife was also a student, and thanks his parents and parents-in-law who also gave continuous support and encouragement. The author is honoured to submit this thesis as an expression of his gratitude to all who have assisted him in its formulation and production.

CHAPTER 1

INTRODUCTION

1.1 Research in Geomechanics

There is a long history of landslips and their effect on centres of population, and much evidence of prehistoric slides exists. As western technology developed, the activities of the engineers of the day began to modify the surface of the earth at an exponentially increasing rate. Because the appreciation of design in works involving soils was virtually non-existent before 1750, it was not surprising that the early approaches to stability and earth pressure analyses were based on field observations of failures in engineering projects. Thus, until the 1920's, the majority of design procedures for soils and foundations followed this philosophy; however, one noteable exception was the Rankine active and passive earth pressure calculation.

The 1920's saw the advent of modern soil mechanics under the leadership of Karl Terzaghi. It was the careful and deliberate study carried out by Terzaghi, and many researchers who succeeded him, which gave the scientific basis to soil mechanics, which for so long had relied on experience and empiricisms alone. Although Australian engineers did not play a prominent role in the initial (1900-1950) development of soil mechanics, there was considerable interest expressed in the discipline, and some earnest research undertaken. Trollope (1973a) discussed the work of Hawken, which concerned the active thrust on a retaining wall. The debate and criticism of Hawken's work (cf. Trollope, ibid.) illustrated another important facet of research into soil mechanics - the existence of several ways for the investigation of a particular problem, each with its advantages and disadvantages.

Thus, the pattern for research in soil mechanics was established; as it had been for many other disciplines created by the technological changes since the industrial revolution. The extent of the discipline of soil mechanics is continually being redefined, and the last two decades have seen an increasing exphasis on the use of the term "geomechanics" to encompass both soil and rock mechanics. As more understanding is gained of the current problems in geomechanics, investigators are able to isolate portions of those problems for more detailed study; or are able to adjust their method of approach so that a more appropriate avenue of thought may be pursued. Current research into problems which have been created by the exploits of modern technology, is also being assisted by the same technology in the solution of those problems; therefore, many innovations may be used to solve problems which were beyond the capacity of researchers in the first half of this century.

1.2 The Study of Slope Stability

The ideal solution to a slope stability investigation would be possible if the stresses at failure were defined everywhere in the soil, and the critical kinematically admissible slip mechanism had been established. This form of solution is not feasible and one of the main factors contributing to this situation is the nature of the soil material, both its variability and its stress-deformation response. Although there have been considerable advances with analytical and numerical procedures in the fields of soil statics and kinematics, many of the methods are under restrictions or assumptions which preclude them from practical application in design problems. Thus, the study of slope stability cannot be described by a single procedure, but each problem must be evaluated so that use may be made of a relevant procedure.

Unfortunately, very few analyses consider the kinematics of failure explicitly, but the simple wedge and slip circle analyses do use slip surfaces which are kinematically admissible. However, when the soil materials under investigation are stratified so that part of the failure mechanism is pre-determined, the kinematics of the slip is necessary information for the adequate assessment of slope stability. It is not uncommon for a soil profile to contain a band of material which is significantly weaker than the surrounding soil; or to have a situation in which a band of weakness may develop due to some change in ground water level or stress condition within the soil. Therefore, a method of stability analysis should be available for consideration of the situation where the kinematics of failure is dominated by the presence of a weak stratum. This research is a detailed investigation of the influence of a weak stratum on the failure of a granular slope.

1.3 Scope of the Research

Trollope (1975) proposed that the failure of a simple granular slope underlain by a weak layer occurred in an identifiable sequence of discrete events, rather than the semi-continuous form of progressive failure. The principal aim of this study was to carry out a quantitatively reliable series of physical model tests which would provide the data for the interpretation of the sequence of failure.

The physical model was limited to a simple slope of dry, cohesionless silica sand which stood at its angle of repose on a weak layer of purely cohesive material. The prime variable in the model was the thickness of the base layer, with all other variables maintained as uniform as practicable. Records of slope failure and their measurement were made photogrammetrically.

The second purpose for which the physical model was used, was to enable recognition of the kinematics of failure; and subsequently, an adequate stability analysis was sought with the incorporation of both static and kinematic considerations. If an acceptable analysis was found, it could be applied to a prototype example which would result in an evaluation of the reliability of the modelling technique and chosen analysis.

Throughout the study, emphasis was placed on the discontinuous nature of the granular material in the slope and the stress-deformation response of the materials under conditions which prevailed in the model. Part of this project was the design of the modelling apparatus so that the response of the model could be interpreted independently from the effects of the apparatus on the materials.

CHAPTER 2

FIELD EXAMPLES

2.1 The Occurrence of Instability

It will be clear to most people who have seen an exposed soil profile, that the nature of the soil is highly variable. One simple example is the change in colour of the earth which may be found in a road cutting. Although the variation of the geotechnical properties of soil cannot be determined at a glance, it may be expected that these properties should vary in any given soil profile.

Just as the performance of a material is dependent on its inherent properties, the effectiveness of these properties may be significantly altered by the action of external agents. It has been found that geotechnical parameters in a soil are affected in varying ways by pore fluid pressure, cyclic loading, and relative displacement, to mention but a few. If these changes strengthen the soil, loads to failure are not reduced; however, there are many instances in which a loss of stability has occurred in a formation which was stable in its previous condition but weakened when disturbed. Common sense dictates that a body is only as strong as its weakest member, so that if a soil profile is adversely affected in one region some instability may develop, even though most of the profile has remained relatively unchanged.

One of the objectives of the geotechnical design engineer should be to identify zones which have a potential to become the critical member in the soil or rock system. The geological process of sedimentation provides an excellent opportunity for weaker materials to be deposited between more competent bands. Thin layers of montmorillonitic clays are known to occur in many shale profiles, and when exposed, or brought into the range of influence of some structure or excavation, often prove to be troublesome. Layered deposits commonly contain some sand, either in lenses of limited extent and thickness or in aquifers from centimetres to tens of metres thick, and because of the natural permeability of sand, ground water under different heads of pressure is often associated with these layers. If one of these smaller deposits which had limited drainage was loaded rapidly by some construction, the subsequent pore pressure increase in the sand would tend to push the soil system closer to the point of instability. Similarly, if for a given situation, pore pressures were to increase due to a rise in the level of ground water supply, then a state of instability would also be brought closer.

The following section considers the modes of instability encountered when a failure is influenced by the presence of a layer which is weaker than the surrounding soil mass.

2.2 Failures Influenced by Subsurface Geology

The types of structure to which the following text refers are limited to natural and man-made slopes and embankments. Terzaghi and Peck (1948) have called these slips "spreading failures", after the nature of the displacements observed. This category is divided further into two forms, with the distinction being made according to the thickness of the weaker layer, as may be seen in Figure 2.1. Unfortunately, the writers did not define how the relevant mode of spreading failure should be determined prior to the occurrence of slip.

In Figure 2.1(a), the thicker layer (e.g. a clay stratum) is shown as allowing some overall volumetric distortion with the embankment coming to rest in "a gentle S-shape". The second part of the figure illustrates the case of a thin weak layer (e.g. sand or silt partings carrying high pore water pressure) which assumes a characteristic two-wedge mechanism in the embankment with a compressed ridge of soil at the toe. The writers refer to several examples of spreading failure at the end of their article; some of which are included in this chapter.

The references to failure thus far have been for embankments and have been used as a matter of convenience for the introduction of this topic, with the intention that slope failures are to be considered as having the same forms as given in Figure 2.1, but with the obvious extension of the crest area so that only one toe region needs to be considered. The mode of spreading failure is not the only possibility for slip when a weaker layer is present. There are a great number of examples of progressive failure and retrogressive failure to which references are made in following sections.

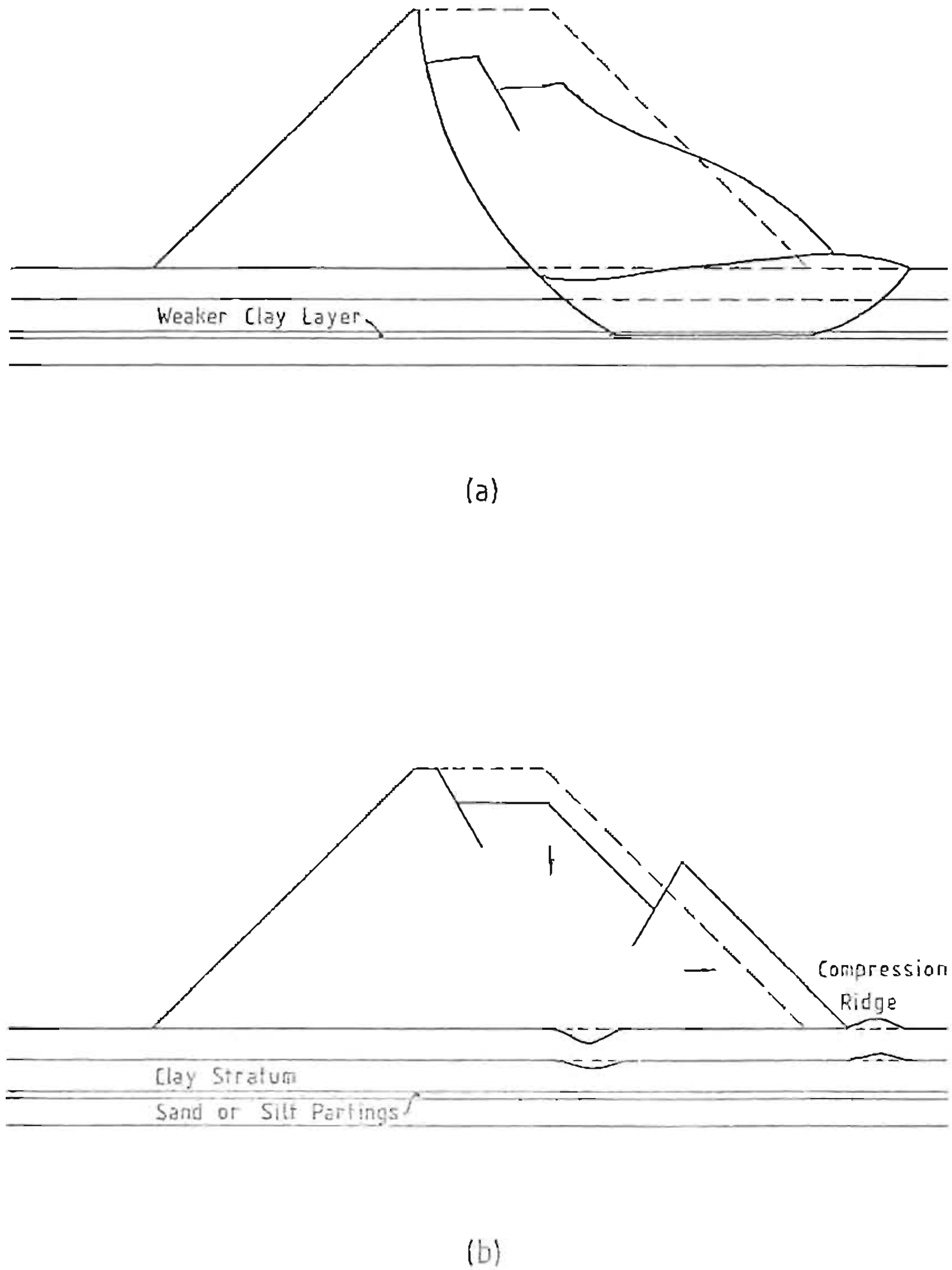

Figure 2.1 Spreading Failure (after Terzaghi and Peck, 1948)

2.3 The Role of Progressive Failure

Wilson, in his 1970 Terzaghi Lecture, stressed the importance of thin zones of weaker material in the development of failure surfaces and supports his argument by a large number of relevant field examples. The majority of cases chosen by the writer were slopes which deformed by progressive failure. The sense of the term "progressive failure" in the text of the lecture and in this thesis means localised failure in an area of stress concentration which in turn causes a stress redistribution bringing a new area into failure, with this process continuing until some force equilibrium is reached (cf. Bjerrum, 1967).[1]

The aim with which Wilson approached his topic was to identify slip patterns from the data which was collected by field observation, and hence, has described the form of progressive failure by its field characteristics. Most of the examples quoted failed as a series of blocks and wedges which gave them an appearance similar to that of a spreading failure, mentioned in the previous section. There is, however, another feature of the progressive failure which distinguishes it from other blocky slips; namely, ground movements increase linearly from the upper edge of the failure to the cut face, the area of initial stress concentration. Thus, the mode of failure pursued in this thesis is not of a progressive nature, but rather one for which the movement of the blocks of material may be simply described as uniform.

2.4 Identification of Weak Layers

In the context of the stability of slopes and embankments, the presence of a weak layer may lead to four types of landslip: spreading, progressive, and retrogressive failures; and flow slides. It is important to be able to recognise weak layers so that any potential hazard may be reduced. The common features of weak layers giving rise to the above mentioned failures are briefly described below, with further attention being paid to spreading failures in the next section. It is convenient to approach the description of the weak layers through

1. The author is primarily concerned with the deformational nature of landslips and has accepted the explanation of progressive failure by Bjerrum (op. cit.) as a matter of convenience rather than conviction, because an investigation of the topic was beyond the scope of this thesis.

their association with earth embankments, mining waste dumps and natural slopes.

2.4.1 Earth embankments

Because of its generally economic construction, the earth embankment has been used widely for a considerable period of time. Thus, valuable experience has been gained from the performance and, in some cases, failure of these structures. Prior to the advent of modern earth-moving machinery, many embankments were constructed by hydraulic filling between two outer shells. This method of placement left a relatively loose core section which for the short term was in a saturated condition, making the fill material a hazard in itself.

The lack of adequate site investigation for many early dams led to unexpected deformations both during and after construction. Seams of highly plastic clay, saturated sand and silt lenses, and peat layers have been labelled as the source of many failures. The results of some post-failure analyses have shown that slip occurred along a thin layer of weak material in the foundation. The movement of these structures may be described as a mobile system of wedges and blocks; for example, Sheffield Dam in Santa Barbara where the toe of the dam was found to have moved bodily over more than a hundred metres, leaving the vegetation on the face undisturbed.

The foundations of the Fort Peck Dam had the unfortunate property of a high brittleness index (cf. Bishop (1967)), and with the dam being of hydraulic fill construction, its failure resulted in a flow slide with considerable loss of life. Further reference to flow slides is made in Section 2.4.3.

2.4.2 Mining waste dumps

Any given mining operation needs to be considered as an enterprise which has a monetary profit as one of its objectives. Thus, the disposal of waste material in the least expensive manner is sought after. A natural consequence of this constraint is that waste dumps are often situated on land which is unsuitable for other industrial or residential use. When land is acquired, there is little or no site investigation and preparation. In many large strip mining operations, areas from which the mineral has been recovered are back filled with overburden material from the advancing pit face. If the base of the pit is wet and the waste material soft, failures will often result when a weak layer forms due to the rapid break-down of the dumped material by crushing and chemical weathering. Subsurface geology still has an important influence on dump instability, especially in the case of hillside dumps where the natural water table may be close to ground level.

Several authors have recognised the existence of spreading failures in waste dumps and have been able to associate some with slip through a thin zone of weak material. The coal mining industry appears to be the sector most troubled by these failures and endeavours to bring the situation under control are continuing, especially since the Aberfan (South Wales) and Buffalo Creek (West Virginia) disasters. There seems to be a general consensus among researchers in this area that three distinct factors must be considered before a particular situation is defined: the properties of the dumped material, the properties of the foundation material beneath the dump, and the level of ground- or ponded-water at the dump site.

2.4.3 Natural slopes

The materials found in earth embankments and mining waste dumps are generally limited and in the former case well controlled, however, natural slopes are normally a mixture of soils of varying properties, with an inherent relationship to subsurface geology and the groundwater table; consequently, failures in natural slopes are diverse. It is not the purpose of this section to describe all failures, but to demonstrate that a weak layer may induce a spreading failure in a natural slope, as well as in the man-made structures previously considered.

There exists a difference between spreading failure and progressive and retrogressive failures which needs to be expanded upon so that the identity of the former will be clear. Spreading failure is assumed to have occurred when a deep seated landslip becomes evident over a short period of time, implying that the major cause of weakness in the slip layer was not due to the pre-failure movement of the soil material. Progressive and retrogressive failures are commonly found in areas where a soil is moderately sensitive or has a moderate brittleness index. The latter failures are initiated in a relatively small region compared to the full extent of the slide; with the progress of failure primarily due to a stress redistribution resulting from a decrease in load capacity of the area which has just slipped. Both the former and latter mechanisms may be complicated by the presence of pore water pressure induced by seepage or earthquake loading.

Any of the above modes of failure may develop into a flow slide if the toe region of the slip surface becomes lubricated, or if the potential energy released by the subsiding mass cannot be spent in work on the slip plane(s) and thus must be represented as kinetic energy. The Aberfan, Fort Peck, and Turnagain Heights slides are classic examples of flow slide formation.

The simple form of spreading failure has been actively linked with the occurrence of plastic clay seams, sand or silt laminations, and increase in pore pressure levels. A list of references to some further examples, beyond those studied in detail in the following section, is included at the end of this chapter.

2.5 Particular Examples of Spreading Failure

In recent times, the study of progressive and retrogressive failures has taken precedence over the study of spreading failures. One area in which considerable research towards spreading failure has been conducted was the response of sloping core earth dams to earthquake loading (Sultan and Seed (1967)), however, no specific field examples have shed any light onto the overall mechanism of spreading failure. The main benefit derived from this research was gained in the field of physical model testing, to which further attention has been given elsewhere. Significant field cases have been documented for failures in waste dumps and earth embankments, however, only one case containing enough detail for review has been found for a natural landslip. Eight failures have been considered individually, with particular emphasis placed on the mechanism of failure. Very little comment may be made about the sequence of development of these failures because of a general lack of records of the time at which various events took place.

2.5.1 Rockfill slopes, South Africa (Blight, 1969)

Gold and uranium mining operations in the Witwatersrand region resulted in large quantities of quartzite rock waste, which was disposed of by dumping on flat marshy ground. The dumps were formed by building a low grade haulage ramp to a height of about 50 m and then tipping over the crest to advance the face of the dump. The foundation material was mostly a stiff fissured sandy to silty clay to a depth of about 5 m where it was underlain by shale at various states of weathering. The water table was generally 2 m below the surface and in some cases there was surface water.

Blight has given details of four failures, which exhibit many similarities. Only one of these slides, the first at Vlakfontein, was considered for review in this section. Figure 2.2 shows a profile of the Vlakfontein tip from which the key features to note are the compressed ridge of foundation material in front of the toe, the formation of a berm at approximately the mid-height of the dump, a relatively uniform lateral movement of the lower half of the dump, and the position of the slip surface at the top of the dump. The lateral extent of these failures across the face of the dumps allowed the assumption of plane strain conditions to be made with confidence.

Blight has used a back-analysis technique to determine the angle of the slip plane through the dump (α_R in Figure 2.2). However, he has been able to locate the position of the crest of the dump before failure and presumably the diagram shows the actual position after failure, so that by drawing a trace through these two points the line formed will give another approximation of the angle of the slip plane. It was unlikely that the dumped rock had a dilatant angle of more than a couple of degrees because of its loose state, so that the new estimate of α_R was lowered to between 53^0 and 55^0, which may cast some suspicion on the relevance of the methods of analysis used for the original calculations. It was unfortunate that more attention had not been given to the mid-height berm and the slip plane that gave this effect, as this data may have helped in more accurate location of the slip surface and a better description of the failure mechanism.

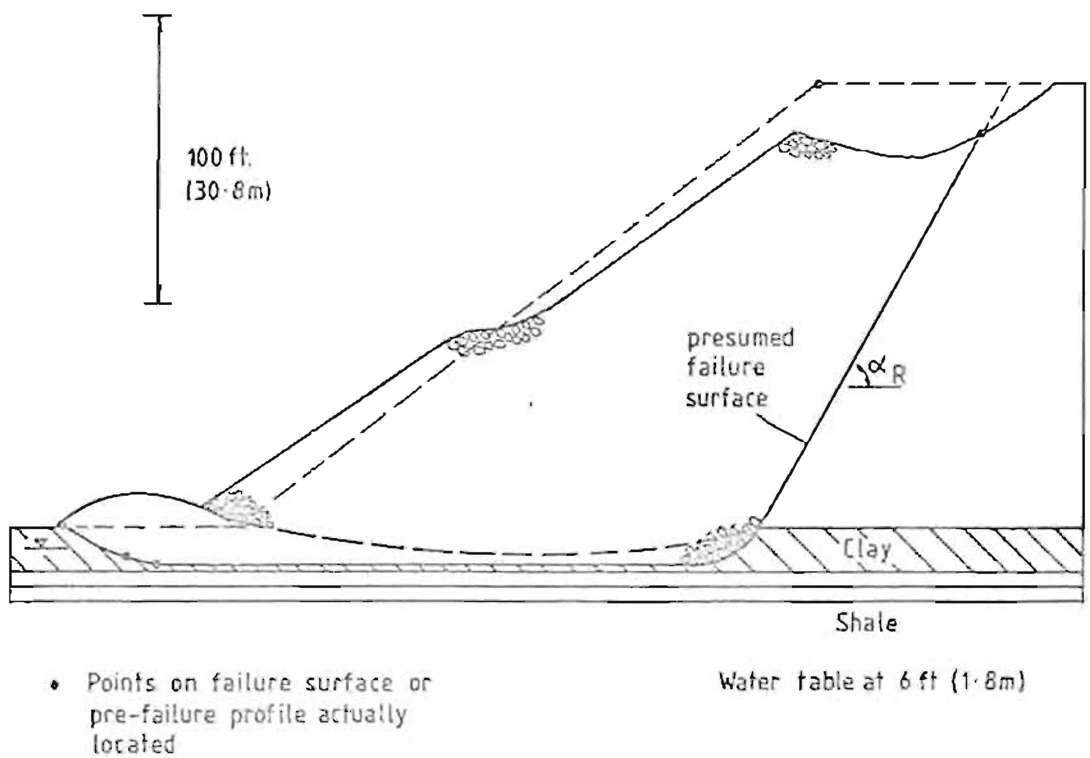

Figure 2.2 First Vlakfontein Slide (after Blight, 1969)

Another comment made by Blight about the Vlakfontein slides was that they were of a progressive nature. It would appear from the large number of observed slip planes in the second slide, that a progressive failure was a good interpretation; however, the first slide was very different in this respect. The type of deformation associated with progressive failure has been described in Section 2.3 as being linearly increasing from the back slip plane to the toe. A comparison between progressive and rigid block failures was made by the author by superimposing the three slip planes of the two wedge mechanism onto Figure 2.2, using the revised estimate of 54^0 for the inclination of the back slip plane. The distance travelled by the toe block was about 7.5 m for the recorded slump of 6 m at the crest. This value closely corresponded to the observed displacement shown in Figure 2.2; thus confirming the uniform nature of the movement and demonstrating that progressive failure was not likely for that slide.

Hence, the existence of a sequential mode of failure is plausible, with a characteristic two-wedge deformation pattern resulting from the formation of a base slip plane through a clay layer which proved to be incompetent for the loads applied.

2.5.2 Spoil pile failures, Goonyella (Boyd et al., 1978)

Open pit strip mining of coal has been carried out at Goonyella in Queensland's Bowen Basin for a number of years during which failures in both the highwall (unmined side of the pit) and spoil piles have occurred. The spoil failures were of interest to this study since research into the instability problem has shown that failures were associated with ingress of water into the piles, causing a loss of strength along the base.

Figure 2.3 shows some observed slip patterns which follow the two-wedge mechanism, with a layer of saturated low shear strength clay along the base. This weak layer was generated from the spoil material by crushing of the large fragments under high consolidation loads and subsequent softening of this material after an increase in moisture content. Standpipes in some piles have shown that high pore pressures were not necessary for the formation of the weak layer; and in some areas the plastic material had been intruded into 20 mm tubes to an

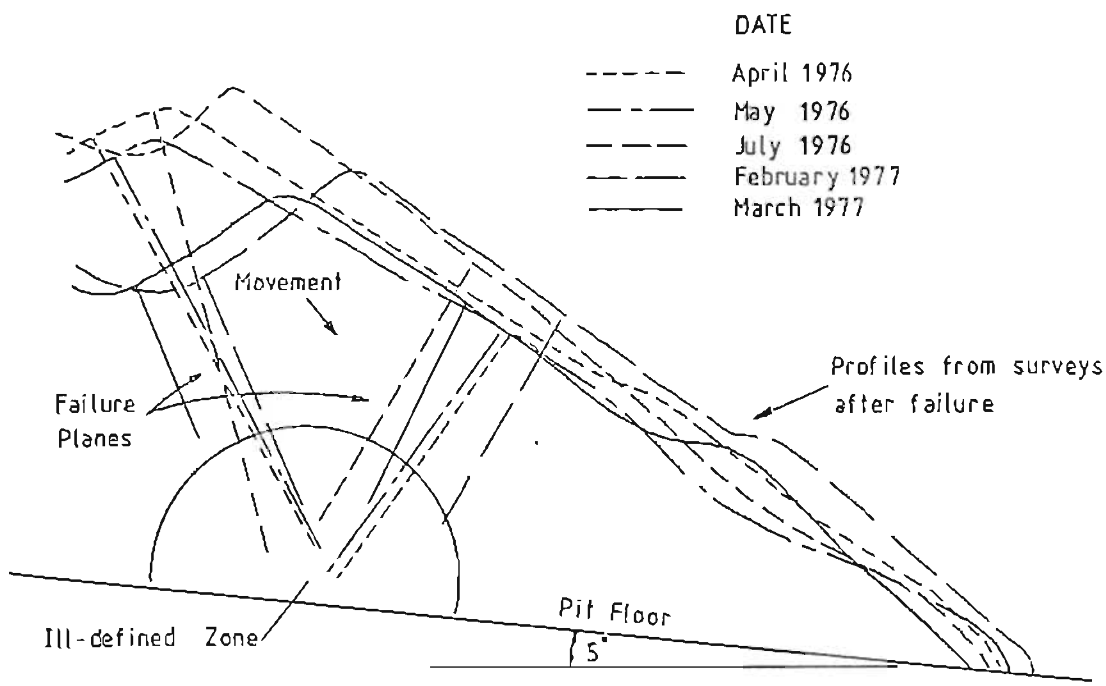

Figure 2.3 Goonyella Spoil Pile Failures (after Boyd, et. al., 1978)

elevation of 45 m above the pit floor. Other characteristic slip geometry was: a pit floor slope of 5^0, and a back slip angle of about 63^0 emerging behind the most recently formed crest of the spoil pile.

2.5.3 The Aberfan Disaster, 1966 (Bishop et al., 1969)

Because of the tragic loss of life suffered at Aberfan on 21st October, 1966, an intensive geotechnical study into the causes of the slide was undertaken. There seems little doubt that the slip was due to high seepage pressures along the base of the tip from a spring located behind the toe.

The stability analysis carried out was based on circular slip surfaces in the majority of cases. The scarp left at the tip site after the slide stood at 40^0 to 50^0 for about one month; but, if the slip surface had been circular, this angle would be expected to vary from the top to the base of the tip. If the upper part were to fail, it would be natural for the material to take up its angle of repose (about 35^0) so that neither this reason nor the circular slip failure explained the final scarp angle. Model studies carried out at Imperial College, London, showed a two-wedge failure mechanism had formed when a weakness was induced along the base in the form of seepage flow: this information seemed to be given little attention by the compilers of the geotechnical report. It would seem possible that the slip mechanism began in a two-wedge form rather than in the circular form favoured in the report, from the consideration of both the post-failure scarp at the tip and the model studies. Trollope (1975) had previously suggested that failures at Goonyella, Queensland, and the Aberfan disaster were the result of the activation of a third-order (two-wedge) sequential failure mechanism. The writer described the kinematics of the two-wedge mechanism, and gave a method of stability analysis which will be commented on in a later chapter. The relationship between the two-wedge mechanism and the subsequent development of a flow slide was also discussed.

2.5.4 Failure at Lafayette Dam (Engineering News Record, January 31, 1929)

Lafayette Dam consisted of rolled earthfill, and was under construction and within 6 m of final crest level when the failure occurred. The slip was attributed to slip along a layer of plastic alluvium in the site foundations. Figure 2.4 shows a profile of the dam before and after failure, exhibiting many characteristics in common with a two-wedge failure mechanism. Some of the more important features noted were the uniform lateral movement of the lower half of the face, the mid-height berm, and the subsidence of the crest area.

2.5.5 Failure of Marshall Creek Dam, Kansas (Engineering News Record, September 30, 1937)

A much lower foundation strength than originally anticipated was identified as the cause of the failure of the dam. Figure 2.5 shows a cross-section of the failed dam, which had many features of a spreading failure; such as the uniform lateral movement of the lower half of the embankment with a subsequent downward movement of the crest. The report mentioned that an engineer at the site commented on the similarity between the failures of the Lafayette and Marshall Creek dams.

Hammond (1956) included a more informative discussion on the Marshall Creek failure with the advantage of a report of a committee of engineers appointed to investigate the incident. The failure was still attributed to the weakness of the foundation material; however, the composition of the soils showed that high pore water pressures may have developed to significantly reduce the soils' effective strength. Post-failure site investigation had shown that the foundation materials were originally in a loose, saturated condition at depths only a little below the surface. It was further noted that parts of the site contained sand and silt laminations which would probably have been subject to high pore water pressures under the combined effects of increased normal load and foundation settlement caused by embankment construction.

The investigating committee considered the stability of the dam by applying the slip circle method to find a factor of safety of .84 at the time of failure. This result implied that the dam should have failed at a time prior to the end of construction. However, there is evidence to suggest that a wedge failure mechanism was active: namely, the report stated that "a secondary fracture area having a similar crescent shape was present in the downstream slope in the general region of the upper berm (El.807)". Thus, it seemed unlikely that a circular slip analysis was relevant to this case.

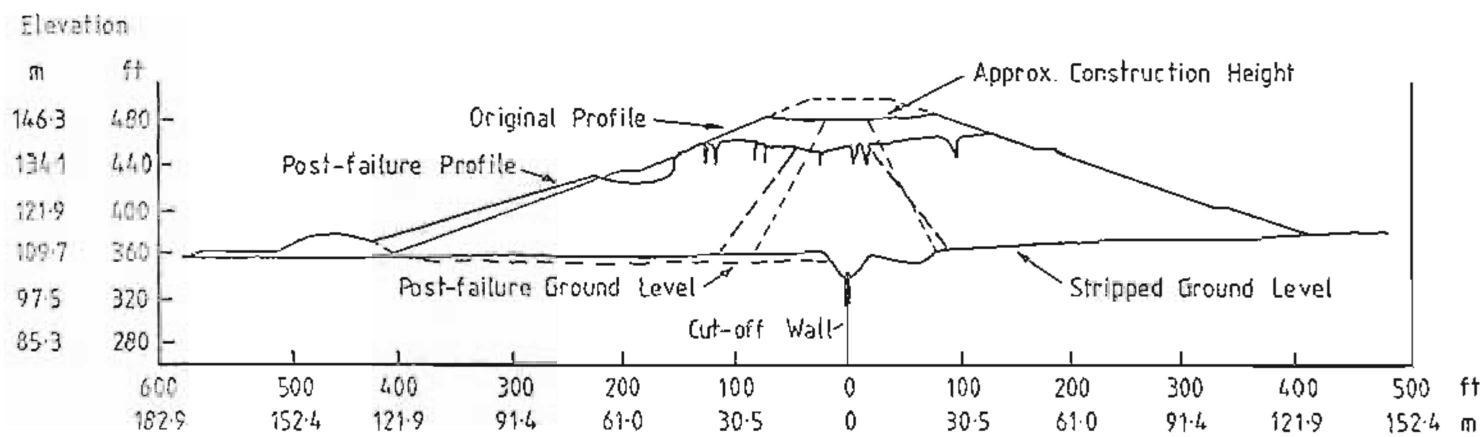

Figure 2.4 Cross-section of Lafayette Dam near Centre (vide Engineering News Record, January 31, 1929)

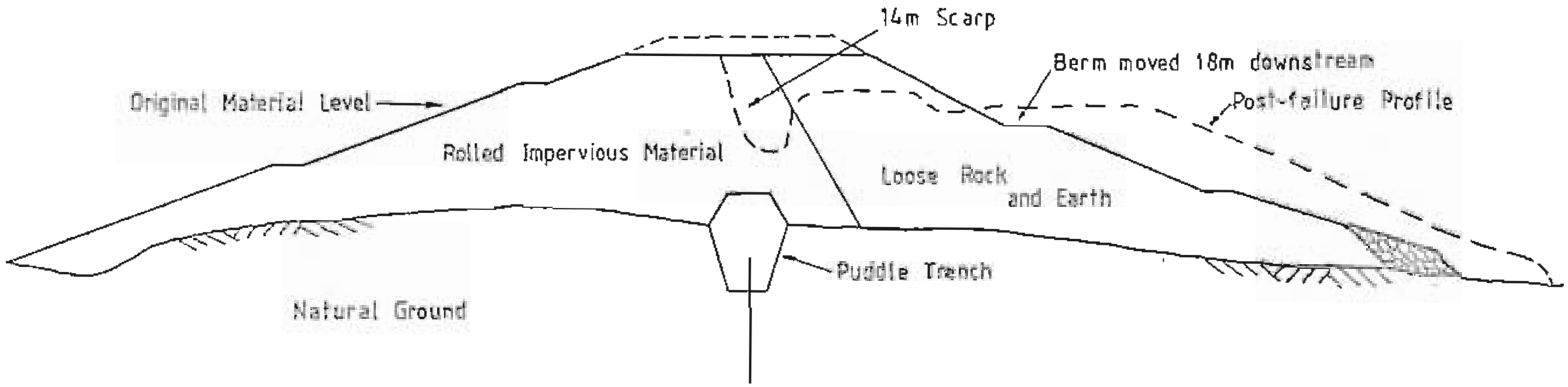

Figure 2.5 Cross-section of Marshall Creek Dam (vide Engineering News Record, September 30, 1937)

2.5.6 Failure of flood-control dike, Hartford (Engineering News Record, July 31, 1941)

A deep seated circular slip through a foundation of soft varved clay was assumed to have taken place while hydraulic sand fill was being placed behind a recently completed flood-control dike on the banks of the Connecticut River. Before the slip, placement of material behind the dike continued even though a warning had been given after preliminary calculations showed the possibility of instability unless the foundations were allowed to consolidate for a few months. A profile of the dike and the assumed slip circle are given in Figure 2.6. Observations after the slip showed that the crest had slumped about 7.5 m, and the highway fill and dike had moved laterally about 15 m. Measurements of the diagram gave the radius of the slip circle as 41 m. If the slump of 7.5 m was assumed to be at the middle of the crest, then rotation of the failed mass would be about 16^0. The lateral displacement of the mass could be only 6 m at the most, and not the 15 m observed. Again it was pertinent to realise that the foundation was a varved soft clay which allowed the possible development of high pore pressures from extra vertical load, consolidation and seepage from the hydraulic fill. Thus, a wedge form of failure may have occurred along one of these low strength zones and given rise to the deformations observed.

2.5.7 Trial bank on soft alluvium, River Thames (Marsland and Powell, 1977)

The failure of this bank was planned so that members of the Building Research Station could establish design parameters for the construction of storm levees in the Thames Estuary. The location of the levees placed them over very poor foundations consisting of a mixture of very soft organic clays, peat layers, silty clays, clayey silts and sands in various orders of deposition. The estuary ensured that the soils were mostly in a saturated condition.

The bank was constructed of sandy gravel fill with a range of inclinometers, piezometers, extensometers and surface targets in both the foundation material and the bank fill. The pattern of displacements in two of the inclinometers is given in Figure 2.7 and a simplified representation of the movements of the bank during failure is shown in Figure 2.8. With reference to the latter figure, the writers have

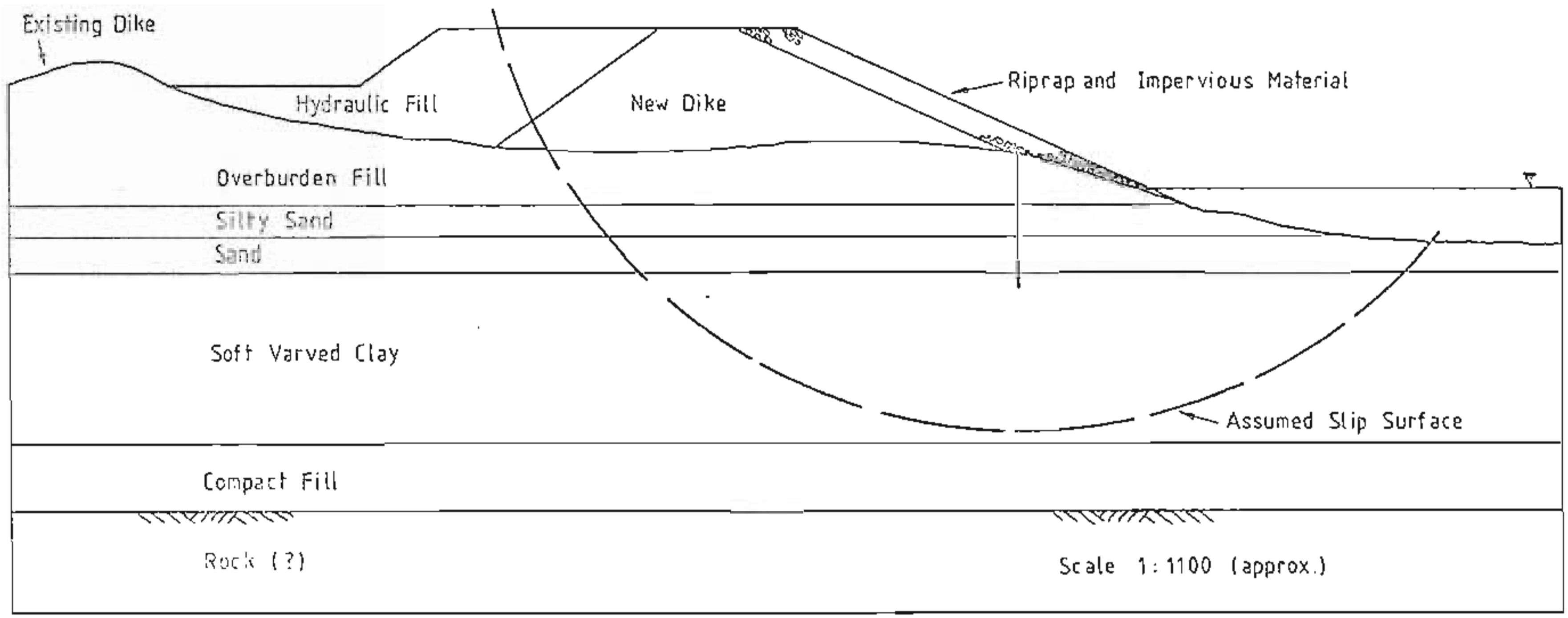

Figure 2.6 Flood-control Dike, Hartford (vide Engineering News Record, July 31, 1941)

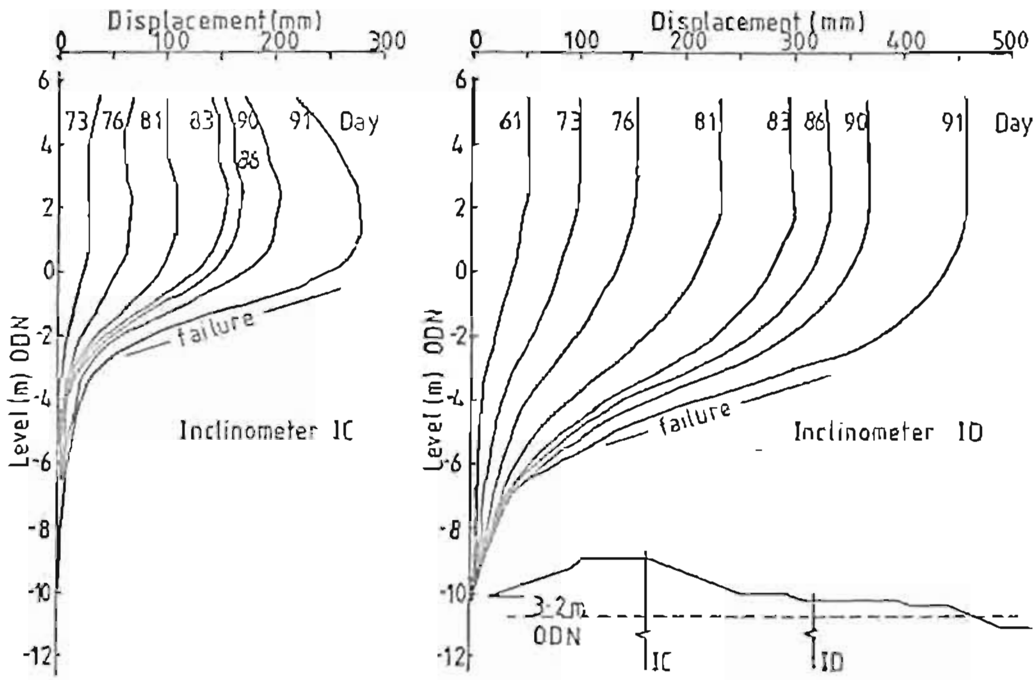

Figure 2.7 Horizontal Displacements measured in Inclinometers (after Marsland and Powell, 1977)

defined the failure surface as "a vertical face ab, a circular portion bc centre o which changed to a near horizontal translation cd culminating in a smaller circular portion de". Because of the reliability of the displacement data, it was re-examined to test for alternative interpretation. In the segment obc (Figure 2.8), the construction of normals to the displacement vectors should have found their intersection in the vicinity of o, however, this was not the case (c.f. Figure 2.9). Also, the overall heave at the toe did not support a circular failure mode as there was little rotation and no consistent rotational direction. If the failure mechanism proposed by the writers took place, a fissure would be expected to form along oc with a width of about 150 mm at the surface of the bank, but no such feature was reported.

A wedge mechanism was constructed using the displacement data. This mechanism appeared to be more consistent with the observations than the proposed combination of slip circles and blocks; the dashed line in Figure 2.8 shows one wedge mechanism.

2.5.8 Failure of natural slopes at Herne Bay, Kent (Bromhead, 1978)

The surface geology of the Herne Bay region consists primarily of a 30 m layer of London clay underlain by the slightly dipping Oldhaven beds of silty fine sands, which vary in depth below sea level along the coast. A long history of deep-seated landslips is known, with records dating back to the late nineteenth century. Of the three slides reported by Bromhead, the Miramar landslide was most relevant to this study because it was located close to the place where the Oldhaven beds intersected the shore line.

The landslides of this region have gained the attention of Hutchinson; however, the writer does not refer to more than descriptive material from Hutchinson (c.f. Section 2.7). A reliable description of the slip of 4th February, 1953, in which about 25 m of the top of the cliff was lost, was given as: "sharply dipping sliding surfaces to form a near-horizontal graben structure, while the original cliff face was pushed forward intact to form a sharp crested ridge." Figures 2.10 and 2.11 show a plan and sections of this slide, which may clearly be seen to have a two-wedge failure mechanism. Bromhead reported that surface water seeped down through the graben region into the Oldhaven beds and produced adverse

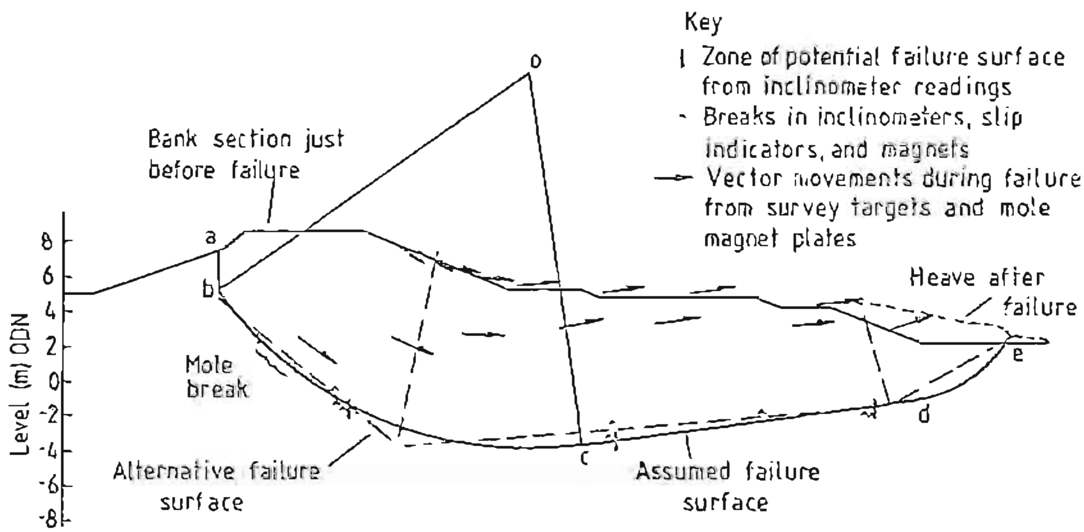

Figure 2.8 Movement of Bank during Failure (after Marsland and Powell, 1977)

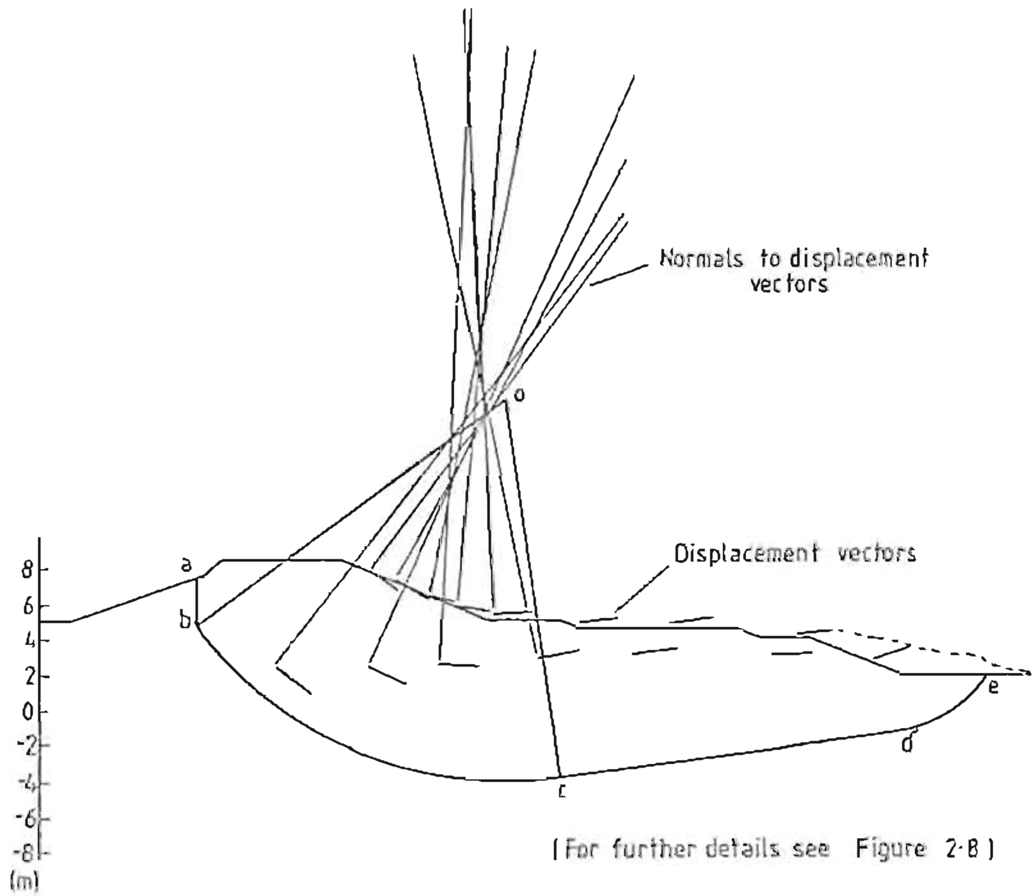

Figure 2.9 Review of Displacements in Segment obc

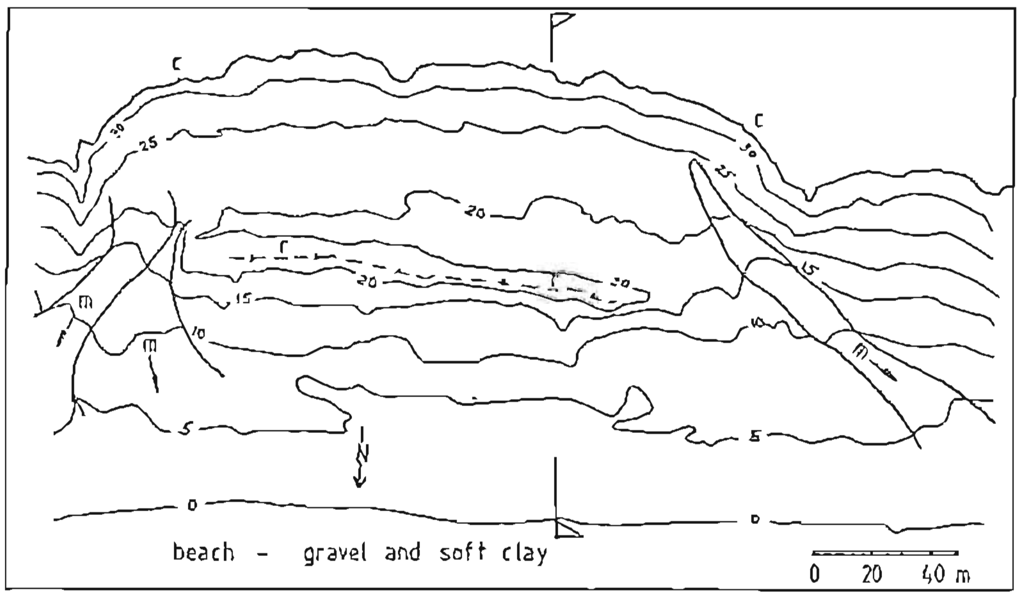

Key:

c cliff top

m lateral mudslide

r crest of ridge of blue clay

Figure 2.10 Contour Plan of Miramar Slide (after Bromhead, 1978)

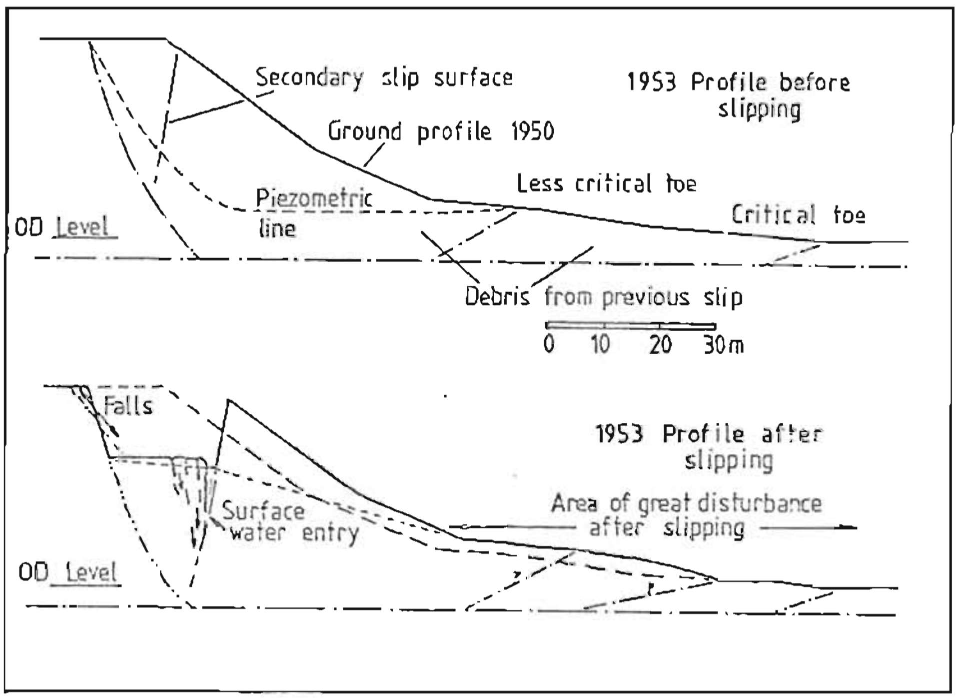

Figure 2.11 Sections through Miramar Slide (after Bromhead, 1978)

The position of these sections is indicated on Figure 2.10.

pore water pressures, which further weakened the strain softened material. A nearby slide at Queen's Avenue was reported to have shown first movement after a tidal surge in 1896. It was interesting to note that the Miramar slide showed large movement between Ordinance Surveys of 1872 and 1898; this activity may have been initiated by a similar surge, although the writer did not comment on this matter.

2.6 Conclusions

The presence of a layer of soil which is weaker than its neighbours has a particular influence on the position of the slip surface, the mechanism of failure, and subsequently the relevance of any stability calculations performed. The two-wedge failure mechanism has been demonstrated as being particularly relevant to the interpretation of slips in mining waste dumps, while other wedge mechanisms may form in embankments, depending on the position of the weak layer. The evidence presented suggests that another form of landslip, the wedge mechanism, should be considered together with progressive and retrogressive failures when studies are being undertaken. The aim of this study is to define clearly the kinematics of the two-wedge mechanism so that it may be readily recognised in the field, and an appropriate design method may be established.

2.7 Additional References to Field Examples

Anderson, J.G.C. and Trigg, C.F. (1976), "Case-Histories in Engineering Geology", Elek Science, London, 204pp.

Bishop, A.W. (1973), The Stability of Tips and Spoil Heaps", Quarterly Journal of Engineering Geology, Vol. 6, pp. 335-376.

Carson, M.A. (1977), "On the Retrogression of Landslides in Sensitive Muddy Sediments", Canadian Geotechnical Journal, Vol. 14, No. 4, pp. 582-602.

Christie, J.H. (1975), "Makohine Tip Fatality", New Zealand Engineering, 15-10-75, pp. 294-295.

Donovan, J.J. (1978), "On the Retrogression of Landslides in Sensitive Muddy Sediments: Discussion", Canadian Geotechnical Journal, Vol. 15, pp. 441-446.

Eden, W.J. (1975), "Mechanism of Landslides in Leda Clay with Special Reference to the Ottawa Area", Proceedings 4th Guelph Symposium on Geomorphology: Mass Wasting, pp. 159-171.

Engineering News Record (1925), "What Happened to Municipal Utilities at Santa Barbara", Vol. 95, July 23, 1925, pp. 146-149.

Gonano, L.P. (1977), "Slope Stability Investigations in Open Pit Mining", Technical Report No. 57, Division of Applied Geomechanics, CSIRO.

Holubec, I. (1976), "Coal Waste Embankments", Canadian Geotechnical Journal, Vol. 13, No. 1, pp. 27-39.

Huang, Y.H. (1977), "Stability of Mine Spoil Banks and Hollow Fills", Proceedings of Conf. on Geotechnical Practice for Disposal of Solid Waste Matter, Ann Arbor, pp. 407-427.

Hutchinson, J.N. (1965a), "The Stability of Cliffs Composed of Soft Rocks with Particular Reference to the Coasts of SE England", Thesis submitted for PhD degree, University of Cambridge.

Hutchinson, J.N. (1965b), "A Survey of the Coastal Landslides of Kent", Building Research Station Note EN/35/65.

Jones, F.O., Embody, D.R. and Peterson, W.L. (1961), "Landslides along the Columbia River Valley, North-western Washington", U.S. Geological Survey, Professional Paper No. 367.

Knights, C.J. and Matthews, W.L. (1976), "A Landslip Study in Tertiary Sediments, Northern Tasmania", Bulletin of the Int. Assoc. of Engineering Geology, No. 14, pp. 17-22.

Sapozhnikov, V.T. (1971), "On the Limiting Height of Banks", Soviet Mining Science, Vol. 7, No. 6, pp. 674-678.

Seed, H.B. and Wilson, S.D. (1967), "The Turnagain Heights Landslide, Anchorage, Alaska", Journal of Soil Mech. and Found. Div., Proceedings ASCE Vol. 93, No. SM4, pp. 325-353.

Tschebotarioff, G.P. (1973), "Block Slides", Article 703 in "Foundations, Retaining and Earth Structures", 2nd. ed., McGraw-Hill Kogakusha, Tokyo, pp. 291-292.

Wahler, W.A. and Schlick, D.P. (1976), "Mine Refuse Impoundments in the United States", Proceedings 12th. Congress of Int. Commission on Large Dams, Mexico, Vol. I, pp. 279-319.

Ward, W.H., Penman, A. and Gibson, R.E. (1955), "Stability of a Bank on a Thin Peat Layer", Geotechnique, Vol. 5, pp. 154-163.

CHAPTER 3

PHYSICAL MODELLING

3.1 Introduction

The role of physical modelling in soil mechanics has a long history. Even before the subject of soil mechanics was recognised, engineers were working with soil in the construction of roads, bridges, and building foundations. The prevailing attitude was to carry out the work required on the assumption that the soil would not cause failure; the essence of this approach was the use of the prototype as a full scale model, although this point was not recognised at the time.

Early researchers in the field of soil mechanics used small scale models to simulate what might occur in the field and many of the advantages, as well as limitations, of physical modelling became apparent. The development of large capacity, rapid computers in recent years has led to an upsurge in the numerical modelling of geotechnical problems, with the result that the emphasis on physical modelling has apparently waned. However, in many ways, physical modelling has been aided by the new technology associated with computers, especially in the area of data acquisition and manipulation.

The following sections of this chapter will explain the current approaches to physical modelling and then give details of the modelling apparatus and materials used to obtain the results for this study.

3.2 Classification of Models

The results of research have provided a better understanding of soil mechanics which has enabled more meaningful model studies to be devised and undertaken. Thus, as physical models became more specialised, it was necessary to describe their purpose more accurately. In the 1971 Roscoe Memorial Symposium on Stress and Strain in Soil, a section was devoted to physical modelling in which the discussion leader defined three classes of model (James, 1971).

Class I models are those which are built to study the response of a particular prototype. Therefore, for any results to be meaningful, the model must obey the principles of similarity. There are four main techniques for constructing similar models: full scale construction, centrifuge, hydraulic gradient, and equivalent material. The first three are more common to soil mechanics problems than is the fourth, which is used for many rock mechanics investigations. Examples of each of these methods are given by Parry (1971), Coxon and Bassett (1976), Zelikson (1969), and Fumagalli (1968) respectively. Although the results from the Class I model are quite reliable, the major limitation of this approach is the restriction of the results to the model's particular prototype, which makes this technique costly if several alternatives are to be investigated.

The second class includes models which are a small-scale version of a general field situation. The purpose of the model study is to consider the sample as a small prototype, and to compare its behaviour with that predicted by some method of analysis, so that a relevant design approach may be used. Thus, it is necessary to make some simplifying assumptions for ease of model construction and then in the analytical stage to use parameters relevant to the low stress levels associated with the model. Because of the different behaviour of some modelling materials at various stress levels, the results observed in the model may not be evident in the prototype. For a Class II model, the relationship between model and prototype is made through the analysis which most effectively describes the performance of the model. Some presumptions about the qualitative performance of the prototype may be made from the evidence provided by the model.

Class III models are similar to those of Class II, however, they are more closely oriented to the study of fundamental soil mechanics as an academic subject, because there never need exist a prototype. The work carried out at Cambridge (e.g. Arthur and Roscoe, 1965) is an excellent example of the application of a Class III model. As implied above, it is not one of the aims of a study using a Class III model to establish a relationship with any prototype; however, the contribution of this type of model to the understanding of soil behaviour is likely to lead to improved design approaches for many types of structure.

The model used for this study is best described as in Class II, because the simplified slope used for the model resembled some field conditions which have been described in an earlier part of this text. However, the model was restricted by a number of idealistic assumptions, with one of the objectives of the study being to gain further understanding in the theory of the kinematics of failure. Two points which need to be realised when reviewing the model used for this study are:

(i) the model did not represent a prototype in reality, and

(ii) the results described the performance of the model, but not necessarily what might occur in a similar situation in the field.

3.3 The Model Developed for the Study of Sequential Failure

3.3.1 The model in relation to field cases

Generally, a Class II model is a simplified, and thus idealised, representation of a field example. From the earlier description of some landslip records, the problem was generally defined as one where a weak planar discontinuity formed the base of a slope which was granular in nature for many cases. Each particular case had special geotechnical features, however, the features which were common to all cases were of primary importance for this study.

To make the study effective, the model was chosen as a particular circumstance within the generalised conditions. The granular material was limited to a well-graded, cohesionless, loose sand which formed a simple slope at its angle of repose with its base bounded by a weak horizontal layer of purely cohesive material. Because of the lateral extent of most of the field cases, the modelling technique was required to simulate plane strain conditions. Thus, the details of the model, both materials and apparatus, centred around the achievement of these initial conditions.

3.3.2 The modelling materials

In previous examples of this type of physical modelling, use had been made of a uniform or a well-graded cohesionless material. Because the material commonly found in spoil piles was not uniform, the well-graded material was selected as being a more suitable approximation to the field material. Cornforth (1964) reported on experiments performed with Brasted sand, and its grading curve was used as a guide to the choice of a sand for use in these experiments. To avoid detrimental effects resulting from particle breakdown, silica sand was selected for its abundance in quartz mineral. The sand was quarried at Herveys Range (west of Townsville) and after washing, drying, and selection of the particles in the sand size range, preparation was complete. The final grading curve is shown in Figure 3.1 and other relevant descriptive properties are listed in Table 3.1. All values were determined in accordance with AS 1289 (1977), "Methods of Testing Soils for Engineering Purposes".

TABLE 3.1

Descriptive Properties of Silica Sand

Specific Gravity	2.60
Minimum Density	1480 kg/m^3
Maximum Density (wet method)	1650 kg/m^3
Air dry moisture content	.1%
Placed density in tank	1500 ± 20 kg/m^3
d_{50}	.40 mm

The method of placement of the sand is described in the following section.

The weak layer was represented by a uniform thickness of bentonite, at a preset moisture content. This layer rested directly on the rubber covered base of the tank. The low yield strength required for the model was achieved by mixing the bentonite to a moisture content of 900% and by keeping the time between placement of the layer and conducting the test as short as practicable. The marked difference in moisture content between the bentonite and the sand created a problem when capillary tension was exhibited by water which had seeped up into the sand from the bentonite. This effect was significantly reduced by the application of a thin water-resistant film of wax-like material at the interface.

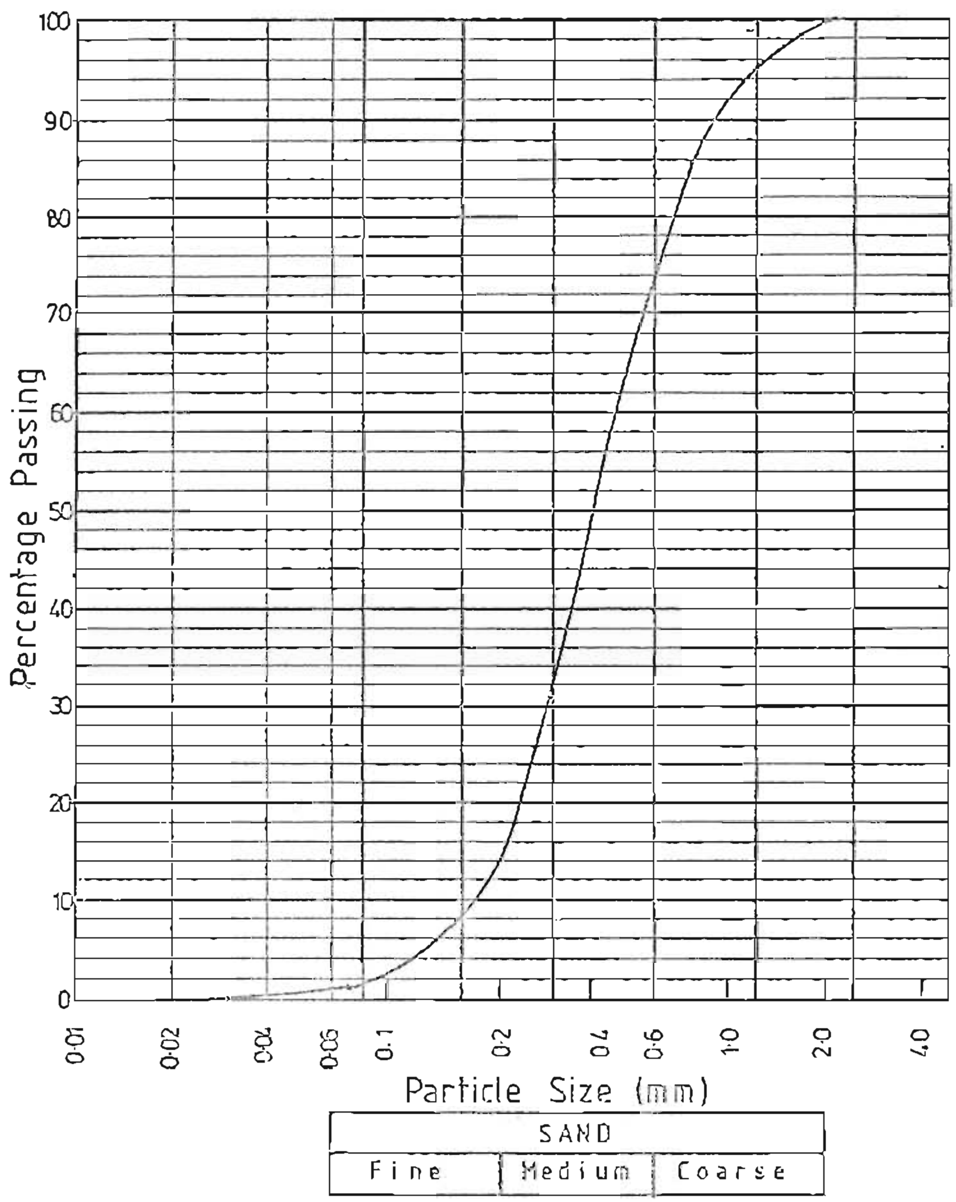

Figure 3.1 Grading Curve for Silica Sand (prepared)

The presence of the film did not perceptibly alter the yield strength of the bentonite. Although the use of bentonite at high moisture content may at first seem unrealistic, it is worthy to recall that bentonite is a member of the family of sodium-montmorillonites, which may have field moisture contents in the range of 300 to 400%. The source of bentonite was a commercial product marketed under the name of "Red Devil Gel" by Petro-Chem Inc., Montana. The water resistant film was Molycote "Metal Protector" manufactured by Dow Chemicals.

3.3.3 The modelling apparatus

The dimensions and mode of operation of the apparatus are given in this section, with the background to their choice and associated experimental techniques presented in the following section. There are three major components of the apparatus: a strengthening mechanism for the bentonite (explained subsequently), a sample enclosure, and an overhead hopper from which the sand was placed.

Before design was attempted, a literature review revealed four methods used by other researchers to induce failure in small slopes: increasing the effective angle of the slope by tilting the base after the model is constructed (e.g. Sultan and Seed, 1967); weakening a layer of material along the base of the model when fully constructed (e.g. Blight, 1969); inducing movement using a mechanical discontinuity (e.g. Holland, 1977); and manipulating effective strength in the base material by increasing pore fluid pressure (e.g. Bishop et. al., 1969). The first method was discarded because the geometry of the model would not accommodate tilting, and the third method was considered to be unrealistic because the direction of shear forces induced through movement of the discontinuity would be markedly different from those existing in the field. Thus, time was devoted to the second and fourth schemes, with the principle of the second leading to the design of the device used in this study.

From the previous section, it will be found that the bentonite was mixed so that it offered little resistance to shear; therefore, if a sand slope was constructed over the bentonite, some additional shear strength would be required in the base layer to maintain its stability until completion. This condition was met by introducing a 50 mm square wire mesh at the interface of the sand and bentonite with the mesh being supported from beneath the sample base by a set of retractible vanes. The bentonite was loaded with the full thrust of the sand when the mesh was lowered by its supports and effectively became the base of the tank. The removal of the mesh was kept uniform by linking all supports to a stiff cradle which was activated by two simple lever mechanisms connected to a common handle for the operator. Illustrations of the tank body and stiffening mechanism are given in Figures 3.2 and 3.3 respectively.

The sample enclosure was a rectangular prism of length 1500 mm, width 745 mm, and depth 600 mm. The two side walls were each a single sheet of 15 mm thick glass; the base was 18 mm reinforced ply covered with 1.5 mm Linatex sheet rubber; one end was 12 mm reinforced ply, and the other end and top were open. The reinforcing for the ply consisted of 25 mm steel equal angle attached at 100 mm centres, with the spacing of the angle dependent on the position in the tank.

The main frame of the apparatus was designed to carry a hopper which would traverse the length of the sample space and the storage capacity of the reservoir was sufficient to enable a 20 mm layer to be placed without any recharge. Figure 3.4 shows the hopper geometry. The flow of sand was regulated by the distance of the hopper from the previous layer and was stopped by rotating the delivery slots in a cylindrical gate at the base of the reservoir. The hopper was elevated by two screw threads and secured in a particular position for placement by pin connectors fixing steel bars on either side of the hopper to the hopper carriage. These bars were drilled at 10 mm centres, thus limiting the variation of placement interval to a multiple of 10 mm. The glass side walls were protected against scratching by the hopper by fixing a plastic (pvc) pad to each side of the discharge fan of the hopper. The carriage was built of steel section and the hopper bin of galvanized sheet. An overall view of the apparatus is shown in Plate 1.

3.3.4 Material - apparatus interaction

Many of the design details for the apparatus were determined by the feasibility of operating the apparatus and the physical constraints

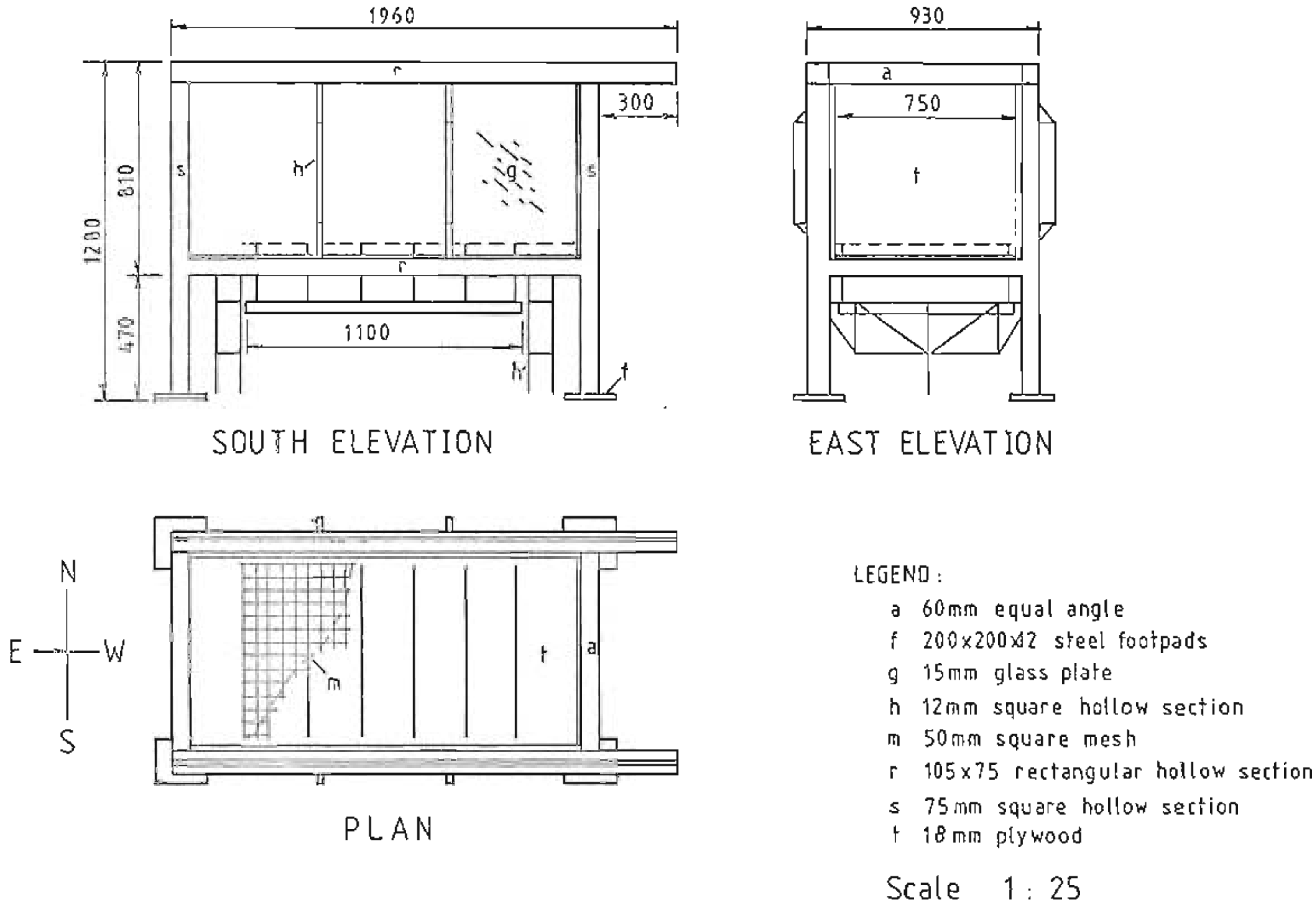

Figure 3.2 Modelling Tank

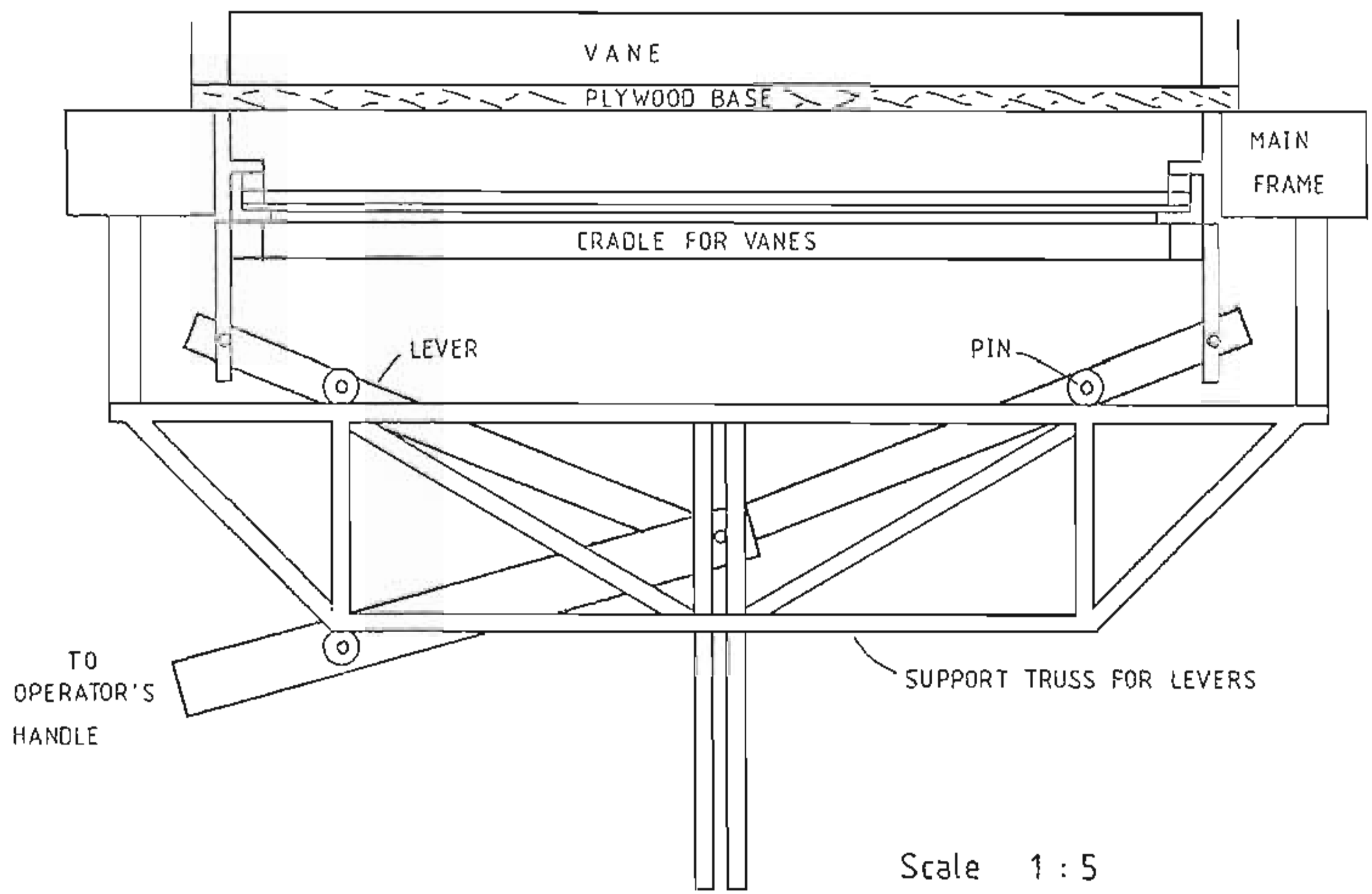

Figure 3.3 Bentonite Stiffening Mechanism

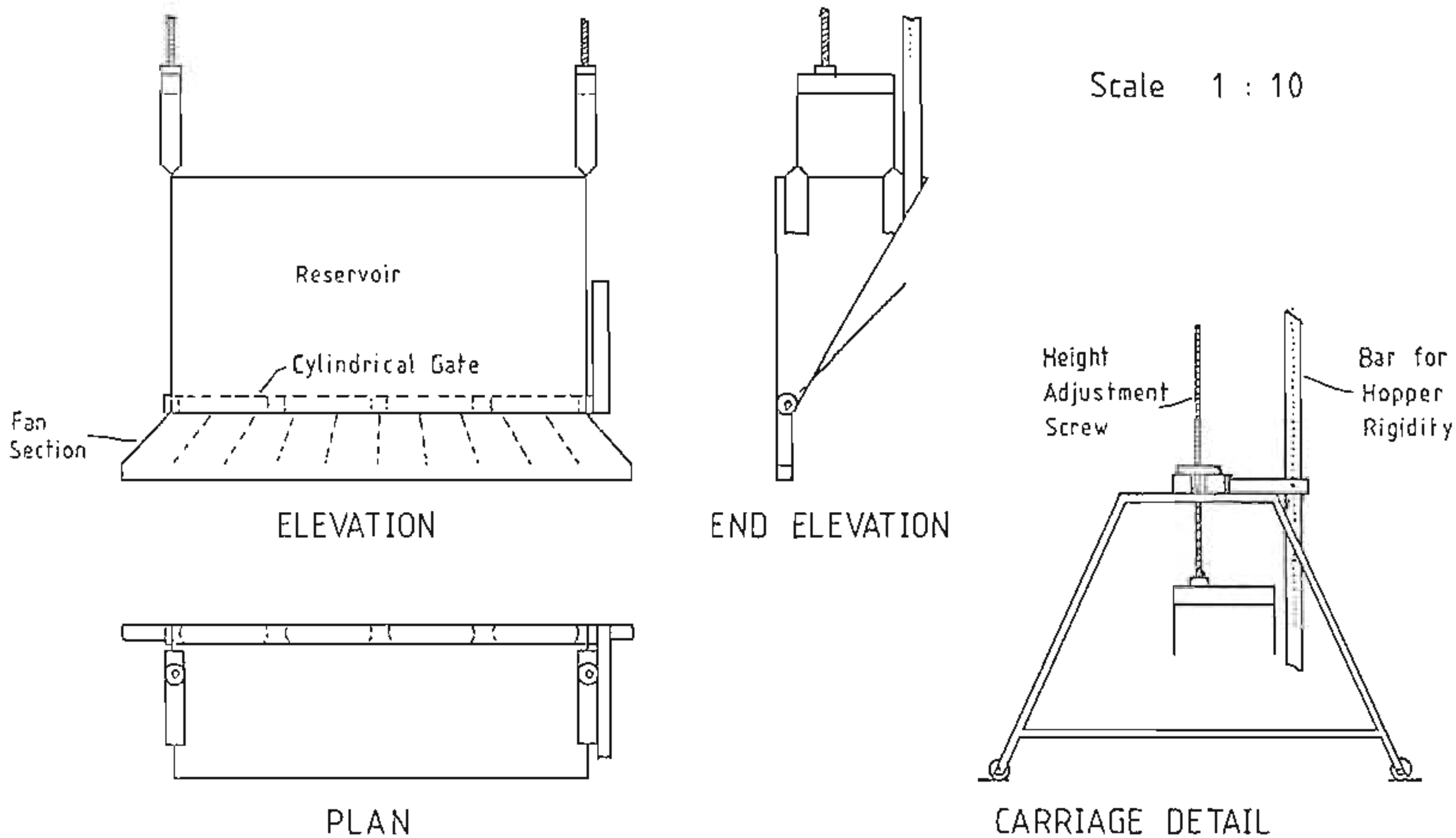

Figure 3.4 Hopper for Sand Placement

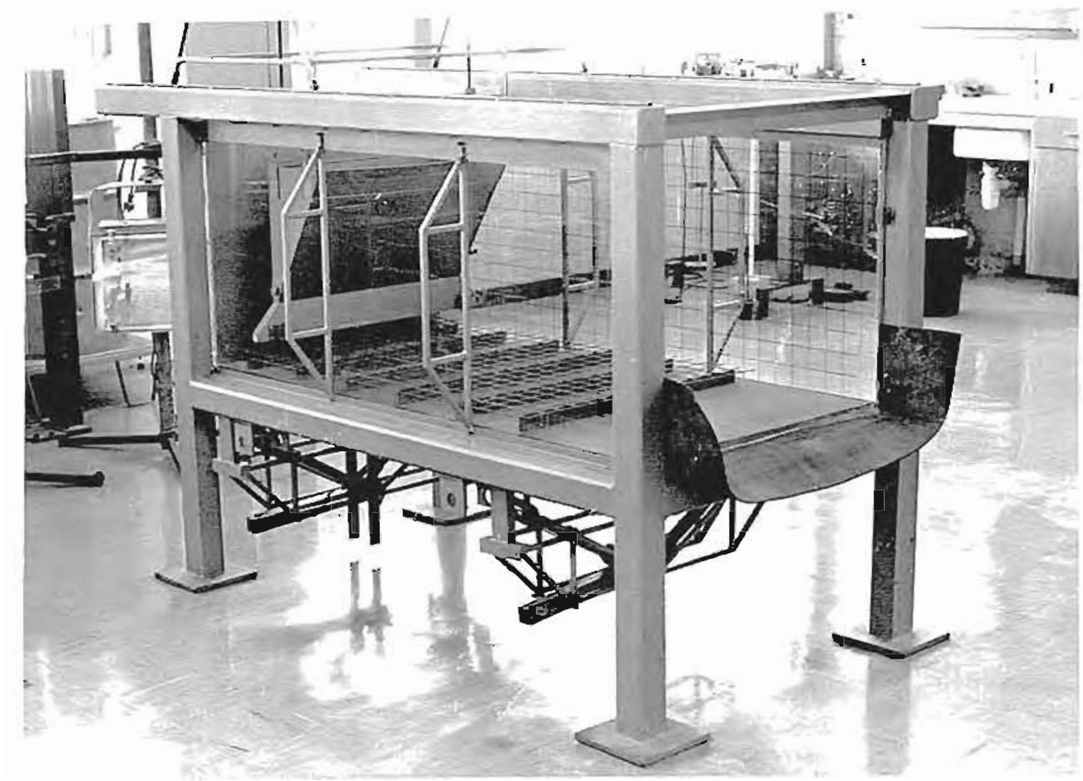

Plate 1 Overall View of Apparatus

necessary to retain the conditions for reliable results. The overall capacity of the sample enclosure was chosen so that no more than one tonne of sand could be used, since the effort required to handle a greater mass would have been excessive, especially within the confines of a laboratory. The time required for placement of sand needed to be in the order of one hour because of the adverse effects of moisture incursion into the sand and the thixotropic nature of the bentonite.

Once the basic size of the sample enclosure had been estimated, the support requirements to promote plane strain conditions, and to minimize other edge effects, were considered. Arthur and Roscoe (1965) reported that the flexibility of the side walls in a model earth pressure apparatus had a significant effect on the intermediate principal stress, and consequently on the behaviour of the soil. It was said that the most reliable results would be given by an apparatus with rigid side walls. This suggestion came in conflict with the need to use a transparent material in the side walls for observation of the model in the plane of movement. A satisfactory solution was reached in which the side walls consisted of 15 mm thick plate glass acting as a slab, simply supported around its perimeter and stiffened at two intermediate positions by members spanning its width. Thus, the area for observation was preserved in three units of approximately 600 mm height and 500 mm width. The maximum deflections expected in the side walls were less than the upper value used for the design of the frame of the apparatus: .05 mm. The actual deflections experienced during an experiment were significantly less than design maximum because of the lower sample density and more restrictive connections than were assumed in calculations. A test loading of the base of the sample enclosure yielded results which were within design limits. A safety check for stress concentrations in the glass was made with a polariscope before any experiments were carried out.

In some experimental methods, the size of the soil particle with respect to the apparatus affects the reliability of results. Kerisel (1972) showed that in triaxial tests and models of shallow footings, results were erroneous when the ratio of working dimension (sample diameter or footing width) to maximum particle diameter was less than about 20. These complications did not affect the results from the model slope or the load deformation tests because the relevant ratios were 325 and 25 respectively.

There has been considerable attention given to the effect of sidewall friction on the performance of models, although the conclusions reached were contradictory. Arthur and Roscoe (op. cit.) stated that "side plate friction is not a large factor in determining the strain, and hence the stress field in this model", when reporting experiments with a model retaining wall which had a width and height of 150 mm (6 inches).

Bransby and Smith (1975) presented a paper which had the effect of side wall friction as its main theme. The writers revealed that previous researchers had recommended minimum height to width ratios for sample enclosures so that the effects of side wall friction would become negligible; Terzaghi suggested that models should be twice as wide as their height, and Rowe suggested a width to height ratio of 1.5 to 3, depending on the surcharge load. Furthermore, Rowe (1971) has concluded that the uniform results recorded by Arthur and Roscoe (op. cit.) indicated that the effects of side friction extended throughout the sample, and not the opposite as suggested by the latter. Thus, the inevitable existence of the effects of side wall friction was recognised and the sample enclosure was designed to have a minimum sample height to width ratio of 1.5. Bransby and Smith (op. cit.) stated that photography through the side wall would record the zone most disturbed by the frictional effects; thus, measurements were taken during experiments so that the movement at the side wall could be related to that at the centre, which was practically free from frictional distortion.

The magnitude of the side friction depended on the coefficient of friction between the wall and the modelling material. Hence, the frictional effect would be minimised if materials were used which gave the lowest practical coefficient of friction. An article by Butterfield and Andrawes (1972) gave important information regarding the frictional coefficients between sand and various plane surfaces. The material most likely to suit the objectives of this study was glass because of its relatively low coefficient of friction, small variation between static and dynamic values of this coefficient, and its time independence.

several surface preparations were applied to a sample glass plate which was then tested in shear over a bed of sand; the lowest coefficient of friction (.15) was achieved when the glass was cleaned with acetone and allowed to dry without any further applications. The results of experiments showed that the central 400 mm of the model was relatively undisturbed by side wall friction.

In an attempt to rationalise the study, it was decided to use an homogeneous slope of well-graded sand. Because of the tendency of the sand to segregate when dropped or rolled, sand placement occurred in horizontal layers rather than by using a wedge construction. AS 1289 (op. cit.) recommends a maximum dropping height of 20 mm when a loose sample is desired; thus, layers were placed at this interval and, as well as creating a loose structure, the amount of segregation was small. Each layer was placed by positioning the hopper at the face of the slope, then opening the reservoir gate. The hopper was moved at an even pace toward the back of the tank, where the gate was closed. Before the reservoir was refilled, the hopper was raised to the next level and moved to the front of the tank. In all experiments, no data were recorded less than 200 mm from the back wall of the tank so that the non-uniform zone caused by the closure of the hopper gate would be avoided. Plates 2(a) and (b) show the bentonite base before any sand was placed and while the first layer was deposited.

The strengthening mechanism for the bentonite was one feature of the model with a high potential to cause misleading results because of the possible alteration of the failure characteristics of the model slope. The retraction system was built so that the mesh would be lowered quickly and uniformly; hence, the main source of distrubance came from the presence of the mechanism rather than from the means by which it was retracted. A quantitative comparison between one experiment, in which the slope was excavated without any artificial support, and those experiments in which the strengthening mechanism was used, revealed negligible difference between the final sets of failure characteristics. Detailed results of these tests are given in a later chapter. Thus, it was confidently concluded that the strengthening mechanism did not adversely affect the performance of the model.

In the design of the apparatus around the model slope there were some ideals to pursue and also physical limitations, both material and

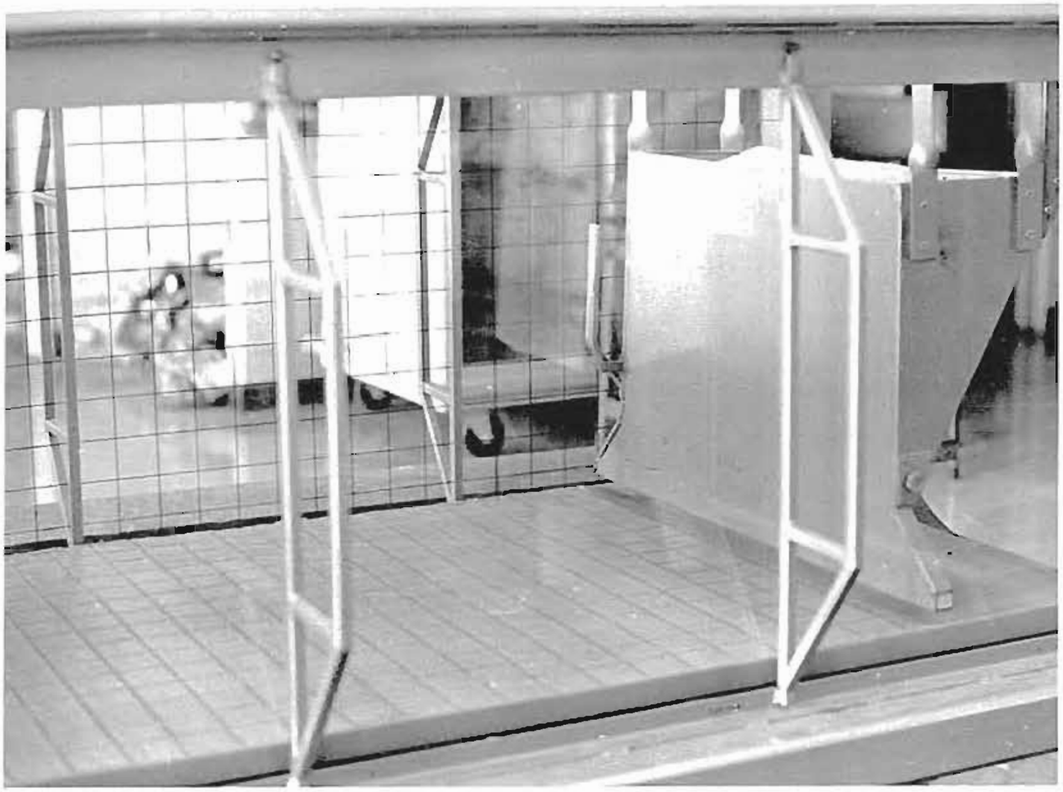

Plate 2a Bentonite Layer Ready for Sand Placement

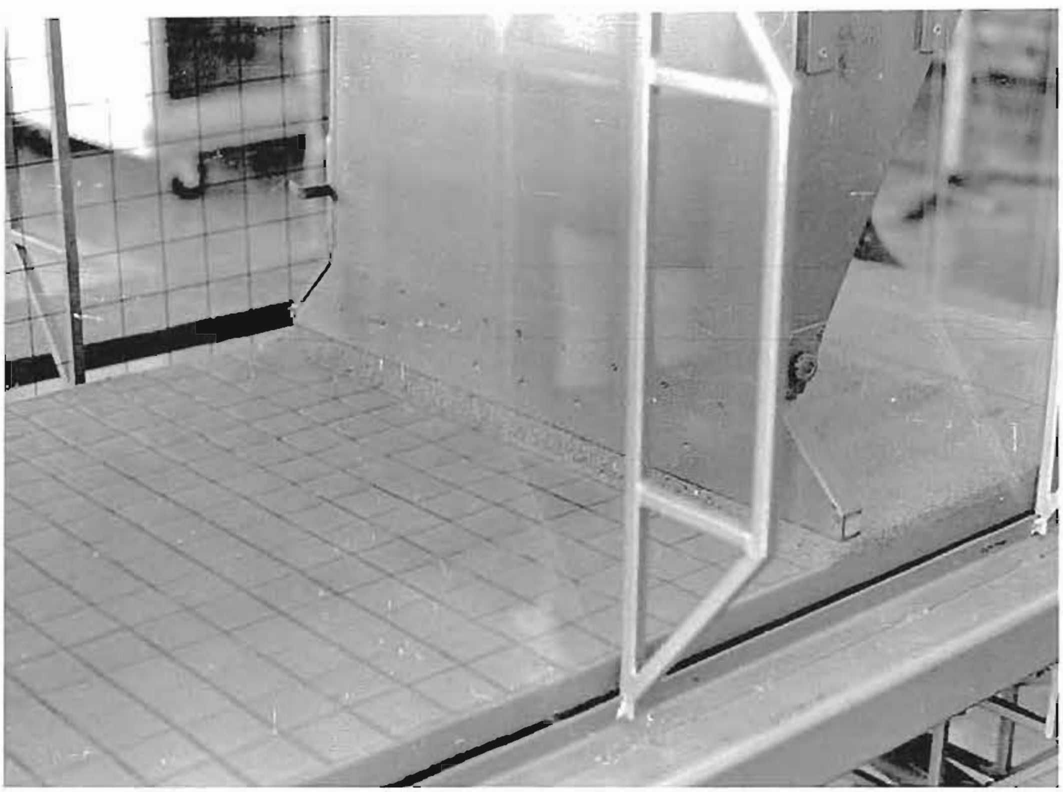

Plate 2b Placement of First Layer of Sand

geometric, which would not allow the ideals to be fully realised. However, the end result of design and construction was a suitable compromise from which reliable results could be expected.

3.4 Data Collection

The physical size of the model slope produced relatively low working stresses under natural gravitational conditions; therefore, any device considered for force or displacement measurement would have to be sensitive to the quantity to be measured, but not alter that quantity in the process of obtaining a record. Because of physical difficulties of placing apparatus in the sample space, and other problems associated with peripheral equipment, photogrammetry was chosen as the method for recording displacement. No attempt was made to measure forces or stresses because of the concentration of this study on the kinematics of slope movement.

The apparatus was designed to promote a plane strain condition in the sample; thus, the most effective area for photography was in a plane perpendicular to the plane strain axis. The major requirement for success was a transparent wall which would still meet the deflection restrictions discussed previously. The problems of photographing a zone affected by side wall friction and the methods used to correct the differences has also been given earlier in this text.

Two methods exist for the measurement of data from a photographic record of displacement: the first relies on measuring the coordinates of a group of target points over a number of time steps, enabling displacements to be calculated from comparison of the data; the second requires a stereo-pair of photographs so that displacements may be measured by the method of false parallax (vide Harley, 1967). The efficient use of stereo-photogrammetry can only be achieved when large format plate cameras are employed and when it is practical for the movement to be recorded as a series of exposures of the same plate; otherwise, the accuracy afforded by this technique is impaired by the poor definition and low reliability of the photographs. Thus, the first method was used for measurement in this study, allowing conventional camera equipment to be used. Examples of measurement by stereo-photogrammetry are given by Butterfield, Harkness and Andrawes (1970), and Andrawes (1976); an example of the first method is given by Roscoe, Arthur and James (1963), although the film was exposed to X-rays rather than light.

The qualitative results of this study were gained by using a 16 mm Bolex movie camera driven at constant speed by a motor and battery pack. The films were projected onto sheets of cartridge paper where the movements of the targets in the slope were plotted. Individual frames of the movies were examined with a control being provided by a reference grid marked on the glass wall. More detailed measurements were taken using an Olympus OM-2 single lens reflex camera with a motor drive attachment. A Nikon Data-back camera with motor drive and a large magazine had been successfully used, but was not available for the final test run; this camera was more suited to the task than was the Olympus. Measurement of the 35 mm film was directly from the negatives using monocular vision through a Zeiss Stecometer linked to a Dell-Forster digitiser, with data being typed record as well as paper tape. The Stecometer was located in the Surveying Department, University of Melbourne. The control and analysis of these results is presented in a later chapter.

The form of the targets finally developed for the identification of movement throughout the slope was a 50 mm length of aluminium rod of 3 mm diameter. The end in contact with the glass wall was finely polished and then half the area was blackened using a spirit marking pen for better definition in the Stecometer. The rods were placed in the slope through a templet, which resulted in the formation of a triangular pattern with all sides being approximately 45 mm. Plate 3 shows a row of targets in the process of being covered by the next sand layer.

3.5 Expectations and Goals

The principal aim of this study was to determine the kinematics of failure for the small-scale slope constructed in the modelling apparatus. Thus, the apparatus had to aid in the control of the sample so that the assumptions made in the definition of the study were upheld and that a suitable photographic record was obtained during each test run. The photographs had to provide both qualitative and quantitative

Plate 3 Target Arrangement

information for the results of the experiments to be meaningful.

Once the principal aim was fulfilled, the purpose of the study was to formulate comments on current engineering approaches to this particular problem by analysing, or numerically modelling, the laboratory slope as a prototype. The most significant information required for the majority of the work was the load-deformation function for each material; hence, an effort was made to identify relevant parameters with the expectation that these would lead to a satisfactory result. The following chapter is devoted to the description and results of the load-deformation tests conducted.

CHAPTER 4

STRESS-DEFORMATION PARAMETERS

4.1 Introduction

The deformation of the model slope was the result of the interaction of two materials, sand and bentonite, under self-weight loading. The model container restricted movements so that a plane strain state existed for most of the sample. Therefore, to establish suitable stress-deformation characteristics to aid in the interpretation of test data, tests on the materials had to be carried out in plane strain conditions and within the stress range imposed by self-weight loads in the model.

Another very important point to be considered in the interpretation of model test results was the nature of the material itself. For example, the high moisture content of the bentonite effectively transformed it from a soil into a suspension of clay particles in water, which required testing practices used for non-Newtonian fluids. Similarly, it is the author's belief that sand should be considered as a discontinuum when inter-particle frictional contacts are the major means of force transmission through the soil structure. Considerable credibility has been given to the clastic approach to granular materials by Trollope (1968), Rowe (1963), and several other authors. The use of clastic mechanics does not negate the concept of stress as a measurement of the intensity of load, but requires that its magnitude be found as an average force intensity distributed over an area which is at least an order of magnitude larger than a representative particle cross sectional area (i.e. there is no meaning for "stress at a point" in a discontinuum). Therefore, the emphasis in the interpretation of the tests on sand was on the stress-deformation response of the sample, rather than on the usual stress-strain characteristics.

Because of the widely different nature of the sand and bentonite materials, the descriptions of testing procedures and stress-deformation responses will be considered in two parts: Section 4.2 for sand, and Section 4.3 for bentonite.

4.2 Tests on Loose Sand

4.2.1 Background to the choice of tests

The low levels of stress in the model slope proved very difficult to achieve in conventional laboratory testing apparatus, and the very loose state of the sand necessitated the development of a special sample former and some skill so that the loose matrix was disturbed as little as possible prior to testing.

Two types of stress-deformation test were used: the plane strain and direct shear tests. Of the two, the plane strain test was by far the more important. Sultan and Seed (1967) emphasised the need to use relevant strength parameters when computing slope stability, even though the slope may only be of small scale. It is well known that the difference between strength parameters derived from triaxial and plane strain tests on loose sand is quite small; however, it will be shown that the variation in deformational response between the two tests justifies the use of the plane strain apparatus.

The choice of the direct shear test stemmed from the test's simplicity and convenience. The purpose of the tests was to provide a rough check against the results gained from the plane strain tests by using a primarily qualitative comparison. The results from the plane strain tests are used for comparisons made with existing stress-strain (stress-deformation) theories. The following sections provide a description of the plane strain apparatus, sample preparation, plane strain results, direct shear results, comparisons with existing theories, some further observations on the response of the sand, and a summary of results for tests on loose sand.

4.2.2 Plane strain apparatus

A plane strain device was developed at James Cook University by Ford (1970). The sample tested was 101.6 x 101.6 x 50.8 mm (4" x 4" x 2") and was contained in a thin rubber membrane moulded to suit rectangular end plattens, rather than those of circular origin which rely on a transition section to fit the sample shape (e.g. Green, 1971). The cuboidal cell was assembled from three parts: the base plate, the side walls, and top plate; which were held together by ten tie rods on the perimeter and tightened to a torque of 27.1 Nm (20 ft lb). The cell was fabricated from steel, and two small observation ports were provided in the longer side walls, although these were ineffectual. Axial load to the sample was carried by a standard plunger arrangement through the top plate with the load being indicated by a 450 N (100 lbf) proving ring. Detailed design drawings of the device were given by Ford (op. cit.).

During familiarisation trials of the device, the end clamp which controlled the plane strain condition was found to be insufficiently sensitive to measure the load in the intermediate direction. The original design used a cylindrical ram rigidly attached to a platten which was in contact with the sample membrane, however, the O-ring seals in the ram offered too much resistance to sliding for a reliable value of the lateral load to be recorded. As there appeared to be no simple solution to overcome the problem of poor response, a second end clamp was designed and manufactured. The new device consisted of one rigid platten and a reservoir covered by a flexible membrane, which were joined by four 12 mm diameter steel rods. The separation between the ends was controlled by nuts on each of the four bolts. This device is illustrated in Figure 4.1 and is similar to that used by Cornforth (1964). The flexible membrane was 1.5 mm Neoprene rubber which was fixed by a polyester resin to the steel reservoir. The shape and position of the reservoir was machined so that it corresponded to the sample area. The contact surface of the rigid platten was covered with the same neoprene to provide even contact conditions in the intermediate direction. The reservoir was connected by a flexible tube into the cell base and then to a null indicator; therefore, by ensuring zero volume change in the reservoir, a plane strain condition was maintained and the lateral pressure was also monitored. One problem which was often present in devices which used flexible membranes was poor membrane restraint near the edge of the reservoir. Sutherland and Mesdary (1969) gave a solution to the problem, however, no difficulties were experienced in these tests because of the relatively low differential pressures between the cell and end clamp reservoir.

The use of low confining pressures in the plane strain tests required the calibration of all parts of the apparatus for operational

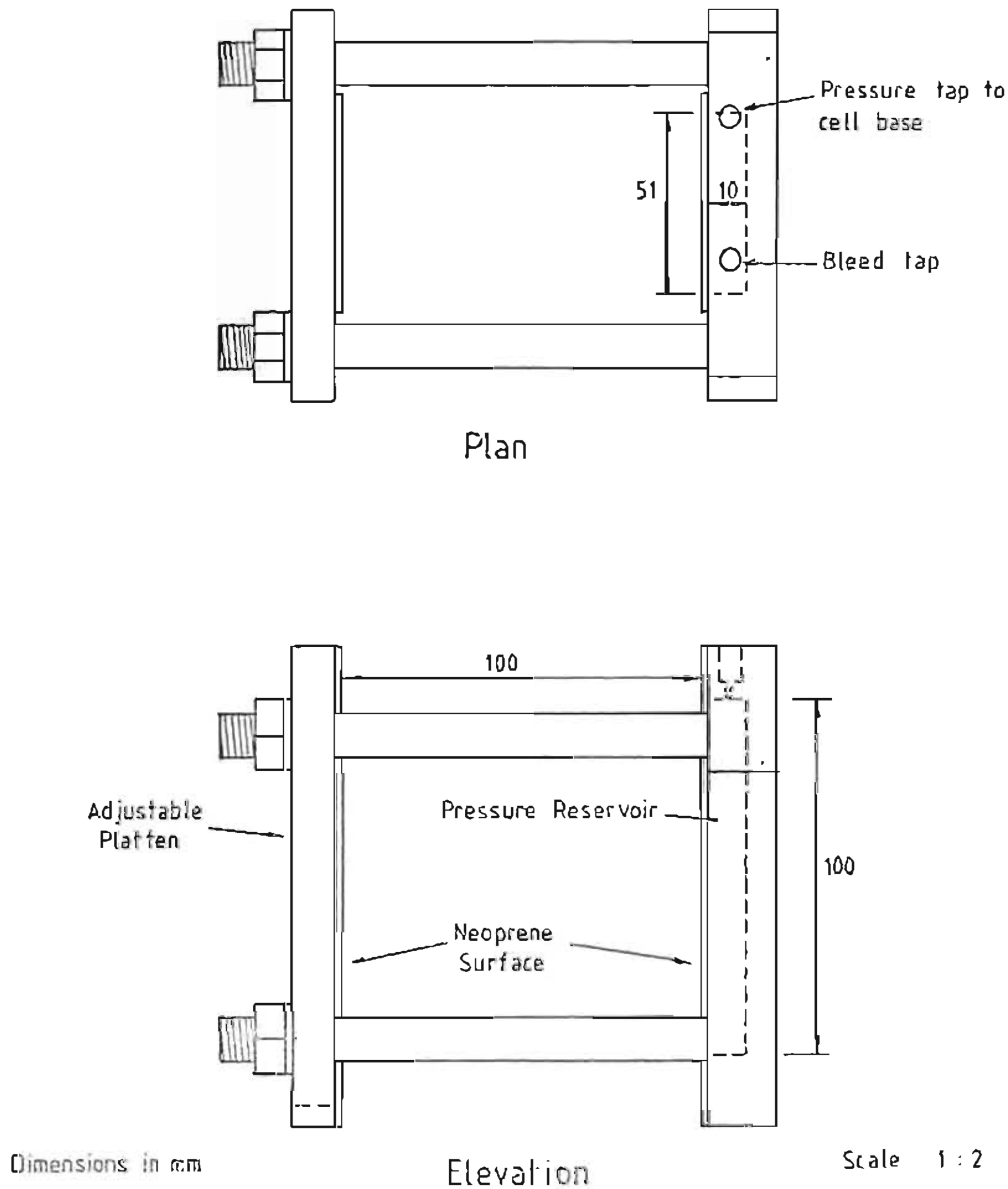

Figure 4.1 End Clamp Device

reliability. The record of volume change with pressure in the cell included the component due to membrane impression around sand grains. For this test, a dummy sample was made from a block of steel which had sand grains adhered to its surface by a poly-urethane lacquer so that the overall dimensions of the finished article closely resembled those of the actual sample. Figures 4.2, 4.3, and 4.4 show the calibration curves for the 450 N proving ring, the cell volume change, and the end clamp response respectively.

4.2.3 Sample preparation

All samples were formed in a loose, dry state and were separated from the cell water by a rubber membrane with a thickness of .254 to .330 mm (.010" to .013"). Each membrane was of relatively uniform thickness, but the thickness of individual envelopes varied. The sample was sealed at both ends around the perimeter of the end caps by clamping the membrane between an O-ring and a smooth metal surface. The lack of a complete seal at the top cap or the puncturing of a membrane wall led to the abandonment of several tests.

The sample former consisted of four interlocking steel plates which were tied together with brass bolts to form a rectangular enclosure around the membrane which was fixed in position on the cell base by the lower sample platten. The former had to be machined to a very close tolerance to ensure satisfactory sample dimensions for the test. The membrane was stretched over the top of the former where it was held with the aid of rubber bands, after which a vacuum was applied between the membrane and the former. With the membrane thus extended, the sample was poured through a funnel into the space, with care being exercised so that the sand did not drop through more than 20 mm to preserve similarity between the sample and the sand in the model slope.

When the sample reached its full height, the top surface was gently levelled out and the top cap placed in position with the membrane being released from the former and clamped by the top cap as quickly as possible. To maintain the sample's shape, a slight sub-atmospheric pressure was placed inside the sample before the former was removed. In this operation, care was taken so that the effect of the lower pore

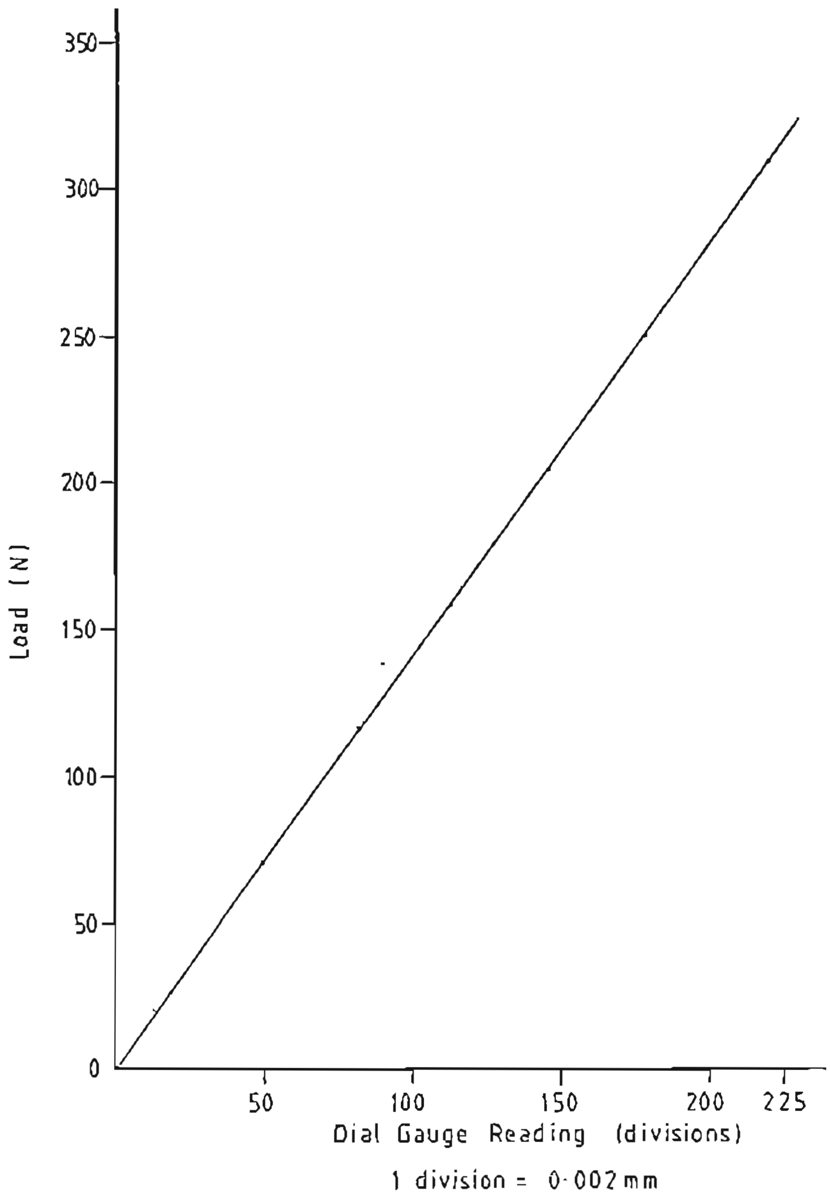

Figure 4.2 Calibration Curve for 450N Proving Ring

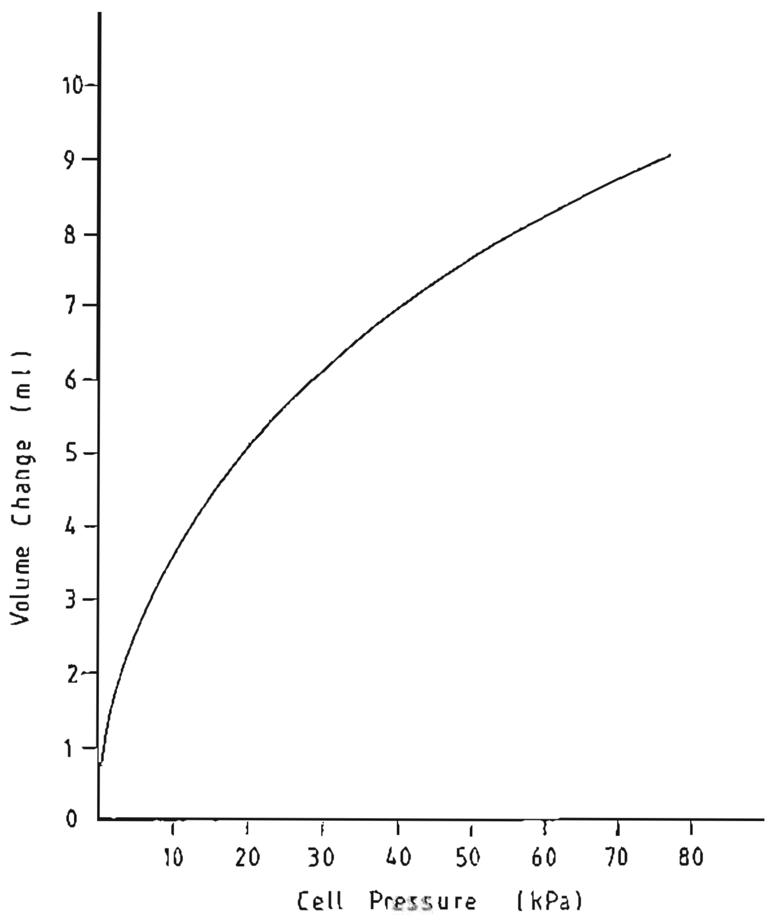

Figure 4.3 Calibration for Cell Volume Change with Pressure

n.b. includes membrane impression

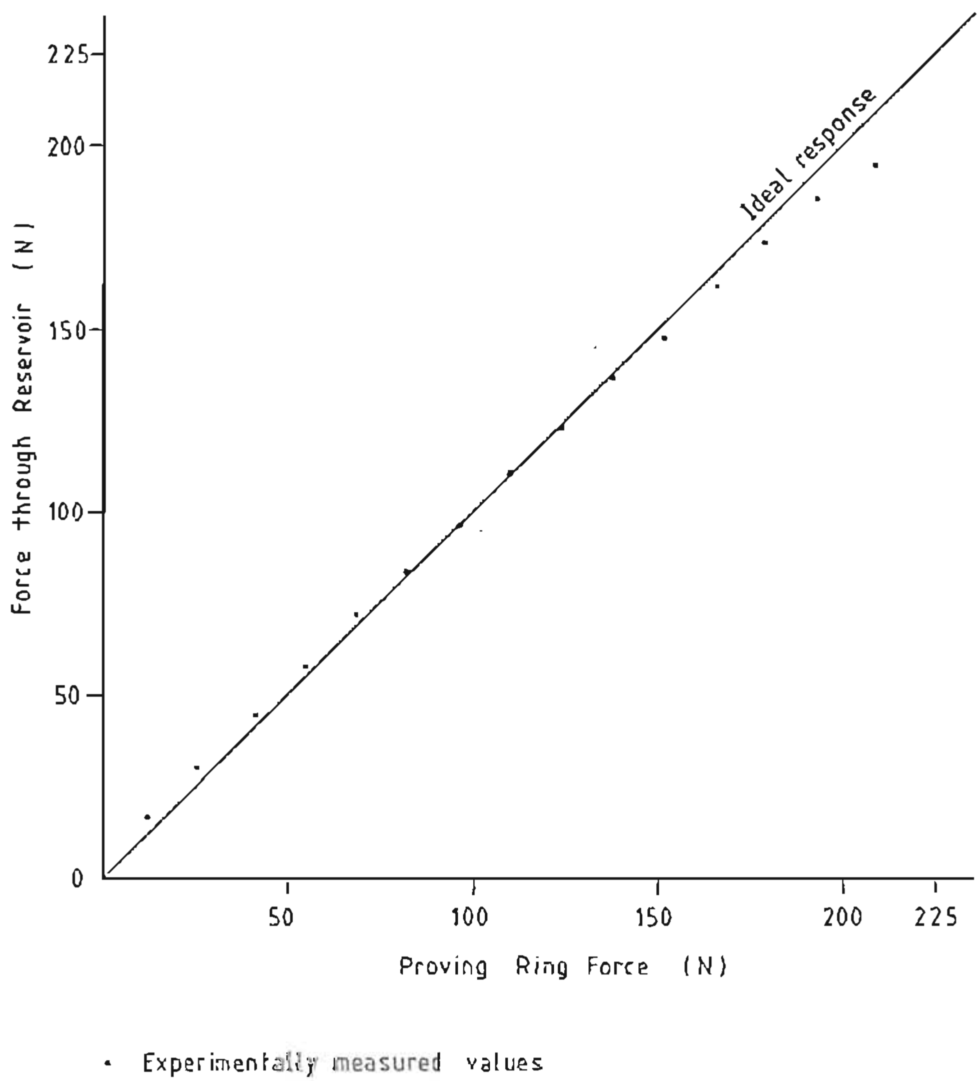

Figure 4.4 Calibration Curve for End Clamp

pressure did not exceed that of the initial cell pressure proposed for that particular test. Before further preparation was made, the dimensions of the sample were determined using a set of verneer callipers which were able to be read to .02 mm. The slight curvature at the corners of the sample was also measured and taken into account when the sample volume was calculated.

When measurement of the sample was complete, the end clamp was placed in position and adjusted so that the plattens were just touching the ends of the sample. The null indicator was set and the remainder of the cell was assembled with all bolts being tightened to the required torque. The cell space was filled with tap water at a rate which did not induce turbulence, which would tend to trap air pockets around the sample and end clamp. The upper few millimetres were filled with oil to reduce leakage of water through the plunger bearing. After the cell was sealed, the cell pressure was slowly increased as the pressure inside the sample was brought back to atmospheric level. The sample was kept in a drained condition under isotropic consolidation for several hours before any load was applied.

Some attention was paid to the possibility of frictional effects from the plattens which might influence failure characteristics. Thus, the contact faces of the end clamp were coated with silicone grease before the clamp was put in position. Simple block sliding tests showed an extremely low drag at all normal loads for the surface materials and lubricant in use (.48 kPa, which represents a total force of 2.4 N against the deviatoric load). Bishop and Green (1965) showed for triaxial tests that the effects of end restraint on both strength and deformation were negligible for loose samples with a height to diameter ratio greater than or equal to 2. Thus, it was considered unnecessary to provide lubricated plattens at the top and base of the sample because the height to depth ratio was 2. Cornforth (op. cit.) explained that if platten friction was a problem, then the slip plane would be expected to pass through an edge of the top platten because of the shear stress concentration in that zone; however, all slip planes in these tests were observed to intersect the sample edge about 5 to 10 mm below the top platten. This evidence was considered to support the assumption that there was no significant effects from the unlubricated end plattens.

4.2.4 Test results

The upper limit for stresses in the model slope was 10 kPa, therefore, plane strain tests were carried out with confining pressures of 4, 6, and 8 kPa. The testing technique took some time to develop and only a limited number of tests were of sufficient reliability to warrant inclusion in this section. The tests considered were: 4A, 6B, and 8C for which the nomenclature indicates the approximate cell pressure and the particular test at that pressure; all tests were conducted at a constant rate of axial deformation of .127 mm/min (.005 in/min). The stress-deformation plots are given in Figure 4.5, and relevant test details are in Table 4.1.

Table 4.1

Test Details

Test	Cell Pressure kPa	Density kg/m^3	Relative Density
4A	4.02	1514	.200
6B	5.93	1518	.224
8C	7.99	1513	.194

The sample density was reasonably consistent, although it was at the upper end of the range of the model slope density which was 1500 ± 20 kg/m^3. Thus, the samples could be compared with each other, but there was no attempt made to determine the effect of the higher relative density of the samples.

One of the more common methods for representing triaxial and plane strain test results is using the Mohr diagram for stress coupled with a Coulomb failure envelope. Figures 4.6 and 4.7 show these plots for peak and residual stress conditions. The determination of the angle of maximum obliquity led to an estimate of the angle of the plane along which slip might take place; however, more detailed discussion of the predicted and observed slip directions is given in Sections 4.2.6 and 4.2.7. The slip plane was observed to make an angle of 54° with the direction of the minor principal stress (horizontal), and the Coulomb

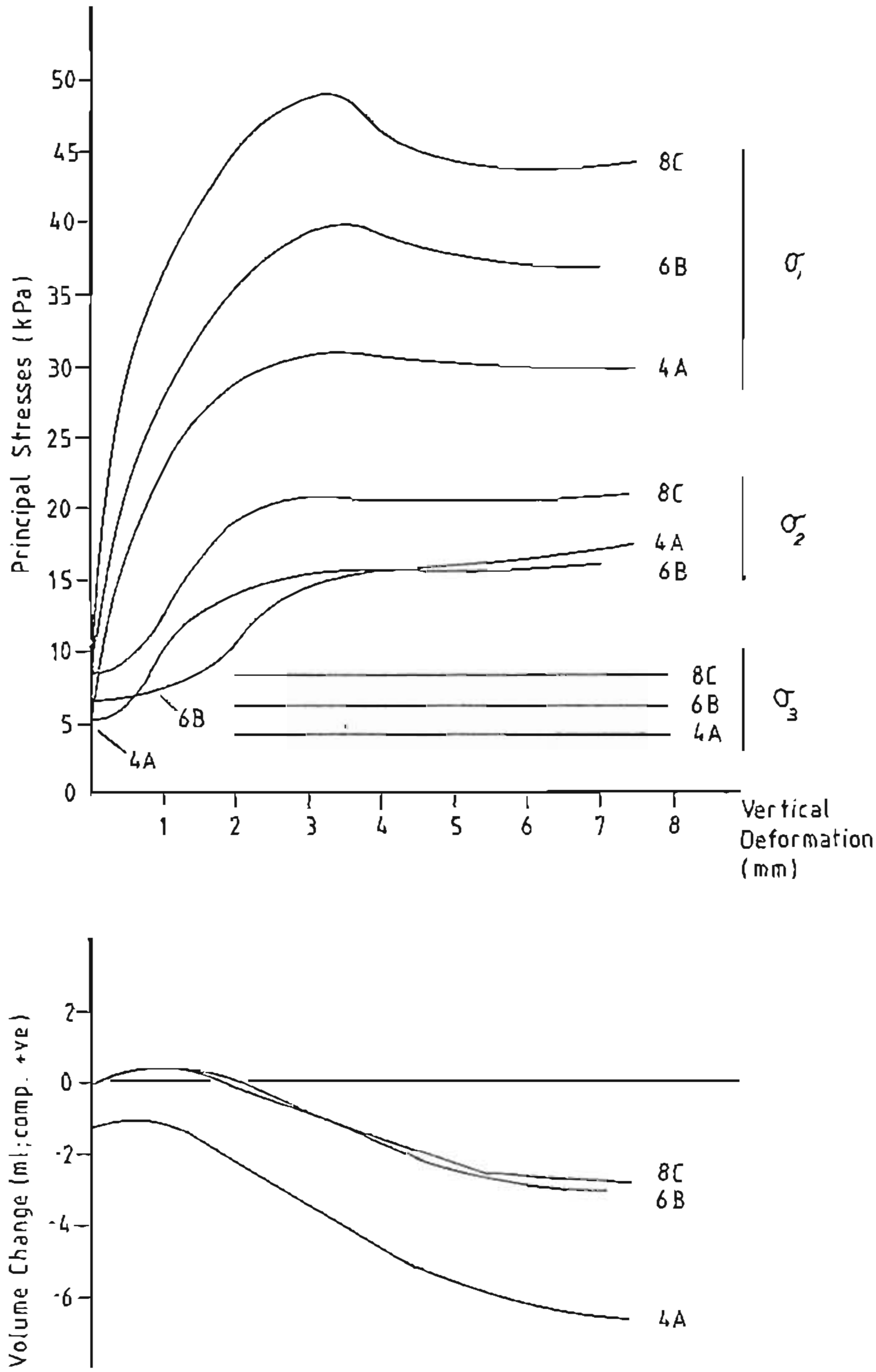

Figure 4.5   Plane Strain Stress-Deformation Results

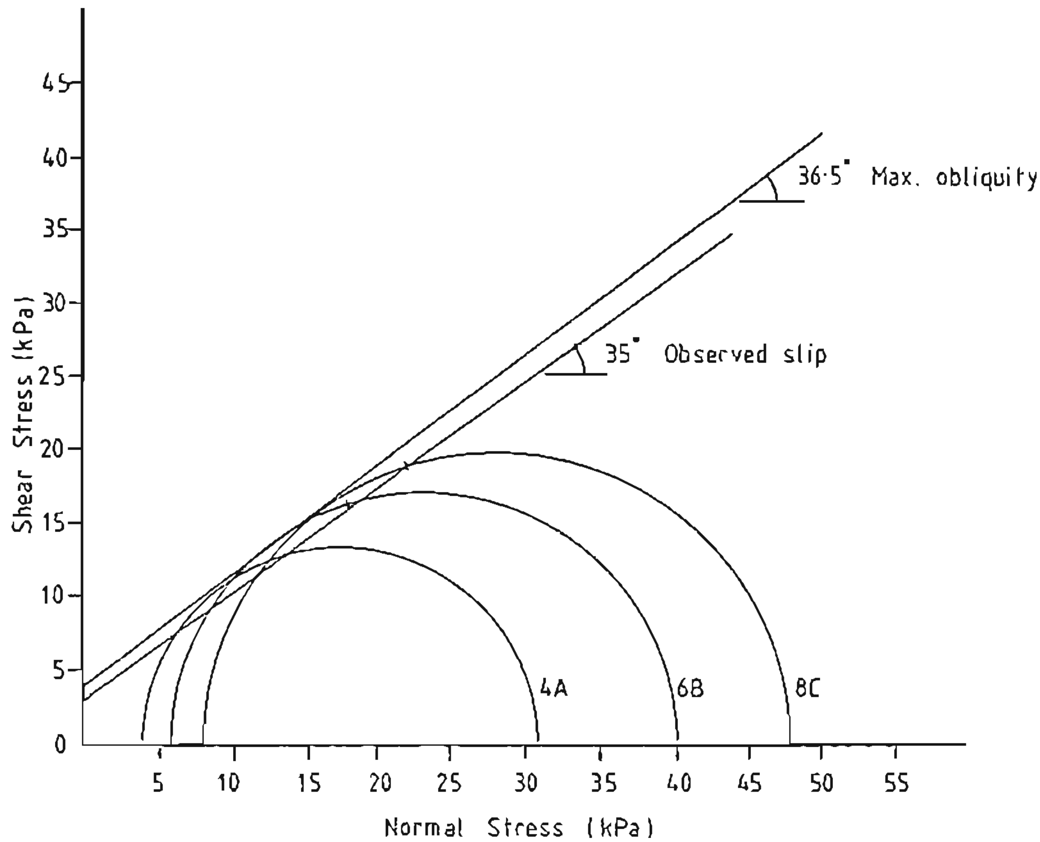

Figure 4.6 Mohr-Coulomb Diagram - Peak Stress

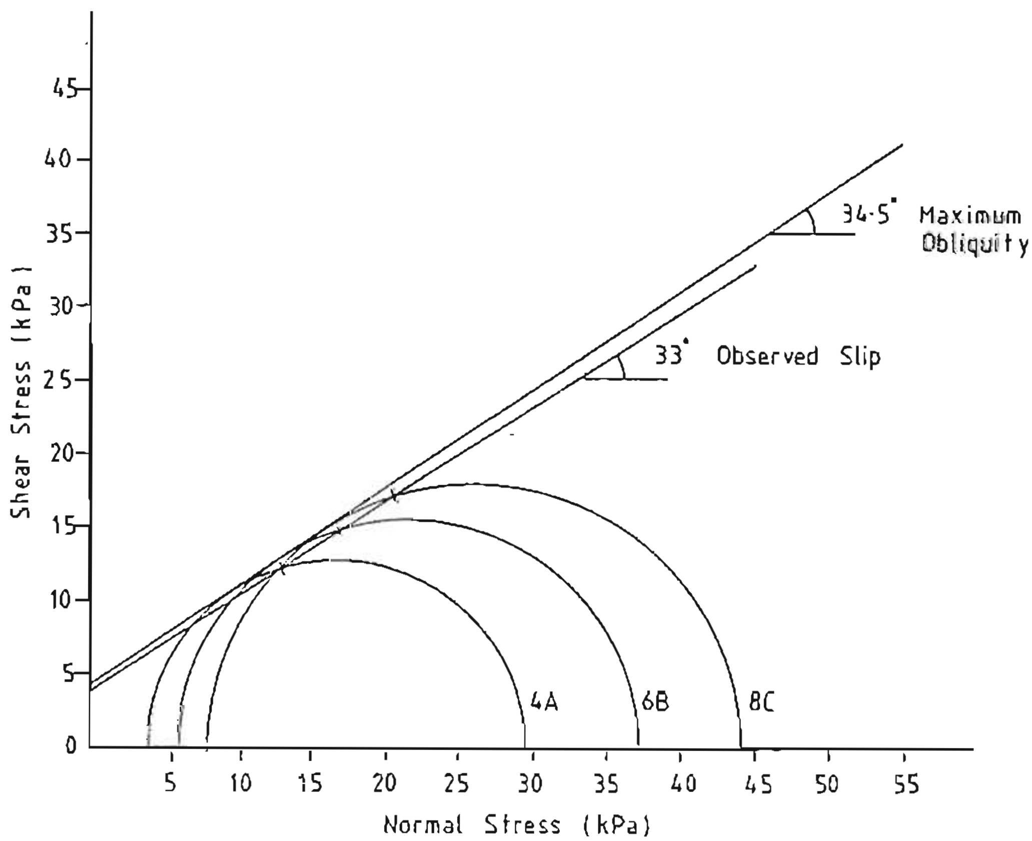

Figure 4.7 Mohr-Coulomb Diagram - Residual Stress

failure envelope relevant to the slip plane is also shown in Figures 4.6 and 4.7. Both King and Dickin (1970) and Bransby (1971) noted that the slip plane in a plane strain test formed soon after the peak stress ratio was reached and did not vary significantly after that; therefore, the slip angle of 54^0 was assumed to be applicable to both peak and residual stress conditions for representation on the Mohr diagrams. One observation which was made from both Mohr-Coulomb diagrams was the considerable difference in stress levels at points of failure on the planes of maximum obliquity and observed slip angle. All envelopes showed an intercept on the ordinate, however, it is quite likely that the envelope was curved toward the origin.

Several important observations about the stress-deformation behaviour of this sand were made by further consideration of Figure 4.5. The deformation to the peak values of major and intermediate principal stresses was the same; this agreed in general with findings by other researchers (e.g. Cornforth (op.cit.), and Green (op.cit.)). The plot of intermediate principal stress for test 6B was inconsistent with the other plots and it was concluded that there was an error in the adjustment of the end clamp which led to the later development of the stress. The loose clamp allowed less restricted movement of the sample in the lateral direction which resulted in less sample volume change than expected. Because of the low pressures used during testing, the cell and lateral pressures were recorded with their datum at the mid-height of the sample so that the values were close to the equivalent average pressure acting over the relevant surfaces.

In sharp contrast to the deformational response of loose sand under usual working pressures, both triaxial and plane strain samples exhibit expansion when sheared (in compression) at low confining pressures, in the order of 10 kPa. Lee (1970) illustrated an example of this characteristic with Antioch sand tested in both triaxial and plane strain devices at cell pressures of 9.8 and 49 kPa (1.0 and 5.0 kg/sq. cm). The results for plane strain tests on Antioch sand agreed well with the author's test results in many qualitative aspects, which included an early realisation of the peak stresses compared with the axial deformation required for a similar triaxial test.

The volume change for all tests (cf. Figure 4.5) showed an initial decrease, but reversed sign to assume a basically constant expansion rate until the trace altered to a value slightly above the zero volume change rate. This volume change characteristic was very similar to the characteristic for a medium-dense sand sample in a plane strain test at a much higher cell pressure; e.g. Cornforth (op. cit.) conducted a test at 275 kPa (40 psi) and Green and Reades (1975) ran several tests at 207 kPa (30 psi).

It is of considerable importance to determine when failure in the sand occurred. Some writers claimed that failure occurred just after the peak stress was reached, when first evidence of a slip plane was observed (e.g. King and Dickin (op. cit.), Bransby (op. cit.); however, this interpretation did not explain the relationship between volume change characteristics and the failure mechanism. Roscoe (1970) presented a review of some of the significant work which was carried out at the University of Cambridge using various versions of the simple shear apparatus. The writer commented on work by Cole, who had shown that the failure of Leighton-Buzzard sand started on as thin a band as possible and grew to a zone of about 10 grain diameters (3 to 6 mm) thick. Cole also found that the angle of dilatancy calculated from boundary deformations grossly underestimated the local values measured in the region of the shear zone by using X-radiography.

The role of the kinematics of failure in granular materials has been demonstrated recently by Mandl, de Jong, and Maltha (1977). The writers gave a very accurate account of the movement of particles and the mechanics of formation and growth of a shear zone. Although the majority of their work was based on shearing at high confining pressures, considerable insight was given into many fundamental characteristics of shear in granular materials. Likewise, Cornforth (op. cit.) concluded that many of the differences in stress-deformation characteristics between plane strain and triaxial tests were attributable to the modification of the kinematics of slip due to the lateral restraint in the plane strain test. Trollope (1971) has considered a more theoretical approach to the kinematics of granular shearing by proposing the "strong systone hypothesis".

The writer proposed that sand could be considered as a random arrangement of groups of grains (systones), and that the load carrying capacity of individual systones was dependent on the packing within the systone, the interparticle friction, and the orientation of the systone with respect to the load. Therefore, before shearing occurred throughout a sample, systones would have to be reoriented to a direction which favoured slip at the ambient load. Thus, the kinematics of failure would be expected to exhibit a sequence of three stages: an initial collapse to overcome packing irregularities; an expansion during which grain movements occurred to realign systones to a suitable slip direction which subsequently allowed shear at constant volume.[1]

The author supports this three-stage concept for shear in granular materials, and found that the volume change data recorded during the author's plane strain tests were able to be classified into distinct stages. The first stage was to the point of zero rate of volume change, the second to the point of decrease in volume change rate, and the third continued for the remainder of the deformation.
The initiation of failure was defined by the point of zero rate of volume change which occurred immediately after a slight compression of the sample. The second stage of volume change represented the growth of the shear zone from the initial slip line to the band, which has also been observed by other researchers to vary between 5 and 10 mm. Some theoretical aspects of, and further evidence for this opinion are presented in Section 4.2.7.

Thus, the failure condition was described by the amount of deformation in the direction of the major principal stress as: initiation after 1 mm, growth of the shear zone up to 5 mm, and rigid block motion with slip inside the shear zone for deformations beyond 5 mm. An alternative approach was to use the deformations along the slip direction as a gauge, giving: initiation after 1.25 mm, growth of the shear zone up to 6.2 mm, et cetera. The author also considered that the level of force at individual interparticle contacts determined the dilatant characteristics of the granular samples during shearing. The support for the previous statement came only from qualitative argument, because the research required to produce a quantitative argument would be a

---

1. The author is indebted to Professor Trollope for his extended explanation of the implications of the strong systone hypothesis.

large project in itself and was beyond the scope of this study (e.g. work by Mandl et al.,(1977). The magnitude of the force transmitted through an interparticle contact is directly influenced by the number of contact points and the ambient stress level (n.b. the definition of "stress" is the same as was given in paragraph two of Section 4.1). Thus, it was postulated that the dilatant behaviour of a medium-dense sand sample at an ambient pressure of 250 kPa would be similar to the behaviour of a loose sample (fewer interparticle contacts) at a pressure of 10 kPa (lower force intensity). The author considered that this proposal could lead to a significant advance in the interpretation of the response of small scale physical models; however, much more research is required to establish any working relationships between model and prototype.

4.2.5 Direct shear tests and results

The apparatus used was a standard (Casagrande) 60 mm square shear box. Normal load to the slip plane was applied by a weighted hanger through a rigid top cap to the sample and the shearing force required to drive the apparatus was measured by the same 450 N proving ring as was used in the plane strain tests. The sample was poured in a loose state with an average sample thickness of 20 mm. Volume changes within the sample were assumed to be uniform over its horizontal section and calculations were made from a single measurement of the vertical deflection of the top cap and hanger over the centre of the sample. The effects of container friction were reduced by application of a PFTE film to the contact surfaces.

Four direct shear tests were conducted on loose samples, each at a normal stress of 40.28 kPa, which was roughly double the load intensity at failure in the plane strain tests carried out at a cell pressure of 8 kPa. Table 4.2 shows the relevant test details and Figure 4.8 gives the stress-deformation and vertical deformation responses for each test.

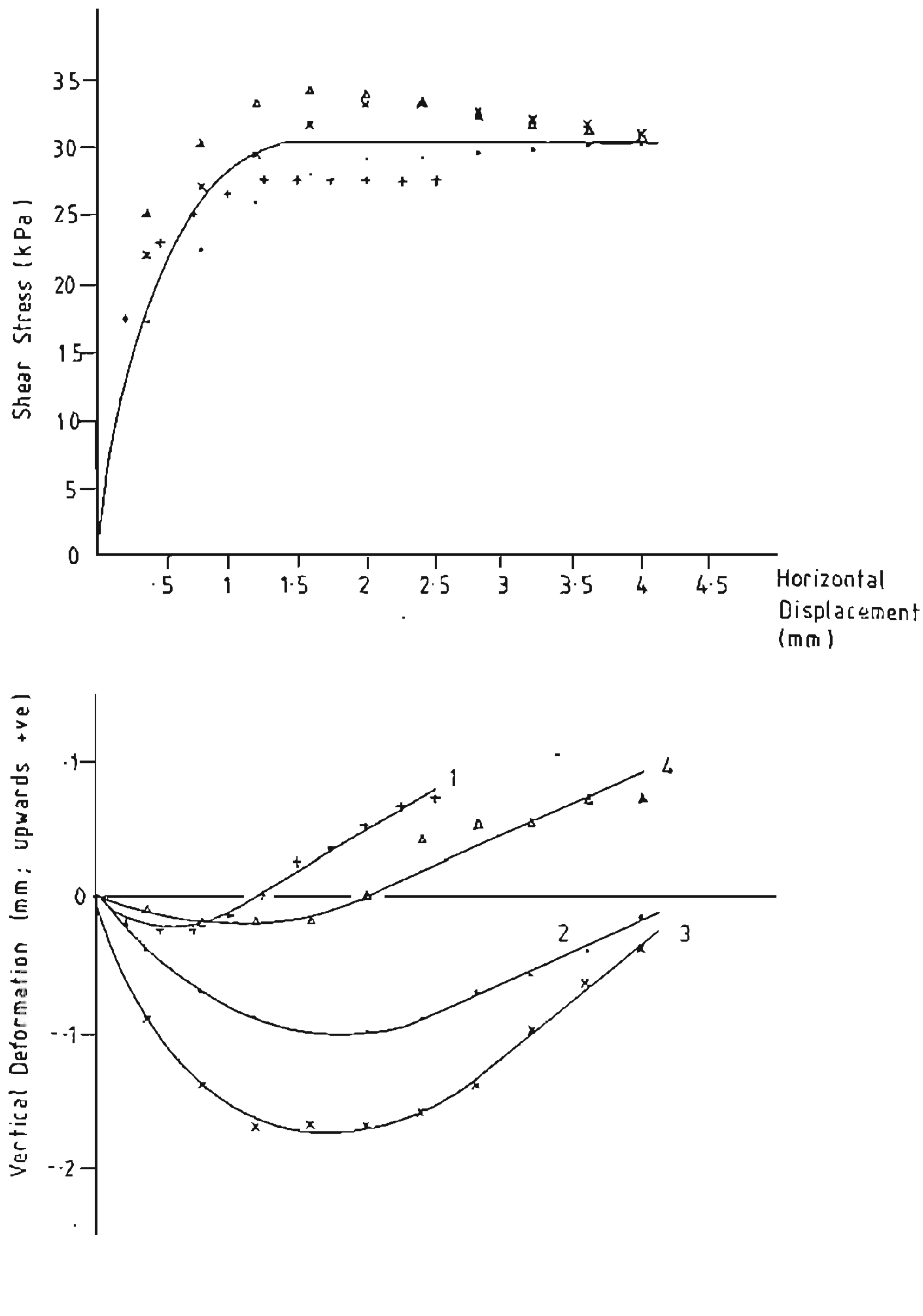

Figure 4.8   Direct Shear Test Results

Table 4.2

Direct Shear Test Details

Test	Density kg/m^3	Relative Density
1	1520	.235
2	1423*	-
3	1417*	-
4	1572	.541

* loose samples, but unreliable values.

The laboratory techniques used for the direct shear tests were not as refined as those used for the plane strain tests, and this was reflected in the variability of the sample and the subsequent variation in results. In some samples the shear strength showed a slight peak; however, the trend overall was found to be a rise to ultimate strength (about 30 kPa) within 1.5 mm horizontal deformation (i.e. along the slip path). The distance travelled to mobilise full strength compares favourably with the proposed distance of 1.25 mm required to induce failure in the plane strain tests. In terms of angle of internal friction, the direct shear tests gave a value of about 37^0, which was marginally higher than the peak ($36\frac{1}{2}^0$) and residual ($34\frac{1}{2}^0$) values obtained from the plane strain tests.

All the direct shear tests showed an increase in sample volume after an initial decrease. Because the maximum horizontal displacement was 4.5 mm, it was not possible to observe the third stage of volume change in these tests, which was expected to become evident after about 6 mm displacement. The amount of displacement required to reach the point of zero rate of volume change varied between .5 and 1.7 mm. This value was close to the displacement required for development of full shear strength, and may reasonably be considered as the initiation of failure to add support to the definition of failure proposed in the previous section.

4.2.6 Discussion of test results with reference to contemporary interpretations

During the past twenty years, substantial advances have been made in the design and use of apparatus which gauge the stress-deformation response of soils. As more information was gathered from studies, researchers were able to propose more meaningful, and often more sophisticated, functions to represent the strength and deformation characteristics of the materials they were investigating. The plane strain device used for this study did not represent any advance on those used by previous researchers, and many of the recently developed true triaxial devices have improvements in a number of aspects, including load and deformation measurement, platten control, and localised measurements within the sample.

The approaches to interpretation of data used in this section are associated with - the prediction of the level of intermediate principal stress during plane strain testing; the classification of failure as a collection of discrete interparticle slips; the correlation of the data with stress-dilatancy theory and critical state soil mechanics equations; and a comparison of the observed and predicted angles of slip planes. Section 4.2.7 contains the author's interpretation of the test results. The purpose in making these comparisons was to try to find a suitable stress-deformation relationship which could be used for the interpretation of the data from the physical model tests of the slope.

(i) Estimation of the Intermediate Principal Stress, σ_2

Bishop (1966) gave an equation for the estimation of σ_2:

$$\sigma_2' = \left(\frac{\sigma'_1 + \sigma'_3}{2}\right) \cos^2 \phi' \qquad (4.1)$$

(n.b. the value of ϕ' is for peak stress ratio)

Because the tests used in this study were all with fully drained samples, the total stresses equalled the effective stresses; thus, by dividing equation 4.1 throughout by the minor principal stress, a modified equation incorporating total stresses was produced:

$$\frac{\sigma_2}{\sigma_3} = \left(\frac{\sigma_1}{\sigma_3} + 1\right) \frac{\cos^2\phi}{2} \qquad (4.2)$$

Green (1969) gave an alternative equation for σ_2, which was ceded by Bishop (1971) to give a closer approximation of σ_2 for granular materials:

$$\sigma_2' = \sqrt{\sigma_1'\sigma_3'} \tag{4.3}$$

By performing the same modifications as were used for equation 4.1, equation 4.3 yielded:

$$\frac{\sigma_2}{\sigma_3} = \sqrt{\frac{\sigma_1}{\sigma_3}} \tag{4.4}$$

Both relationships in equations 4.2 and 4.4 were graphed with the observed values from tests 4A, 6B, and 8C in Figures 4.9(a), (b), and (c) respectively. The difference between predicted values of σ_2 from equations 4.2 and 4.4 were smaller than their deviation from the observed values. The trend of both observed and predicted values was basically the same in the post-peak region, however, the shape of the observed pre-peak curves was not reflected in the predictions. Therefore, the author does not accept that either equation adequately predicted the level of intermediate principal stress for these conditions.

(ii) Failure by Discrete Particle Slips

Parkin (1965) has used a close-packed system of uniform frictional spheres to model a cohesionless, granular material. The analysis was based on the minimisation of a function which related the number of interparticle contacts involved, the external load, the orientation of the packing to the load, and the coefficient of interparticle friction. Because the theory was essentially a stress relationship for failure, the deformational restriction of plane strain was not able to be included without considerable difficulty. Trollope (1971) has demonstrated that some plane strain data followed the general trend predicted by Parkin's theory, and highlighted the theoretical relationship for intermediate principal stress under plane strain conditions:

$$\sigma_2 = \left(\frac{\sigma_1 + \sigma_3}{3}\right) \tag{4.5}$$

This equation was supported by data from tests in both loose and dense sand in which σ_3 had been decreased to failure. By assuming a value of $\mu = .4$ ($\phi_\mu = 21.8^0$) for interparticle friction, the author compared

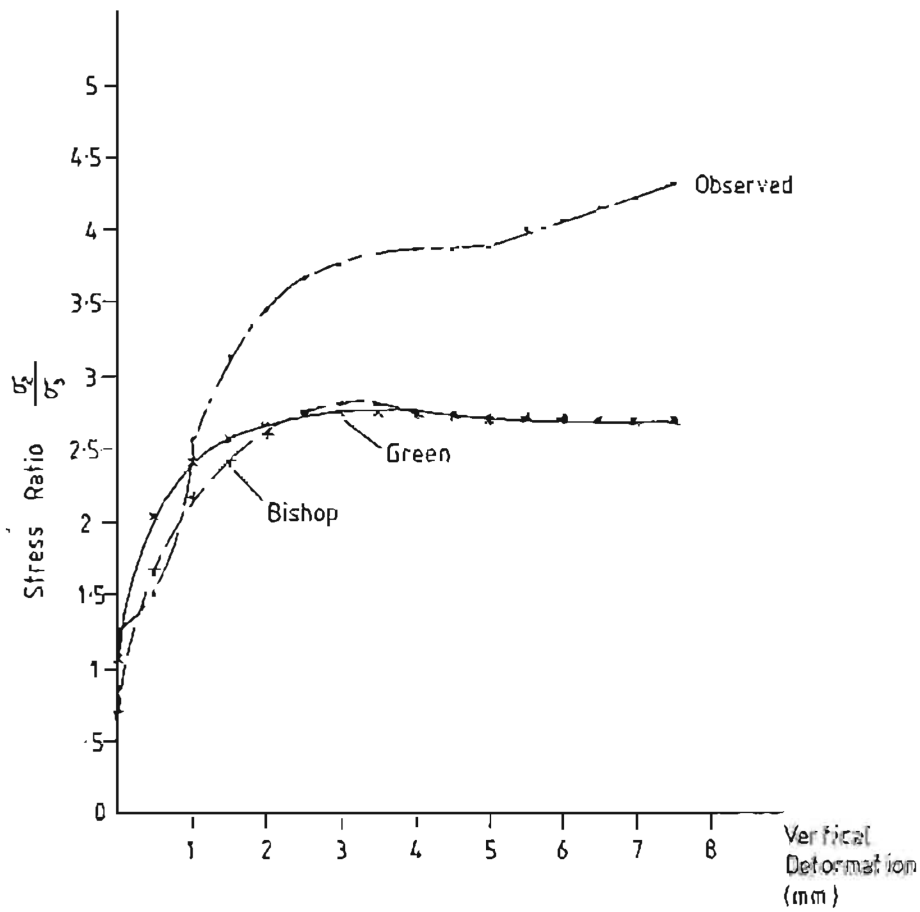

Figure 4.9a Prediction of Intermediate Principal Stress - Test 4A

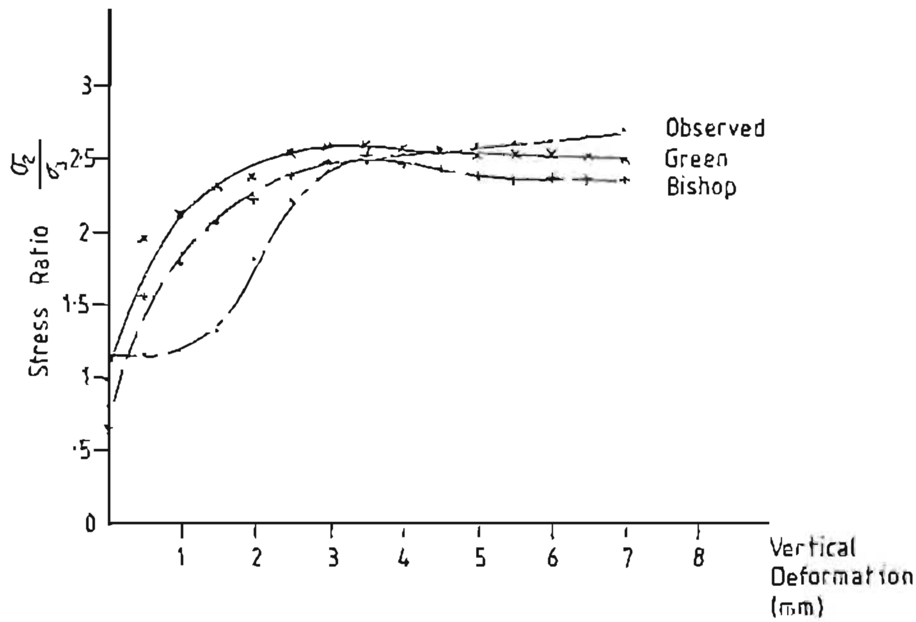

Figure 4.9b Prediction of Intermediate Principal Stress - Test 6B

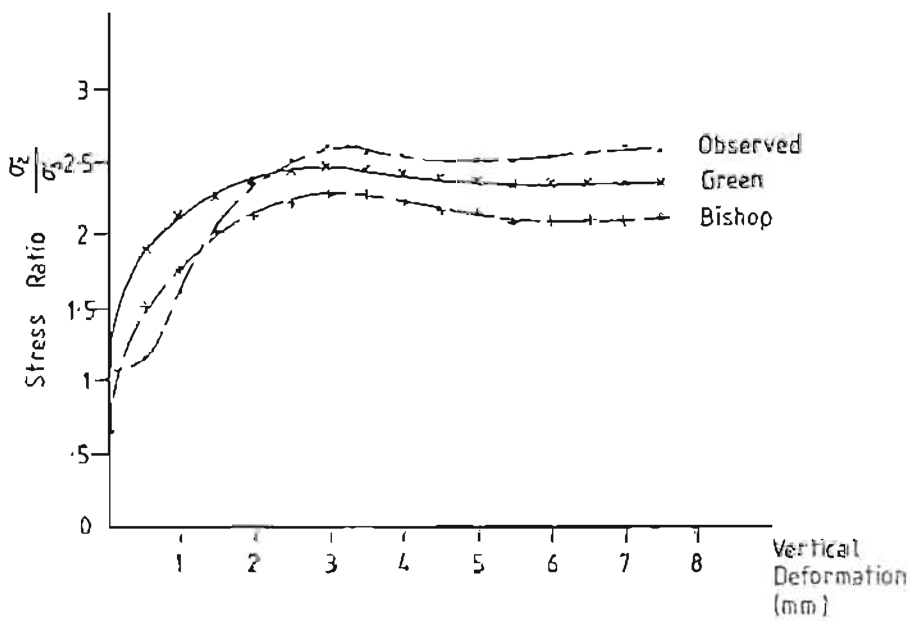

Figure 4.9c Prediction of Intermediate Principal Stress - Test 8C

the plane strain data from this study with Parkin's theoretical prediction of σ_2 from equation 4.5. The result is illustrated in Figure 4.10. It did not appear that the predicted stress relationship was any better than those discussed previously. The general form of Parkin's relationship was reflected in the test data, however, there appeared to be considerable difficulty in defining an appropriate value for the coefficient of interparticle friction, μ. Even if the theory had been able to accurately explain the failure characteristics of sand; in its present form the only information predicted about deformation was the angle between the principal axes of stress and strain. Roscoe (1970) has shown that the direction of the slip plane in model retaining wall tests was dependent on the direction of the major principal stress and the material's dilatancy. Although Parkin's theory agreed with the findings of the Cambridge research team, it did not yield any information on either the orientation of the slip plane or the expected dilatancy. If more understanding was gained about interparticle relationships in real soils, then the application of the approach used by Parkin would be likely to succeed because of its consideration of the clastic nature of granular materials.

(iii) Stress-Dilatancy Theories

King and Dickin (1970) reviewed two stress-dilatancy theories, the widely published theory of Rowe and a lesser known, but earlier, work by Newland and Allely. Although the two theories had the same background, the equations used in the development of the work by Newland and Allely involved an approximation which did not appear in Rowe's work. King and Dickin wrote that Rowe had pointed out this error as "a small approximation"; however, a review of the relevant equation revealed that the error was dependent on sample geometry, and could become considerable. Newland and Allely's equation was:

$$-\frac{dv}{de_1} = \frac{\tan\alpha - \tan(\alpha - \theta)}{\tan(\alpha - \theta)} \qquad (4.6);$$

but an exact analysis gave:

$$-\frac{dv}{de_1} = \frac{h}{h_1} \cdot \frac{\tan\alpha - \tan(\alpha - \theta)}{\tan(\alpha - \theta)} \qquad (4.7),$$

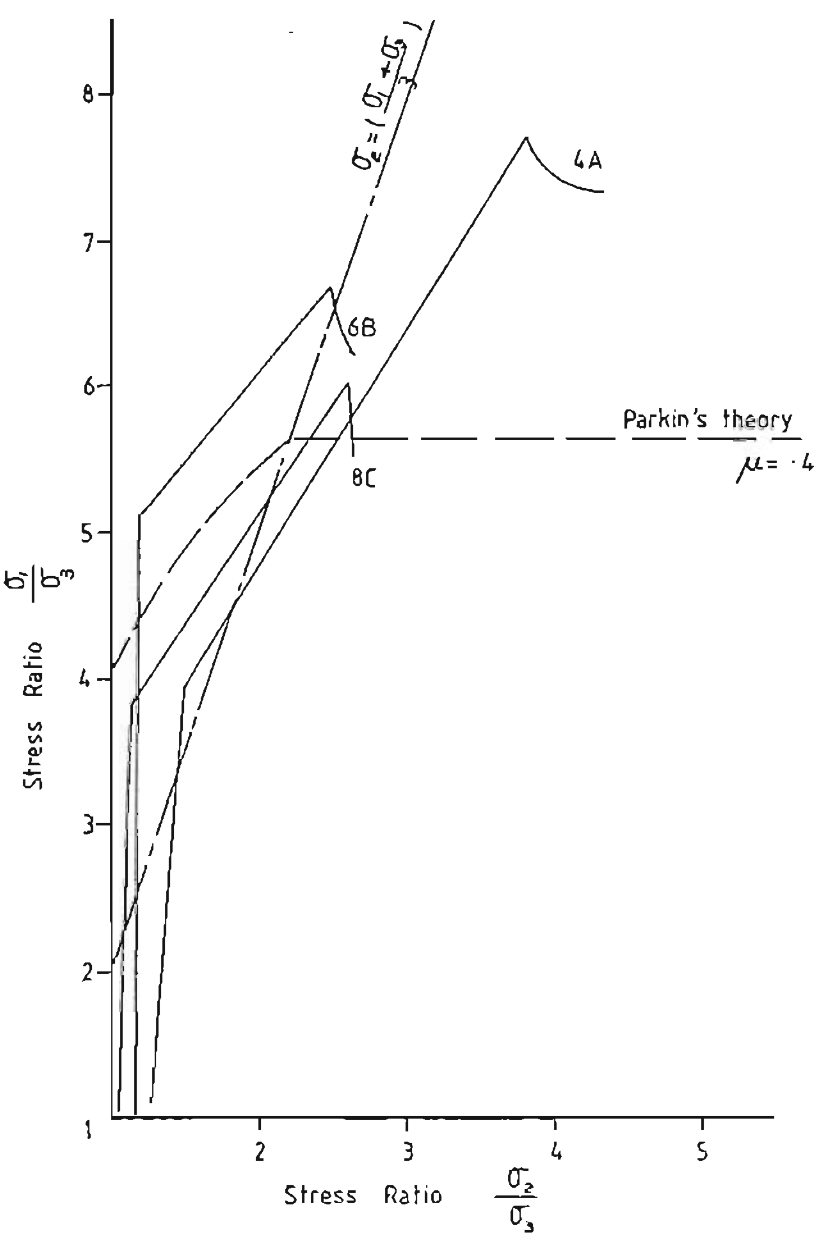

Figure 4.10 Parkin's Discrete Particle Slip Prediction

where h is the total height of a prismatic sample
and h_1 is the vertical component of length of the slip plane.

The small amount of extra calculation involved by using the exact equation did not appear to justify the approximation made, which could easily have resulted in a 10% error. Thus, the calculations presented in this section were based on the stress-dilatancy equation of Rowe (cf. King and Dickin (op. cit.)):

$$\frac{\sigma_1}{\sigma_3} = \left(1 - \frac{dv}{de_1}\right) \tan^2\left(45 + \frac{\phi_f}{2}\right) \qquad (4.8)$$

Figure 4.11 shows the plane strain data plotted with an estimate of the stress-dilatancy line for the critical void ratio state (i.e. shearing with zero rate of volume change), and lines from which an estimate of the value of ϕ_f was taken. The range of ϕ_f found was 39.6^0 to 41.8^0. The writers commented on the results of plane strain tests in two types of medium-dense sand for which they found that ϕ_f values approximately equalled ϕ_{cv} values. However, this was clearly not the case for the tests undertaken for this study. Further discussion of the predictions of the stress-dilatancy theory are included in the section dealing with predicted and observed slip angles.

(iv) Critical State Soil Mechanics

Schofield and Wroth (1968) have published a substantial work explaining the theory and applications of critical state soil mechanics. They have proposed the Granta Gravel model for granular materials, for which the fundamental equations are:

$$q = Mp \qquad (4.9),$$

and $$v = \Gamma - \lambda \ln p \qquad (4.10);$$

where p is spherical pressure
q is deviatoric stress
v is specific volume
λ, Γ are critical state constants.

Figure 4.12 shows that equation 4.9 was readily satisfied by the author's

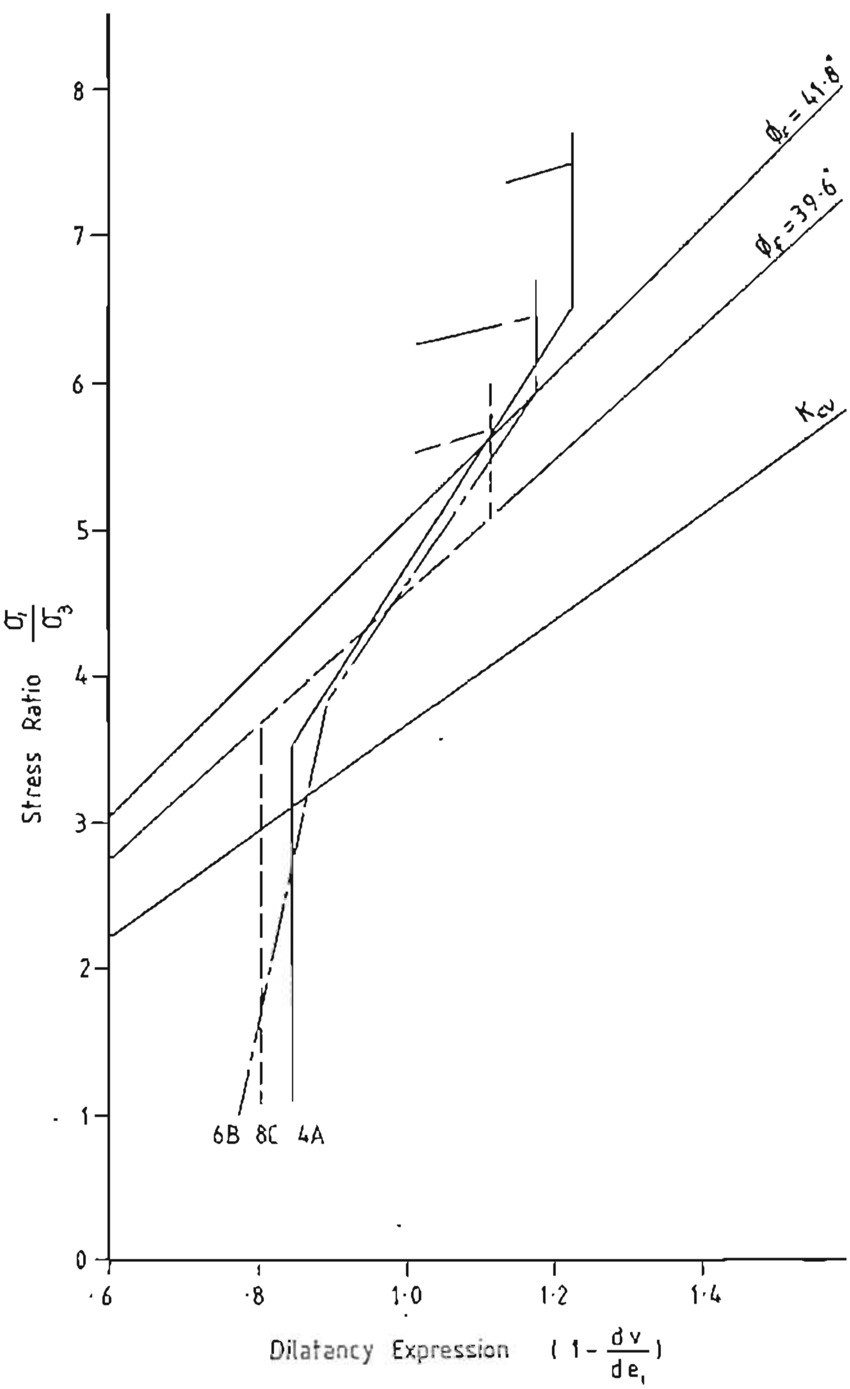

Figure 4.11 Stress-Dilatancy Comparison

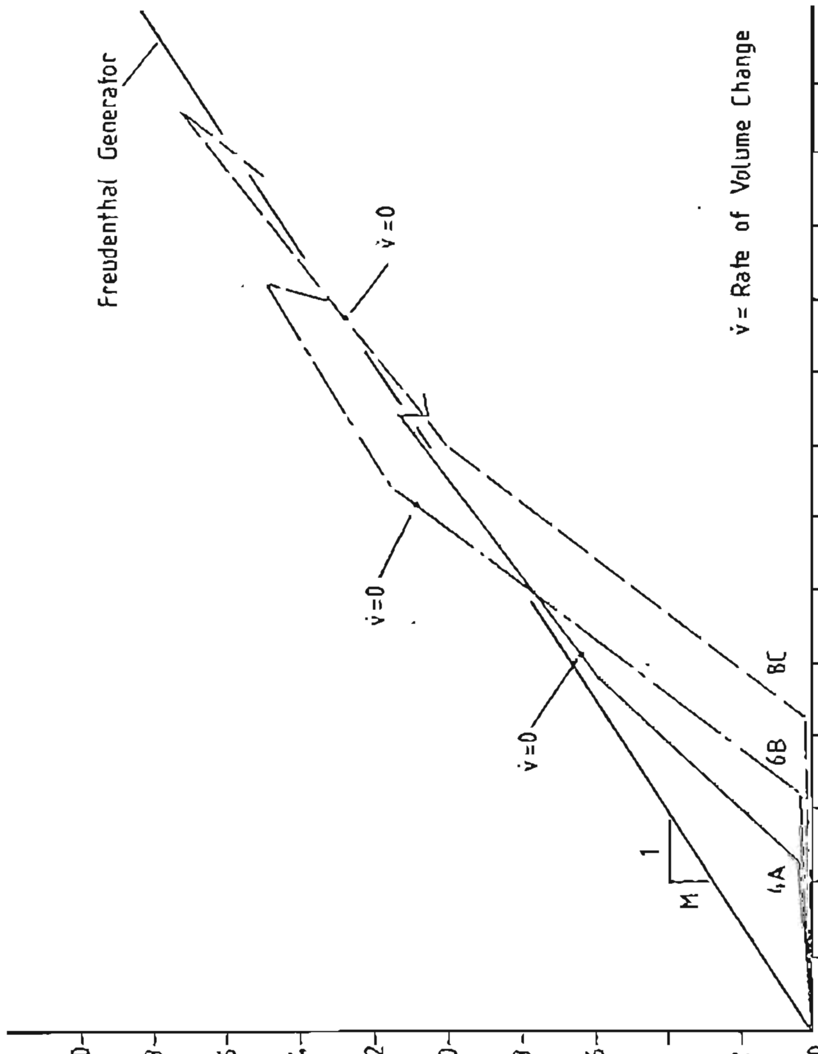

Figure 4.12 Octahedral Stress Plot

plane strain results; however, the results in Figure 4.13 did not satisfy the linearity of equation 4.10. Thus, the author drew the same conclusion as Zienkiewicz and Naylor (1971), that the Granta Gravel model was inadequate to describe the failure characteristics of granular materials. This was not meant to imply the basis of the approach was invalid, but that a new granular material model needed to be developed.

(v) Observed and Predicted Slip Angles

Because of the emphasis in this study on the kinematics of failure, the prediction of the orientation of slip planes was an important aspect of any proposed failure criterion or material model. In the author's plane strain tests, the angle of the slip plane to the horizontal was measured to fall in the range of 53^0 to 57^0. King and Dickin (op. cit.) reported tests in which the observed slip angles were 52^0, 54^0, and 60.5^0, although some doubt was cast on the reliability of the first two values due to frictional effects from the end plattens. Nevertheless, these values were well below the preferred angle of slip predicted by the stress-dilatancy theories of Rowe and Newland and Allely. The writers offered no explanation or criticism for the lapse of the theories in this respect.

Roscoe (1970) reported that the data from several model retaining wall tests led to the conclusion that the axes of stress and strain-rate were coincident, and that slip occurred along lines of zero-extension; i.e. the slip lines made angles of $(45^0 \pm {}^{\nu}/2)$ to the direction of the major principal stress (ν was the dilatant angle of the material). X-radiographic studies of sand in a simple shear apparatus showed that the value of dilatant angle estimated from boundary deformations significantly underestimated actual values of the angle measured in the slip zone. Values of the dilatant angle calculated from boundary deformations in the author's tests were in the range of 3.9^0 to 5.7^0. Roscoe (op. cit.) reported that for a dilatant angle of 4^0 in a sand sample, based on boundary deformations, the angle measured in the shear zone was 8^0; thus, in the author's plane strain tests, a slip angle of about 50^0 might be expected if slip occurred along a zero-extension line. Before further conclusions may be drawn about the applicability of zero-extension lines as slip lines in this study, more detailed

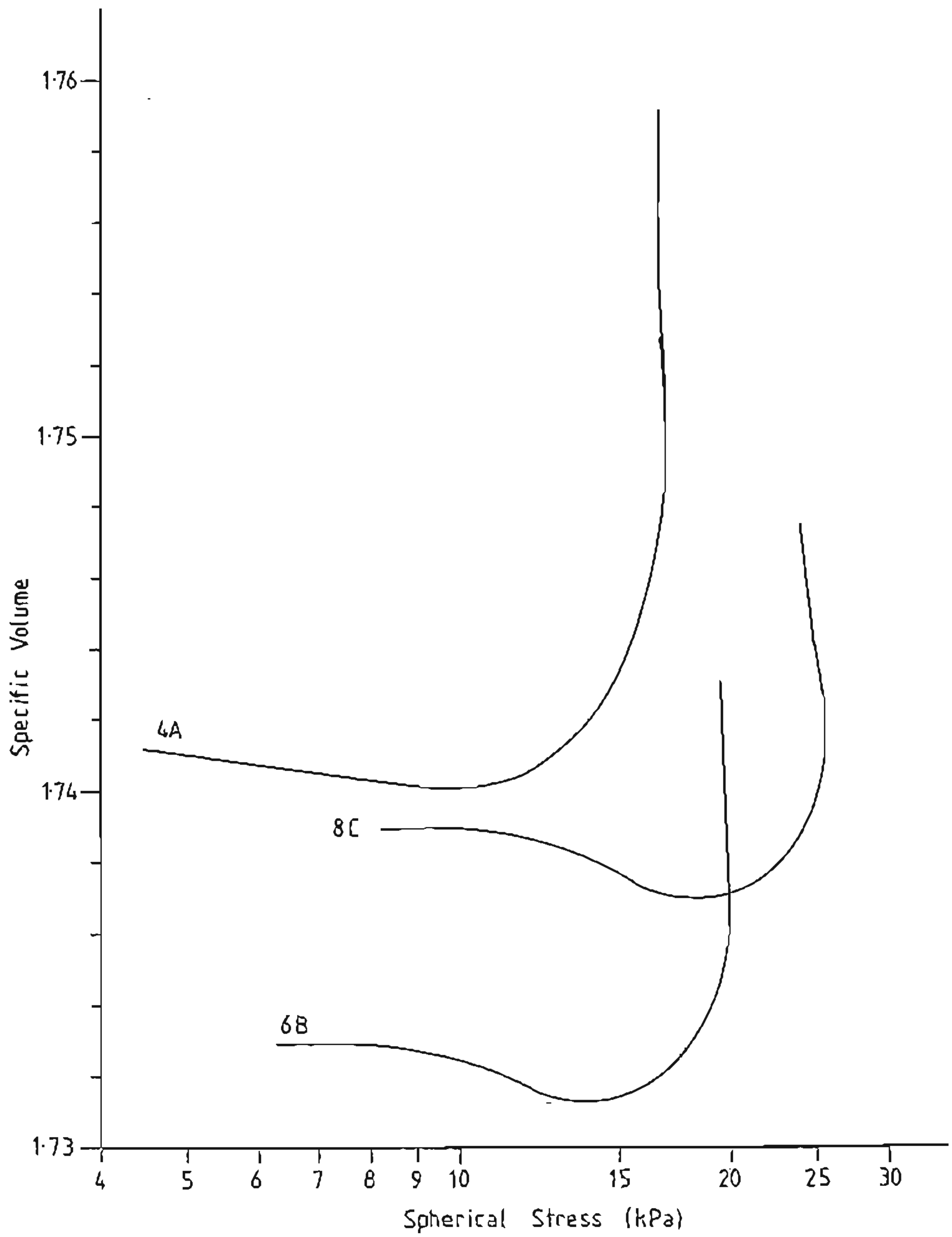

Figure 4.13 Critical State 'Granta Gravel' Model

plane strain testing of sand samples at low confining pressures would be required. Some further comment concerning the slip plane orientation is included in the following section.

4.2.7 Some further observations of the failure of sand in plane strain

Because the level of confining pressure used in this series of plane strain testing was much lower than usual working pressures, there was very little literature with which to compare the data. The previous section showed that none of the theories or models investigated adequately described the test data presented. Test details have been given in Section 4.2.4.

Figure 4.12 is an octahedral stress plot from which it may be seen that a possible yield surface for these tests was a cone in stress space; corresponding to the Freudenthal (or extended von Mises) criterion (cf. Trollope, 1978). Bishop (1971), using data from a true triaxial apparatus, showed that the Mohr-Coulomb failure criterion was the most suitable criterion over the full range of stress conditions from axisymmetric compression ($\sigma_2 = \sigma_3$) to axisymmetric extension ($\sigma_1 = \sigma_2$), having acknowledged that there exists a rise in strength between the two extremities, but that this is small. Bishop said that the range of stress values in which the Freudenthal (extended von Mises) criterion approximated the response of a soil was very limited; however, the combination of a deformational restriction in plane strain and the low confining pressures appeared to have broadened the area of application of this failure criterion to include the results presented for this study.

Although the stresses in plane strain were three-dimensional, the deformation was limited to two dimensions. Thus, to relate the yield function dimensionally to the deformation required a transformation from three dimensions to two, so that movement was restricted to the σ_1-σ_3 plane. Figure 4.14 shows a representation of a Freudenthal cone in stress space, with the point P defining the state of stress at failure in a plane strain sample. Let the projection of the cone generator OP onto the σ_1-σ_3 plane be OP', and define the angle between OP' and the direction of the major principal stress as β (see inset on Figure 4.14).

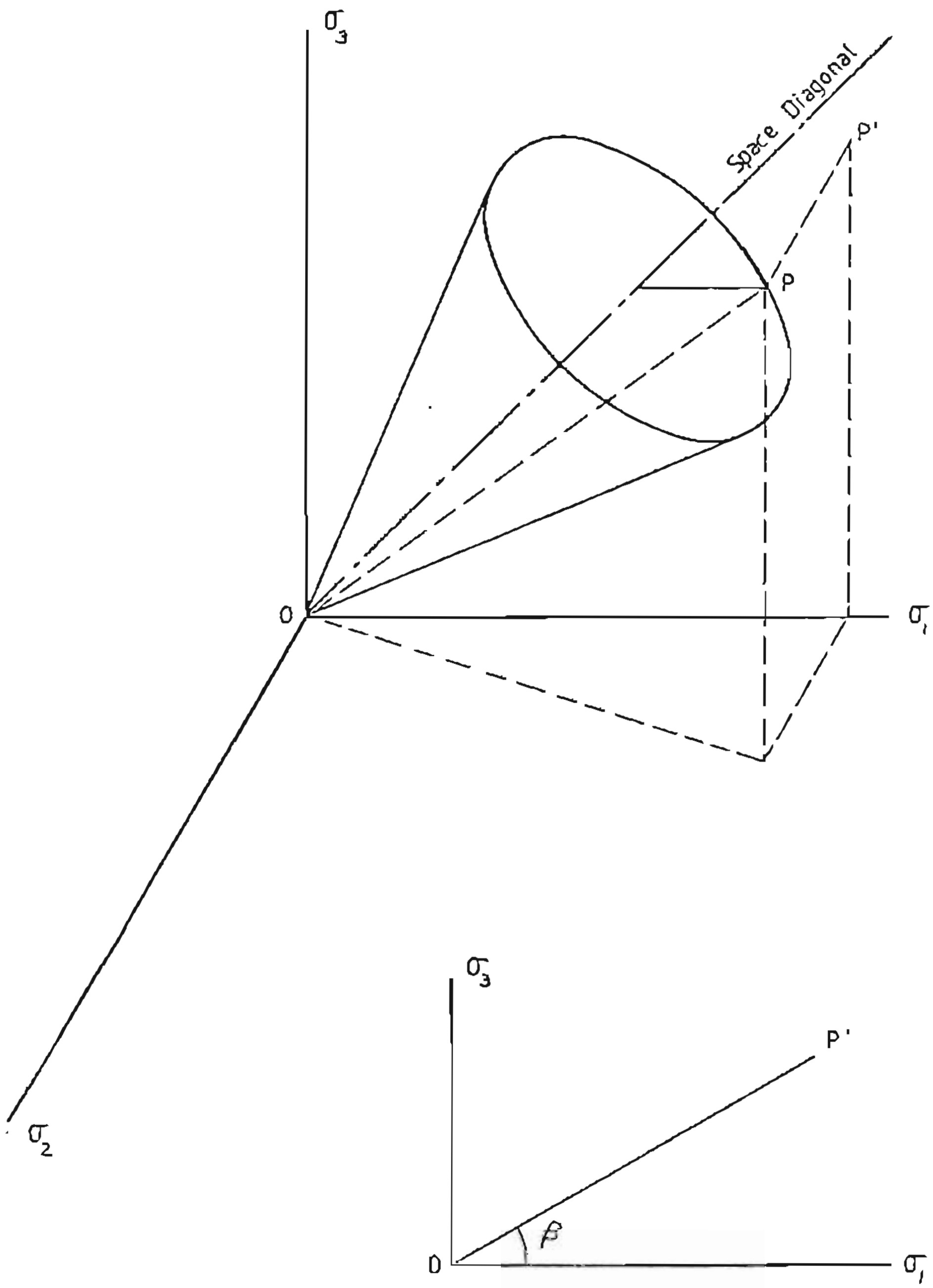

Inset: σ_1-σ_3 plane

Figure 4.14 Freudenthal Cone

Thus, the value of β may be calculated by simple analytical geometry, provided the point P is completely defined:

$$\beta = \arctan\left[\frac{2}{\frac{\sigma_{oct}}{\sigma_3}(1 + \sqrt{6}\tan\rho\cos\alpha) - 1}\right] \qquad (4.11)$$

where $\alpha = \arcsin\left(\frac{\sigma_{oct} - \sigma_3}{\sqrt{2}\,\sigma_{oct}\tan\rho}\right)$

and ρ is the dihedral angle between the space diagonal and the failure surface (i.e. the Freudenthal cone). Equation 4.11 is valid only for those points which lie on the failure surface.

Figure 4.15 gives the values of β calculated for data from plane strain tests 4A, 6B, and 8C, together with the volumetric changes from which the definition of failure was derived in Section 4.2.4. The range of β at residual strength conditions was 16^0 to 21^0. Hence, if normality conditions and coincidence of stress and strain rate were assumed, the expected range of slip plane angle, $(45 + {}^{\beta}/2)$, was 53^0 to 55.5^0, which corresponded closely to the observed range of 53^0 to 57^0. The assumption of normality conditions implied that the sample should also have a dilatant angle equal to β. In the previous discussion of slip angles, the measurements of local dilatant angle reported by Roscoe (op. cit.) gave values which were much higher than those calculated from boundary deformations. Therefore, the verification of predictions of the slip angle by both Roscoe's zero extension line and the author's proposal were dependent on the results of more accurate plane strain testing of samples at low pressures because of the significance of the localised value of dilatant angle in the shear zone.

4.2.8 Summary

The behaviour of loose sand at low confining pressures in plane strain was similar to that of a medium-dense sand at usual confining pressures. Thus, to adequately describe the stress-deformation characteristics of a granular material used in a small scale laboratory model, both similar stress levels and boundary restraints must be used when the sample is tested.

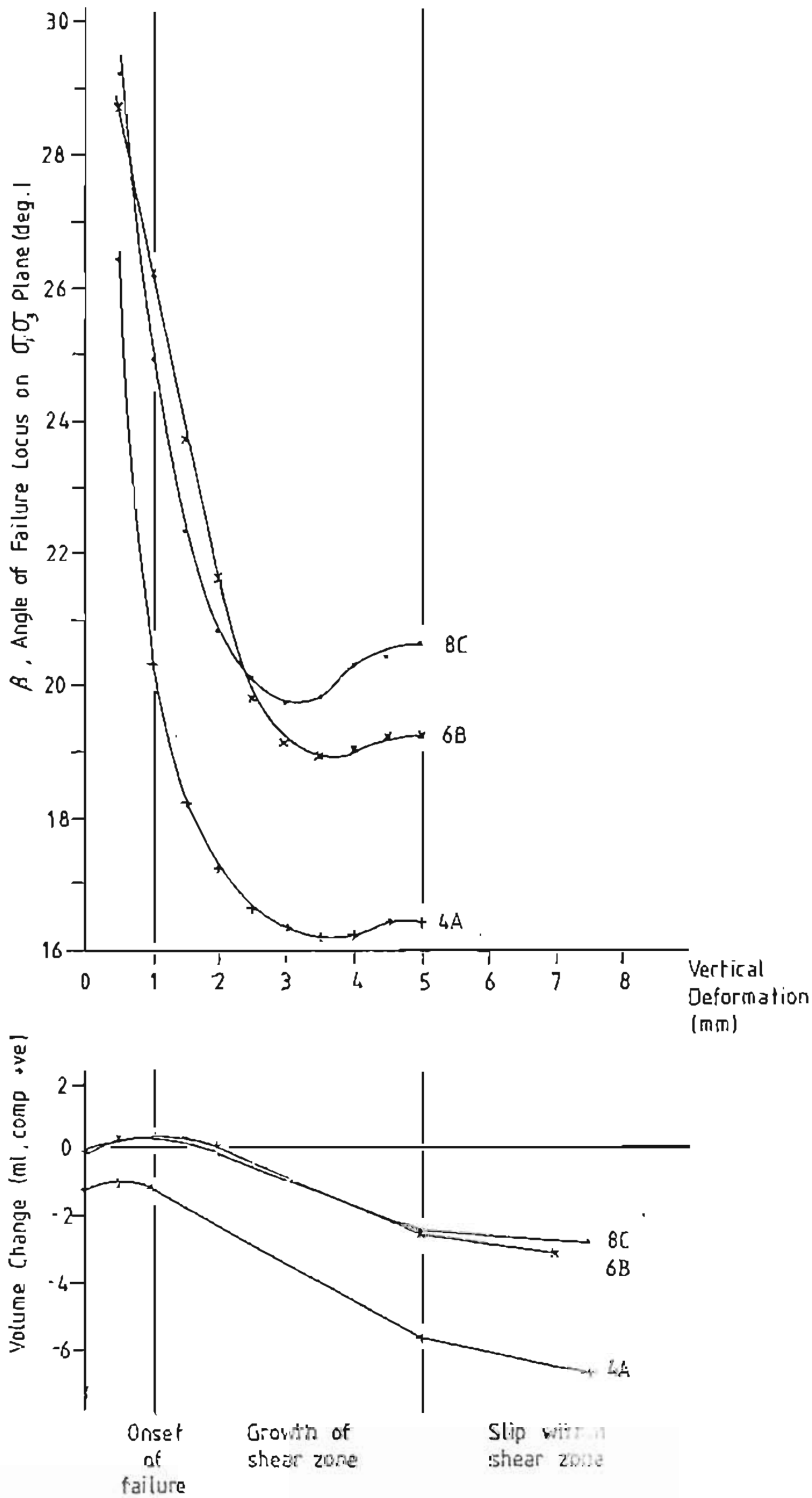

Figure 4.15 Variation of β with Axial Deformation

The data from the plane strain tests conducted by the author were interpreted as conforming to the Freudenthal (extended von Mises) criterion, however, the deformational aspects of the failure were more important to this study. The kinematics of failure were divided into three sections:

(i) an initial compression accompanied by an axial deformation of 1 mm;

(ii) the onset of failure when the rate of volume change becomes zero, followed by growth of the shear zone at constant dilatancy up to an axial deformation of 5 mm;

(iii) cessation of growth of the shear zone with further slip taking place within the zone at practically zero dilation.

Therefore, the observation of slip planes was expected in the laboratory model after vertical deformations in the order of 5 mm had occurred. The deformation characteristics of the loose model slope were likely to predict those of a medium-dense slope of the same material at the prototype scale (e.g. a slope 8 m high).

4.3 Tests on Bentonite

4.3.1 Flow properties of bentonite suspensions

Jones (1963) presented a concise description of many important properties of bentonite, from its mineralogical composition through to its flow properties when combined with chemical additives used in grouting practice. The range for the liquid limit of bentonite was quoted as 350 to 500%; therefore, the bentonite used for the foundation of the model slope was well into the liquid phase with its moisture content at 900% (i.e. a clay concentration of 11%). Jones (op. cit.) illustrated that the flow properties of bentonite suspensions with clay concentrations in the range of 1 to 15% exhibited anomalous characteristics, which matched the flow properties of a Bingham body. The description of bentonite suspensions as Bingham bodies was also given by Marsland and Loudon (1963); however, Robertson and Stiff (1976) preferred the Power Law model (or a similar law proposed by the writers). Skelland (1967) gave a review of many analytical models, as well as laboratory procedures and equations for the determination of flow properties. Another important property of bentonite suspensions was their thixotropy: i.e. their increase of yield strength with time. It was also noted that this process was fully reversible.

Therefore, the basic flow properties of bentonite were considered to be those illustrated in Figure 4.16. The Bingham body was defined by two parameters: τ_y, the yield stress, and η, the apparent viscosity; and the shear strength, τ, was calculated using:

$$\tau = \tau_y + \eta\dot{\gamma} \qquad (4.12).$$

The Power Law model used the same two parameters, and a third, $\frac{1}{m}$ (an index) to give:

$$\tau = \tau_y + \eta(\dot{\gamma})^{\frac{1}{m}} \qquad (4.13),$$

where $\dot{\gamma}$ in the previous two equations is the rate of shear.

4.3.2 Tests on bentonite suspensions

The bentonite mixture used for the base layer differed fundamentally from a soil in that it consisted of a suspension of clay particles in a water matrix, rather than being a soil particle matrix with water in the voids. Thus, it was not surprising to find that standard soil testing apparatus (e.g. direct shear box, laboratory vane) were inadequate for the determination of the suspension's shear characteristics. Skelland (op. cit.) recommended an extrusion rheometer for the task, and Figure 4.17 gives a schematic diagram of the apparatus used. The equations used for the determination of the flow properties and their method of interpretation were taken from Skelland (op. cit. pp. 28 to 39) and were not repeated in this text.

The bentonite used in the model was purchased on two occasions, and it was found that the properties of the product differed greatly

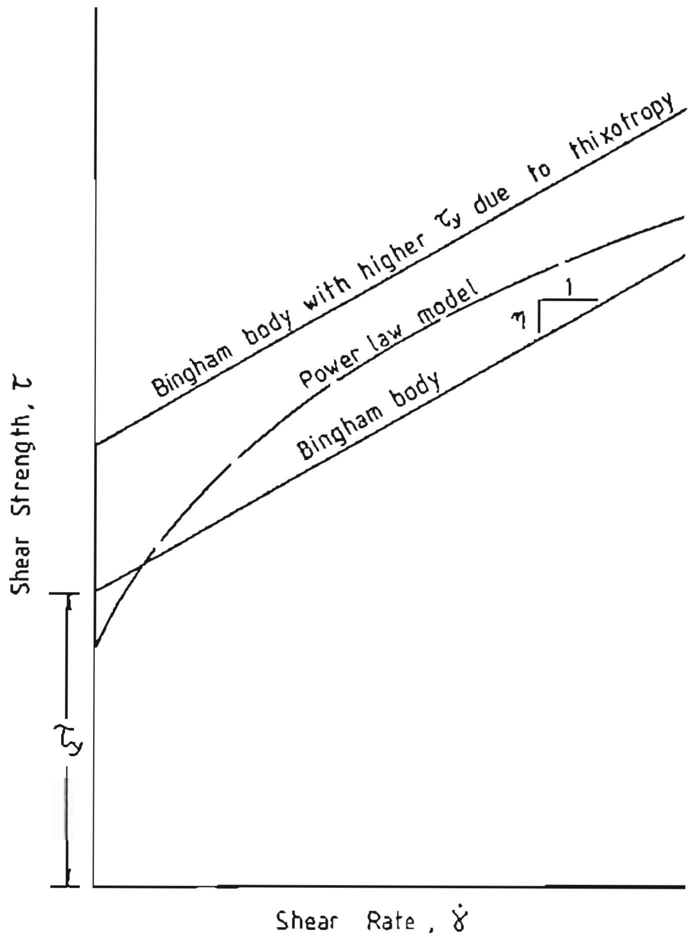

Figure 4.16 Flow Properties of Bentonite

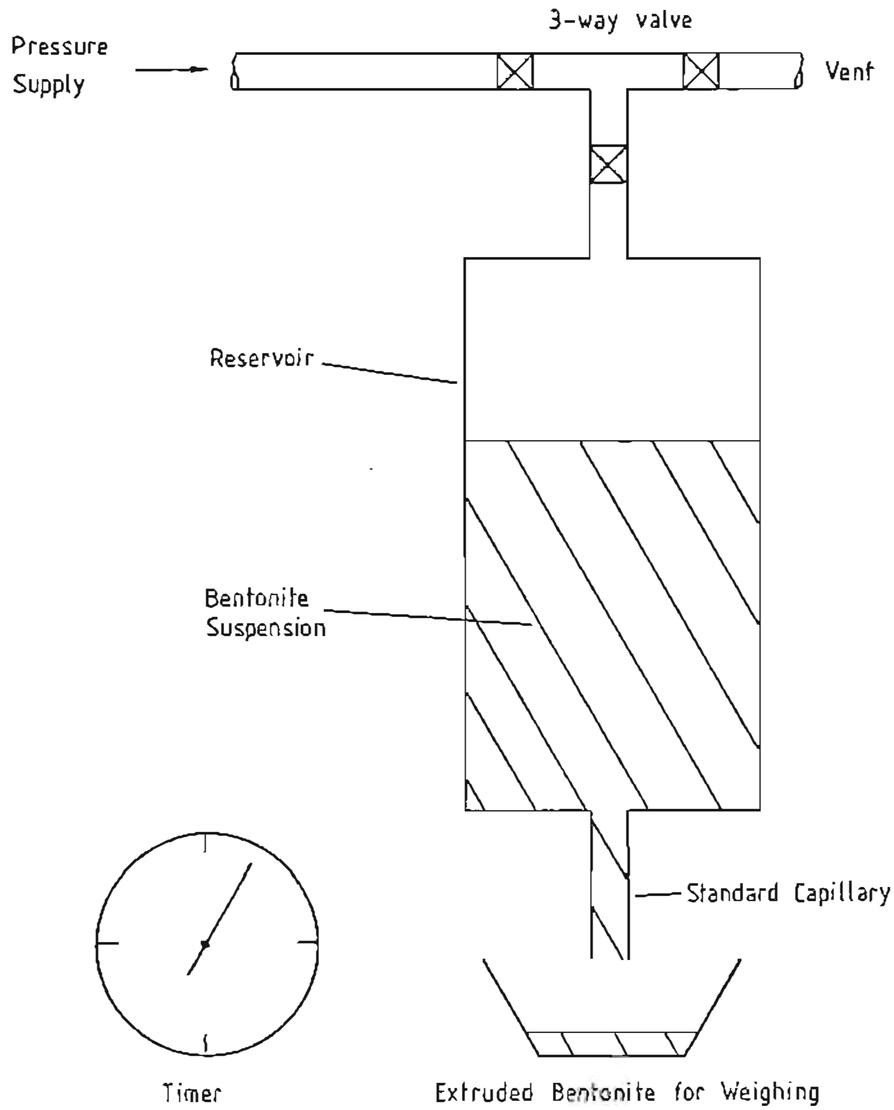

Figure 4.17 Schematic View of Extrusion Rheometer

between the two batches, even though the product name and supplier had not changed. The first batch, consisting of two 25 kg bags, gave a suspension which could be described as a Bingham body; however, the second batch, again of two 25 kg bags, gave a suspension which matched the Power Law model, but had approximately the same yield stress as exhibited by the first batch. Figure 4.18 gives the results for tests on the first batch of bentonite, where the yield stress was found to be about .7 kPa and the apparent viscosity was .043 Pℓ. Figure 4.19(a) shows the results for the second batch when it was assumed to be a Bingham body, and Figure 4.19 (b) shows the results when plotted for the Power Law model. The yield stress for the second batch was approximately .7 kPa, the apparent viscosity .42 Pℓ, and the index, $\frac{1}{m}$, equalled .117. The determination of the thixotropy was not possible, but Jones (op. cit.) gave an example of the effect of thixotropy in an 8% clay concentration of "Fulbent 570" bentonite, in which there was about a 10% increase in yield strength during the period from 1 to 2 hours after mixing stopped, and a further 10% increase during the period from 2 to 4 hours. Therefore, assuming that the behaviour of bentonite products does not differ very radically, it would be expected that a 10 to 20% variation of yield strength in the base layer may have occurred in the laboratory model tests.

4.3.3 Summary

The bentonite suspension was identified as a non-Newtonian fluid which had a yield strength and a shear strength which increased with the shear rate. It was also established that the bentonite was thixotropic; a condition which was fully reversible. An estimate of the yield strength gave a value which was small compared with the shear strength of the sand material (this was one of the modelling requirements); however, the reliability of this value could not be determined because the laboratory tests were inadequate.

4.4 Conclusions

Although the materials used for the modelling study were basic minerals, their behaviour under the stress and deformational conditions imposed on them by the testing techniques showed that the characteristics of their response should not be taken for granted.

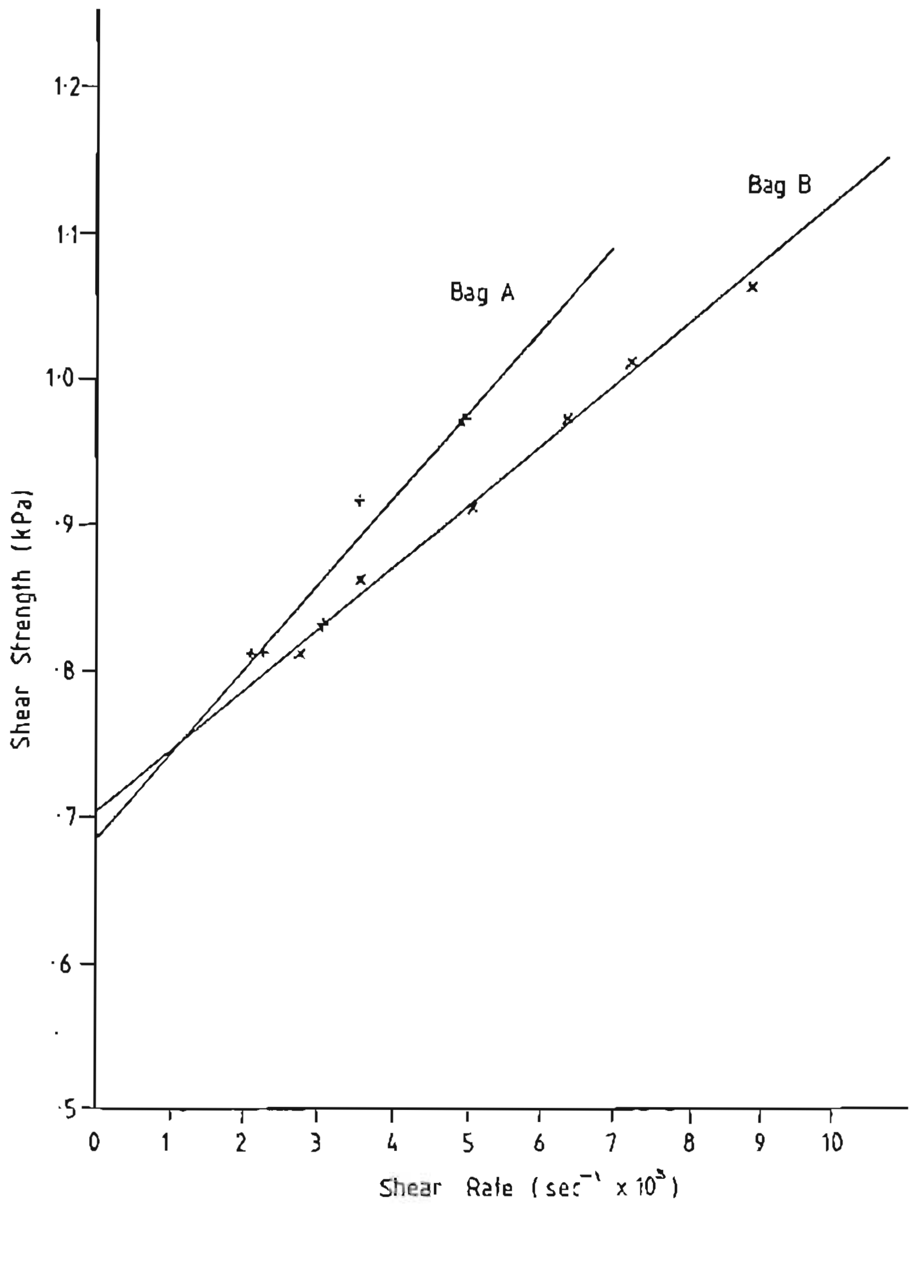

Figure 4.18 Flow Properties of Batch 1 Bentonite

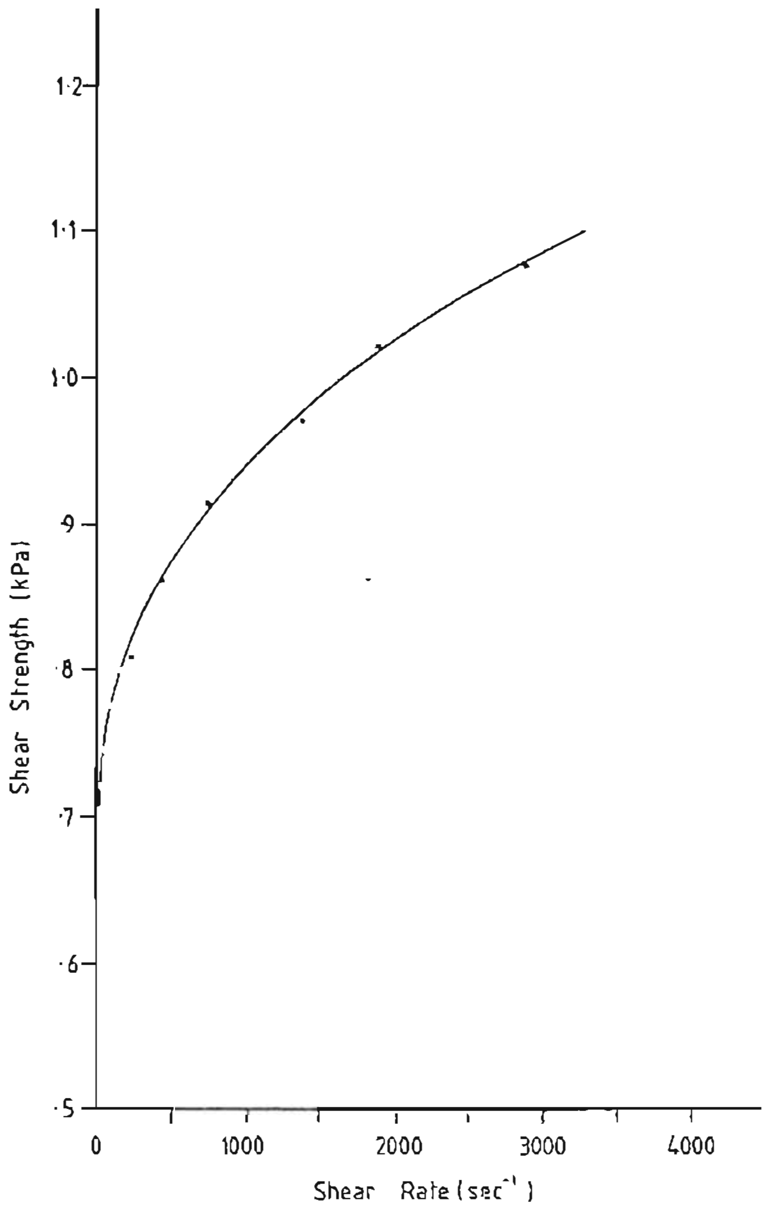

Figure 4.19a Flow Properties of Batch 2 Bentonite - Bingham Body Model

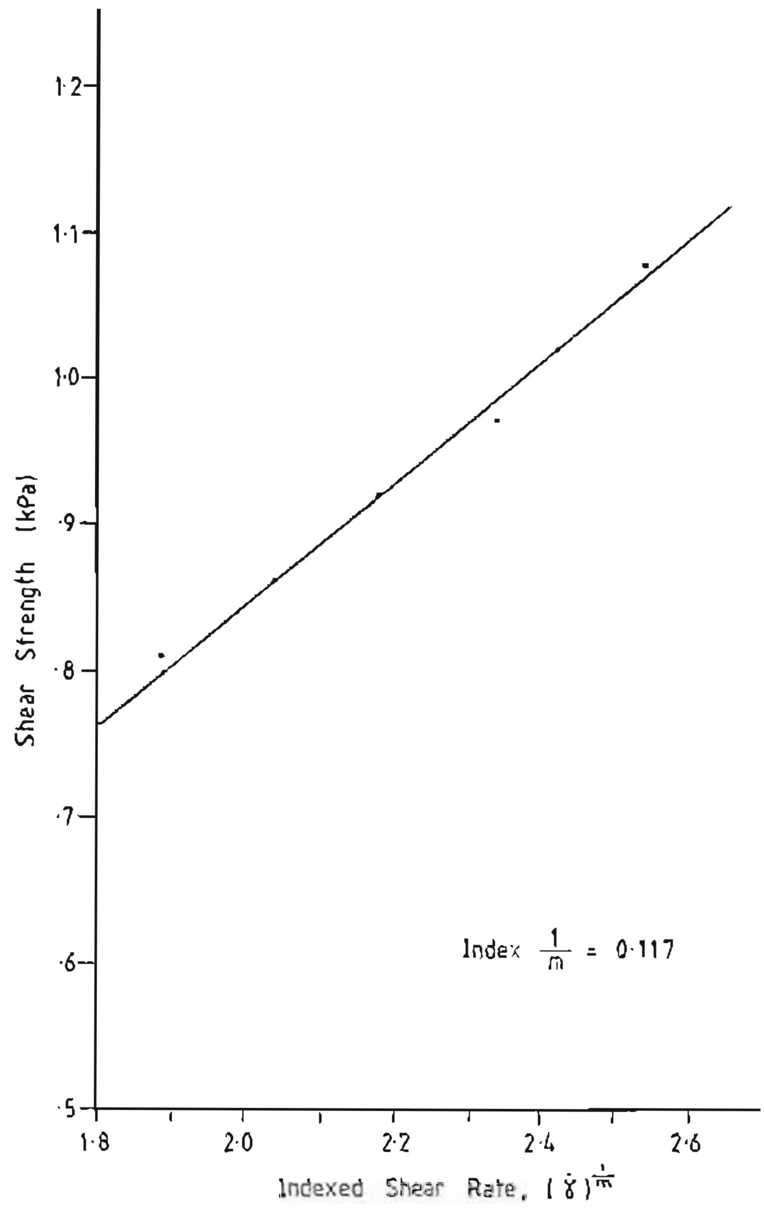

Figure 4.19b Flow Properties of Batch 2 Bentonite - Power Law Model

The plane strain and direct shear testing of the silica sand provided a simple deformational criterion to describe the failure of the sand; a summary of which is given in Section 4.2.8. The strength of the sand was best described by a Mohr-Coulomb diagram in which the failure condition was governed by the angle of the slip plane rather than by the angle of maximum obliquity. The assumption that failure occurred at stresses defined by the latter angle led to greater material shear strengths than could be mobilised, and hence would lead to an overestimate in any subsequent stability calculations. The flow characteristics of the bentonite showed that the material satisfied the requirement of being significantly weaker than the slope material, although an increase in shear strength would be observed if the rate of shear in the bentonite became high which would require a review of the conditions.

Therefore, for sand and bentonite the strength properties were dependent in some way on the deformation or rate of deformation of the model. The response of the sand emphasised its discontinuous nature, especially with the important role played by the dilatant properties. Because the dilatancy is closely linked to the granular structures, or systones, within the sand mass, the deformation of a larger sand mass may be the same as that of a smaller mass provided that the pattern of systones and the ambient stress levels are approximately the same. Thus, the author proposes that the deformational failure criterion, defined from the plane strain results, will also apply to the model slope.

The author's application of the Freudenthal failure criterion and subsequent prediction of the slip angle in plane strain is not supported by sufficient evidence to be reliably used in any stability analysis. Therefore, the matter is left as a topic for future detailed research.

CHAPTER 5

RESULTS FROM PHYSICAL MODELLING

5.1 Introduction

The previous two chapters described the modelling method and the materials used, therefore, only the details for particular tests are included in this chapter. All experiments, except one, had the same sand slope geometry: a crest height of 400 mm, the face of the slope inclined at the angle of repose (approximately 34^0), and a total base length of about 1100 mm. The bentonite layer was horizontal and four different thicknesses were investigated: 5, 10, 20, and 30 mm. At least two tests were conducted at each thickness to ensure repeatability of the results. The test which differed significantly from the others was one in which no stiffening mechanism was used in the base. A rectangular prism of sand was built up in the sample enclosure, which had been modified by the addition of a retaining wall at the open end, so that a 20 mm layer of bentonite was uniformly covered by 300 mm of sand. The sand was excavated from one end by using an air-lift device so that a sand slope resting close to its angle of repose was formed. Further details of the results are given later in this chapter.

Table 5.1 summarises the details of the testing programme carried out. Several preliminary experiments were run in late 1976 and 1977, however, a reliable experimental technique and suitable targets to indicate movement were not developed until early 1978. The results of the early tests proved to be valuable indicators of the results observed in the ensuing testing programme. One of the most significant features of the early tests was the development of flow slides which travelled about 2 m (5 times the height of the slope). Inspection of individual frames of the movie film records of the flow slides showed that the initial failure mechanism was the two-wedge type, with characteristics resembling those found in the slope failures from the testing programme. The occurrence of flow slides was probably due to the very low yield strength of the bentonite used in the preliminary tests. The bentonite was from a different source than that used in the testing programme, and the author believes that its flow properties were significantly

TABLE 5.1

Testing Programme

Test	Date	Bentonite Thickness (mm)	Bentonite Batch	Camera and Speed
25-05-A	04AP78	5	1	16 mm Bolex (movie) 25 frames/sec.
25-05-B	11AP78	5	1	ditto
25-10-A	18AP78	10	1	ditto
25-10-B	02MY78	10	1	ditto
25-20-A	16MY78	20	1	ditto
25-20-B	23MY78	20	1	ditto
25-30-A	30MY78	30	1	ditto
25-30-B	06JN78	30	1	ditto
05-20-A	14FB79	20	1	Nikon Data-back 5 frames/sec.
05-20-B	21MR79	20	1	ditto
05-20-C	24MR79	20	2	Olympus OM2 Variable Speed
05-20-D	25MR79	20	2	ditto
EX20*	09MR79	20	2	Olumpus OM1 Variable Speed

* Test EX20 was the experiment where the slope was made by excavating part of a rectangular prism of sand.

different from those of Batches 1 and 2 reported in Chapter 4. Plate 4 shows an example of one of the flow slides in the apparatus: part (a) is the initial development of the two-wedge mechanism, and part (b) gives the final slope profile.

The central purpose of this study was to determine the sequence of failure of a granular slope, and this is the content of the following section. Other sections discuss observed slip planes, weak layer deformation, and conclusions.

5.2 Observation of the Failure Sequence

5.2.1 Preliminary tests

Test numbers 25-05-A through to 25-30-B (inclusive) were used to study the qualitative aspects of the failure mechanism of the granular slope, as well as to identify any variations in failure caused by the change in the thickness of the bentonite layer. The camera and target configuration used for those tests precluded any accurate measurement of the displacements and volume changes during failure. However, the observations made from these tests enabled the next four tests, 05-20-A to 05-20-D, to be planned so that the measurements could be made to an accuracy which would allow quantitative description.

5.2.2 Description of a model slope failure

The most suitable photographic record of a slope failure was taken in test 05-20-D. The record consisted of 30 single frames taken at varying time intervals during a total run time of about 3½ minutes. The data was collected by measuring the 35 mm negatives in a Zeiss Stecometer (cf. Section 3.4). A subsequent computer analysis gave values of total and incremental displacement, and total and incremental volume change. The displacements were for each target and volumes pertained to triangular prisms whose sections were formed by adjacent targets. The values of volume change were expressed as a percentage of the original volume of the particular prism, with a positive result indicating compression. The time interval between each record was calculated from the number displayed by a frequency integrator which

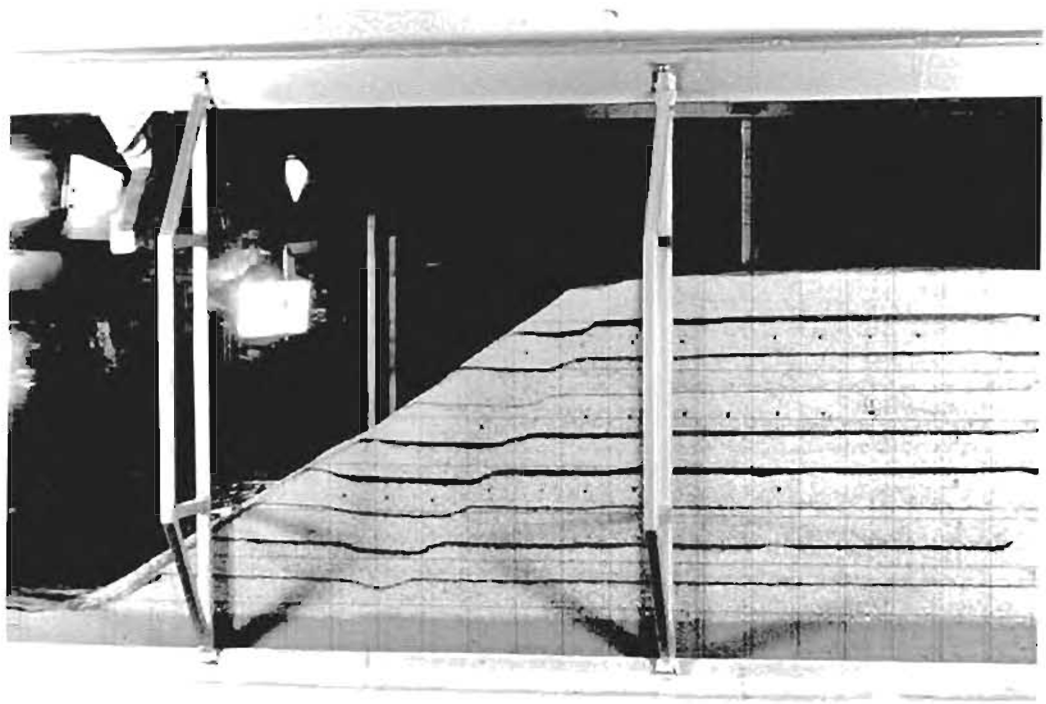

Plate 4a Development of Two-wedge Mechanism

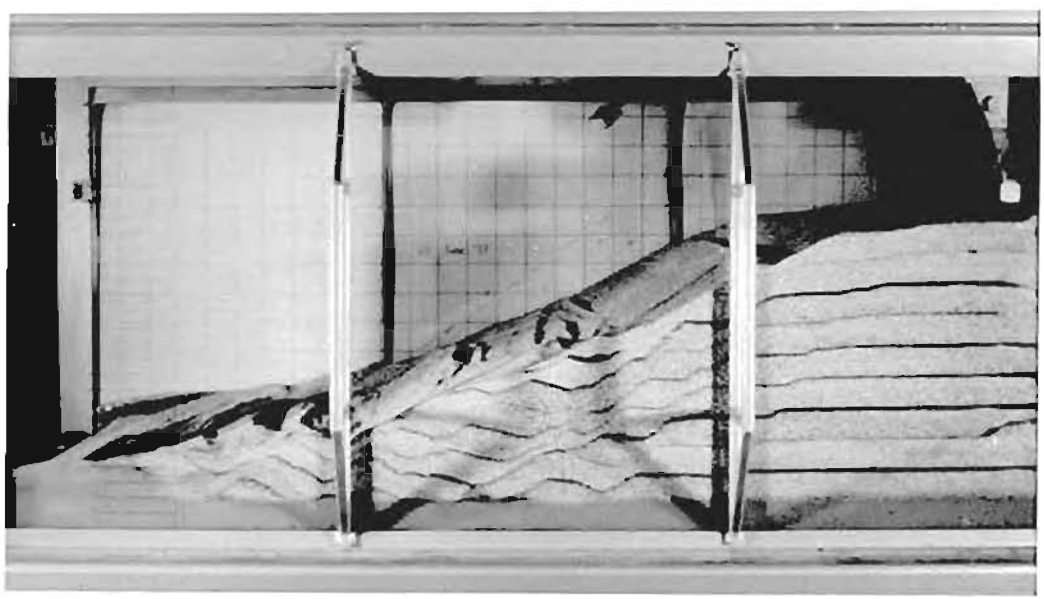

Plate 4b Slope Profile after Flow Slide

was excited by a signal of 50 Hz (main's supply frequency). The initiation of failure, by retraction of vanes and mesh, was indicated by the opening of a circuit which supplied current to a small torch bulb visible in the photographs. The time of initiation was determined to within ±.1 second, and time intervals between successive frames to within ±.01 second, with the error being the same for all frames, and not cumulative.

A statistical analysis was carried out to determine the reliability of the measurements made from this record, and the details of the analysis are presented in Section 5.2.3. It was found that the 95% confidence interval for the magnitude of displacements was ±.4 mm with the corresponding value for volume change being ±2%. The variation in the quality of the target image altered the values calculated for the 95% confidence interval; however, the values quoted above represent the variation for three-quarters of all targets.

It would be difficult to appreciate the data collected for this test if all the information was presented in either tabulated or graphic form, therefore, a selection of seven records from the total is presented as an adequate substitute for the whole. The author has closely examined all the records and has chosen the seven so that no significant events were excluded from the description of the experiment. Figures 5.1 to 5.7 (inclusive) give the details of total displacement and total percentage volume change, in parts (a) and (b) respectively; and remarks about each of the figures are given below.

Figure 5.1: Elapsed time 1.5 seconds

(a) Displacements of up to 10 mm were observed a very short time after the initiation of failure. The slope was divided into three major regions in accordance with the type of displacement exhibited: the first was the toe region which had shown predominantly horizontal movement; the second was the crest region where movement was greater than 5 mm and at an inclination of about 45^0; and the third region was the body of the slope which showed some movement, decreasing in magnitude away from the free surfaces. The boundary between the toe and crest regions was not distinct, but was marked by a broad transition zone.

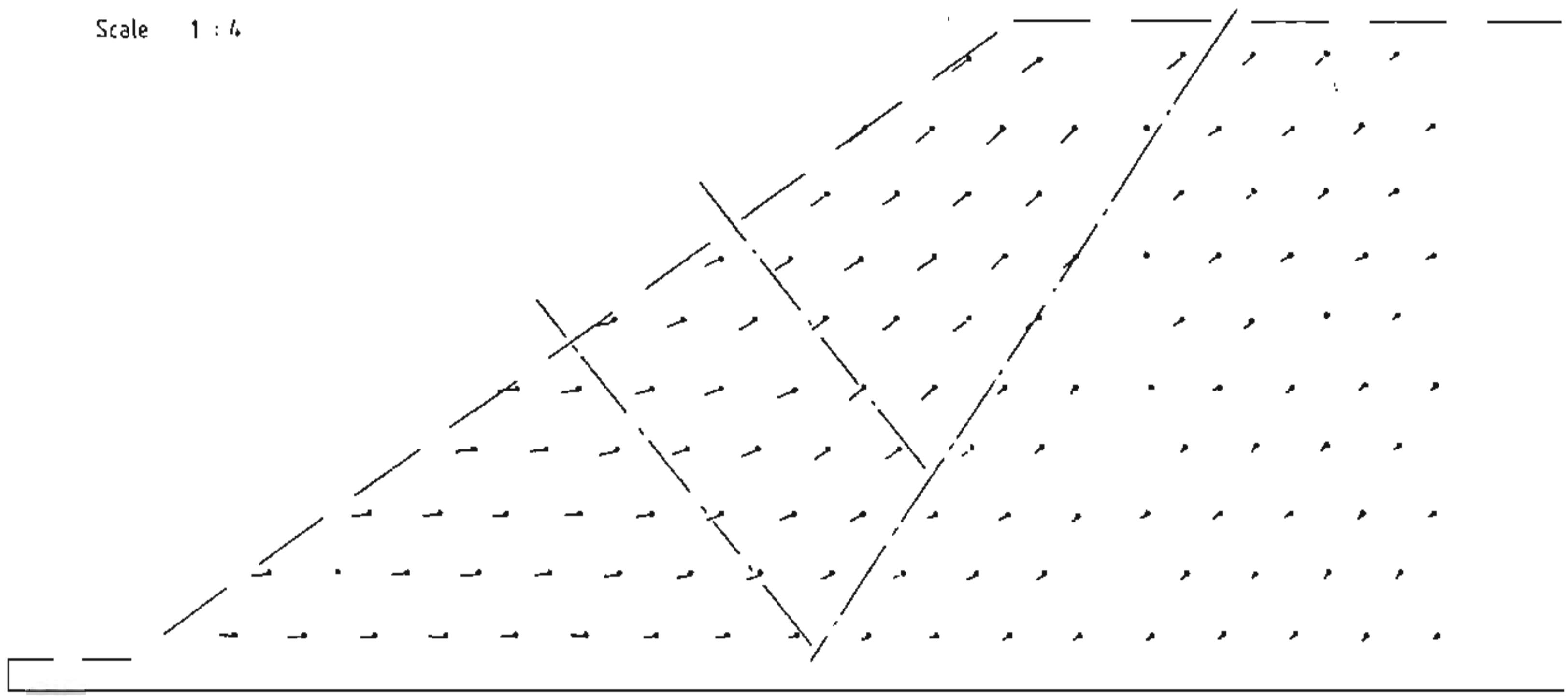

Figure 5.1a Displacements: Test 05-20-D; Elapsed Time 1.5 secs

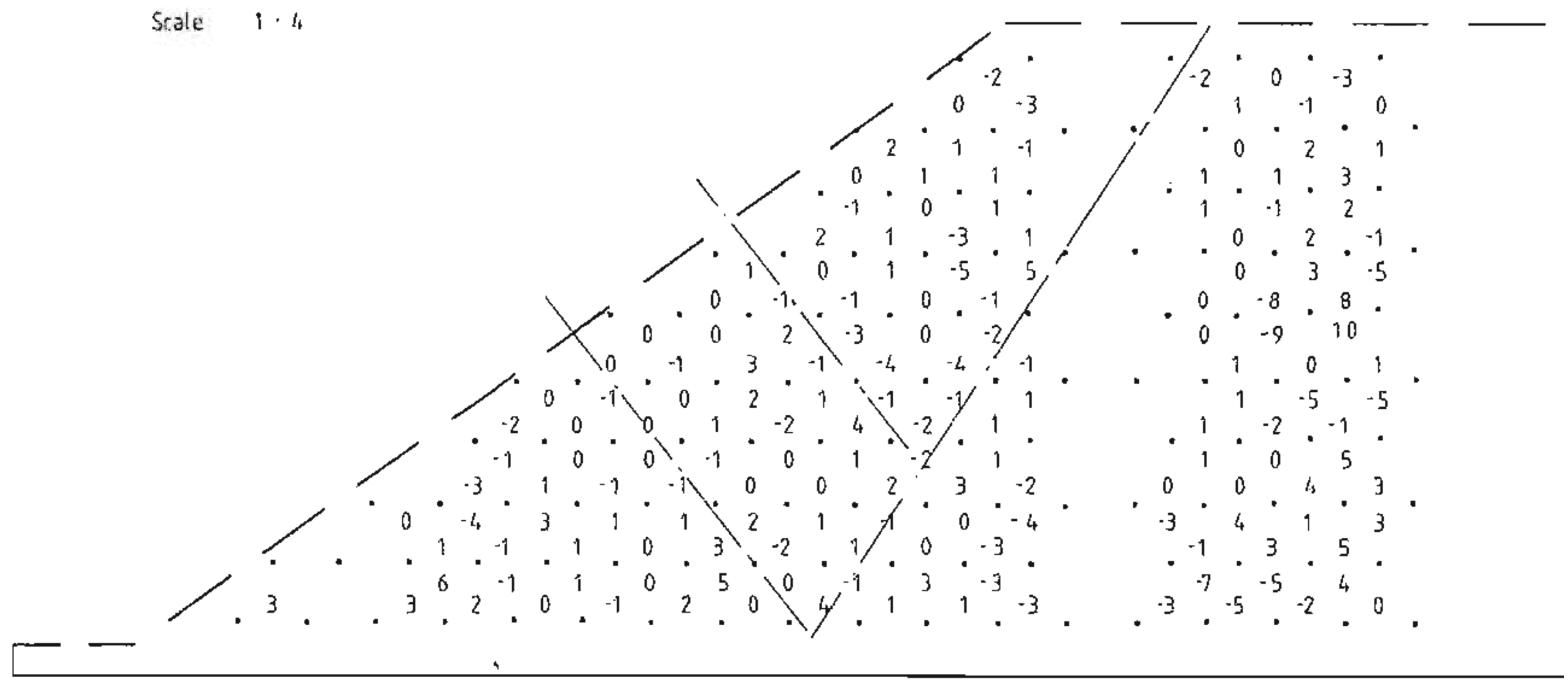

Figure 5.1b Volume Change (%): Test 05-20-D;
Elapsed Time 1.5 secs

The change in inclination of the displacement vectors from the toe to the crest gave the impression that it might have been possible to approximate the regional boundaries by a circular arc; however, the construction of normals to the displacement directions did not show any significant common point of intersection which would have defined the centre of curvature. The magnitudes of the movements within the toe and crest regions were reasonably uniform; thus, the first indications were that the kinematics were described by block movements, if the toe-crest transition zone did not develop any further, and preferably diminished.

(b) The volume changes showed some large magnitudes in the body of the slope, however, the cause of these was unreliable readings of some target positions, which affected all adjacent triangular units in the volume change calculations. The only significant trend found in the figure was the grouping of the larger magnitudes of volume change along the boundary between the crest region and the body of the slope. The variation in the volume change for a 95% confidence interval restricted the usefulness of part (b) of each of the figures until the magnitudes of these changes became large. The volume change indicated was for the prism bounded by the three targets, and not for the original sand mass contained within that prism; thus, the percentage volume change shown cannot be directly related to the dilatancy of the sand material. The sensitivity of volume change as an indicator of movement depended greatly on the orientation of the triangle with respect to the direction of movement; hence, part (b) of Figures 5.1 to 5.7 should be considered in conjunction with part (a) of the relevant figures so that the significance of results may be appreciated.

Figure 5.2: Elapsed time 37.4 seconds.

(a) There was very little displacement change during the interval, which indicated that the initial movements occurred as a result of the retraction of the mesh and vanes. Further comment is made on this matter later in the text. An indicator was drawn on each displacement vector so that the change after the initial movement could be seen. The little additional movement which had occurred to this time reinforced the regional classifications in the slope, however, the changes were too small to indicate if any alteration had occurred in the toe-crest

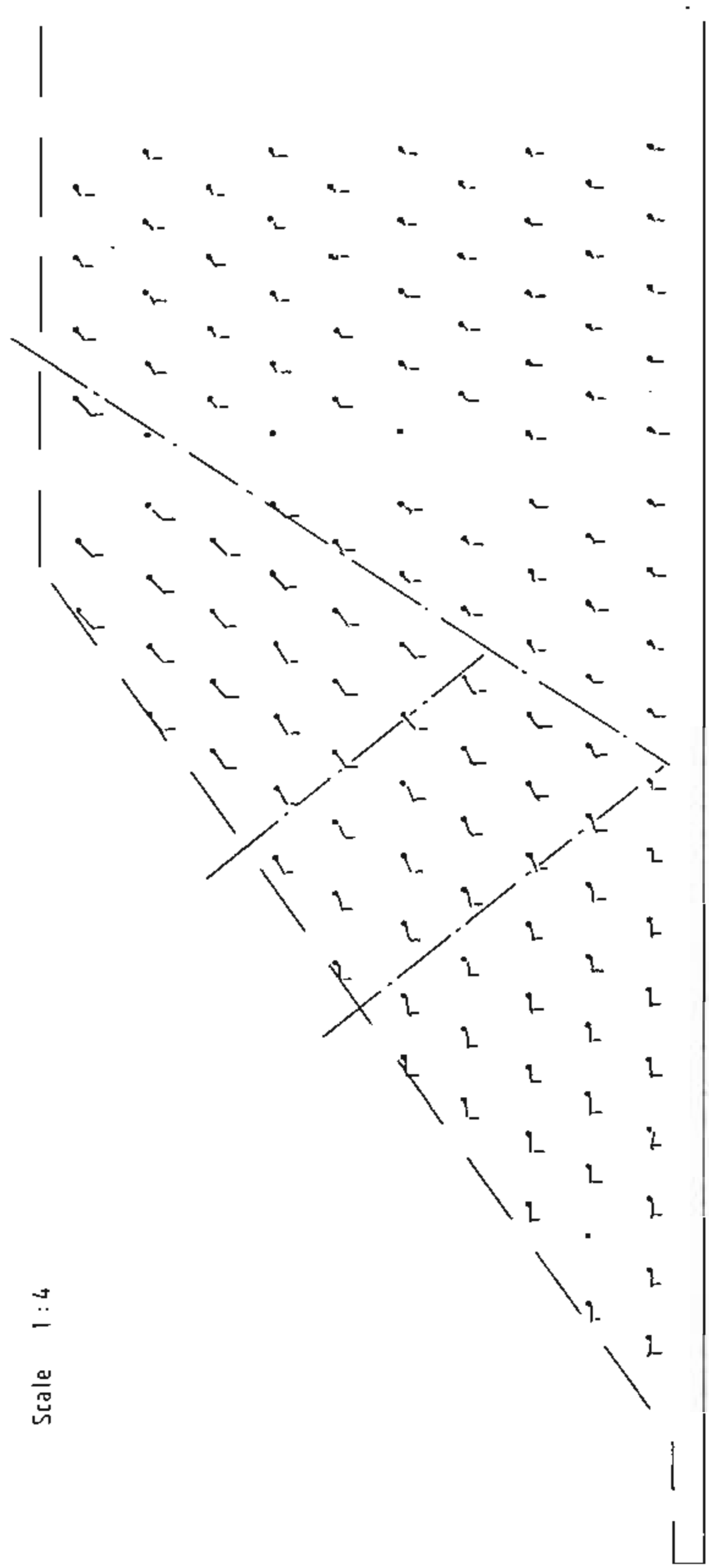

Figure 5.2a Displacements: Test 05-20-D;
Elapsed Time 37.4 secs

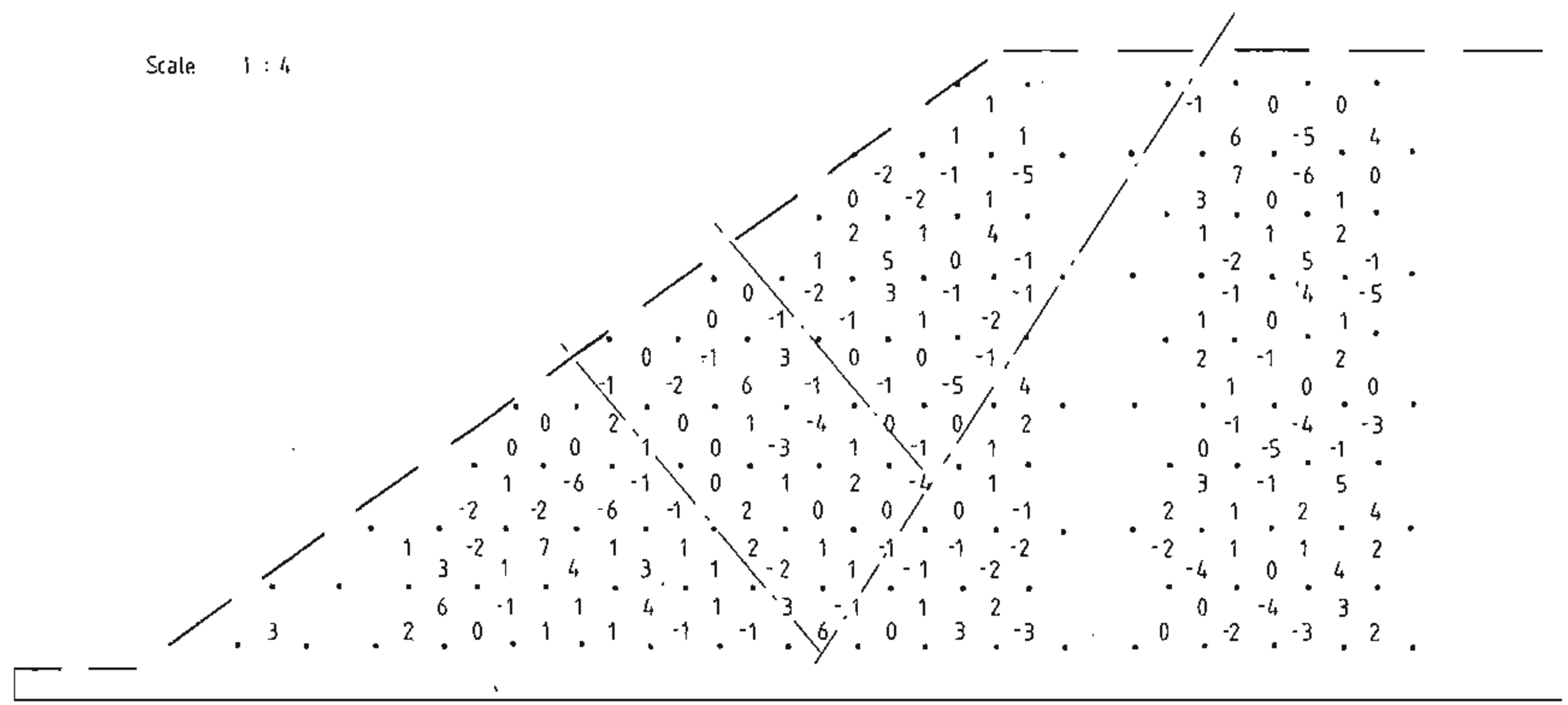

Figure 5.2b Volume Change (%): Test 05-20-D;
Elapsed Time 37.4 secs

transition zone.

(b) The volume changes showed that the transition zone was approximately the same as it was in the previous figure. Some significant changes were noticed in a couple of isolated sections, and reference back to the displacement plot showed that the target reading had deviated from the trend of the adjacent points, which suggested that the larger values were unreliable. Therefore, the kinematics were still favourably described by block movements.

Figure 5.3: Elapsed time 76.5 seconds.

(a) The magnitude of change in displacements compared with Figure 5.1(a) was large enough to establish that a two-wedge mechanism would result when further displacements occurred. The transition zone between toe and crest regions appeared to have reduced in area to be close to the boundary between the two regions. The body of the slope appeared stationary.

(b) The main changes from the previous figure occurred along the regional boundaries. Along the interface between the crest region and the body of the slope, a large amount of compression continued to occur at the base layer and values towards the top of the slope became more consistent. The magnitudes of these values were about 4%, which showed that the slip was uniform along the interface. The toe-crest boundary showed the first significant signs of formation of a slip line and the transition zone did not undergo any further significant change. Thus, the suggestion that the kinematics of failure could be described as a block movement gained quantitative support.

Figure 5.4: Elapsed time 116.8 seconds.

(a) The dominance of the two-wedge failure mechanism was shown by the trends of movement in the toe and crest regions. There were some isolated deviations in movement from the trend, however, they were probably due to an error in target location or some irregularity which caused the target to diverge from the pattern of sand grain movement.

(b) The major changes in the volume plot were seen along the boundary

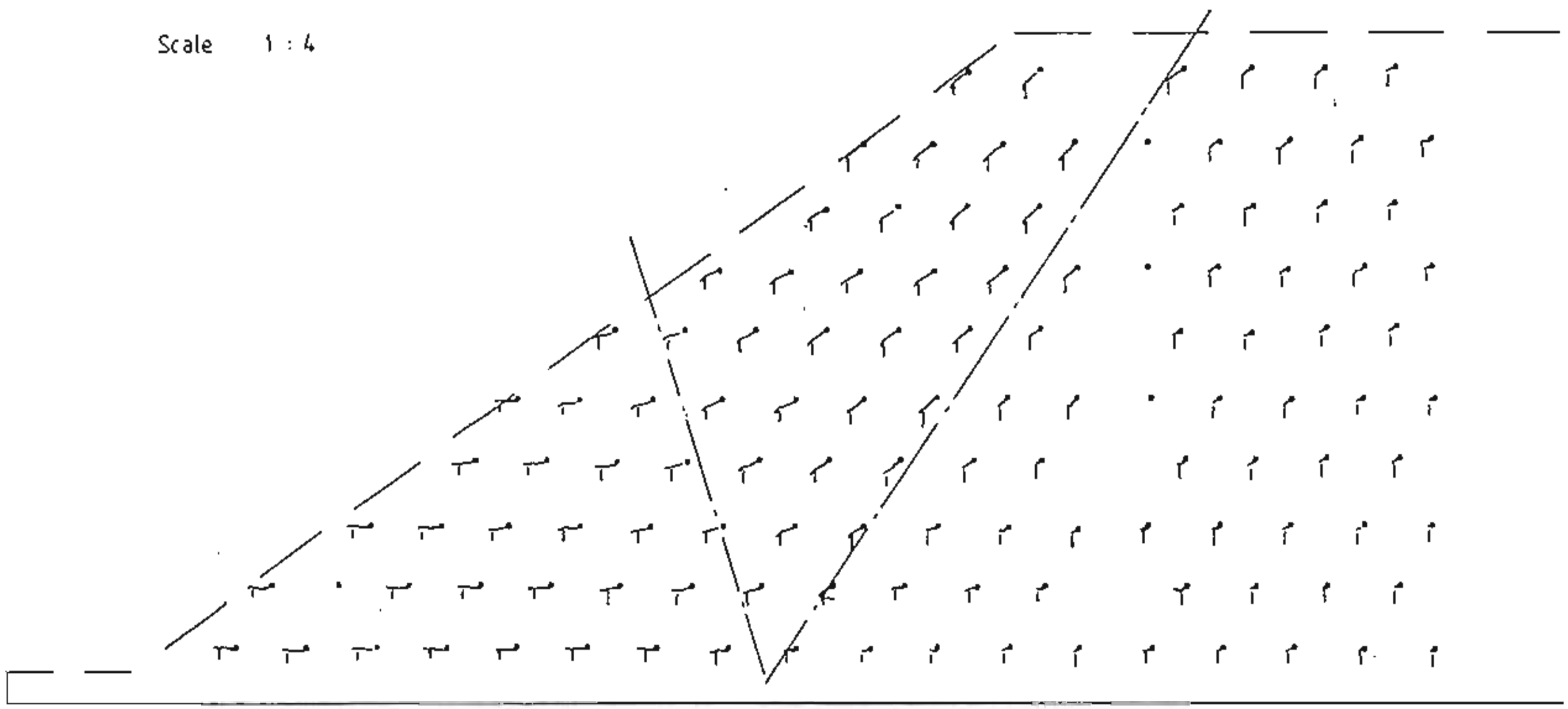

Figure 5.3a Displacements: Test 05-20-D;
Elapsed Time 76.5 secs

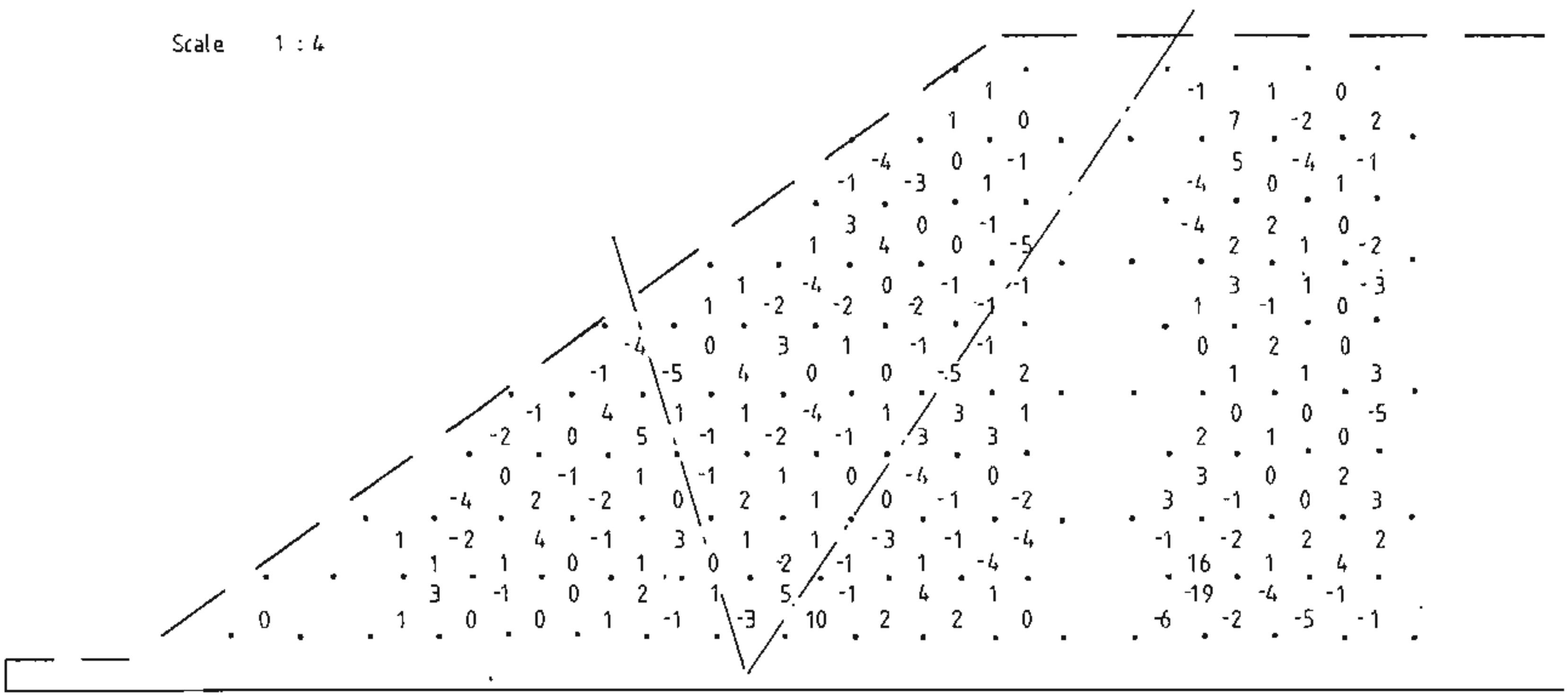

Figure 5.3b Volume Change (%): Test 05-20-D; Elapsed Time 76.5 secs

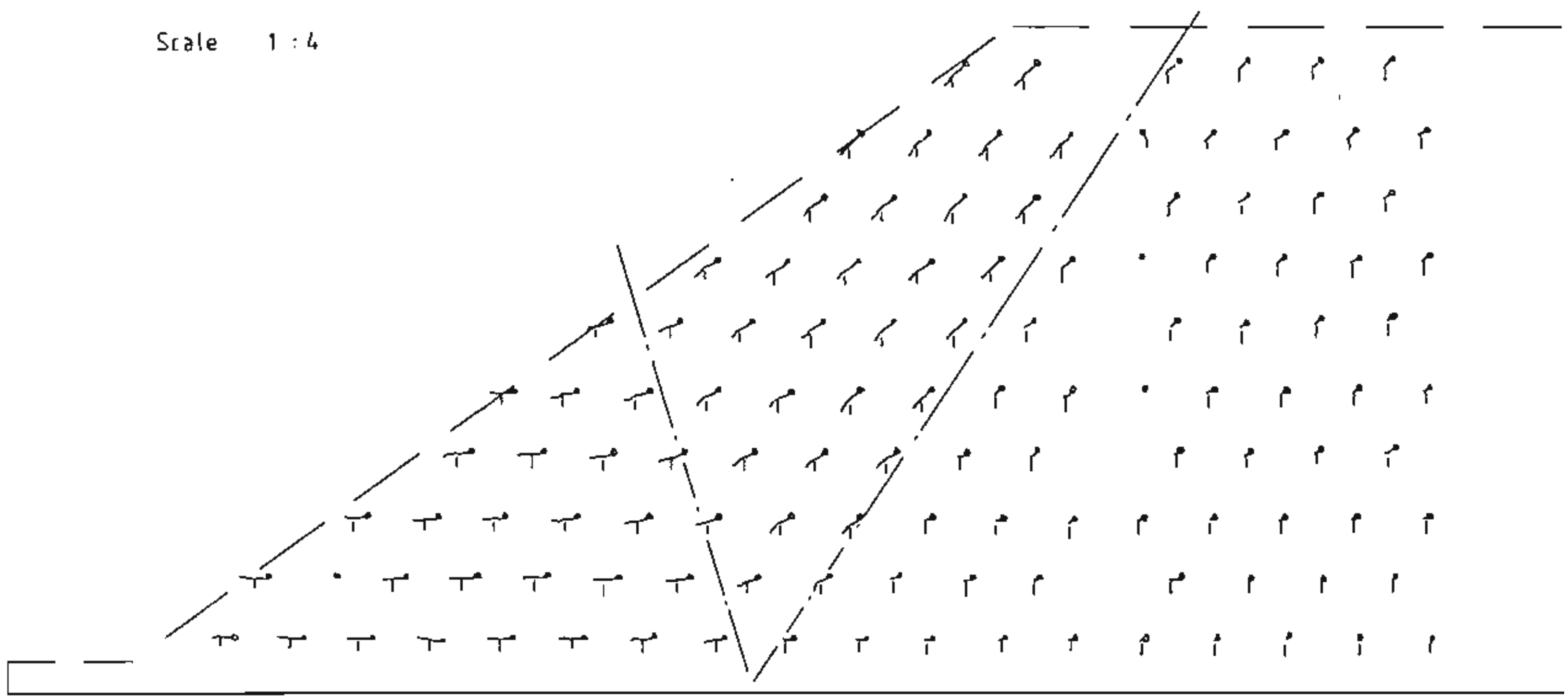

Figure 5.4a Displacements: Test 05-20-D; Elapsed Time 116.8 secs

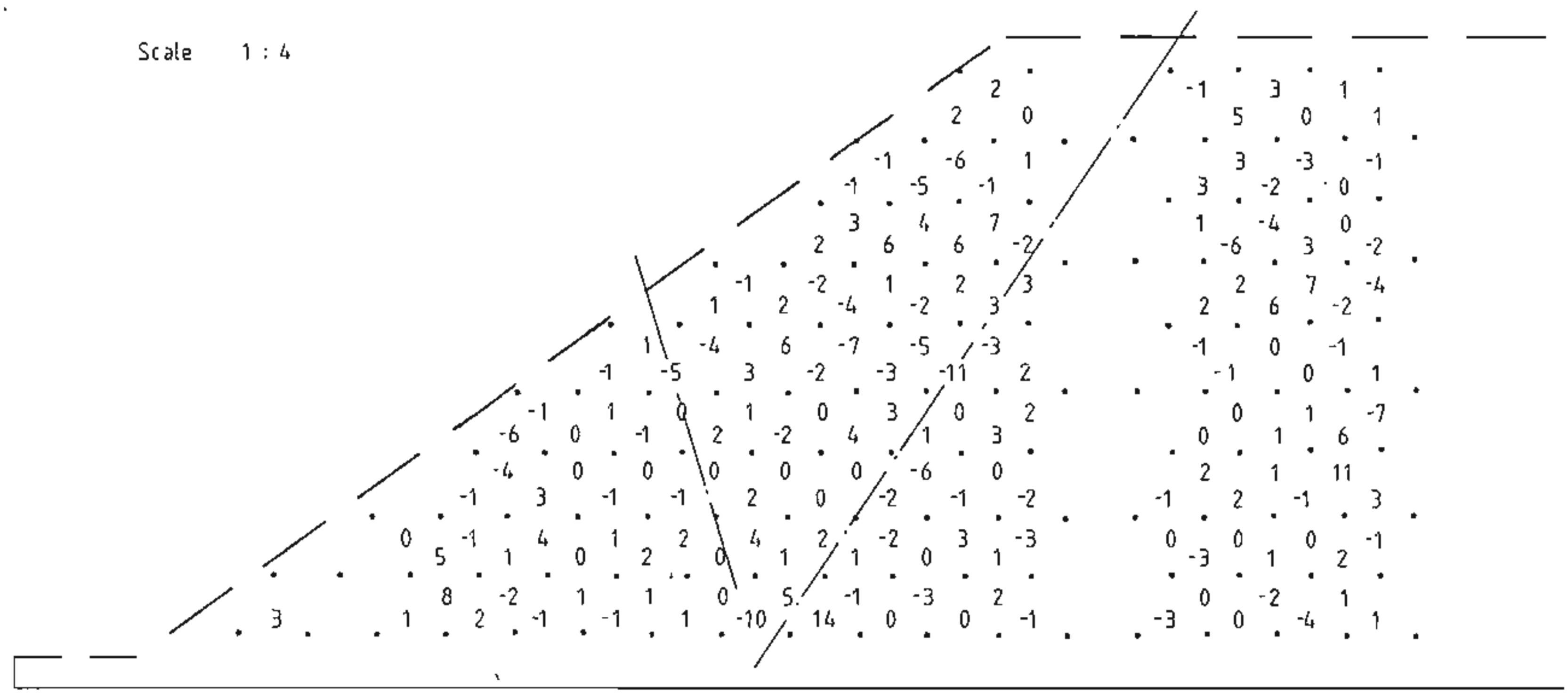

Figure 5.4b Volume Change (%): Test 05-20-D;
Elapsed Time 116.8 secs

between the crest region and the body of the slope, while smaller differences were observed between the toe and crest regions. After allowing for volume changes due to local target deviations from the trend, the movement appeared as two intact blocks slipping relative to one another and relative to the body of the slope, with shearing confined to zones along the regional boundaries, although the existence of a slip zone along the toe-crest boundary was still a matter of judgement.

Figure 5.5: Elapsed time 147.5 seconds.

(a) The pattern of displacement vectors had changed little, except at the toe of a slope where an upward movement of the targets was observed. A compressed ridge of bentonite at the toe had been formed by the movement of the slope; thus, further movement of the slope required a change in deformational pattern at the toe.

(b) The volume change figures showed the first consistent evidence that a slip zone had formed along the toe-crest regional boundary; thus, the failure mechanism had developed into a two-wedge form as was suggested by the early stages of slope deformation.

Figure 5.6: Elapsed time 177.8 seconds.

(a) and (b) There was practically no deviation from the trend of movement or volume change during the interval. Although there were still volume changes recorded, these referred to the volume of the triangular prisms and not to the sand material contained in them. Therefore, no conclusions were possible regarding the state of volume change in the sand for further deformation in the two-wedge mechanism.

Figure 5.7: Elapsed time 207.4 seconds.

(a) and (b) Again there was very little comment to be made as the two-wedge mechanism continued to define the deformation pattern of the slope.

5.2.3 <u>Results from other tests</u>

Qualitative observations showed that the results for tests 05-20-A to 05-20-D were the same as those for tests 25-10-A to 25-30-B. Three

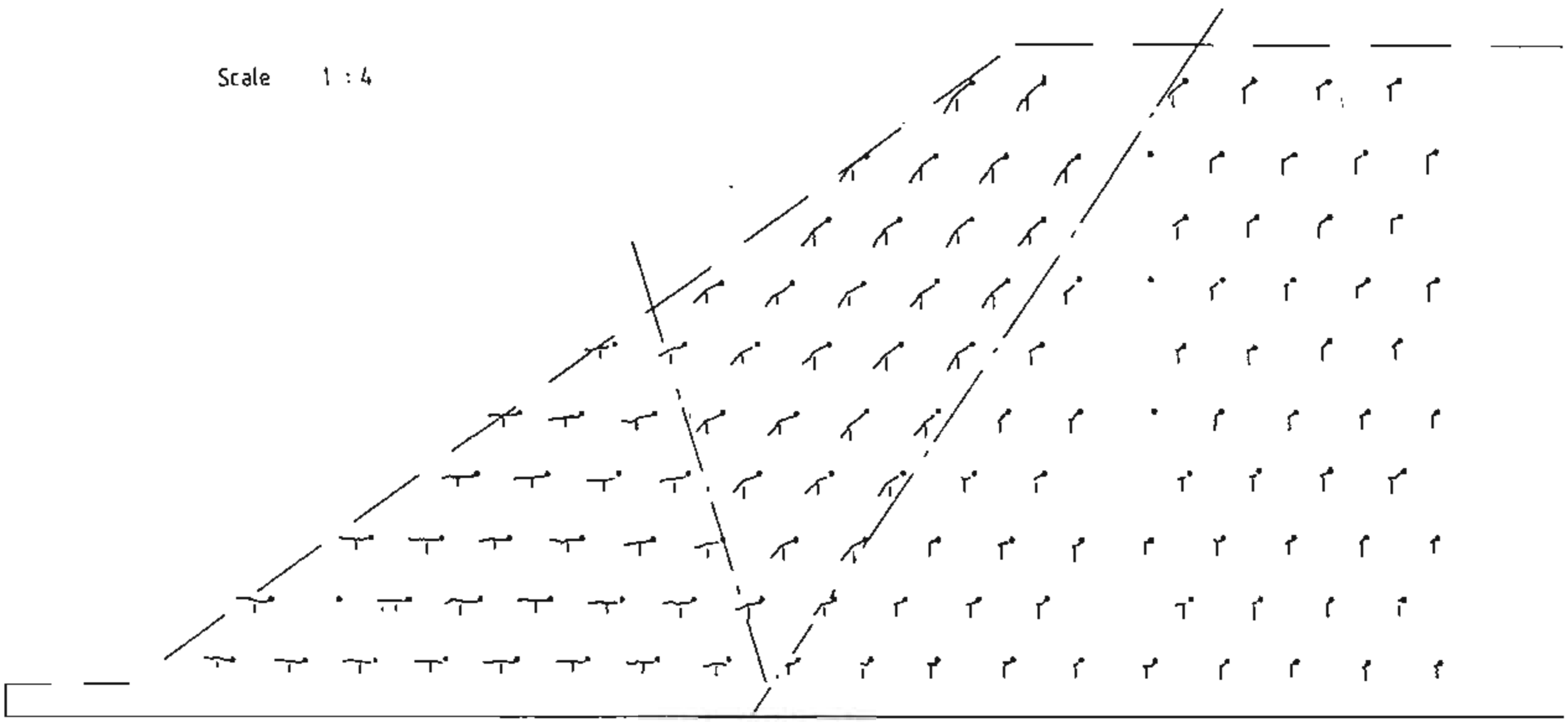

Figure 5.5a Displacements: Test 05-20-D; Elapsed Time 147.5 secs

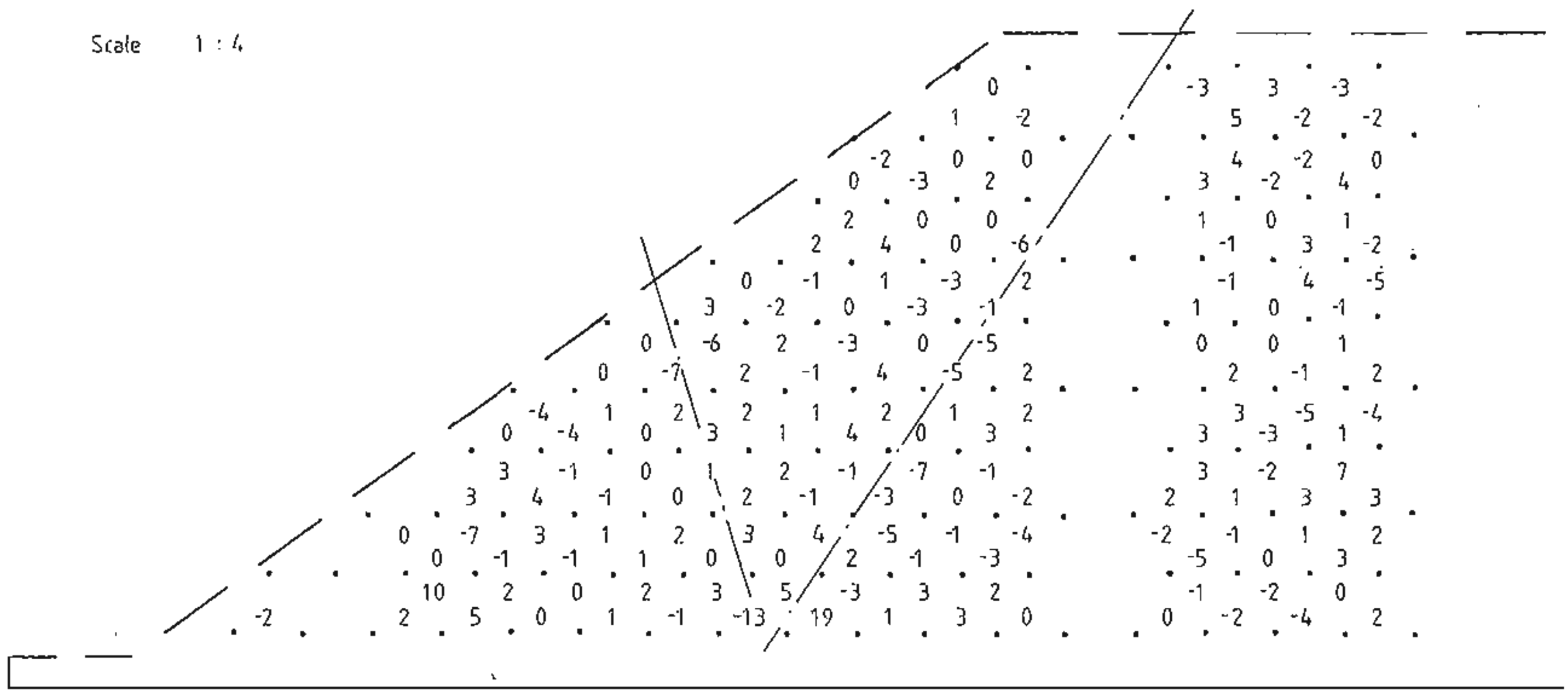

Figure 5.5b Volume Change (%): Test 05-20-D;
Elapsed Time 147.5 secs

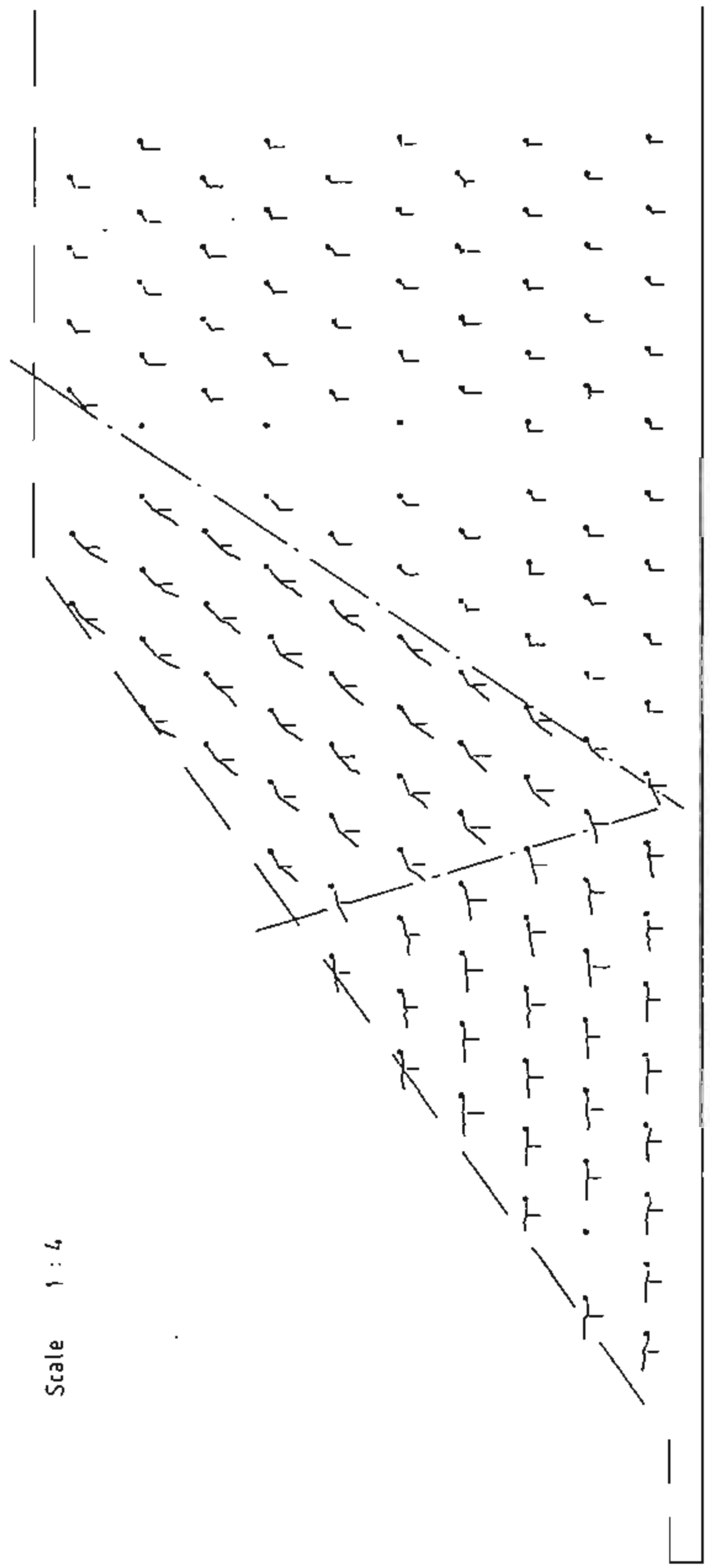

Figure 5.6A Displacements: Test 05-20-D;
Elapsed Time 177.8 secs

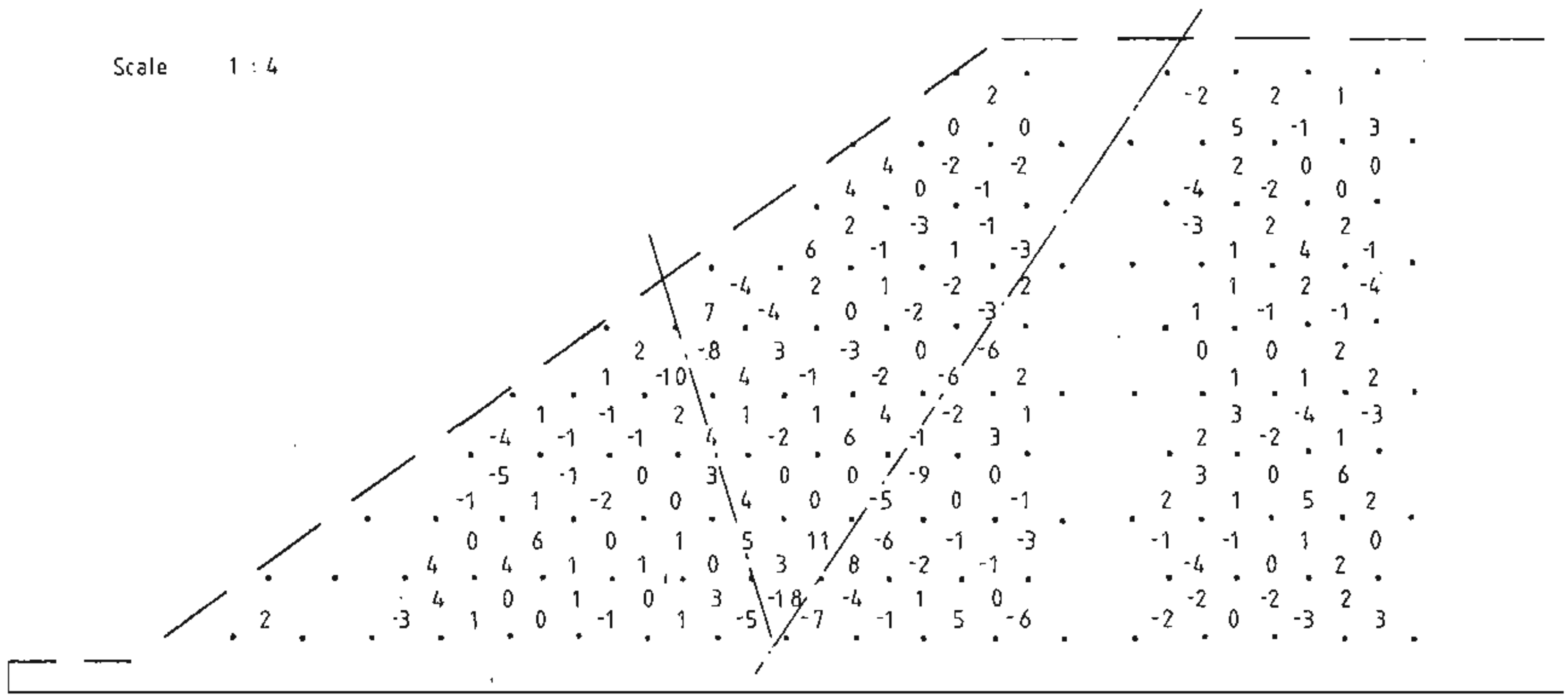

Figure 5.6b Volume Change (%): Test 05-20-D;
Elapsed Time 177.8 secs

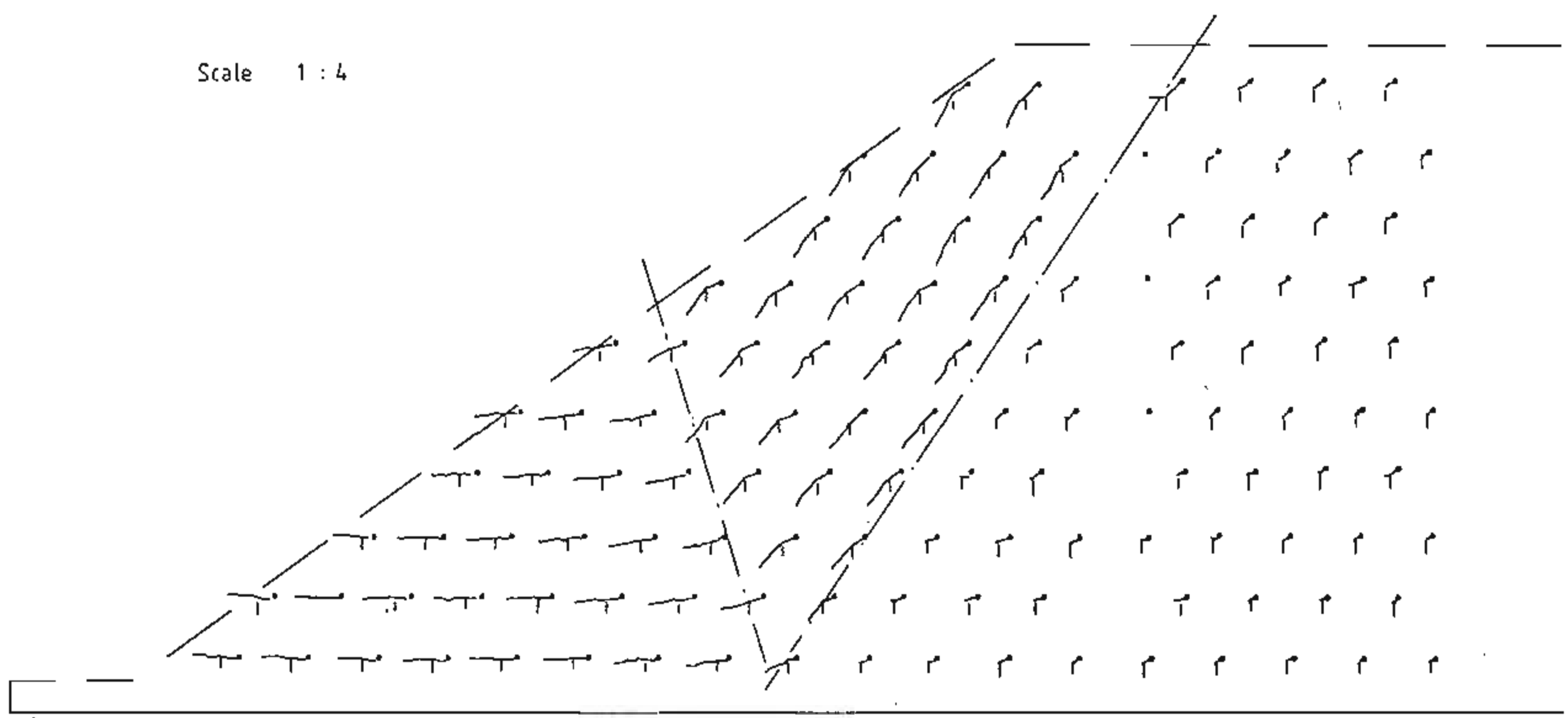

Figure 5.7a Displacements: Test 05-20-D;
Elapsed Time 207.4 secs

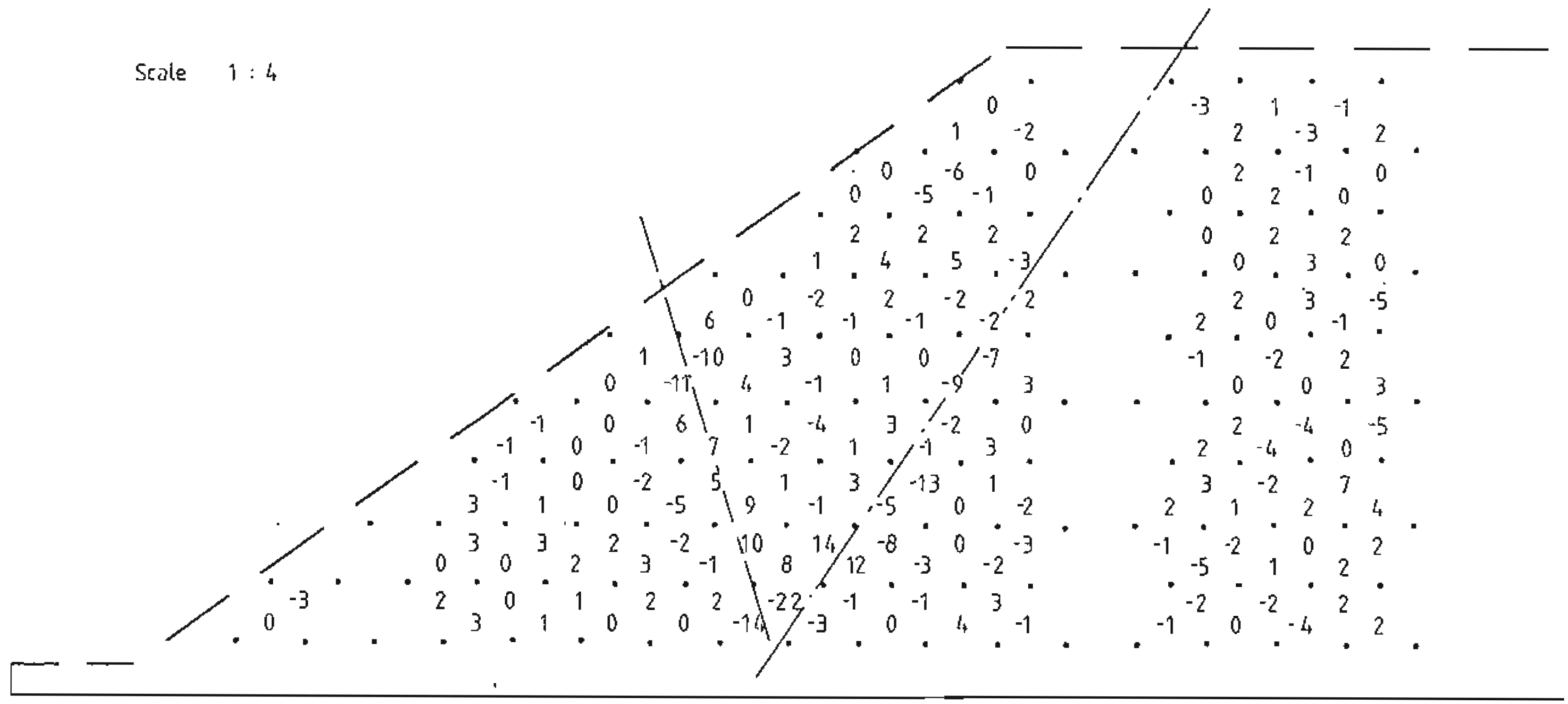

Figure 5.7b Volume Change (%): Test 05-20-D; Elapsed Time 207.4 secs

tests from the latter group and test 25-05-A were measured from the projection of the movie films onto sheets of cartridge paper where target displacements were traced. Although the measurements were of low reliability ($\pm$2.25 mm variation of displacements), they illustrated the similarity among the tests with different bentonite layer thicknesses and among the tests using different batches of bentonite. Figures 5.8 to 5.11 are examples of the results measured from tests which were traced out on cartridge paper. Further results are given later in this chapter.

5.2.4 Definition of the sequence of failure

The detailed description of a modelling test showing typical failure characteristics revealed that the failure was deep-seated from its initiation, and that further development of the failure occurred in a sequence which was clearly evident in both displacement and percentage volume change records. Figure 5.12 shows a simplified interpretation of the sequence which is described as follows:

(i) the original slope before any movement had taken place;

(ii) the first phase where slip occurred along planes 1 and 2, with a zone of shear between the toe and crest regions;

(iii) the second phase where the slip plane 2 became evident in the displacement diagram and the shear zone showed some angular distortion (tilting of the shear zone into the back of the slope);

(iv) thirdly, the formation of a slip plane within the shear zone which resulted in the distinct two-wedge failure mechanism, confirming the third-order sequential failure concept proposed by Trollope (1973);

(v) the final phase was the continued deformation of the slope, with slip occurring along the three bands defined in part (iv) of Figure 5.12, i.e. basically a rigid block motion.

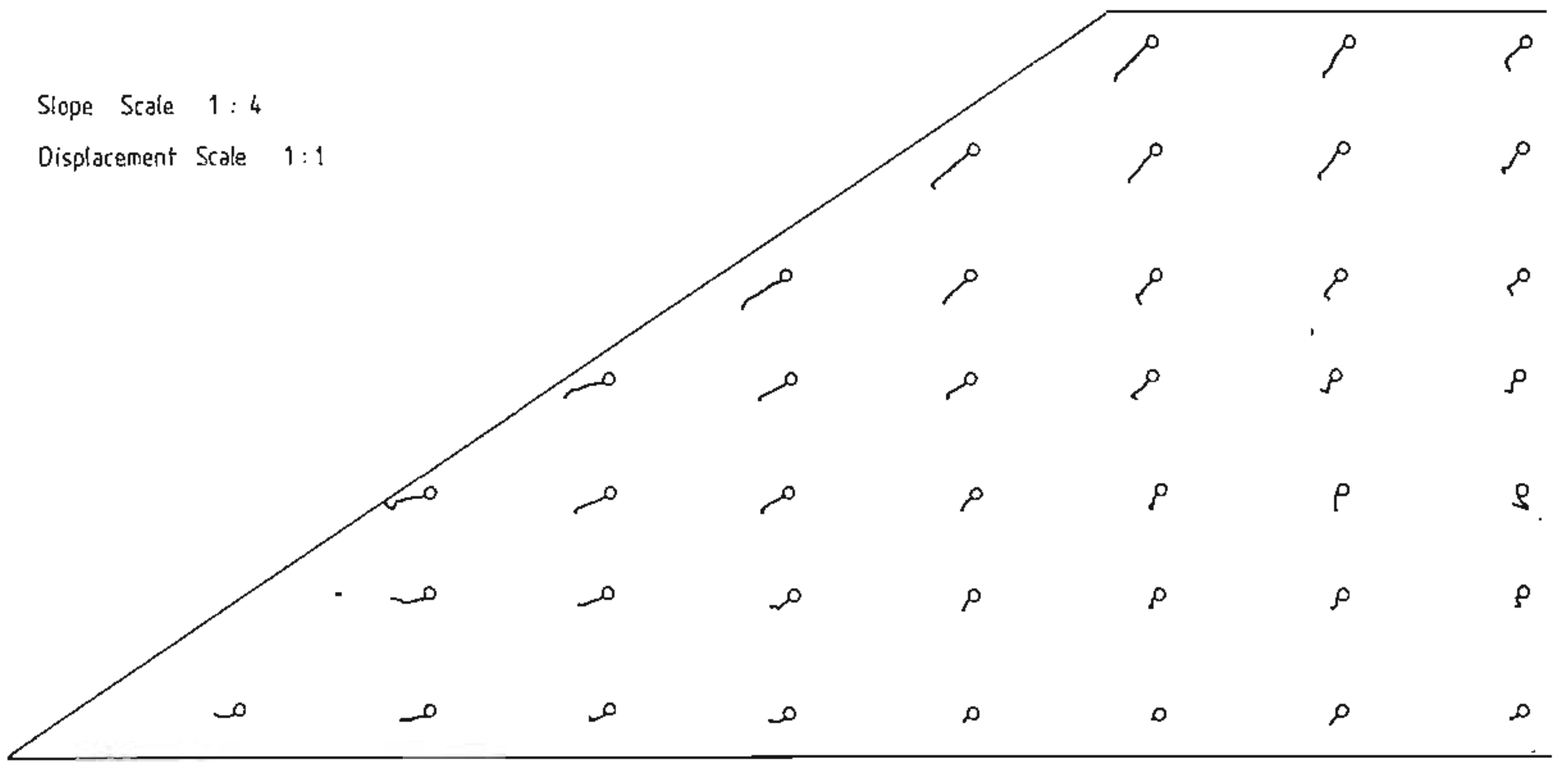

Figure 5.8 Displacements: Test 25-05-A; Elapsed Time 95 secs

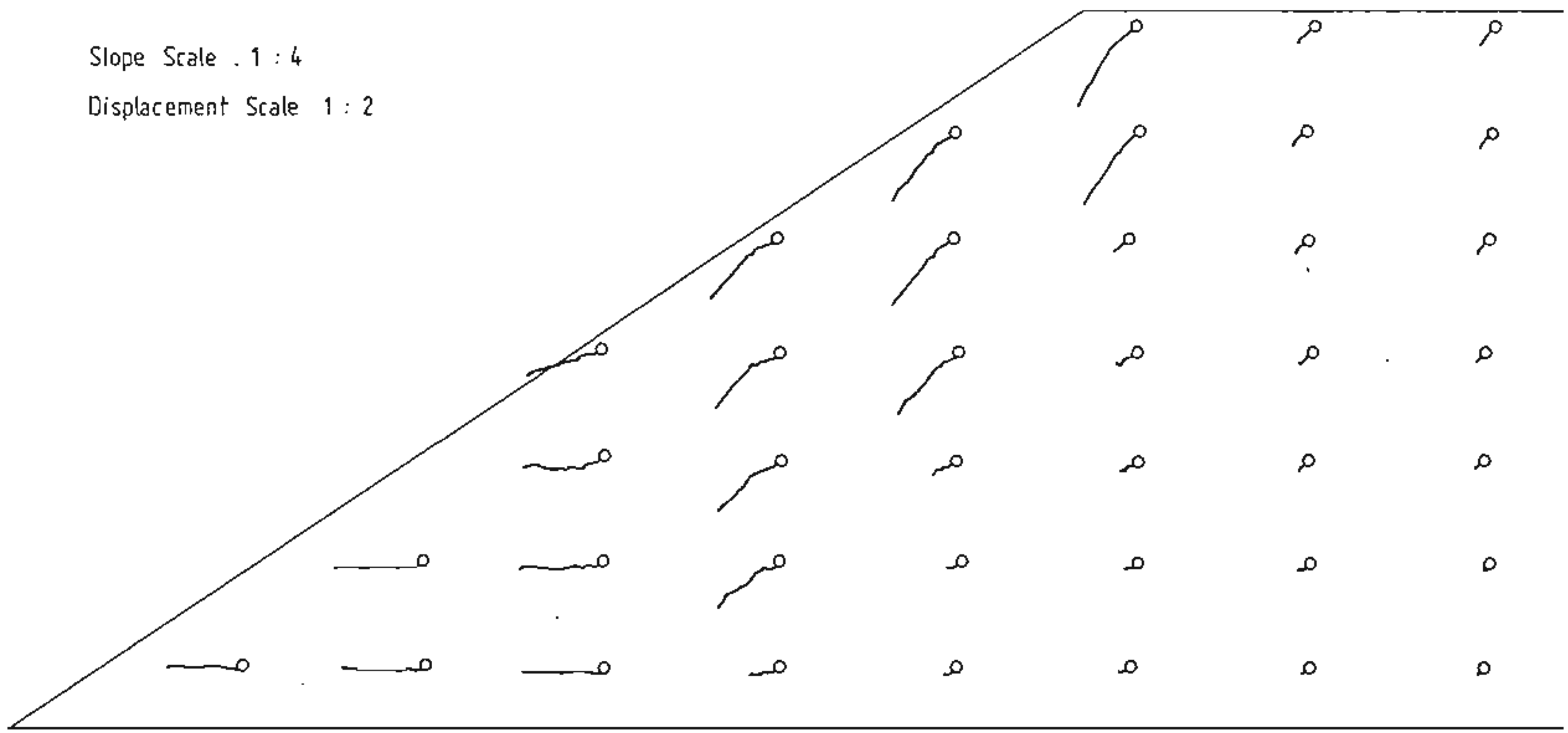

Figure 5.9 Displacements: Test 25-10-A;
Elapsed Time 44 secs

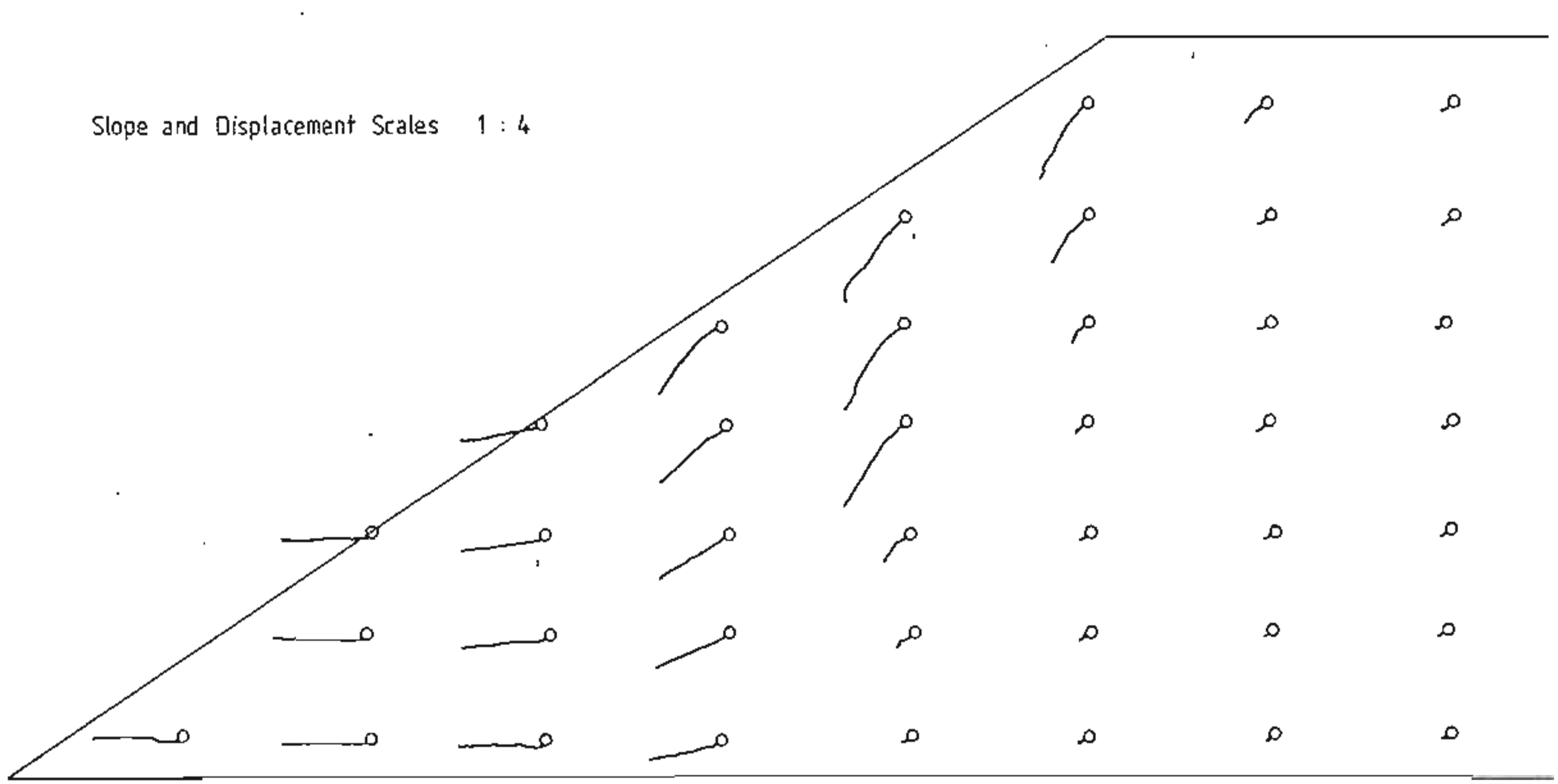

Figure 5.10 Displacements: Test 25-20-A;
Elapsed Time 6 secs

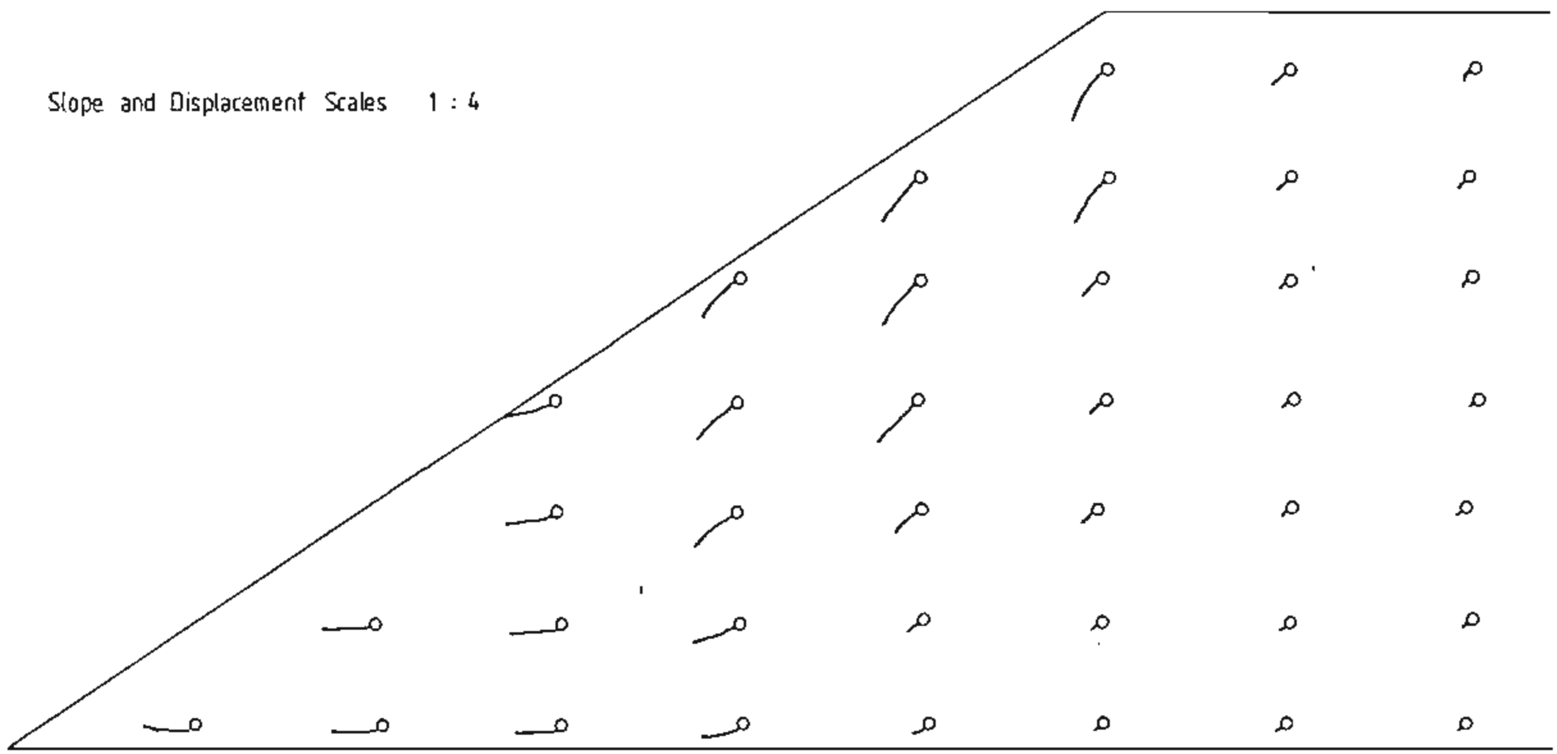

Figure 5.11 Displacements: Test 25-30-A;
Elapsed Time 3.2 secs

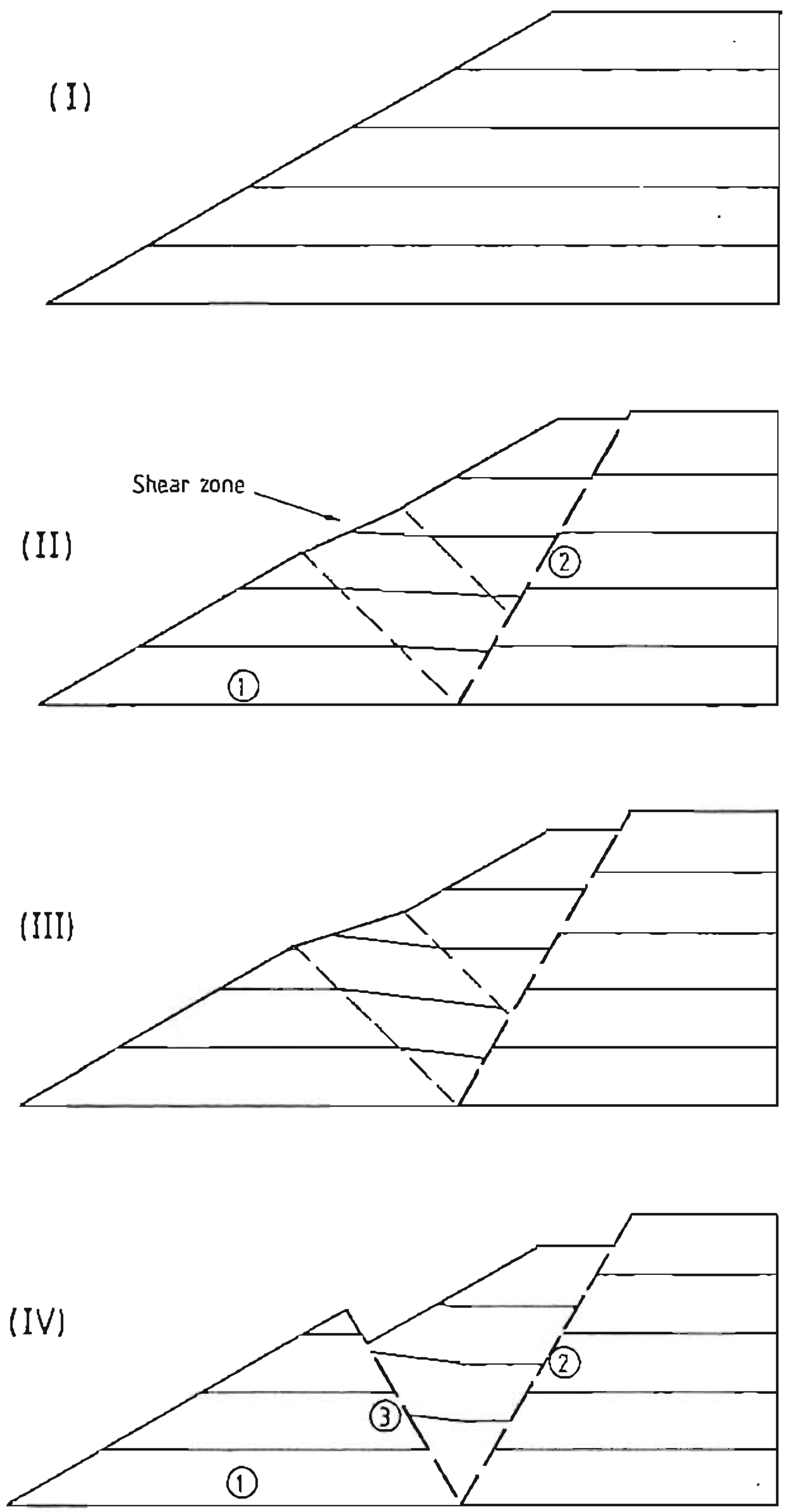

Figure 5.12 Sequence of Failure

This sequence of failure explained the important characteristics of the model tests conducted, as well as many features of two-wedge land slips in the field. Some points of particular interest were: deformation of the slope which left the toe region undisturbed; the gentle S-shape of the face of the slope; the graben formation with one of the slip planes lying behind the crest; the berm near the mid-height of the slope; and the formation of planar, rather than curved surfaces.

It was evident from the displacements shown in Figure 5.1(a), and the comparatively long time interval before further significant movement was observed, that the retraction of the mesh had some effect on the initial displacements in the model slope. Therefore, it was important to determine to what extent the stiffening mechanism affected the failure mechanism and position of the slip surfaces in the model slope. Test EX20 was designed to study the behaviour of a sand slope on a bentonite layer without any interference from the stiffening mechanism. The sequence of failure observed in test EX20 was the same as that described above. Plate 5 shows the evolution of the two-wedge mechanism for this test with frame (a) showing the slip zone on the boundary between the crest region and the body of the slope, frame (b) showing the angular distortion in the lower part of the crest region due to deformation with the broad shear zone, frame (c) showing the formation of the slip zone between the toe and crest regions and the appearance of the mid-height berm on the face of the slope, and frame (d) showing the model slope after about 20 mm horizontal movement of the toe region, clearly illustrating the two-wedge mechanism and the compressed ridge of bentonite at the toe of the slope. Thus, the conclusion was reached that the failure mechanism, its geometry and sequence of development, was not adversely affected by the use of the stiffening mechanism. One feature induced by the stiffening mechanism was the initial rapid displacements in the slope immediately after the mechanism was activated.

5.2.5 Statistical analysis of reliability

The synthesis of the sequence of failure was highly dependent on the evidence of Figures 5.1 to 5.7; therefore, it was necessary to assess the variation in target measurement so that the changes in values

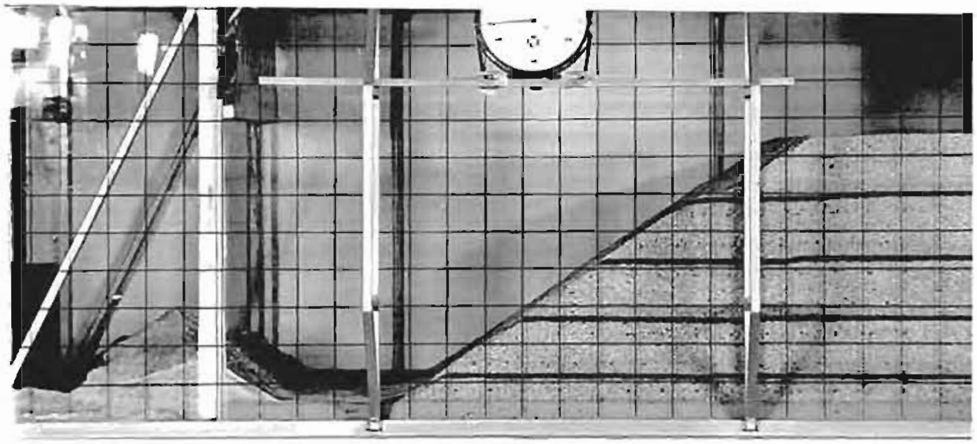

(a) Single Plane through Sand

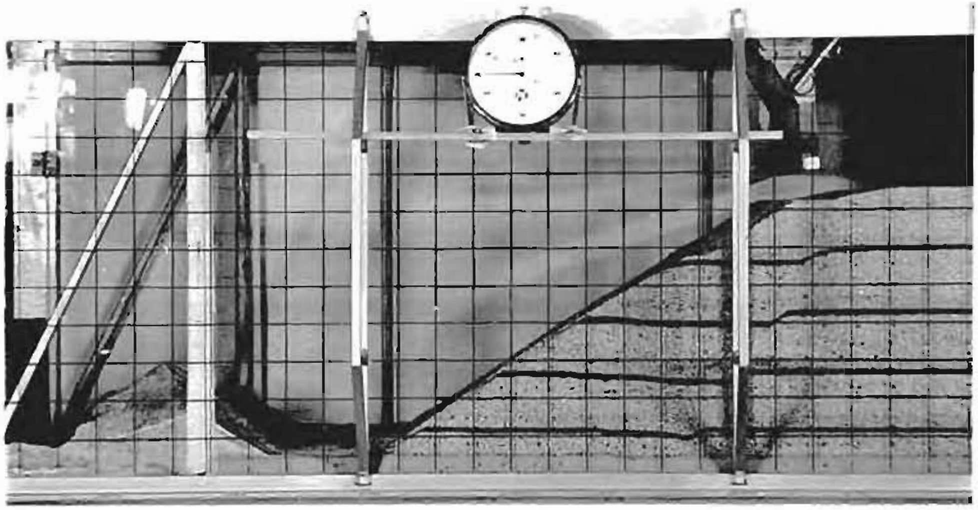

(b) Shear Zone Distortion

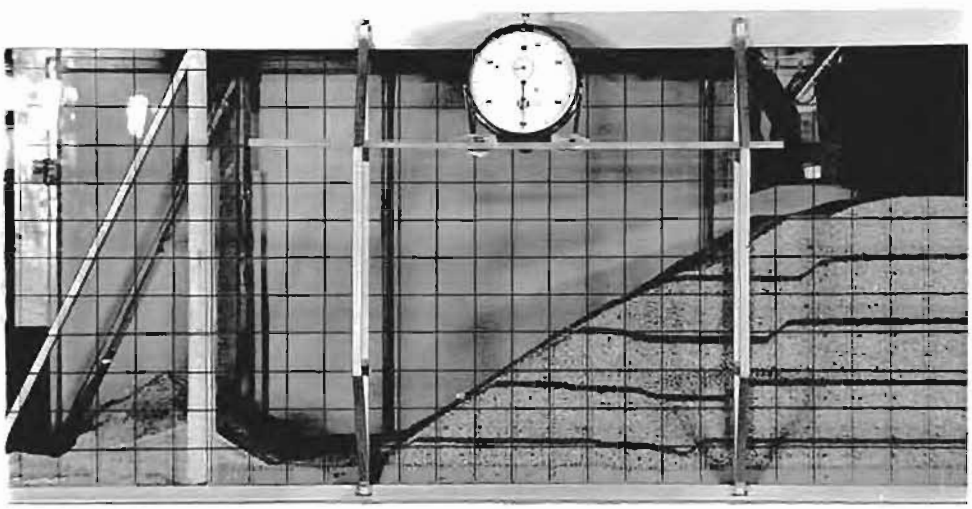

(c) Formation of Two-wedge Mechanism

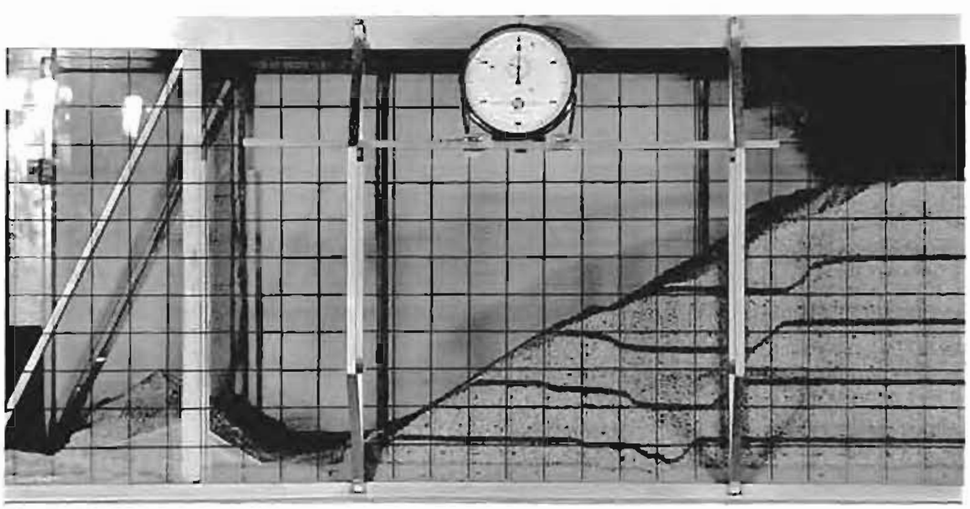

(d) After about 20 mm Horizontal Displacement

Plate 5 Sequence from Test FY20

could be considered at a realistic level of significance. Because thirty frames were measured from the record of test 05-20-D, a group of control records large enough for a Poisson distribution analysis was collected. Therefore, the correlation of datum grids between frames and the scaling of the measurements back to full size was carried out with reliable relationships. The horizontal and vertical scaling factors were 42.04 and 41.93 with standard deviations of .07 and .08 respectively. A linear regression analysis was carried out to arrive at a set of equations which would counteract the distortions due to the curvature of the camera lens. The relationship for the horizontal direction was:

$$x' = 2.83 + .98974\ x \qquad (5.1)$$

with 95% confidence intervals of:

$$-.01 < \alpha < 5.67, \text{ and}$$
$$.98524 < \beta < .99424:$$

where x' = corrected value, and
x = reading after magnification to full scale.

The relationship for the vertical direction was:

$$y' = .12 + .99747\ y \qquad (5.2)$$

with 95% confidence intervals of:

$$-1.73 < \alpha < 1.97\ ,$$
$$.98938 < \beta < 1.00556;$$

where y' = corrected value, and
y = reading after magnification to full scale.

Because the results shown in Figures 5.1 to 5.7 were based on a comparative analysis, the translation of axes (i.e. the α parameter) did not affect the displacements, which were able to be altered in absolute magnitude, but not relative magnitude, by the scaling factors.

Variation in target manufacture, light conditions during the experiment, and local contrast against the sand grains caused the quality of the image of the targets in the photographs to differ. A scale number of 1 to 5 was given to each target according to its image, with a higher number for a better quality of image; a value of zero was given to targets which were obscured from view by either of the support struts for the glass. Table 5.2 gives a descriptive key for the image quality assessment; Figure 5.13 gives the frequency distribution of the image quality; and Figure 5.14 relates the image quality to target position throughout the model slope for test 05-20-D.

TABLE 5.2

Image Quality Assessment

Scale	Remarks
0	Obscured from view
1	Just visible, very blurred image
2	Visible, blurred image
3	Fair image, able to locate target centre
4	Good image, easily locate target centre
5	Excellent image

The errors associated with the manipulation of the data from reading to a full scale value tended to counteract each other in the comparative analysis; therefore, the major limitation to the accuracy of the measurements was the reliability of the location of the target image. Ten sets of readings were taken of a target in each of the image quality classifications from the one photographic frame so that a statistical analysis of the variation of recorded image position could be carried out. The data available was most suited to a Student t-distribution. Table 5.3 gives the variation in displacement and percentage volume change for a 95% confidence interval. The numbers for percentage volume change were calculated assuming that all three targets around the end of the prism had the same image quality number.

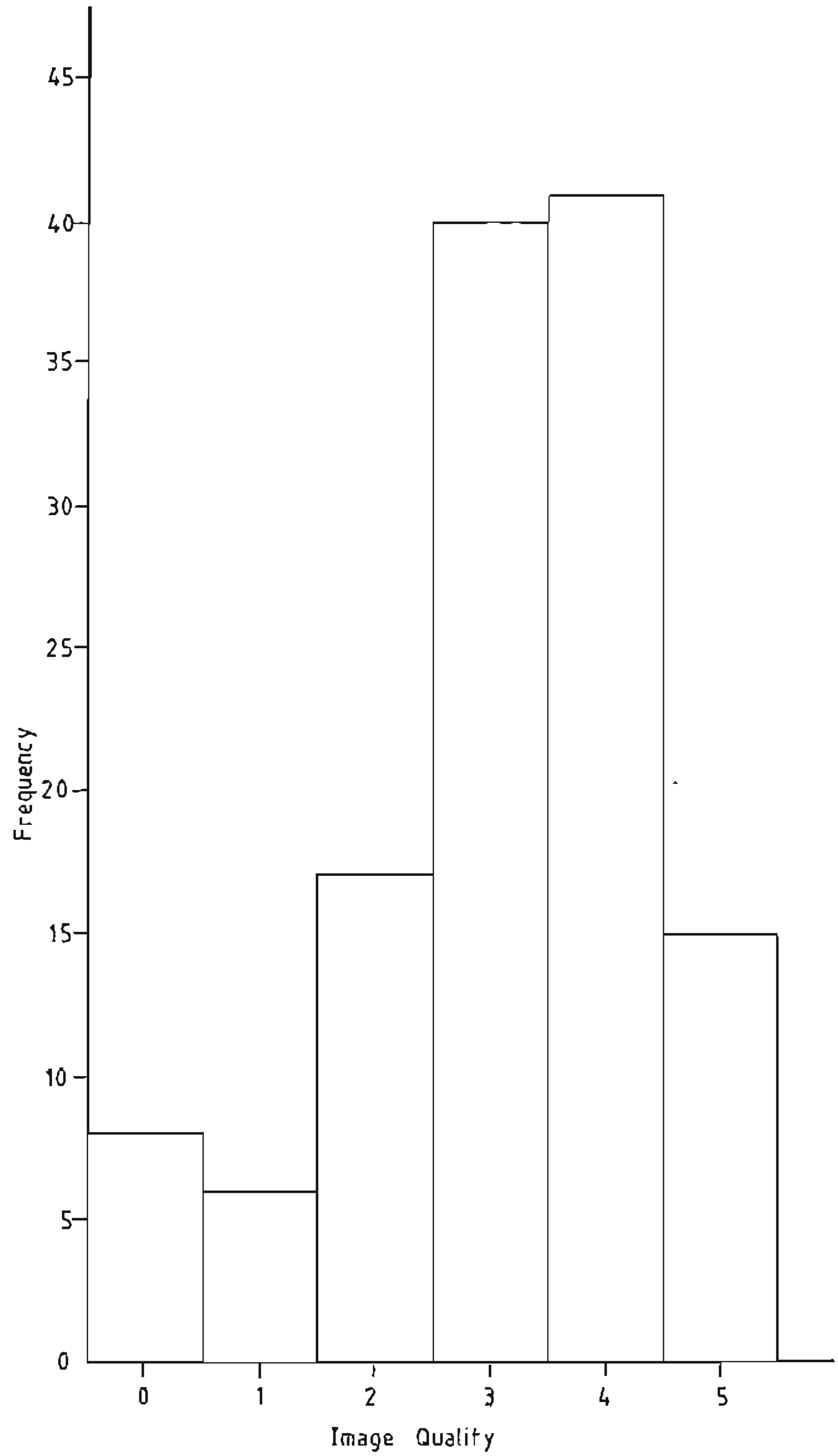

Figure 5.13 Frequency Distribution of Image Quality

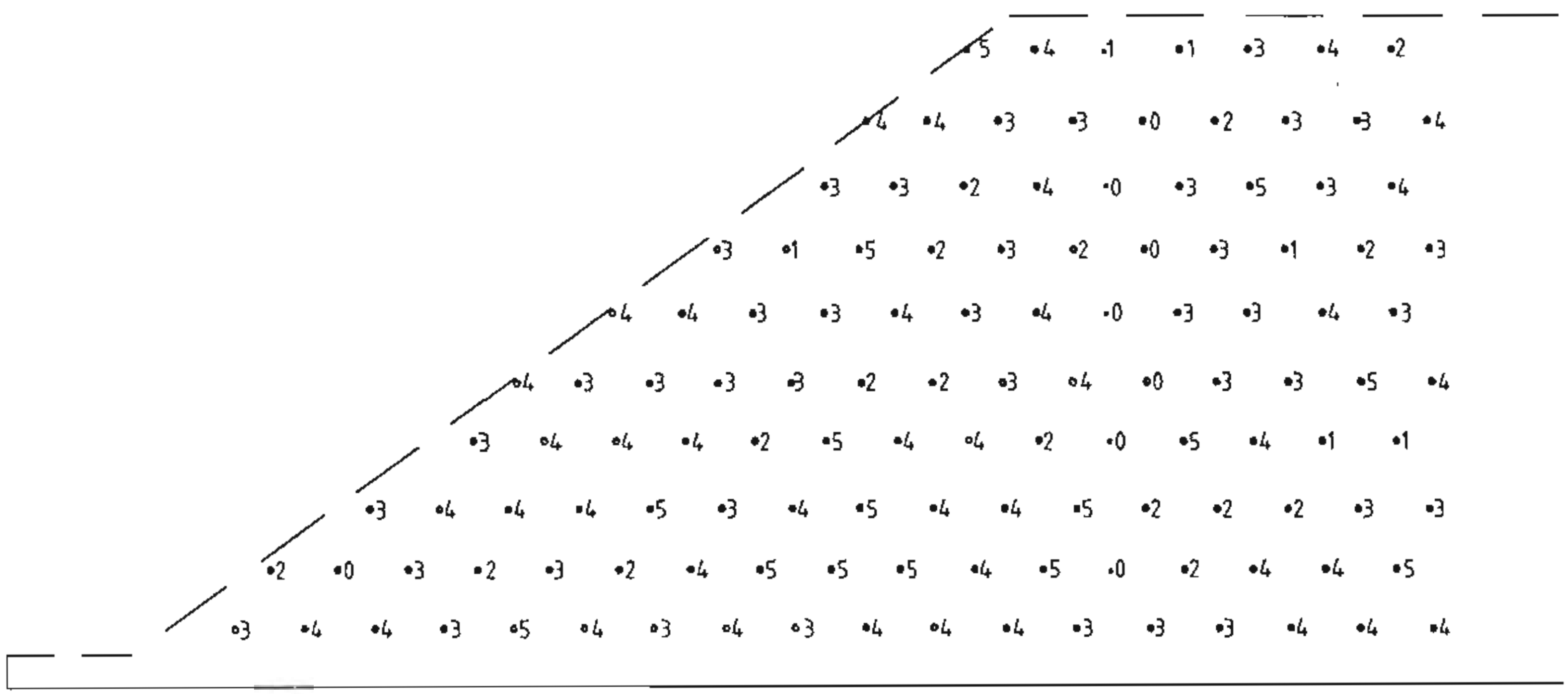

Figure 5.14 Spacial Distribution of Image Quality

TABLE 5.3

Reliability of Target Location

Scale	Displacement (mm)	Volume Change (%)
1	.59	2.8
2	.51	2.4
3	.45	2.1
4	.39	1.8
5	.28	1.3

Thus, the overall variation in results was assumed to be ±.4 mm for displacements and ±2% for volume change.

5.3 Slip Plane Characteristics

5.3.1 Observed characteristics

The position and inclination of the two slip planes which passed through the sand were readily ascertained from photographs taken when the two-wedge mechanism had just become distinct, and before further displacements occurred. Three parameters were used to define the slip planes in the mechanism: the angle to the horizontal of the two planes through the sand, and the distance in from the original toe position to the point where the two inclined planes were coincident with the horizontal slip plane through the base layer. The use of the term "slip plane" with reference to the failure mechanism should be interpreted to mean the plane which follows the centre line of the shear band, where it has been demonstrated that most deformation occurred in the slope when the two-wedge mechanism was dominant. Table 5.4 gives a summary of the characteristics observed during the testing programme, and uses the following symbols:

- H - height of slope;
- α - inclination of slip plane between toe and crest;
- β - inclination of slip plane between crest and body of slope; and

TABLE 5.4

Summary of Failure Characteristics

Test	North Elevation			South Elevation		
	α	β	x (mm)	α	β	x (mm)
25-10-A	70	56	475	70	57	425
25-10-B	75	52	350	72	51½	375
25-20-A	71½-74	57-58½	420	63-84½	60	450
25-20-B	72½	57½	440	75	57	410
25-30-A	76½-78	54-57½	350	75	53½-57	380
25-30-B	74	53-56	450	71½	63	425
EX20	-	-	315	71	58	370
25-20-A	-	-	410	-	-	390
25-20-B	-	-	400	-	-	400
05-20-C	-	-	400	-	-	450
05-20-D	-	-	445	-	-	455

x - distance from original toe position to point of intersection of slip planes.

Although there was variation in the results, the trend of results was consistent enough to allow an average value of the characteristics to be calculated. The resultant values and an estimate of the variations expected were:

α - $73^0 \pm 10^0$

β - $56^0 \pm 5^0$

x - 415 mm ± 40 mm (excluding test EX20)

$^x/_H$ - 1.0 ± .1 (including test EX20)

Bransby and Smith (1975) commented that the deformation of a model is recorded in its most disturbed state next to the sidewall because of the frictional effects of the boundary. The results reported above were measured at the sidewalls, and it was obvious from the curvature of the slip scarps across the tank that the failure characteristics were different at the centre of the model. Thus, the following section deals with the relationship between the characteristics at the sidewalls and those at the centre.

5.3.2 Relationship between sidewalls and centre

Plate 6 shows an example of the curvature of the slip scarps near the sidewalls. The curvature was apparent for both slip planes through the sand, but did not affect the face of the toe region which moved out as an intact block on a practically straight front. The post-failure profiles of the sand surface and the surface of the bentonite (when it was cleared of sand) for test 05-20-D are given in Figures 5.15 and 5.16, respectively. Assuming that all slip surfaces remained straight in the direction of movement, the traces of these surface profiles enabled the calculation of the difference in inclination of the slip planes between the centre of the model and the sidewalls.

An estimate of the angle of the front slip plane from Figure 5.7(a) was 70^0, and other relevant details of the calculation of the central angle are given in Figure 5.17. The central angle was found to be 72^0,

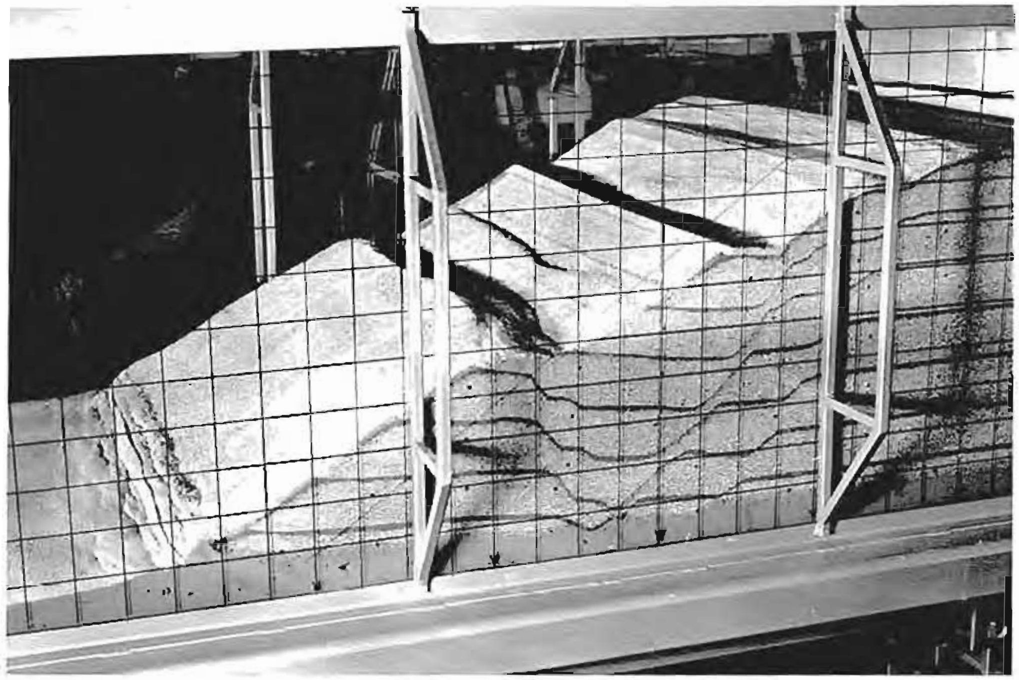

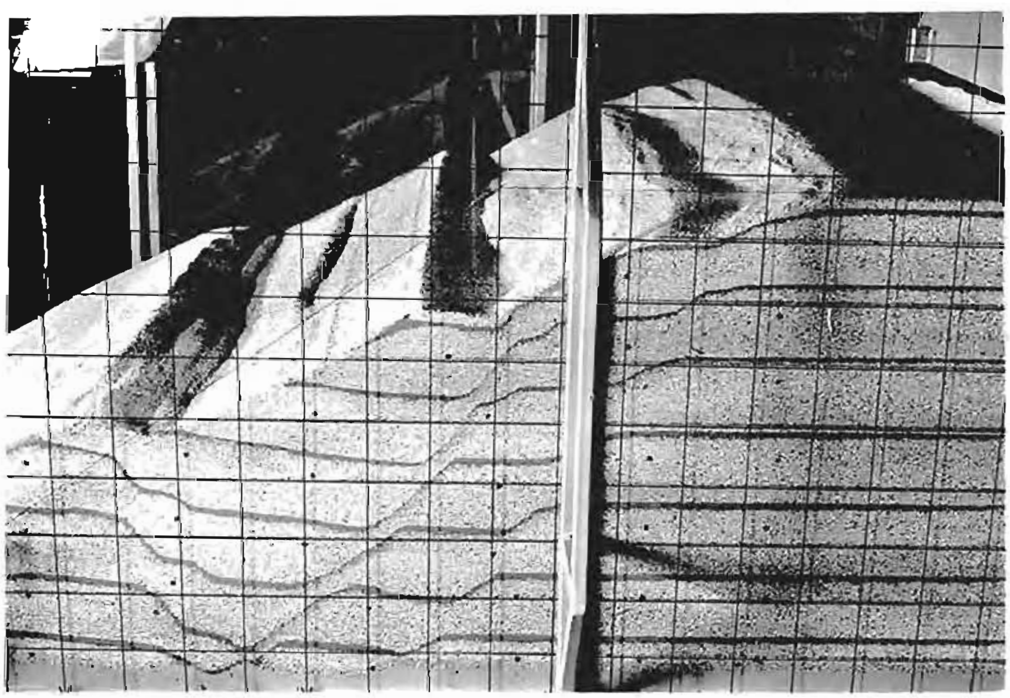

Plate 6 Scarp Curvature near Side Walls

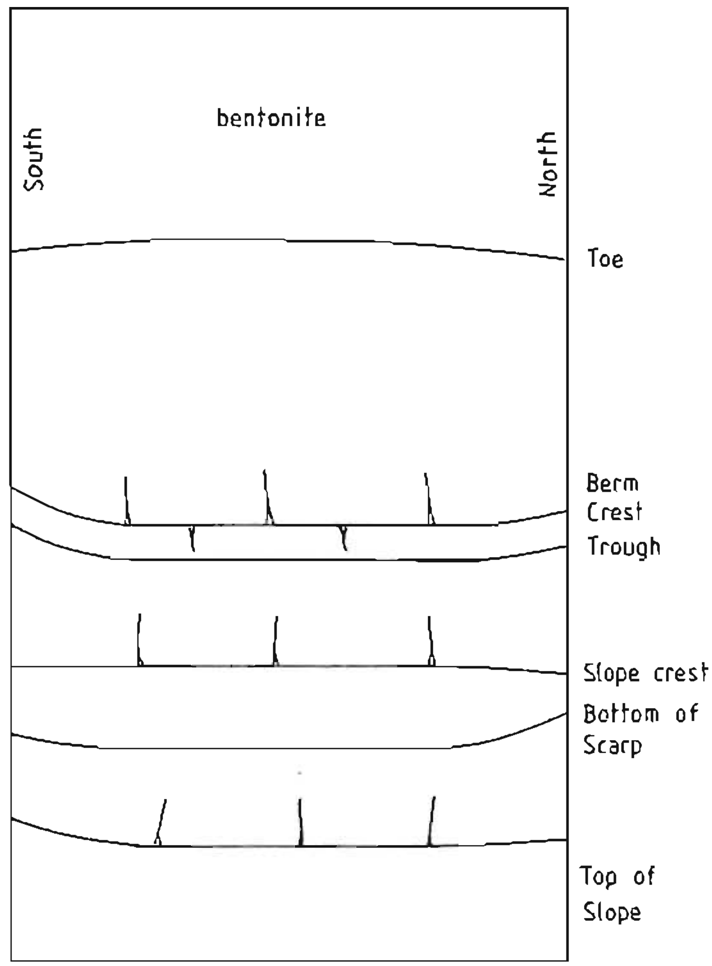

Scale 1 : 10

Figure 5.15 Sand Surface Profile: Test 05-20-D

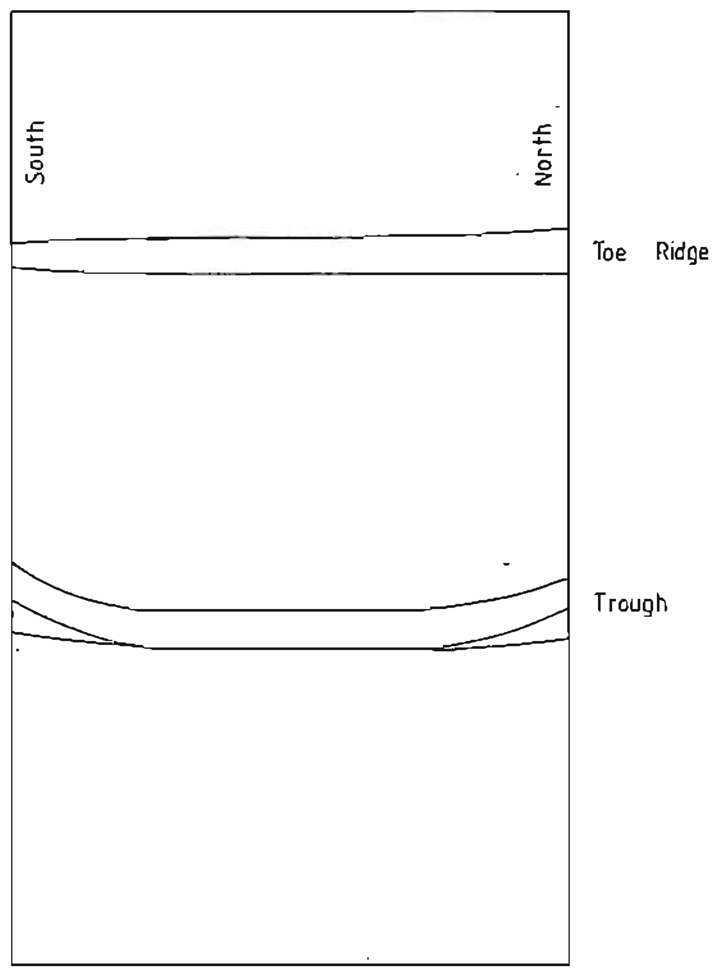

Scale 1 : 10

Figure 5.16 Bentonite Profile: Test 05-20-D

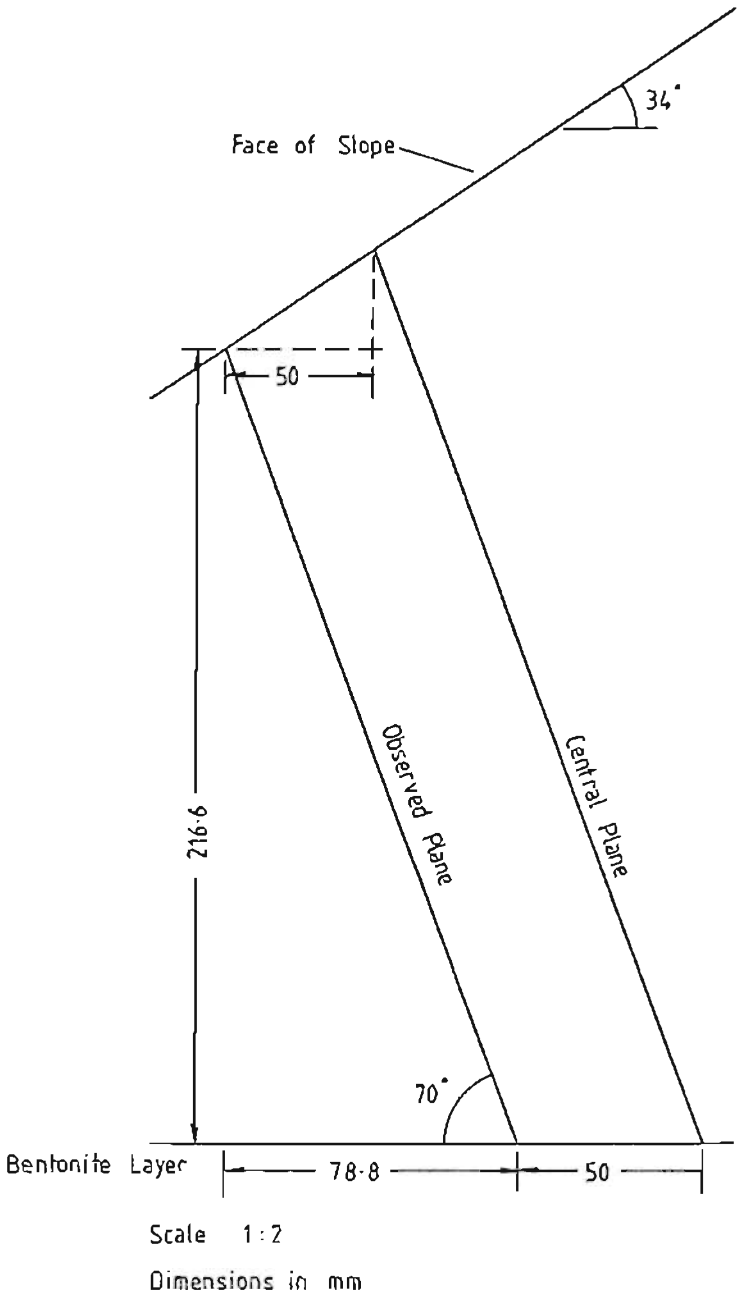

Figure 5.17 Calculation of Central Parameters from Side Wall

and therefore the difference between the two was small when the variation in the measurement of the angle was considered. The influence which led to the change in the front angle was the sloping face of the toe region; however, the back slip plane intersected an horizontal free surface which did not induce any change in angle. A study of Figures 5.15 and 5.16 showed that the dominant offset distance due to the edge curvature was about 50 mm, and this was observed to be a reasonably common distance when other tests were considered. Therefore, the average characteristic values observed at the sidewalls were transformed to values in the central region (which was considered to represent the plane strain condition more realistically than the region adjacent to the sidewalls), and yielded:

α - $75^0 \pm 10^0$

β - $56^0 \pm 5^0$

x - 465 mm ± 40 mm

$^x/_H$ - 1.15 ± .1

Figure 5.16 shows that noticeable deformation of the bentonite layer occurred, because the impression of the descending crest region was clearly visible. The following section considers the base layer deformation in more detail.

5.3.3 Deformation of the base layer

Plate 7(a) illustrates a typical example of the disruption which occurred in the originally smooth bentonite layer. The same features were observed in test EX20, and hence, it was accepted that the patterns were not a side-effect of the stiffening mechanism. These patterns also exhibited alterations due to the boundary friction; thus, the comments in this section are confined to the features of the central region of the base. Three main features of the post-failure base layer are discussed in this section: the toe ridge, the layer thickness (including the indented region corresponding to the point of intersection of the slip planes), and the horizontal displacement.

i) The Toe Ridge:

A common approach in soil mechanics analysis, when dealing with

Plate 7b   Compression Ridge of Bentonite at Toe

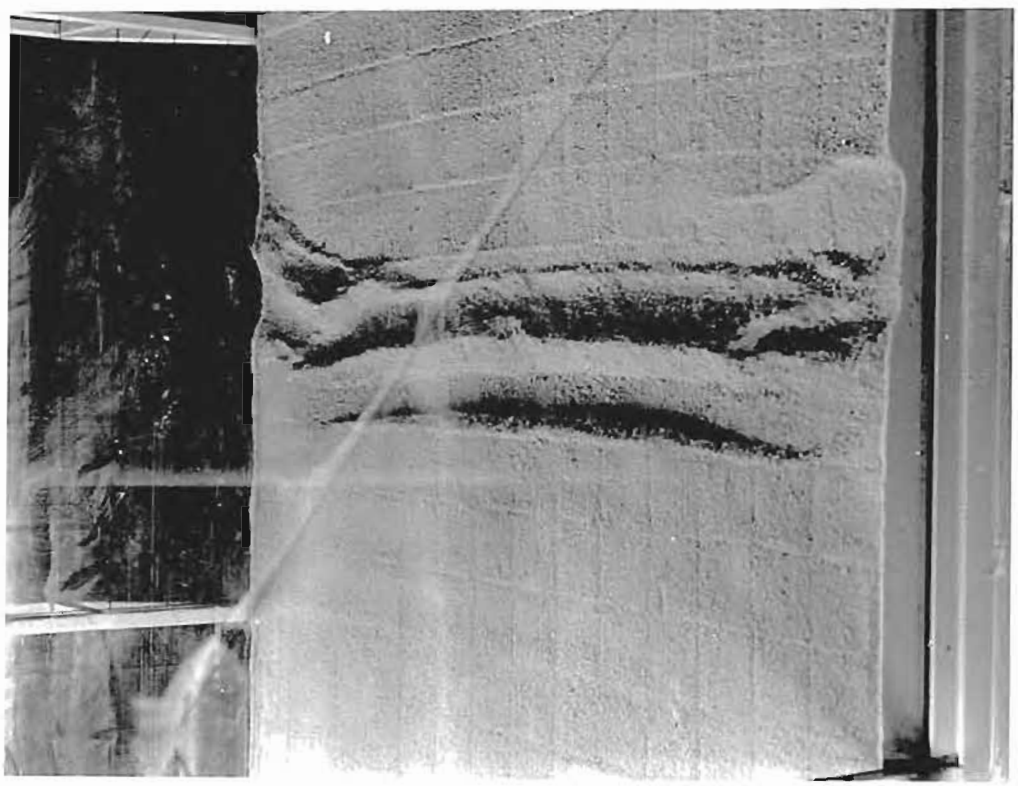

Plate 7a   Disruption of Bentonite Layer by Sand

a blocky failure, is to represent the end blocks as active and passive wedges separated by a number of intermediate blocks, depending on the geometry of the land mass. Thus, the toe region was expected to show the features of a passive thrust block. Plate 7(b) shows that the nature of deformation of the bentonite layer at the toe was in the form of an effective buckling of the clay. When large amounts of displacement occurred (circa 40 mm), the volume of bentonite pushed up into the ridge began to cause the adjacent part of the toe region to change its deformation pattern so that it tended to override the ridge. The post-failure profile exhibited some signs of the formation of a passive wedge in the bentonite, however, the ridge formation was always dominant.

ii) Layer Thickness:

At the end of most tests the sand was removed with minimal disturbance to the bentonite layer, whose post-failure characteristics were then recorded. Figure 5.18 gives several records of base thickness profile. The overall trend of these profiles is shown in Figure 5.18(e) and is described as: an increase in thickness within 100 mm of the toe, corresponding to the formation of the compression ridge; an even thickness slightly below the nominal thickness for 100 to 300 mm from the toe; a uniform decrease to about half nominal thickness over the next 100 mm; a steep trough which extended down to the floor of the tank, followed by a ridge and another trough which was broader than the first but not as deep; and a return to an even profile at the nominal thickness at a distance of 450 to 500 mm in from the toe.

The formation of this profile may be explained by referring to the sequence of failure described earlier. The initiation of the sequence, with the formation of the regions of deformation within the slope also established the position of the trough closer to the toe. Subsequent deformation of the crest region deepened the trough and the angular deformation of the shear zone may have been accompanied by the changing of slope in the bentonite layer in the region of 300 to 400 mm from the toe. The second trough formed when the two-wedge mechanism in the sand became dominant. The width of the second trough may have resulted from the width of the shear bands within the sand. If these shear bands were 20 mm wide (10 times maximum particle diameter), then

Figure 5.18 Bentonite Thickness Profiles

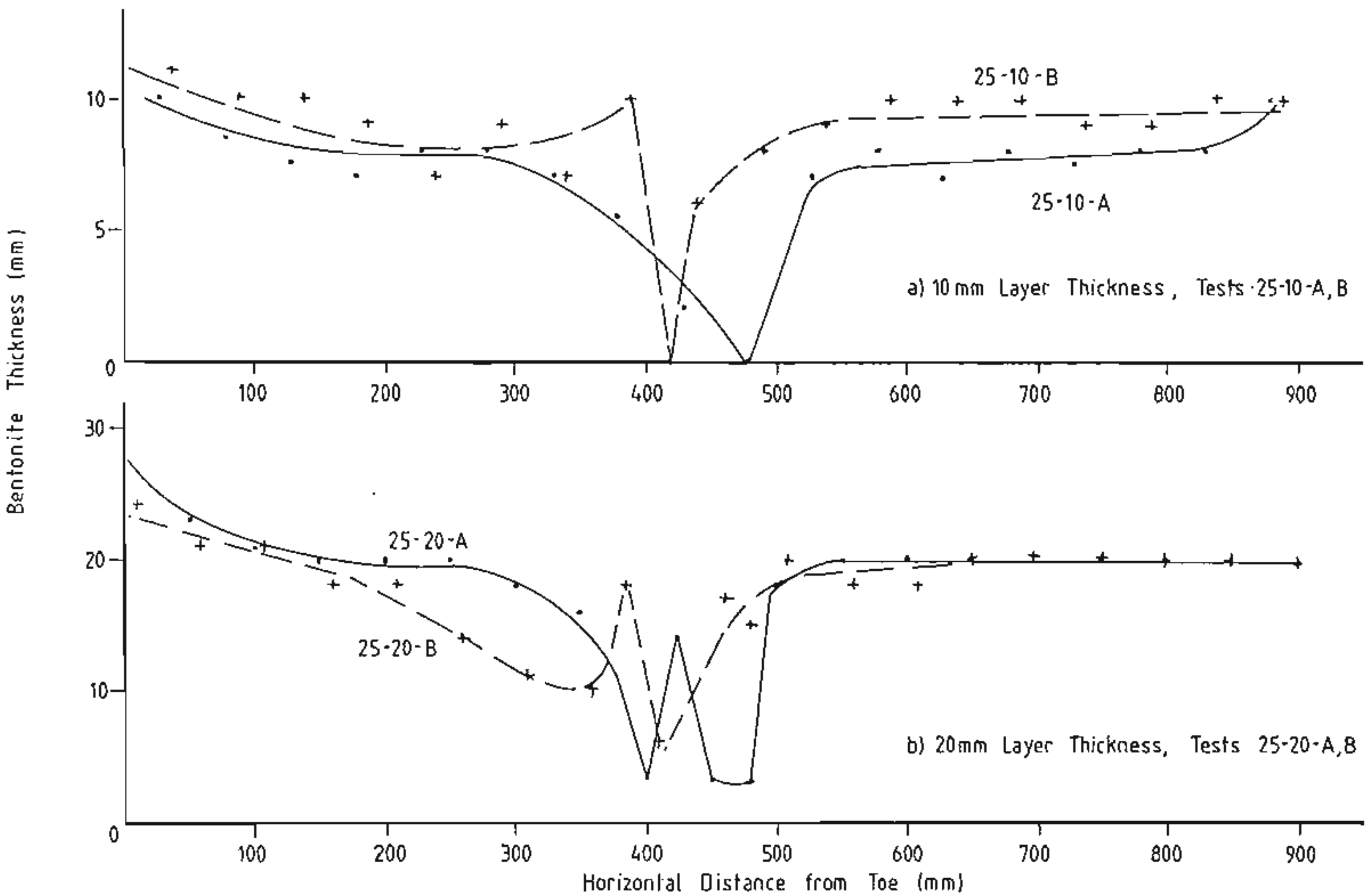

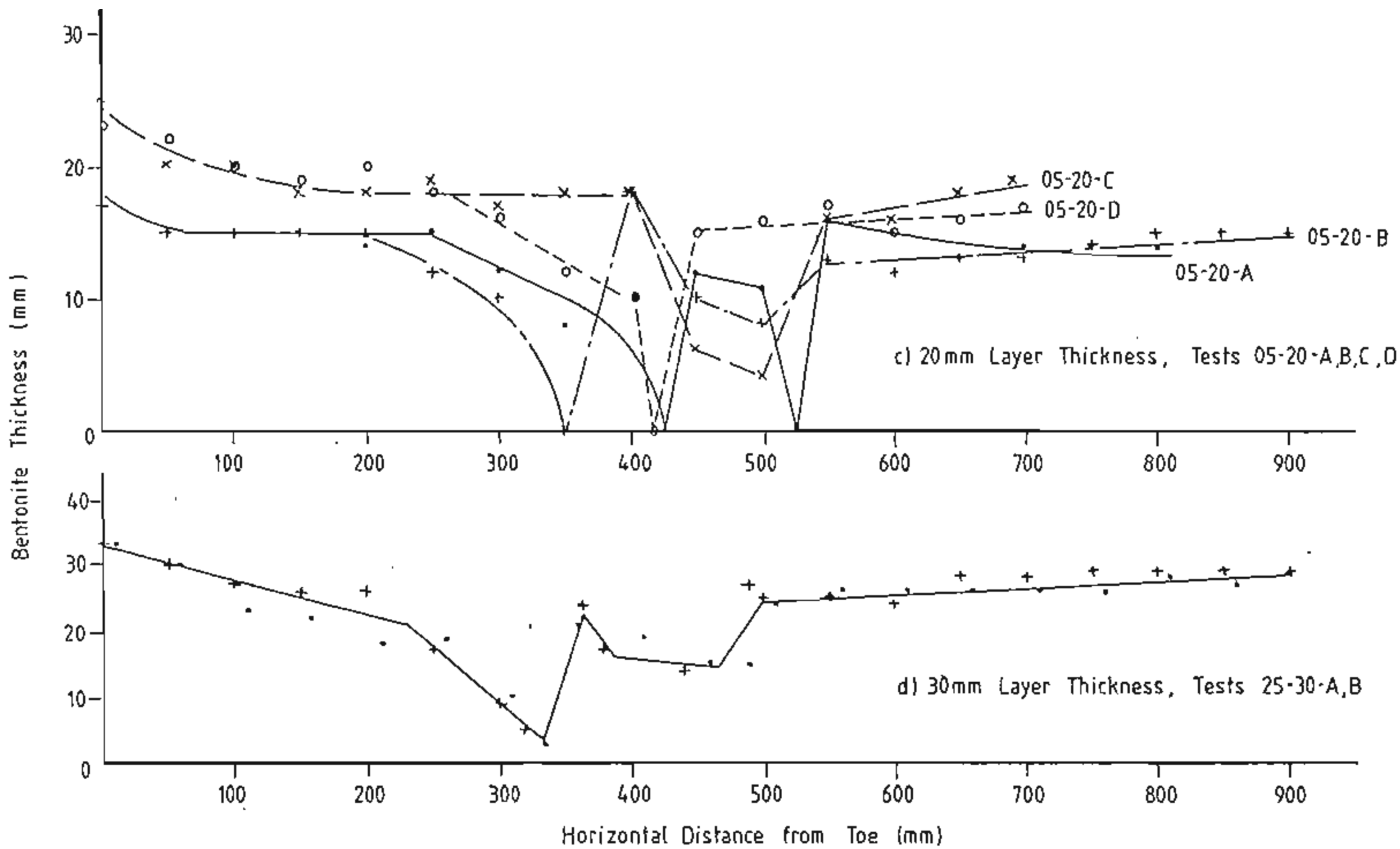

Figure 5.18 Bentonite Thickness Profiles (contd.)

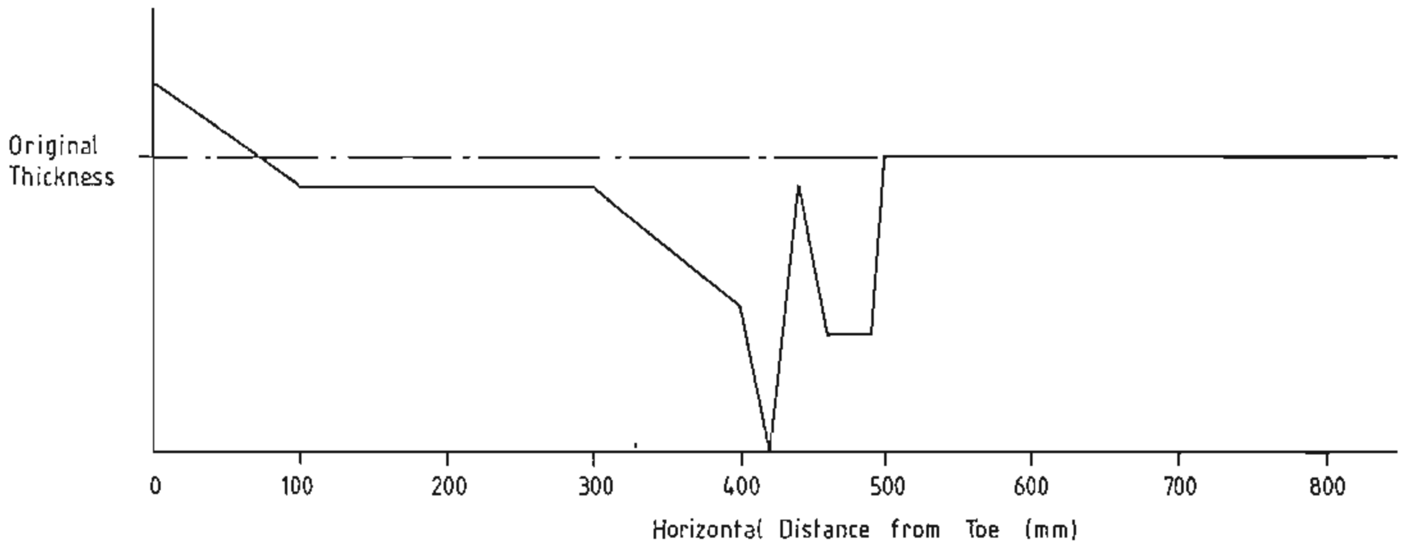

e) Trend of Bentonite Thickness Profiles

Figure B.18 Bentonite Thickness Profiles (contd.)

their area of intersection was about 25 mm wide, which was similar to the width of some of the troughs observed. Some decrease in the area immediately behind the troughs occurred, however, this was correlated to the formation of a second slip mechanism which happened after considerable displacement had taken place via the first mechanism.

iii) Horizontal Displacement

Figure 5.19 shows the amount of horizontal displacement which occurred in the bentonite layer during each test. The intact motion of the toe region was confirmed by the uniformity of the displacements between the toe and the point of intersection of the slip planes. Several dye-lines were placed vertically in the bentonite layer so that the deformation within the layer could be observed. The changes in the position of the dye-lines during test 25-30-A are shown in Figure 5.20, together with the positions of dye-lines with reference to the slope. After the initial movement due to the retraction of the vanes and mesh, the slip in the bentonite appeared as a zone of shear distortion in the lower 10 mm of the 30 mm base layer. There were two possible ways of inducing the base distortions: shear failure in the lower 10 mm with an intact mass movement of the overlying base material, or an extrusion of the base material due to the vertical pressure, which resulted in the displacement of the sand with its foundation. If the latter proposal occurred, the top of the dye-lines were expected to show some curvature away from the toe with the distortion caused by the force transfer from the bentonite to the sand, however, this feature was not apparent. Thus, it was concluded that the distortion of the base was due to shear failure of the lower portion of the material under the self-weight stresses imposed by the sand slope.

5.3.4 Use of the deformational failure criterion

The derivation of a deformational failure criterion for loose sand at low confining pressures was given in Chapter 4, from which the observation of slip planes in a deforming sand mass was expected when a relative displacement of about 6 mm occurred between two sliding blocks. Because no horizontal trace lines were included in the slope

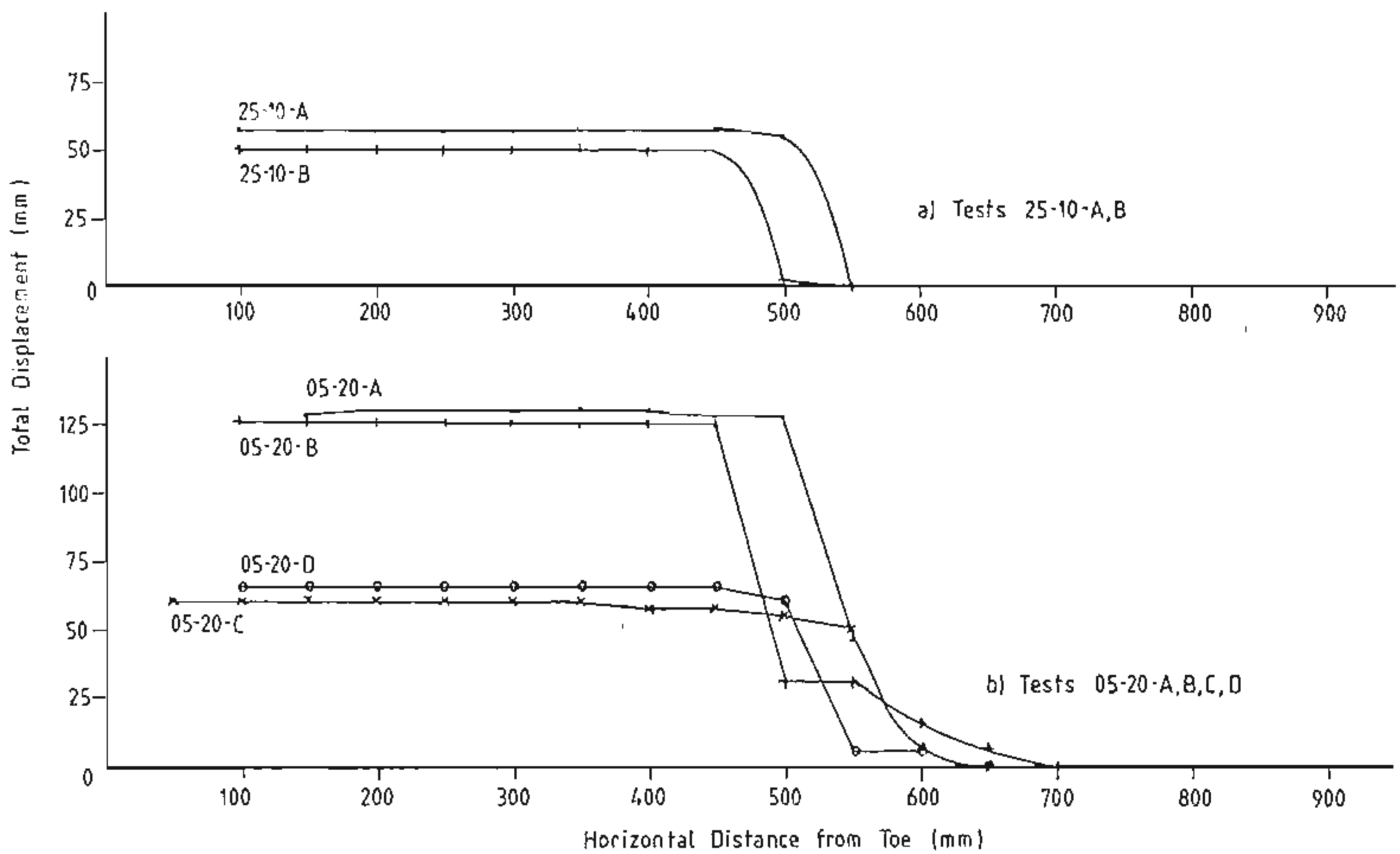

Figure 5.19 Total Displacements along Base

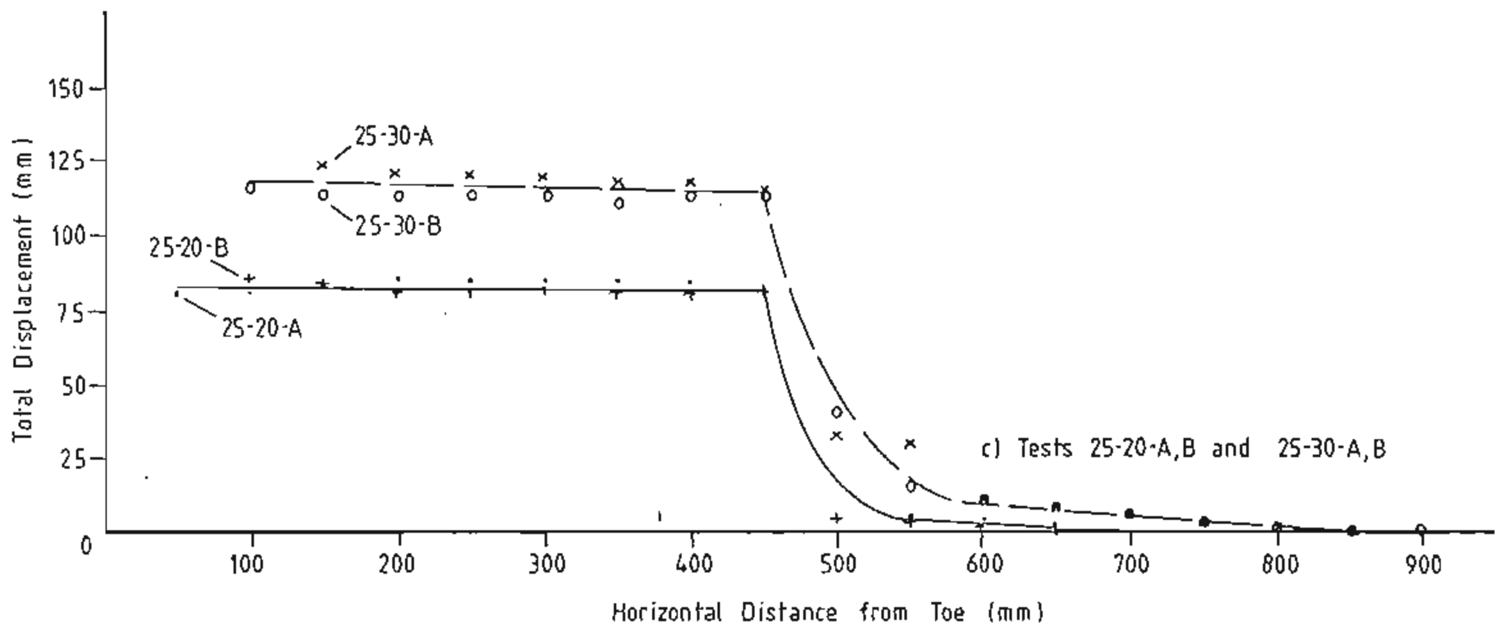

Figure 5.19 Total Displacements along Base (contd.)

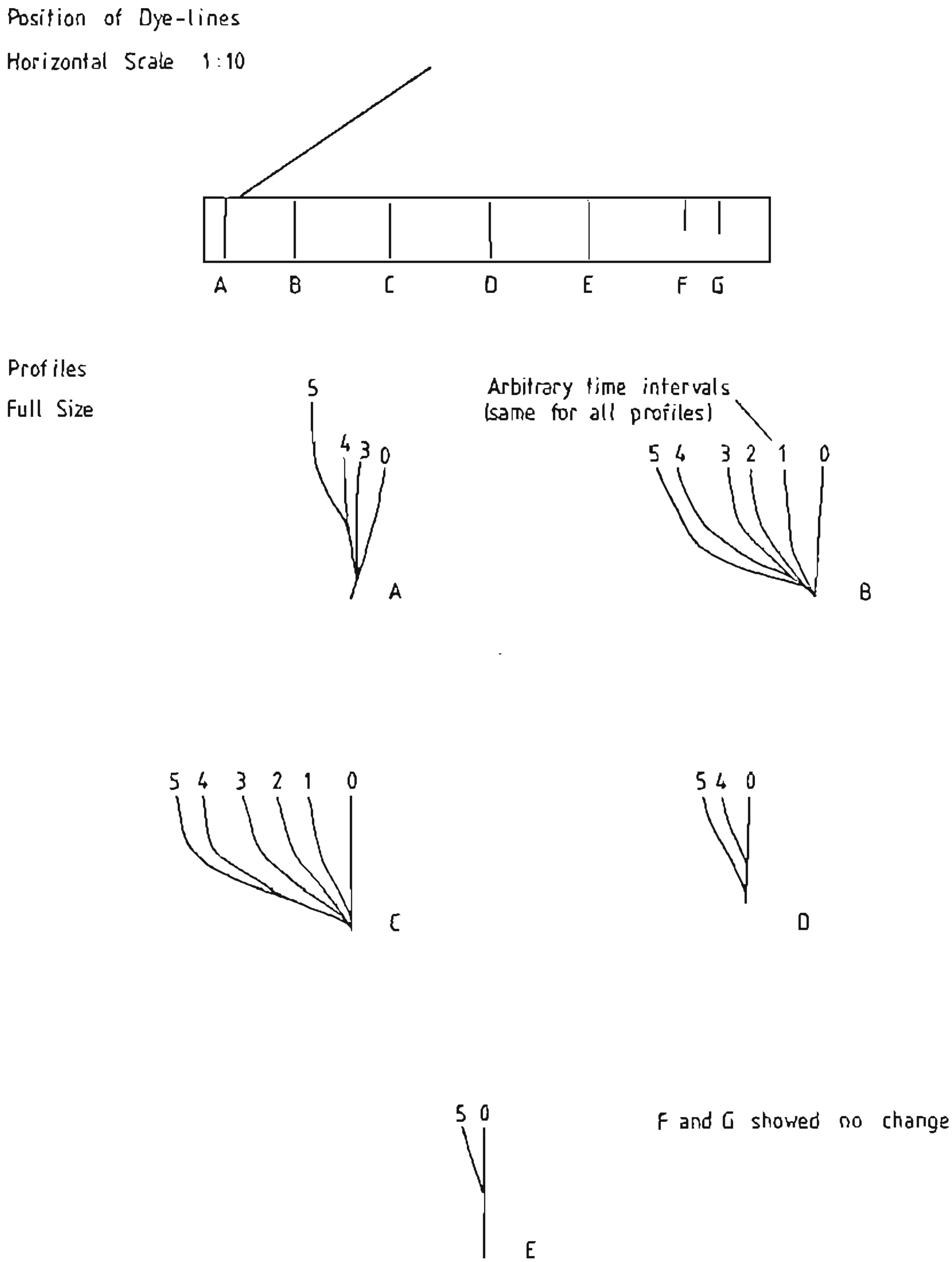

Figure 5.20 Vertical Dye-line Trace: Test 25-30-A

for test 05-20-D, a quantitative comparison was not possible with the most reliable displacement measurements. However, enough information was available for the comparison to be made for tests 25-10-A to 25-30-B. Table 5.5 gives estimates of the relative displacements between the crest region and the body of the slope at the time when the appearance of the slip plane between the two regions was noted. The reliability of the displacement readings was ±2.25 mm; however, an incorrect judgement of the time of formation of the slip plane would have increased the error for that reading. Nevertheless, half of the results compare very favourably with the assumed value of 6 mm.

TABLE 5.5

Displacements to the Formation of a Slip Plane

Test	Time to formation (secs)	Displacement (mm)
25-10-A	12	7.5
25-10-B	85	6.0
25-20-A	.4	6.5
25-20-B	5	13.0
25-30-A	1.2	11.0
25-30-B	.4	9.5

An alternative interpretation of the results which gave rise to the deformational failure criterion was to express the plane strain sample deformations as axial strain instead of vertical distance. Because the model slope had a vertical dimension four times that of the plane strain sample, the vertical deformation of the slope required to satisfy the failure strain would be 25 mm. The results shown in the previous table strongly supported the use of the deformational failure criterion in preference to one based on a failure strain.

5.4 Conclusions

5.4.1 Sequence of failure

The fundamental aim of this study was to determine the sequence of development of the kinematics of failure of a granular slope underlain by a weak cohesive layer. A reliable body of evidence from relevant physical model studies was collected and interpreted. The resultant description of the sequence of failure was in four phases (cf. Figure 5.12):

i) the slope was divided into three major regions by kinematic discontinuities; one slip plane through the weak layer and another through the sand with a larger zone of shear distortion between the two so that there existed two mobile regions, toe and crest, and the body of the slope which was static;

ii) further movement occurred along the slip planes and the angular distortion of the large shear zone tilted the lower half of the crest region back towards the body of the slope;

iii) within the large shear zone, a third slip plane formed so that the three slip planes were coincident and parts of the shear zone on either side of the third slip plane moved with the adjacent region;

iv) as displacement continued along the three slip planes, the toe and crest regions behaved essentially as two rigid blocks, which classified the end result as a two-wedge failure mechanism.

The appearance of the slip planes basically agreed with the prediction made from the deformational failure criterion in Chapter 4. There was no stage in the sequence of failure when the kinematics may have been sensibly interpreted as those of a circular slip.

5.4.2 Failure characteristics

Three parameters were used to define the position and inclination of the slip planes for the two-wedge failure mechanism, assuming that the plane through the weak layer was horizontal. Average values were established for these parameters in the central region of the slope where plane strain conditions existed. These values were more appropriate to the study than were those observed at the sidewall, and are listed below:

$$\alpha \;-\; 75^0 \pm 10^0$$
$$\beta \;-\; 56^0 \pm 5^0$$
$$\dot{x}/_H \;-\; 1.15 \pm .1$$

For the two-wedge mechanism, failure within the sand mass occurred on two planes, each within its own shear band, and in a horizontal shear zone near the base of the weak layer.

The total displacement observed during tests increased with increasing thickness of the bentonite layer, and the rate of displacement also increased. In the two tests with a base layer thickness of 5 mm, the failure did not reach the stage where the slip plane between the crest region and the body of the slope became visible, although some displacements did occur (cf. Figure 5.8). Therefore, it became apparent that the continuation of the sequence of failure through to the development of the two-wedge mechanism depended on the deformability of the base layer, which in this case was proportional to the layer's thickness. The time differences for development of failure may have been due to a limited shearing rate within the base layer, although the information available about the flow properties of the bentonite slurry did not allow any further conclusions to be drawn about this relationship. Figure 5.21 shows the variation in total displacement with base layer thickness. The results are too scattered for any firm relationship to be established, however, the trend appeared to show non-linearity.

5.4.3 Effects of the apparatus on failure

There were two major sources of disturbance from the apparatus to the model slope: the stiffening mechanism in the bentonite layer, and the frictional resistance of the sidewalls. The results of test EX20 showed that, although the retraction of the stiffening mechanism did induce an initial "jump" in displacements, its overall effect on the failure mechanism was negligible. It was possible that the lack of development of the slip planes in tests 25-05-A and B was promoted by the initial displacements which occurred when the vanes and mesh were retracted; however, further studies are required to enable the

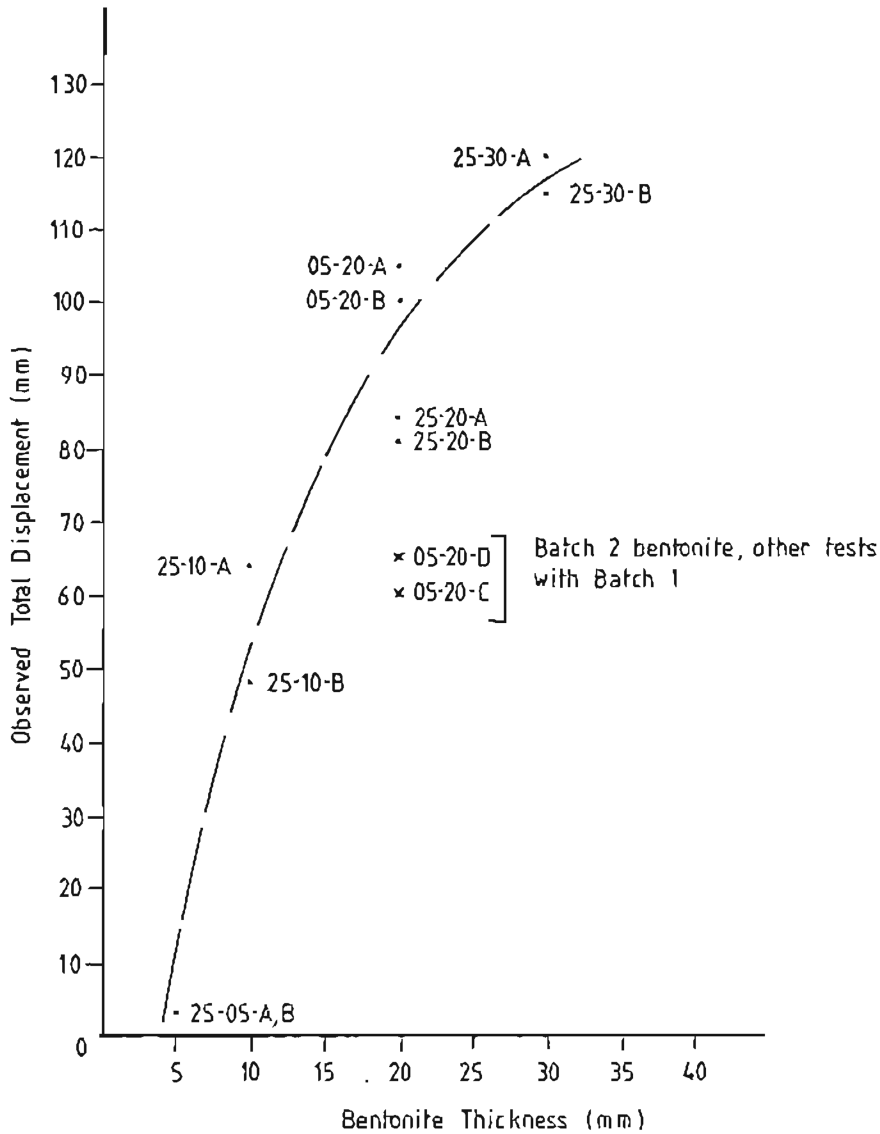

Figure 5.21 Total Displacements vs. Base Layer Thickness

relationship between layer thickness and development of the failure sequence to be explained fully. The author holds the opinion that the stiffening mechanism increased the rate of displacement for the first few millimetres but did not alter its magnitude; thus implying that the results from tests using a 5 mm layer would have been no different from those observed, other than the time taken to achieve the same displacements would have been greater.

The frictional stresses induced by the sidewalls did alter the slip plane characteristics, however, it was possible to determine the relationship between the observed characteristics and those in the central region of the slope. The usual concept of frictional drag on the boundary of a flowing material is that the particles near the boundary are retarded in their movement so that the material advances with a convex front in the direction of material motion. However, the typical curvature observed in all tests was concave in the direction of movement (cf. Plate 5). This apparently contradictory situation was explained by considering the frictional effects in terms of energy dissipation per unit width of slope. Because work was done at the sidewalls during the movement of the slope, to maintain an even rate of energy expenditure across the slope required a reduction in slip surface length towards the sidewalls, which resulted in the concave form of the slip scarps. A quantitative analysis of the stresses associated with friction from the sidewalls was not attempted, but the very complex nature of the relationship of the three-dimensional stresses in the plane strain device showed how difficult any study in this area would become. Thus, a solution to overcome the problems associated with sidewall friction is to ensure that the modelling apparatus promotes a plane strain region in which the model response may be investigated.

CHAPTER 6

ASSESSMENT OF MODEL PERFORMANCE

6.1 Introduction

In Chapter 3, the model studies for this project were placed in Class II, which meant that although the model did resemble some field situation, the results of tests could not be accurately magnified to predict the response of the prototype. The relationship between the model and the full scale situation can only be made by considering the model as a small prototype so that a suitable analytical technique, or numerical model, may be found to describe adequately the observed test data. This analysis is then applied to the field situation with the major assumption being that the analysis still remains relevant even though many differences may exist between the model and the prototype.

The sequential nature of the failure of the sand slope offered many aspects through which the model performance could be considered. To keep within the bounds of the available data, the stages which were considered for analysis were the stable slope just at the point of initiation of failure, and the mobile slope when the two-wedge mechanism had fully developed. The distribution of stress through the slope was investigated for the initiation of failure and several slope stability analyses used in engineering design gave slip surface characteristics which were compared with those of the observed two-wedge mechanism.

Many geotechnical investigations of slopes and embankments consider a numerical model of the prototype to aid in design work. Two different numerical models were used in the course of this study, both of which were especially suited to the clastic nature of the main modelling material. One model was based on the estimation of inter-particle forces which were each evaluated for mobilised strength and gave some insight into the stress conditions at the initiation of failure. The second model described the kinematics of a particulate assembly, and the resulting failure sequence generated by the numerical model was compared with the observed slope deformations.

Some of the kinematics of the slope failure appeared similar to the discharge patterns of granular material from a hopper. This interpretation of movement not only led to the comparison of deformation characteristics, but also implied some possible stress distributions within the material.

All of the above topics are considered in detail in the following sections, together with an approach based on the virtual work principle, with which the author achieved close correlation between predicted and observed parameters for the two-wedge failure mechanism.

6.2 Stability Analyses

6.2.1 Popular methods of analysis

Before the turn of this century, there were only three widely recognised methods relating to stability analysis: Coulomb's wedge, Rankine's active and passive stress states, and Culmann's wedge procedure. The first two were basically designed for retaining wall analysis, and Culmann's procedure was a slope stability analysis. In the first two decades of this century, significant impetus was given to stability calculations using a cylindrical failure surface after several landslips in Sweden showed this characteristic pattern; however, the detailed work of Collin (1846) on landslides in clays should be given the place of honour as the first work concentrating on curved slip surfaces.

As engineering technology developed, the scale and frequency of construction of cut slopes and embankments increased, creating a demand for more reliable design procedures and stability analyses. The techniques of stability analysis were enhanced by the advent of the electronic computer because of its large computational and storage capacity. The limit equilibrium methods which relied on an iterative process to reach a solution, were particularly adaptable to computer programming. A new approach to slope stability was achieved through the numerical solution of Kötter's equations (cf. Sokolovski, 1960), however, the physical restrictions of the solution did not make the analysis flexible enough to be applied to most situations. Further advances in the analysis of slopes, and geotechnical problems in general, were made with the introduction of the systematic arching theory (Trollope, 1957), stress-dilatancy theories (e.g. Rowe, 1962), critical state soil mechanics (Schofield and Wroth, 1968), and numerous finite element and finite difference numerical models. It was not practical to mention the vast number of new failure theories or variations on the application of a number of stability analyses; therefore, only those approaches which were found to be relevant to the modelling situation are given further attention in this chapter.

A simplistic view of slope stability analyses placed each in one of three categories: slip circle analyses, non-circular analyses, and analyses based on soil plasticity. The results of the physical model studies reported earlier showed that the slope failure was not circular, and the observed slip plane characteristics throughout the failure sequence did not show trends which might be described by theories of soil plasticity. If a more exhaustive investigation of the soil plasticity predictions for the modelling situation was conducted, the likelihood of a successful prediction would be small because of the continual change in stress conditions and the difficulty in selecting a suitable yield function for the material. Thus, the most acceptable type of analysis was that based on the non-circular slip, which is considered in detail in the next section.

6.2.2 Stability considerations for non-circular slips

One of the simplest stability analyses was based on static equilibrium of a wedge of soil without regard to the stress distribution within the soil. Coulomb used this method for the prediction of his active earth pressures on retaining walls in 1776, with the only change being the substitution of wall friction instead of the material friction which exists in a slope. The modern equivalents of this method are given in Seed and Sultan (1967) and Wu (1976). The application of this method to a two-wedge failure mechanism was simple because the major variables were the positions and inclinations of the slip planes.

Rendulic (cf. Parcher and Means, 1968) developed a method for the analysis spreading failure which used a simple wedge analysis at several vertical sections along the base of the embankment (or slope), with a number of trial wedges at each section. The two slip planes which formed the trial wedges were symmetrical about the vertical line of the section, and a third plane passed through the weak base layer.

The resurgence of interest in wedge-type failures in embankments in the United States of America led to the publication of a manual by the U.S. Army Corps of Engineers (Anon, 1970), which proposed several approaches to the assessment of stability depending on the type of structure and the information available. Once again, the calculations were based on simple wedge equilibrium; however, the boundary between the two wedges was restricted to the vertical. The critical case was found by varying the position of the wedge and the angle of its second slip plane so that the least degree of stability existed. The methods of analysis presented by Chugaev (1964) were of the same form as those in the U.S. Army manual (ibid.), with the restriction of a vertical interface between the two sliding blocks.

Trollope (1973b, 1975, and 1979) has presented a number of papers in which an equation based on the principle of virtual work was used to estimate the stability of slopes, especially those which fail by a two-wedge (Trollope's third order) mechanism. The writer proposed, on the basis of the available experimental evidence, that the failure mechanism developed sequentially with the separate formation of each of the slip planes. Hence, the conditions for the initiation of failure along a weak base layer were estimated from a virtual work equation applied to that layer for which the relevant stress levels were derived from the writer's systematic arching theory (cf. Trollope, 1968). The important features of this approach were the use of a stress distribution within the slope and the estimate of stability based on the energy balance in the virtual work equation, rather than the usual comparison of strength parameters.

The development of the limit equilibrium (slices) method for use with the slip circle analysis prompted the establishment of a similar method for a general slip surface (e.g. Janbu, 1957). An extension of this method was presented by Morgenstern and Price (1965), with particular reference to the use of electronic computers. The limit equilibrium method created a set of indeterminate equations which required a number of assumptions be made before their solution could proceed.

Even though the assumptions may have been reasonable, the solution given by the method was only approximate. The slices into which the soil mass was divided were hypothetical, and the kinematics of failure were not considered, although the slip boundary used may have followed some of the slip planes which formed a kinematically admissible mechanism.

The solution mentioned above was based on a predetermined slip surface and numerical techniques which required the use of a computer for efficiency; however, Baker and Garber (1978) demonstrated an analytical method for the solution of the limit equilibrium equations. Variational calculus was used to determine the slip surface which had the minimum factor of safety. Unfortunately, there were some kinematic constraints placed on the change of direction of the slip plane across the boundary between two materials which could not accommodate the angular changes observed in the model studies.

After an extensive series of model retaining wall tests using granular materials, Reimbert and Reimbert (1974) proposed a generalised equation for thrust on a retaining wall, with a formulation significantly different from the Rankine and Coulomb analyses (cf. Wu, 1976). The writers derived an empirical formula which considered the angle of internal friction of the material, the inclination of the backfill, the slope of the wall, and the material density; however, the test results reported showed the thrust was independent of the friction mobilised at the wall. The approach was applied to the model slope by considering the toe region as a rigid mass which appeared effectively as a retaining wall to the crest region. Stability was calculated by comparing the thrust from the crest region with the shear force available along the base of the toe region.

It is theoretically possible to find an exact solution to a slope stability problem by using limit analysis; however, there are a large number of mathematical restrictions on the use of the method, which render it impractical for most cases. Chen (1975) gave a detailed review of this topic in which the restrictions on the material for use in limit analysis were:

(i) perfectly plastic (no work hardening or softening);

(ii) convex yield surface and applicability of normality conditions; and

(iii) small changes in geometry up to the limit load.

The reason for the impracticality of limit analysis becomes obvious when the above restrictions were applied to any real situation, especially when the failure mechanism developed sequentially.

The majority of stability analyses required a number of specific parameters with a single value to be input so that a solution may be achieved. It is evident from any field records that soil parameters are not a particular value, but may be described statistically by a mean value with a variance or a confidence interval. An example of a probabilistic approach to slope stability was given by Vanmarcke (1977), who used limit equilibrium analyses for estimation of the factor of safety. A recognised statistical approach was not used for the interpretation of results or the definition of material parameters for this study, although the two-wedge slip plane characteristics were averaged values. The small number of tests from which the stress-deformation response was determined precluded any form of averaging. Thus, the statistical approach was considered to be relevant to a prototype example, but not suitable for the data available from the modelling situation for this study.

The purpose of a Class II model is fulfilled when the data collected from the experiments is adequately described by some analytical procedure or numerical model. Therefore, several of the above slope stability analyses were applied to the specific case of the model slope used for this study, in an effort to establish an analysis which might be relevant to the estimation of the stability of a prototype slope. The particular analyses used were: the simple wedge analysis, with the variations of the U.S. Army Corps of Engineers wedge method and Rendulic's spreading failure analysis; the Morgenstern and Price analysis; Trollope's virtual work approach; and a wedge method using Reimbert and Reimbert's general thrust formula.

6.2.3 Application of stability analyses

All of the analyses, except one, were carried out under the assumption that the sequence of failure had continued to the point where the two-wedge failure mechanism was dominant, even though the analysis may not have recognised the kinematics of the slip mechanism. The virtual work approach proposed by Trollope (1975) considered the slope at the beginning of the failure sequence. Because the rigid block conditions of the two-wedge mechanism did not apply during the initial stages of the failure sequence, the distribution of the shear stresses in the weak layer were not tacitly assumed to be uniform. Therefore, the stability analysis for the initial stages of failure depended on the interaction between the sand and the bentonite, for which the only observation was that the movement appeared relatively uniform over the whole of the toe region (see Figure 5.1(a)).

6.2.3.1 Wedge methods

The simple form of the two-wedge planar failure mechanism made force equilibrium calculations for both wedges quite feasible. The values of these forces were dependent on the failure surfaces chosen; therefore, the estimation of the slip plane characteristics which promoted the maximum average shear stress along the base layer was the purpose of these analyses, rather than the analysis of a particular slope and failure mechanism. This section considers three wedge methods for which the calculated values of maximum average base shear stress and the associated slip plane characteristics are given. For ease of comparison among methods, the parameters involved have been rendered dimensionless where applicable: e.g. the average shear stress along the base layer became $\frac{\tau}{\gamma H}$, and the distance from the toe to the point of intersection of the slip planes became $\frac{x}{H}$; where γ was the unit weight of the sand and H was the crest height of the slope.

(i) The generalised two-wedge failure

Figure 6.1(a) defines the parameters used for these calculations and the same nomenclature was retained throughout this chapter. The variables for the calculation of shear stress were $\frac{x}{H}$, α, and β; while

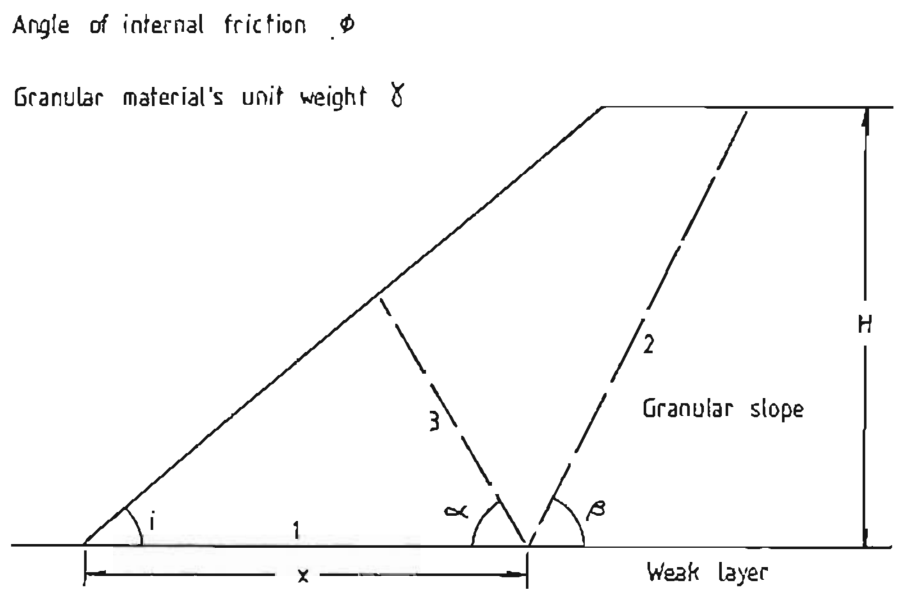

Figure 6.1a Parameters for the Two-wedge Mechanism

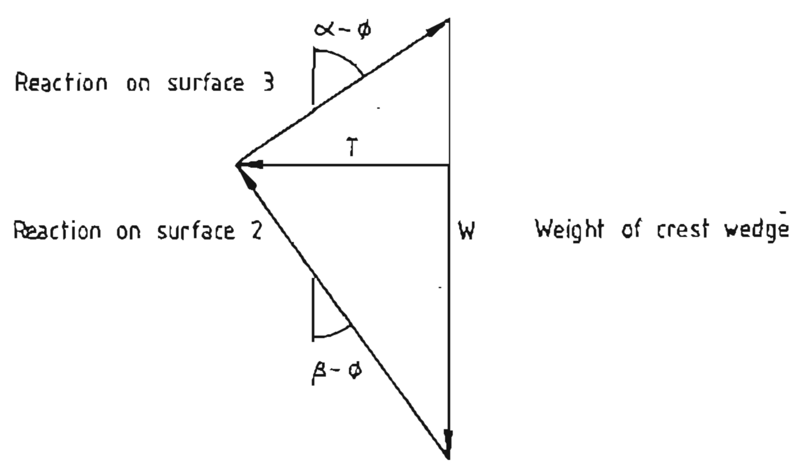

Figure 6.1b Force Equilibrium Polygon

γ, H, the angle of internal friction, and the slope angle remained constant. Figure 6.1(b) shows the force equilibrium polygon from which the thrust (T) on the toe wedge was calculated:

$$\frac{\tau}{\gamma H} = \left(\frac{T}{\gamma H^2}\right) / \left(\frac{x}{H}\right) \tag{6.1}$$

Equation 6.1 may be represented analytically as a single-valued function in the variables $\frac{x}{H}$, α and β. A computer study of this function showed that the value of the shear stress calculated did have an optimum. Therefore, the analysis of this failure mechanism was made very efficient by the application of numerical optimisation techniques to the function for the non-dimensional shear stress.

Because of the changes in geometry, a single continuous function for shear stress for all realistic values of the variables could not be derived; however, a piecewise continuous function in three parts satisfied the geometrical constraints. The three sections were defined by the location of the intersections of the slip planes with the slope's free surface:

(i) both planes intersected the face of the slope between the toe and the crest;

(ii) one plane cut the face of the slope and the other cut behind the crest; and

(iii) both planes emerged behind the crest, in the plateau region of the slope. The functions and their ranges of application were as follows:

$0 < \frac{x}{H} < (\cot i - \cot \beta)$

$$\frac{W}{\gamma H^2} = \frac{\left(\frac{x}{H} \sin i\right)^2 \sin (\alpha + \beta)}{2 \sin (i + \alpha) \sin (\beta - i)} \tag{6.2}$$

$(\cot i - \cot \beta) \leq \frac{x}{H} \leq (\cot i + \cot \alpha)$

$$\frac{W}{\gamma H^2} = \frac{x}{H} + \frac{\cot \beta - \cot i}{2} - \frac{(\frac{x}{H})^2 \sin i \sin \alpha}{2 \sin (i + \alpha)} \qquad (6.3)$$

$(\cot i + \cot \alpha) \leq \frac{x}{H}$

$$\frac{W}{\gamma H^2} = \frac{\cot \alpha + \cot \beta}{2} \qquad (6.4)$$

The shear stress was calculated for all ranges of $\frac{x}{H}$ using:

$$\frac{\tau}{\gamma H} = \frac{W}{\gamma H^2} \cdot \frac{\sin (\beta - \phi) \sin (\alpha - \phi)}{\sin (\beta + \alpha - 2\phi) \, (\frac{x}{H})} \qquad (6.5)$$

Numerical optimisation techniques are partitioned into two categories: bounded or unbounded functions; which may be evaluated with the aid of the function's derivative or without. Although there were physical bounds to the shear stress function (e.g. $\frac{x}{H} \geq 0$), these bounds were not mathematically necessary for the calculation of the optimum; thus, the function was treated as if it were unbounded. The multi-staged nature of the function and the number of variables made an optimisation without the use of derivatives the more convenient way to approach the analysis. Kuester and Means (1973) list several search methods for unconstrained multivariable functions with particular emphasis on their application to computing using the FORTRAN language. The techniques considered for use with the shear stress function were those which were based on the Nelder and Mead, Hooke and Jeeves, Rosenbrock, and Powell algorithms. The Powell algorithm (ibid, pp. 331-343) was found to be the most useful for this particular function because it gave rapid convergence to the optimum and the accuracy of the variables in the end result was able to be specified.

The results for this and subsequent analyses are given in Table 6.2, included in Section 6.2.5. The method considered by Seed and Sultan (op. cit.) took the same form as the above analysis, with the major difference being the location of the pre-determined slip plane which lay along a sloping clay core instead of in a weak base layer.

The writers did not use numerical optimisation techniques, but found the optimum by a graphical procedure after a number of mechanisms were considered.

(ii) U.S. Army Corps of Engineers wedge method

The design procedures recommended in the manual restricted the value of α to 90^0, and it was suggested that the thrust between the toe and crest blocks be inclined at the slope face angle, or half that value. Therefore, this method was a specific case of the generalised two-wedge method discussed previously, and equations 6.2, 6.3 and 6.4 were used in the calculation. The shear stress equation became:

$$\frac{\tau}{\gamma H} = \frac{W}{\gamma H^2} \cdot \frac{\tan(\beta - i)}{(\frac{x}{H})} \qquad (6.6a)$$

or

$$\frac{\bar{\tau}}{\gamma H} = \frac{W}{\gamma H^2} \cdot \frac{\tan(\beta - \frac{i}{2})}{(\frac{x}{H})} \qquad (6.6b)$$

depending on the angle of thrust on the toe wedge. The Powell algorithm was used to find the optimum value of shear stress; however, the function was reduced to two variables, $\frac{x}{H}$ and β, for this example because the boundary between the toe and crest wedges was always vertical.

(iii) Rendulic's spreading failure analysis

Parcher and Means (op. cit., p. 419 f) described the Engesser graphical procedure for calculating the average shear force along the base of an embankment due to the thrust of a graben block of material. The procedure was based on the closure of a force polygon and was not modified for application to the model slope. Figure 6.2 shows the variation of average shear stress along the base and the corresponding slip plane angles for the case of the model slope.

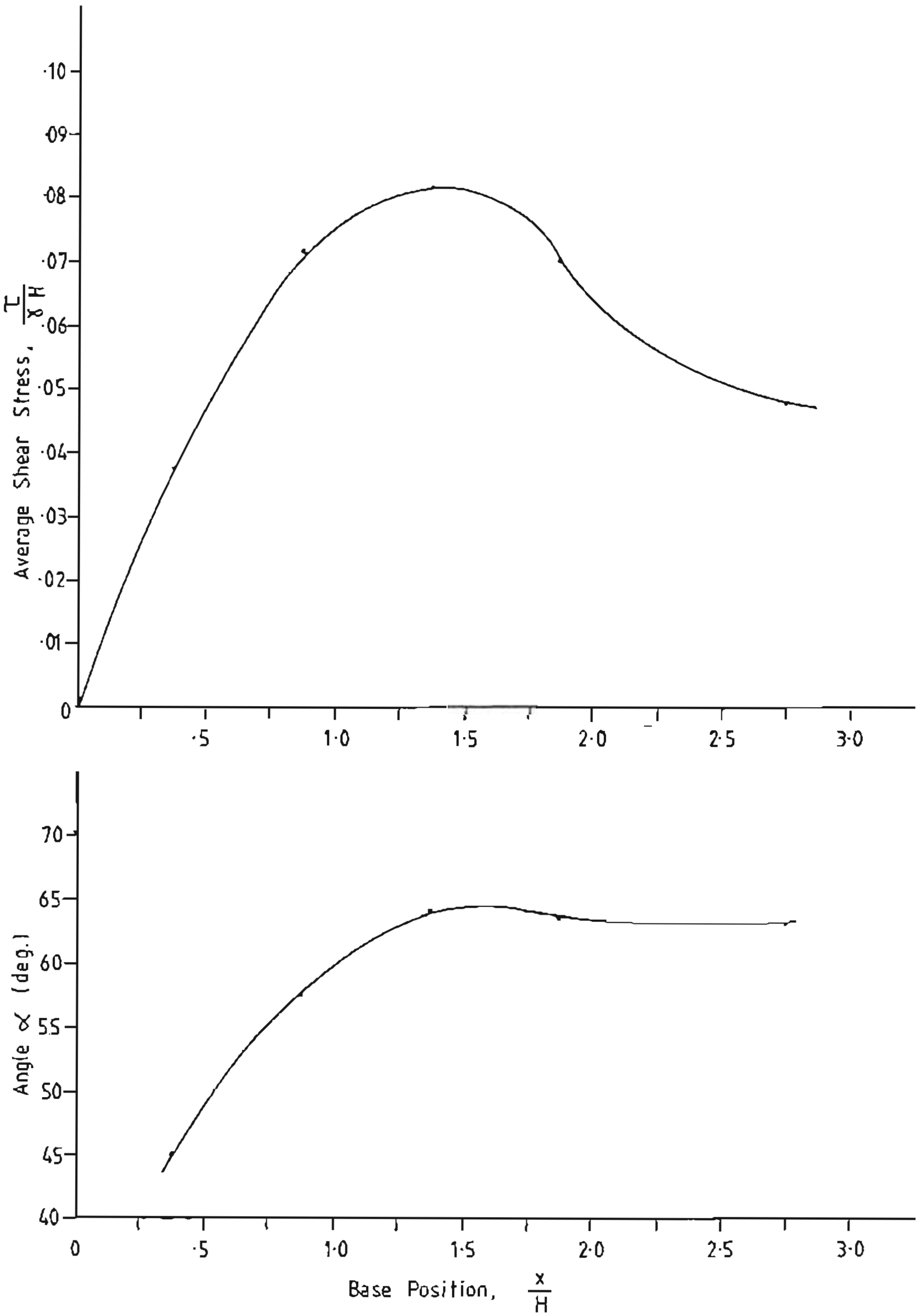

Figure 6.2 Rendulic Spreading Failure

6.2.3.2 Morgenstern and Price analysis

The generalised method of slices proposed by Morgenstern and Price (op. cit.) used the same basic formulation as previous researchers had proposed; however, the writers' scheme to overcome the static indeterminacy inherent in the limit equilibrium equations used a method which paid some attention to the magnitude of the interslice forces and the ratio of the vertical to horizontal components of those forces. This method was not exact (although the errors involved were small) and some assumptions had to be made, including the position of the slip boundary. One point in favour of this method of slices was that the ratio of the interslice forces and the position of the thrust line through the slices were included as part of the results output by the computer program.

Whitman and Bailey (1967) published an article which reviewed the use of computers for slope stability analysis, in which particular attention was given to a program based on the Morgenstern and Price analysis. The writers concluded that the method should be used to check the acceptability of results obtained from simpler methods of analysis (e.g. the simple wedge method). The conclusions drawn from a computer analysis should not be based on one or two calculations, but on a planned series of calculations in which the position of the failure surface and the assumption of the thrust distribution between slices were varied. The position of the thrust line and the ratio of the vertical to the horizontal interslice forces should also be checked so that a reasonable assessment of the stability of the slope may be made.

A series of stability analyses was prepared for the study of the model slope, for which a general diagram is shown in Figure 6.3 along with the thrust distribution found most suitable after preliminary tests. A summary of the results of nine slip conditions is given in Table 6.1 and the results are presented graphically in Figures 6.4(a) and 6.4(b). Thus, it was possible to ascertain a combination of the variables, $\frac{X}{H}$ and β, which produced the lowest factor of safety. The analysis required that the base layer should be given a definite value for shear strength so that a factor of safety along the slip surface could be calculated; hence, an appropriate value for the shear

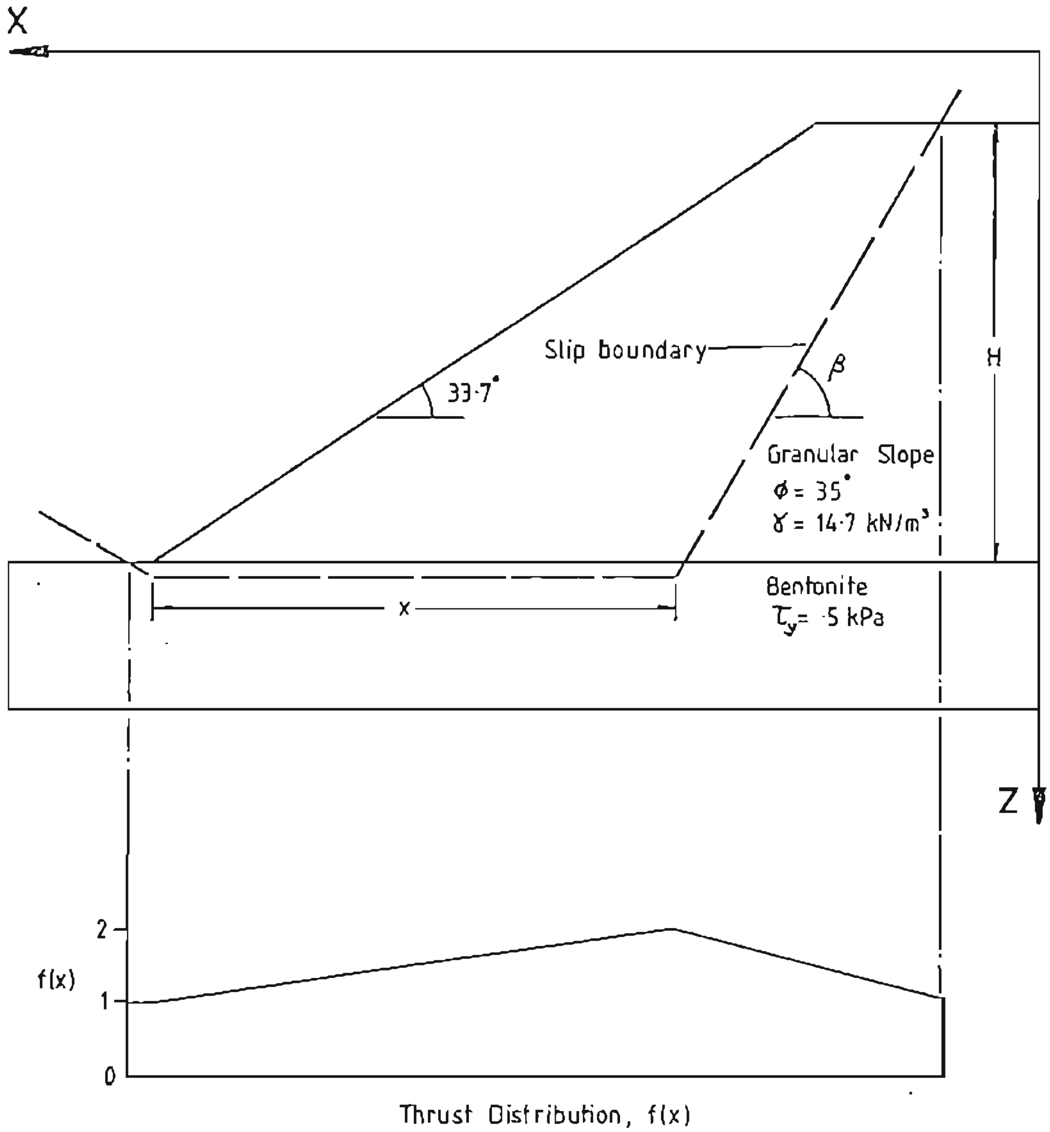

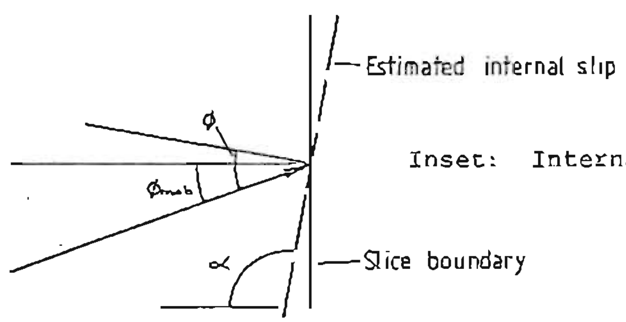

Inset: Internal Slip Plane

Figure 6.3 Morgenstern-Price Analysis - Generalised Diagram

TABLE 6.1

Summary of Results from Morgenstern-Price Analysis

Surface	$\frac{x}{H}$	β	F of S	λ	ϕ_{mob}*	α
1	.75	45^0	1.070	.281	29.3^0	95.7^0
2	.75	55.2^0	1.130	.300	31.0^0	94.0^0
3	.75	64.4^0	1.367	.286	29.8^0	95.2^0
4	1.125	45^0	1.060	.213	23.1^0	101.9^0
5	1.125	55.2^0	.999	.249	26.5^0	98.5^0
6	1.125	64.4^0	1.080	.279	29.2^0	95.8^0
7	1.5	45^0	1.111	.169	18.7^0	106.3^0
8	1.5	55.2^0	1.035	.192	21.0^0	104.0^0
9	1.5	64.4^0	1.070	.212	23.0^0	102.0^0

* on slice boundaries

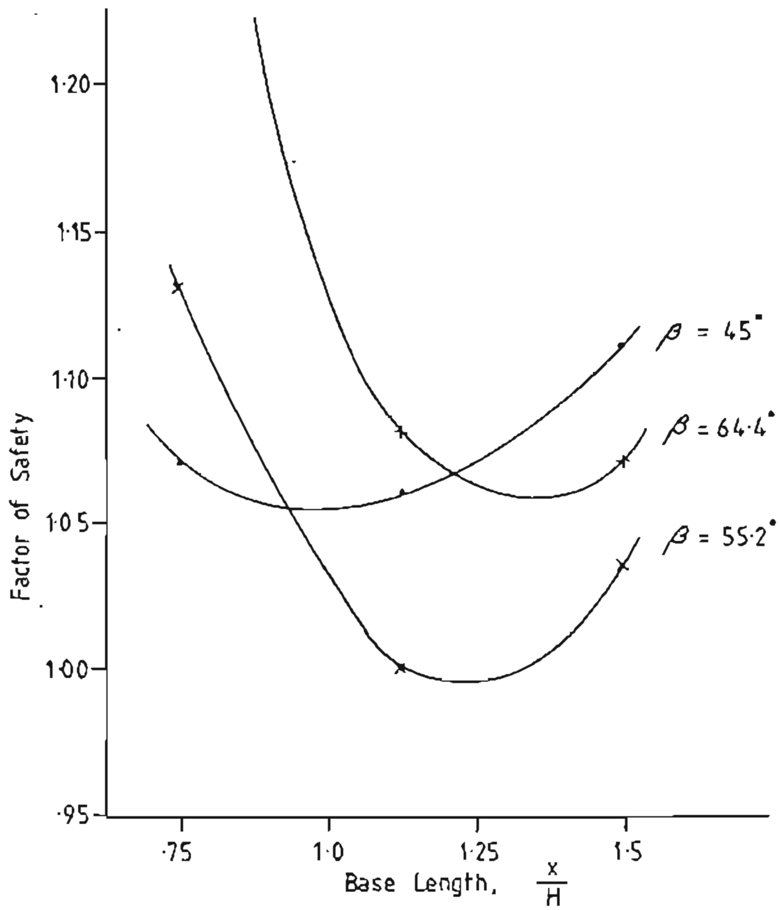

Figure 6.4a Variation of Factor of Safety

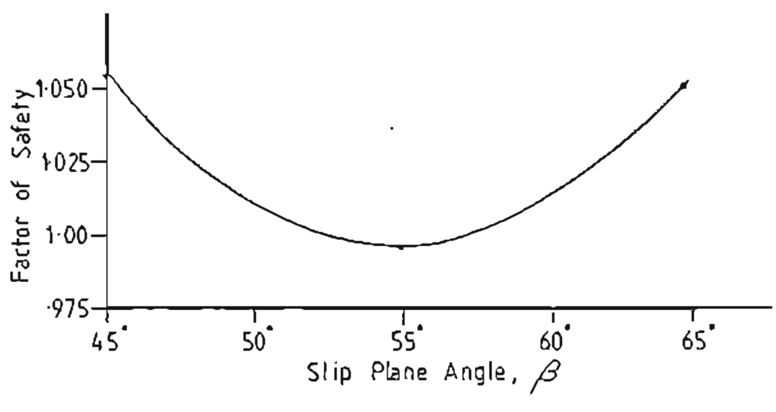

Figure 6.4b Plot of Minima

strength was estimated by an iterative process in which the shear strength was varied until the factor of safety for the observed slip boundary equalled 1.0. Although the value of the factor of safety was pre-determined at 1.0 for the observed failure surface, the values of parameters used for the calculations did not influence the conditions for the minimum factor of safety, which could have gone below 1.0 in the analysis, but would have been meaningless in reality.

One of the assumptions made for the analysis involved the relationship between the vertical and horizontal interslice forces, which was represented by:

$$X = \lambda f(x) E \tag{6.7}$$

where X = vertical force

E = horizontal force

λ = constant (produced by the analysis)

$f(x)$ = thrust distribution (see Figure 6.3)

Therefore, the coefficient $\lambda f(x)$ determined the level of mobilised friction at the slice boundaries, which had a maximum value corresponding to the maximum of $f(x)$. The mobilised friction angle represented the inclination of the interslice reaction to the horizontal from which an estimate of the angle of an internal slip plane, α, was made (see inset in Figure 6.3). Values of λ, ϕ_{mob} and α for the stability analyses carried out are included in Table 6.1. Although this limit equilibrium method did not explicitly consider the kinematics of the possible slips investigated, some estimate of the characteristics of a two-wedge mechanism were estimated from the results produced by the computer program used.

6.2.3.3 Reimbert and Reimbert's thrust analysis

As mentioned earlier, the empirical thrust analysis proposed by Reimbert and Reimbert (op. cit.) offered a new approach to retaining wall design, and was centred on the following general equation:

$$T = \frac{\gamma h^2}{2} \left(\frac{\pi - 2\phi}{\pi + 2\phi}\right)^2 \left(1 \pm \frac{2\psi}{\pi}\right) \left(\frac{\pi - (\alpha + \phi)}{\frac{\pi}{2} - \phi}\right) \qquad (6.8)$$

where T was the total thrust (force), γ was the material unit weight, ϕ was the angle of internal friction, and the parameters α and ψ are defined in Figure 6.5(a). Figure 6.5(b) illustrates the way in which the thrust analysis was related to the conditions in the model slope. Equation 6.8 was adjusted for the calculation of the average shear stress induced along the base of the toe wedge, and using a value of $\phi = 34^{o}$ (.5934 radians) yielded:

$$\frac{\tau}{\gamma H} = .03321 \left(\frac{h}{H}\right)^2 \frac{(\pi + 2\psi)(\pi - (\alpha + .5934))}{\left(\frac{x}{H}\right)} \qquad (6.9)$$

The slope geometry was not specifically catered for by the generalised thrust equation because the angle of the backfill changed abruptly at the crest of the slope, but the analysis was based on a constant angle, ψ, in the region affected by the active wedge. Therefore, an effective value of ψ was estimated from the slope of the single free surface which enclosed an area equal to that in the real wedge (see Figure 6.6). This procedure resulted in a complex set of equations which ultimately gave ψ as a function of $\frac{x}{H}$ and α. It can be shown that the variable $\frac{h}{H}$ was also a function of $\frac{x}{H}$ and α; thus, equation 6.9 can be reduced to an equation in two variables: $\frac{x}{H}$ and α.

The analytical approach to find the condition which promoted the highest average shear stress along the base was similar to that used with the simple wedge analysis; however, the rate of change of slope of equation 6.9 near the optimum was small. Thus, a graphical check was used in conjunction with the numerical optimisation technique so that confidence could be placed in the values corresponding to the optimum.

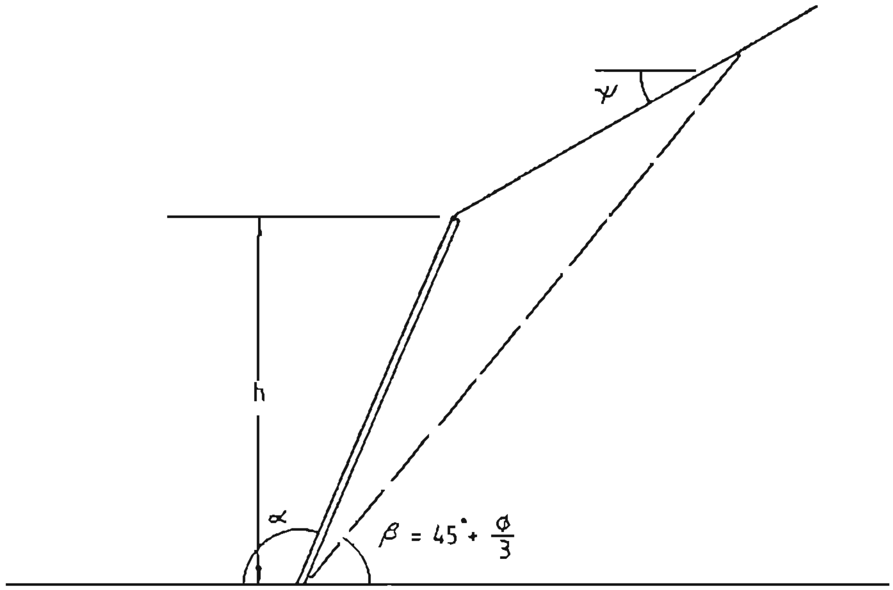

<u>Figure 6.5a</u> Retaining Wall Parameters

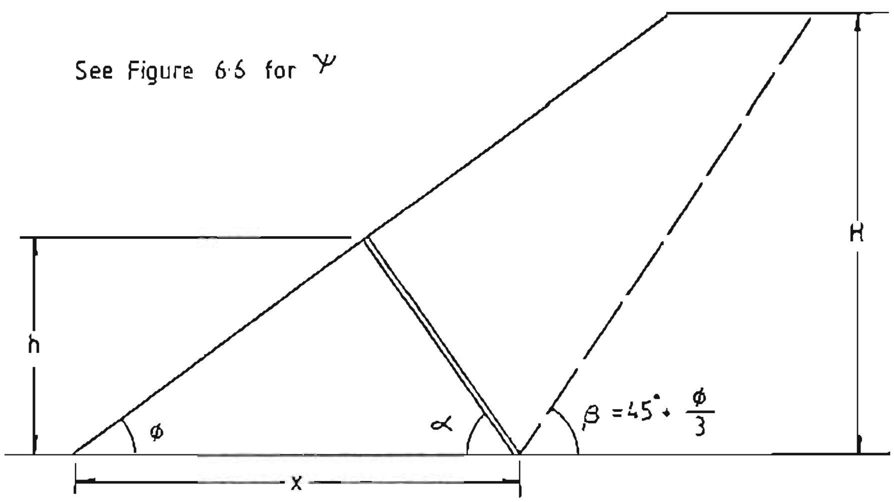

<u>Figure 6.5b</u> Retaining Wall Related to Model Slope

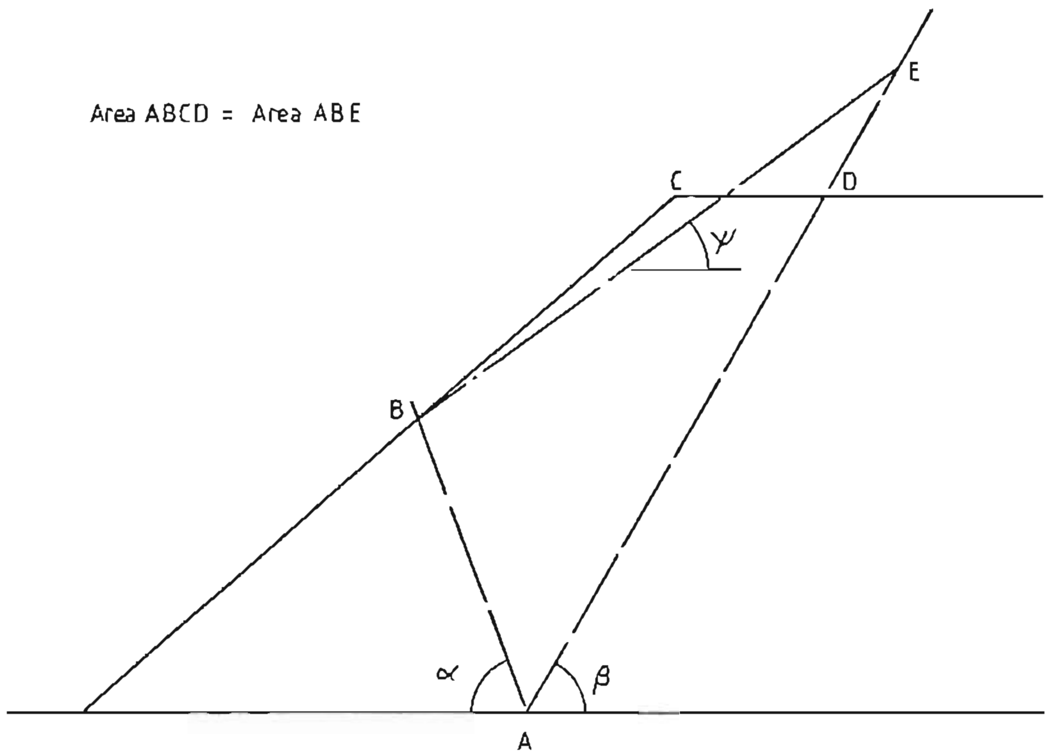

Figure 6.6   Effective Backfill Angle

The retaining wall formula was applicable to a state of active slip within the fill when a slip plane formed at an angle of $(45 + \phi/3)$ to the horizontal. Because the condition of slip was used both at the wall and in the fill, this analysis pertained to the slope when the two-wedge mechanism had formed, and not to an earlier stage in the failure sequence.

6.2.3.4 Trollope's virtual work approach

Trollope (1975) described a physical model study which led the wrtier to conclude that the observed third order (two-wedge) failure mechanism formed sequentially, rather than having all slip planes appear at the same time. The scope of this thesis was centred around a more detailed investigation of the sequence of failure which was given the first serious consideration by the writer. The sequential failure concept was used by Trollope (ibid.) with the stresses predicted by the writer's systematic arching theory to propose a design method for slopes in strain-softening materials, one example of which was a simple granular slope underlain by a weaker layer. Thus, the model slope was easily evaluated by the design method, and the shear stress distribution along the base for the no arching case is shown in Figure 6.7.

Trollope assumed that the slip plane along the base layer would be formed beneath the slope from the toe to the point of maximum shear stress, located by the distribution line BC in Figure 6.7. The stability of the slope was assessed by calculating the minimum allowable strength along the base by balancing an equation based on the virtual work principle for which the work input was derived from the energy released by the shear stress in the base of the slope moving through a uniform virtual displacement of Δ. The value calculated for the minimum allowable strength along the base of the slope was:

$$\text{no arching} \quad (k = 1) \quad \frac{\tau}{\gamma H} = .081;$$

with the slope angle being 34^0. The dimensionless length of the base slip plane, $\frac{x}{H}$, was .905.

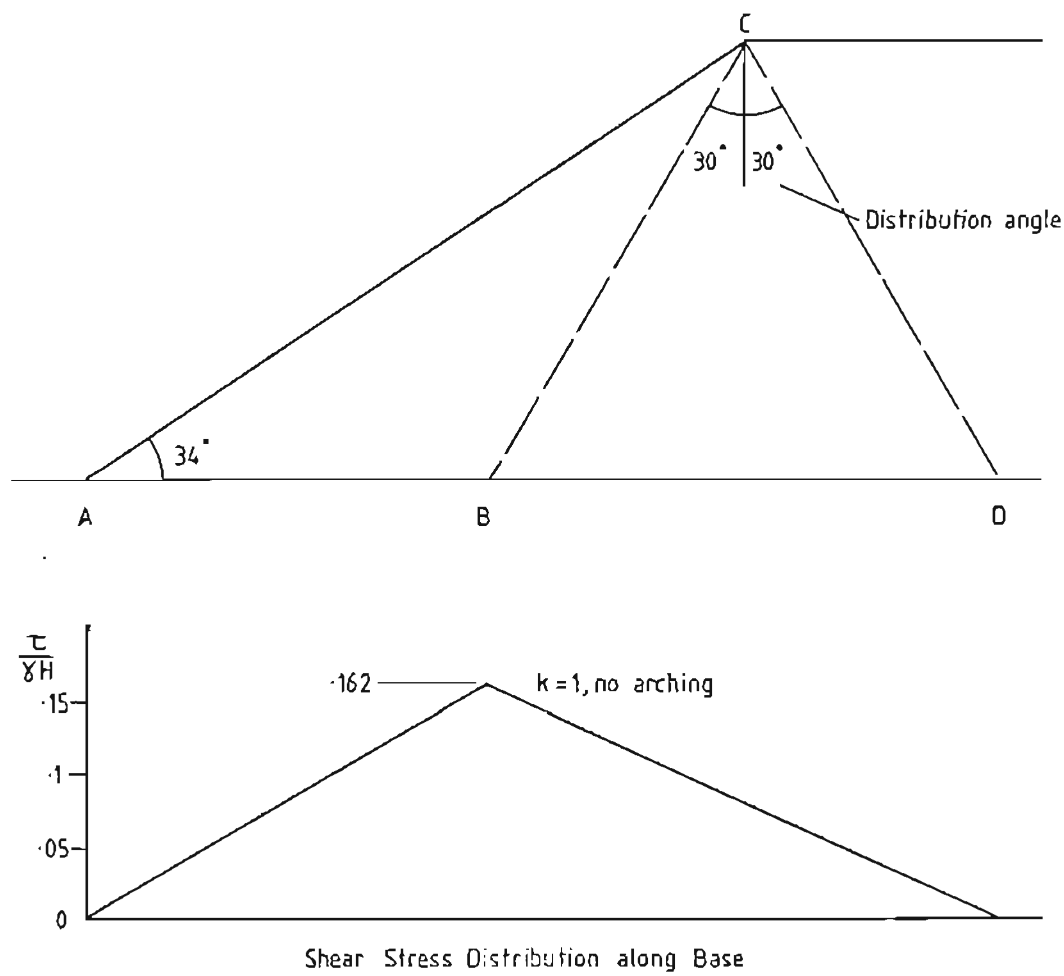

Figure 6.7 Clastic Stress Distribution

The writer recommended that after the third order mechanism had fully developed, it would be appropriate to carry out a simple statical analysis using residual strength parameters to determine the final state of stability of the slope. The use of the systematic arching theory in the virtual work approach implied that the gravitationally induced shear stress along the base was attributable to the weight of the soil material in front of the distribution line BC (see Figure 6.7); and unless a failure criterion was adopted to determine the preferred slip directions, no predictions were possible regarding the inclination of the slip planes through the granular material.

A variation on this analysis, which was more consistent with energy principles, was to assume that the location of the slip plane was determined for the condition where the virtual work expended per unit length of the slip plane was a maximum. That is, the length of the slip plane, x, was defined so that:

$$\frac{\int_{o}^{x} \tau ds.\Delta}{x} = \text{maximum} \qquad (6.10)$$

where τ was the clastic shear stress along the base, ds the distance variable and Δ was a virtual displacement. The linear form of the clastic stress distribution made the evaluation of equation 6.10 simple, and yielded:

$$\text{no arching} \quad (k = 1) \qquad \frac{\tau}{\gamma H} = .097$$

Thus, the value of minimum allowable shear strength of the base material was roughly 20% higher than that calculated from Trollope's analysis. The new dimensionless length of the slip plane was 1.366. Further attention is given to this form of analysis in the following section and also when numerical models are discussed.

6.2.4 An analysis based on virtual work

Karaal (1977a,b) presented a method of stability analysis which was fundamentally an upper bound limit analysis for the case of a general slope. The use of the limit analysis technique required that a number of assumptions be made. The assumptions may have been acceptable when considering purely cohesive materials, however, the stress-deformation response of the loose sand in the modelling situation and the sequential development of the failure mechanism made Karaal's approach impractical. The difficulties encountered when attempting to formulate a yield function for the granular material were discussed in Chapter 4, and attention is drawn to the fact that a successful failure criterion was based on deformation rather than stress. The author considers that the method of energy balance used by Karaal (op. cit) was very important, but a different technique to express this balance needed to be sought for granular materials.

The virtual work procedure proposed by Trollope (1975) was another method which considered the energy balance for a slip mechanism, however, the predictions made by this technique did not anticipate the observed characteristics, and a static equilibrium equation was suggested for assessment of ultimate stability. The virtual work approach was extended to a study similar to that of the generalised two-wedge mechanism, so that a kinematically admissible mechanism was always considered. To keep the analysis as uncomplicated as possible, the elastic stress distribution was not included in the development.

The virtual work approach was not a mathematically rigorous method similar to that for limit analysis (cf. Chen, 1975), but simply introduced a virtual displacement to the two-wedge mechanism so that the magnitudes of work input and output could be calculated. The analysis in this section was relevant to a slope in which the two-wedge mechanism had fully developed, and when strength parameters along the slip planes were in their residual states. That is, the analysis was for the end of the failure sequence and not its initiation, which was the stage considered by Trollope (op. cit.). The virtual work equations for the two-wedge mechanism are given in a simplified form by:

$$\text{External virtual work} = W.c \tag{6.11a}$$

$$\text{Internal virtual work} = R\sin\phi.a + S\sin\phi.b + T.a \tag{6.11b}$$

whence,

$$T.l = W.c - R\sin\phi.a - S\sin\phi.b \tag{6.11c}$$

Figure 6.8 illustrates the nomenclature used in the above equations. The value of the weight of the crest block, W, was calculated from equations 6.2, 6.3 and 6.4. The critical slip mechanism which maximised the energy dissipated per unit length of the base slip plane was determined by the Powell algorithm, which was referred to in more detail in Section 6.2.3.1.

Because the two-wedge mechanism was statically determinate, the results of the simple wedge analysis and the virtual work approach were identical. However, the advantage of the virtual work approach was revealed when the critical slip mechanism for the slope had to be defined. The location of the critical mechanism for the simple wedge analysis might have been chosen using a number of different criteria: e.g. the characteristics giving the maximum acceleration of the toe wedge (cf. Seed and Goodman, 1964), or the region associated with the maximum shear stress beneath the slope (cf. Trollope, 1975), or the location giving the maximum average stress within the base layer. There could be many arguments proposed to support any of the above criteria; however, to the author's knowledge, there was only one reasonable energy based criterion: the slip mechanism was positioned so that the energy dissipated per unit length of the base slip plane was a maximum. The dissipation function was restricted to the base layer because it was the dominant feature of the case under investigation.

The use of an energy balance instead of the usual strength comparison with the level of applied stress enabled a substitute for the factor of safety to be introduced. In most methods of stability analysis, the factor of safety was assumed to apply at all points on the assumed failure surface, which may be a false interpretation of the

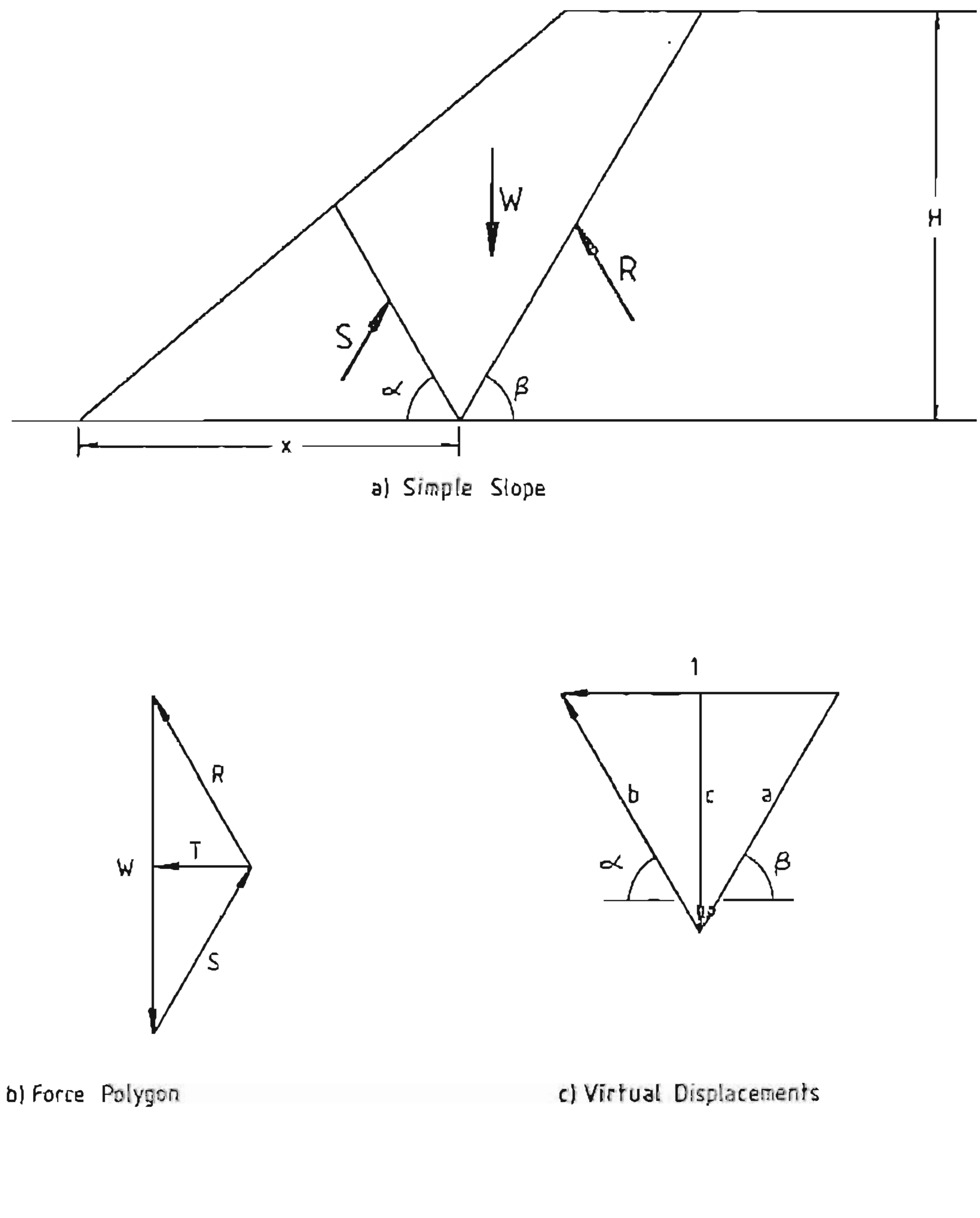

Figure 6.8 Components for Virtual Work Approach

real situation. Trollope (1979) proposed a factor of safety, F, for circular slips based on the writer's virtual work approach which incorporated a variable arching factor ($0 \leq k \leq 1$):

$$F = \frac{\text{Internal virtual work}}{\text{External virtual work}} \qquad (6.12)$$

The author concurs with this definition, however, the description of the work ratio as a factor of safety tended to imply that the ratio should be treated in a similar way to the mobilised strength ratio of stability analyses based on force and moment calculations. Therefore, to emphasise the different nature of the assessment of stability, the author suggests that an energy quotient, Q, be used to define the likelihood of slope failure:

$$Q = \frac{\text{Internal virtual work - External v.w.}}{\text{External virtual work}} \qquad (6.13)$$

Thus, a negative value of Q implies instability, while a positive or zero value implies stability, where the quantities of virtual work are evaluated for the critical slip mechanism. It is important to realise that the parameter Q indicates the likelihood of activation of the mechanism, and does not lead to an evaluation of the degree of mobilised strength on the slip surfaces when the slope is stable.

The physical interpretation of a factor of safety (other than F in equation 6.12) which was less than 1.0 was meaningless, because it implied that the strength parameters on the slip surface were required to be greater than their fully mobilised values. However, the energy quotient has a physically acceptable meaning when it has positive or negative values. A positive Q indicates that more energy has to be provided for the slip mechanism to become active (i.e. the slope is stable), and a negative Q shows that the slip mechanism will be active and that the excess energy (the difference between the external and internal virtual work) will be converted to another form; e.g. the energy may manifest itself as kinetic energy in the sliding mass, which could contribute to the formation of a flow slide.

Thus, it is loosely implied that a lower value of Q will indicate a faster rate of landslip.

The use of the virtual work approach involved relatively simple operations which would not become excessively congested if a statistical estimation of material parameters was available. Thus, in a prototype situation where parameters with a mean value and a variance were available, the energy quotient could be estimated with a knowledge of the risk of failure involved.

6.2.5 Summary of results from stability analyses

Table 6.2 gives a list of results from the analyses discussed in the previous two sections, together with the average slip mechanism characteristics estimated for plane strain conditions from the physical model. An estimate of the dimensionless yield stress of the bentonite was .12, however, this value should only be used to give an order of magnitude estimate because of the many uncertainties associated with its determination (cf. Section 4.3). Although many of the stability analyses gave slip mechanism characteristics similar to those observed, the one which gave best correspondence to all three variables was the author's virtual work approach. For reasons which have been discussed in detail in the previous section, the virtual work approach was preferred to the simple wedge method, although both methods gave the same results.

Because of the apparent success of the virtual work approach, a numerical study was made to ascertain the variation of the three critical slip mechanism characteristics $\frac{x}{H}$, α and β, and the dimensionless base shear stress $\frac{\tau}{\gamma H}$ with changes in the value of the angle of internal friction, ϕ. Figures 6.9a, b, c and d show these variations over a range of ϕ from 25^0 to 40^0. There were no unreasonable trends observed from the results produced, and the increase of the angle β with an increase in ϕ followed the generally acknowledged increase in steepness of the active slip plane with ϕ.

TABLE 6.2

Summary of Results from Stability Analyses

Analysis	$(\frac{x}{H})$	α	β	$\frac{\tau}{\gamma H}$	Remarks
Simple Wedge	1.22	74^0	57.5^0	.085	$\phi = 35^0$
U.S. Army Corps of Engineers	1.48	90^0	56.8^0	.072	Thrust angle 34^0, $\phi = 34^0$
	1.48	90^0	59.2^0	.036	" " 17^0
Rendulic Spreading Failure	1.3	63.5^0	63.5^0	.082	$\phi = 35^0$
Morgenstern-Price	1.2	$\sim 98^0$	56^0	.082	$\phi = 35^0$, see method of estimation of α in text.
Reimbert and Reimbert	2.1	58.1^0	56.3^0	.13	$\phi = 34^0$
Trollope (clastic)	.91	-	-	.081	k = 1 slip from point of max. shear stress
	1.37	-	-	.097	k = 1 slip from point of max. average shear stress

(continued overleaf)

TABLE 6.2 (contd.)

Analysis	$(\frac{X}{H})$	α	β	$\frac{\tau}{\gamma H}$	Remarks
Virtual Work	1.22	74^0	57.5^0	.085	$\phi = 35^0$
	1.20	75^0	56.5^0	.090	$\phi = 33.5^0$ (residual)
Observation	1.15 ± .1	$75^0 \pm 10^0$	$56^0 \pm 5^0$	-	Values at centre of tank

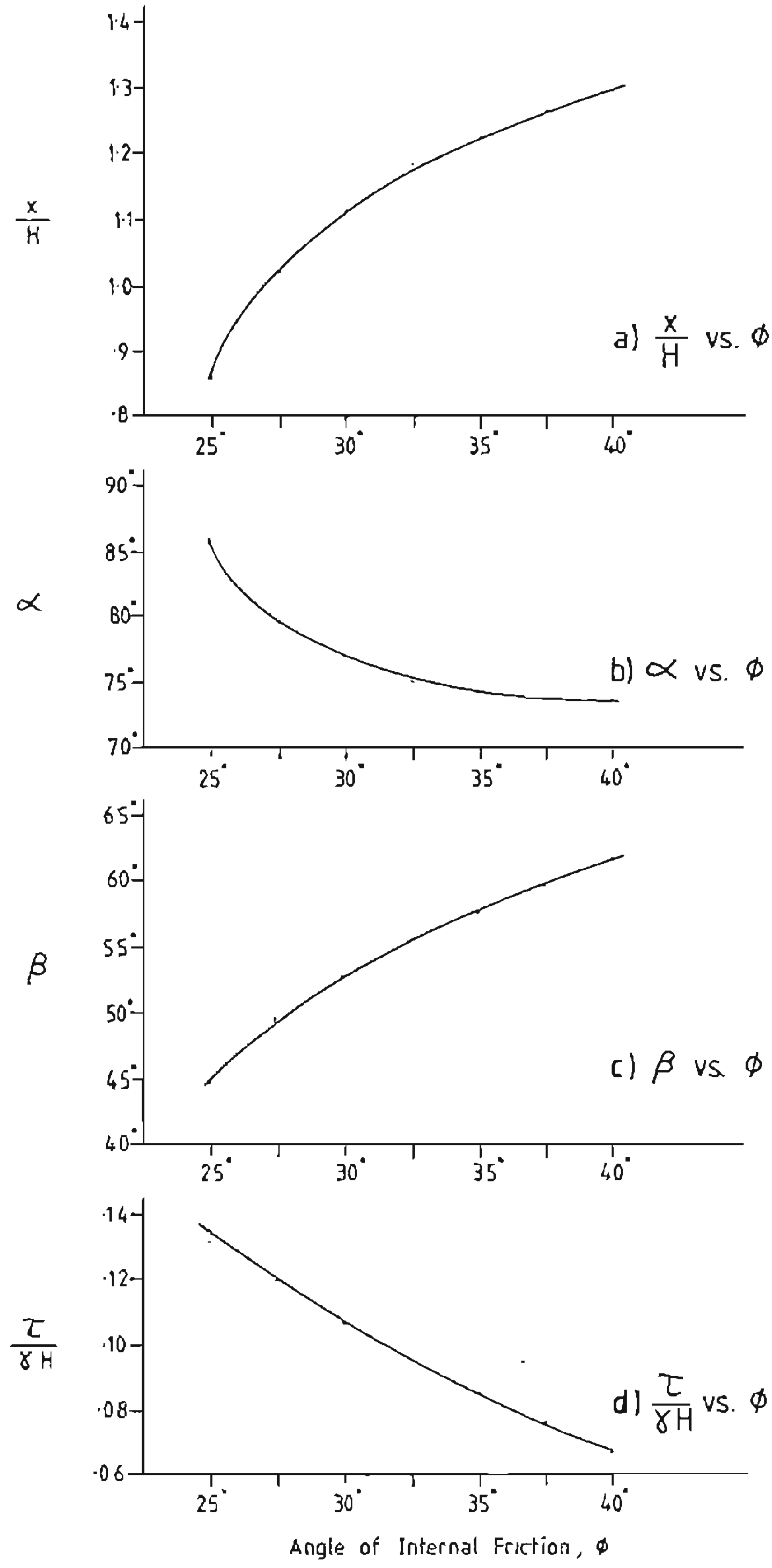

Figure 6.9 Virtual Work Analysis of Model Slope

General support for the virtual work analysis was gained from the work of Seed and Sultan (1967). In the investigation of the stability of a sloping core earth dam model, the writers used a two-wedge force equilibrium analysis, similar to the generalised simple wedge method described earlier in Section 6.2.3.1. The writers used a graphical optimisation technique to determine the position of the critical slip surfaces; therefore, it is reasonable to conclude that the virtual work approach may also be successfully applied to the analysis of sloping core earth dams.

6.3 Numerical Modelling

6.3.1 Application to discontinua

The relevance of any model, physical or numerical, depends on the success of the modelling technique in representing the fundamental characteristics of the material performance. Thus, it was concluded that a numerical model of a discontinuum would be most appropriately modelled by a technique which specifically considered the joint-particle relationship. By far, the most widely publicised numerical models in the field of geomechanics are the finite element techniques based on continuum concepts; however, during the past two decades, there has been continued development of joint-element finite element techniques, in which the contrasting behaviours of the joint material and the solid blocks were accounted for in the overall performance of the structure being modelled. The finite element based methods have not been the only ones developed to consider discontinua, and a different approach using dynamic relaxation techniques was proposed by Cundall (1971).

The laboratory investigation into the stress-deformation response of the silica sand used in this study showed the dependence of the failure conditions on the particulate nature of the material, rather than on one of the commonly used stress dependent yield functions. Therefore, the two numerical models used to approximate the physical model of this study were both particularly suitable for the investigation of a discontinuum. The first model was developed by Burman (1971a) who used the joint-element finite element method, and the second was the kinematically oriented model developed by Cundall (op. cit).

Once the importance of the representation of discontinuities in the material was established, the adequacy of the numerical model depended on the parameters supplied to represent the material characteristics. The difficulties associated with the determination of suitable parameters for use in a numerical discontinuum model were significant, because many assumptions had to be made in the process. The number of individual particles in the physical model was immense and could not possibly be represented numerically on a one to one basis. Thus, the joints in the discontinuum also could not be individually represented, which meant that the joints or contact points in the numerical model had to have a response which would reflect the collective response of a number of real joints.

The scope of this study did not permit the detailed laboratory and numerical investigation which would have led to a reasonable set of parameters for use in the numerical models. Therefore, the results from these models which were related to the deformational response were reliable only from the qualitative aspect. Other limitations in each of the models are discussed in the following sections together with the results of the computer studies.

6.3.2 The discrete stiffness model

Burman (1974) gave a brief history of the development of the discontinuum models based on finite element techniques, after which the writer described the discrete stiffness model he had developed. The model was based on the concept of a system of rigid blocks, whose centroidal positions were fixed, separated from one another by deformable joints of finite length and thickness. The strength and deformation parameters were intended to be modified values which would allow for the response of the block, but keep the computations and storage space to the lowest practical level.

The suitability of the discrete stiffness model, using disc units to simulate a granular material, was demonstrated by Burman (1971a,b) using experimental evidence reported by Trollope (1956), and Lee and Herington (1971), as well as the writer's results from an idealised rod model. The values of the joint stiffness parameters were chosen arbitrarily, however, the values were inter-related so that the shear and moment stiffnesses were about 1% of the direct (normal) stiffness. The angle of internal friction of the granular mass as a whole was assigned to each joint because the rigid block diameter was fifteen times the maximum sand grain diameter. The maximum rigid unit diamter which still gave good agreement with experimental stress measurements for the numerical model was about one tenth of the wedge or slope height.

The computer program of the discrete stiffness model used for this study was an updated version (cf. Fulton, 1979), but the changes were mainly concerned with improved computational efficiency and the choice of input/output modes. Figure 6.10 shows the basic configuration of the blocks and joint elements as well as the boundary conditions. The strength conditions in the joints were a purely frictional contact ($\phi = 35^0$) with no allowable tension within the slope, and purely cohesive joints with a uniform yield strength simulating the weak base layer. Two sets of results are given in Figures 6.11 and 6.12, with base yield stresses of .5 and .75 kPa respectively, and with a rigid disc diameter of 30 mm.

The variation in shear stress distribution along the base for the different base strengths enabled further comment to be made about the relevant arching factor for the elastic stress analysis of a simple granular slope underlain by a weak layer (cf. Trollope, 1975, and Section 6.2.3.4). The parameters used in the computer model revealed that failure was initiated for a base strength of .5 kPa ($\frac{\tau}{\gamma H}$ = .085), but not for a base strength of .75 kPa ($\frac{\tau}{\gamma H}$ = .127). Although a zone of tensile failure was present in both cases, the extent of the zones was different, and some component of tension may have been able to be resolved with a greater number of tension

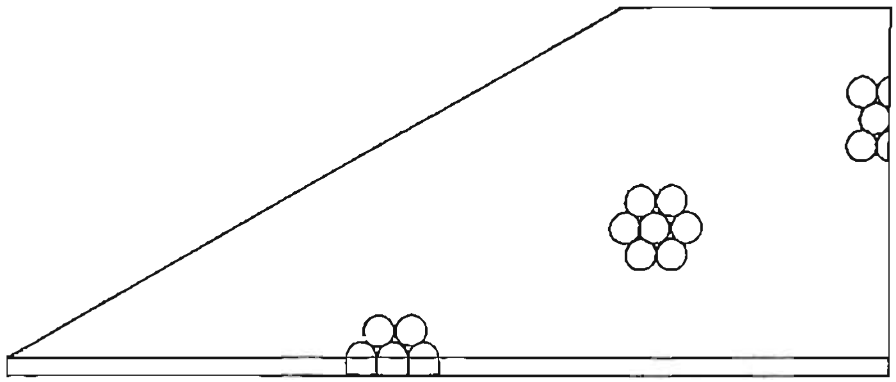

Complete Slope

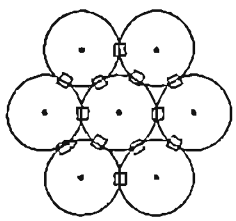

General Configuration

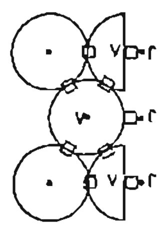

Vertical Boundary

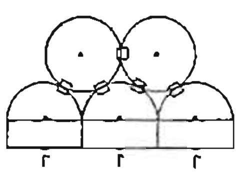

Base

Legend:

- ▪ Node
- □ Joint Element
- r Fully restrained node
- v Vertically unrestrained only

n.b. All other nodes free

Figure 6.10 Basic Configurations for Discrete Stiffness Model

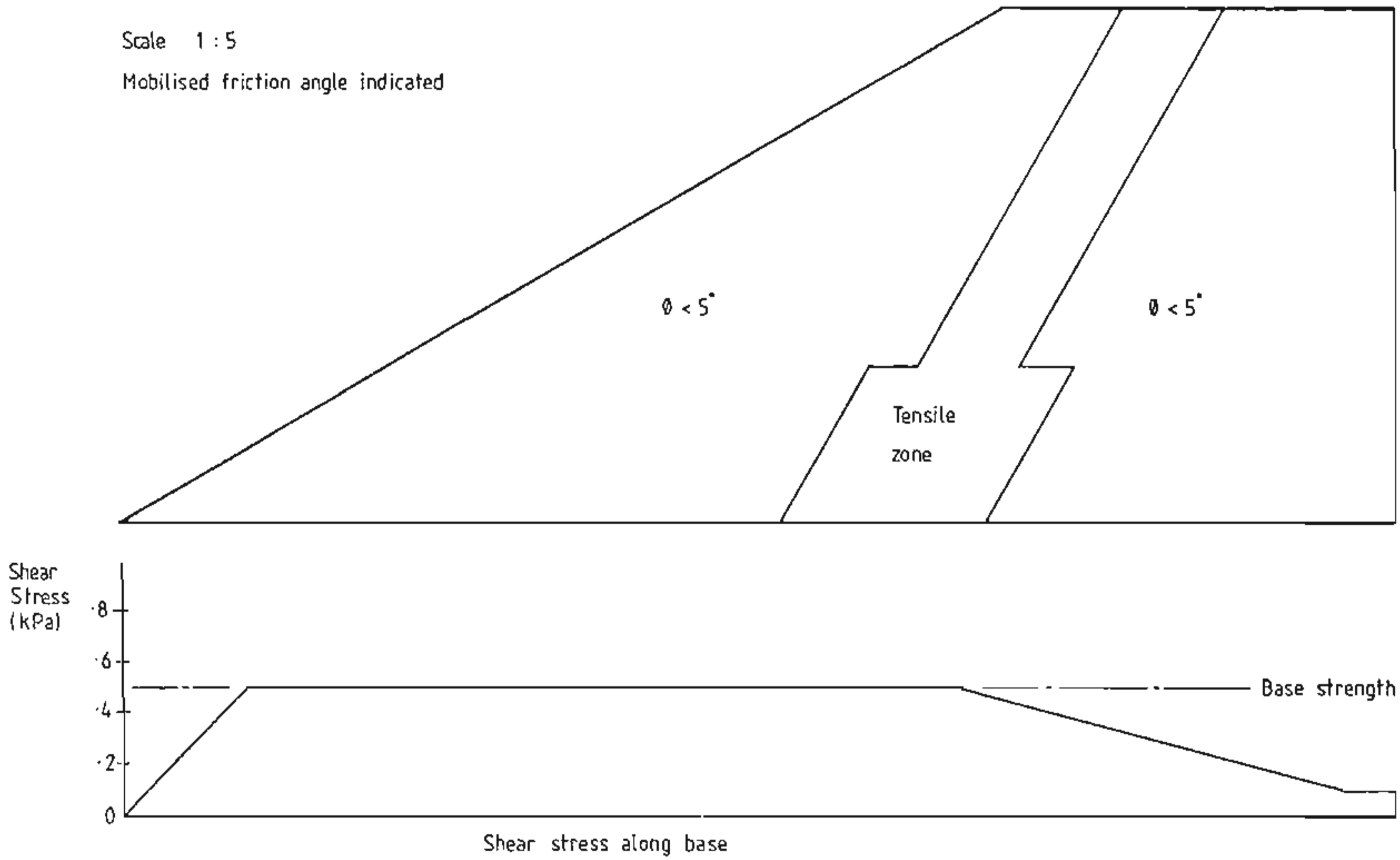

Figure 6.11 Discrete Stiffness Model Results:
Base Strength = .5 kPa

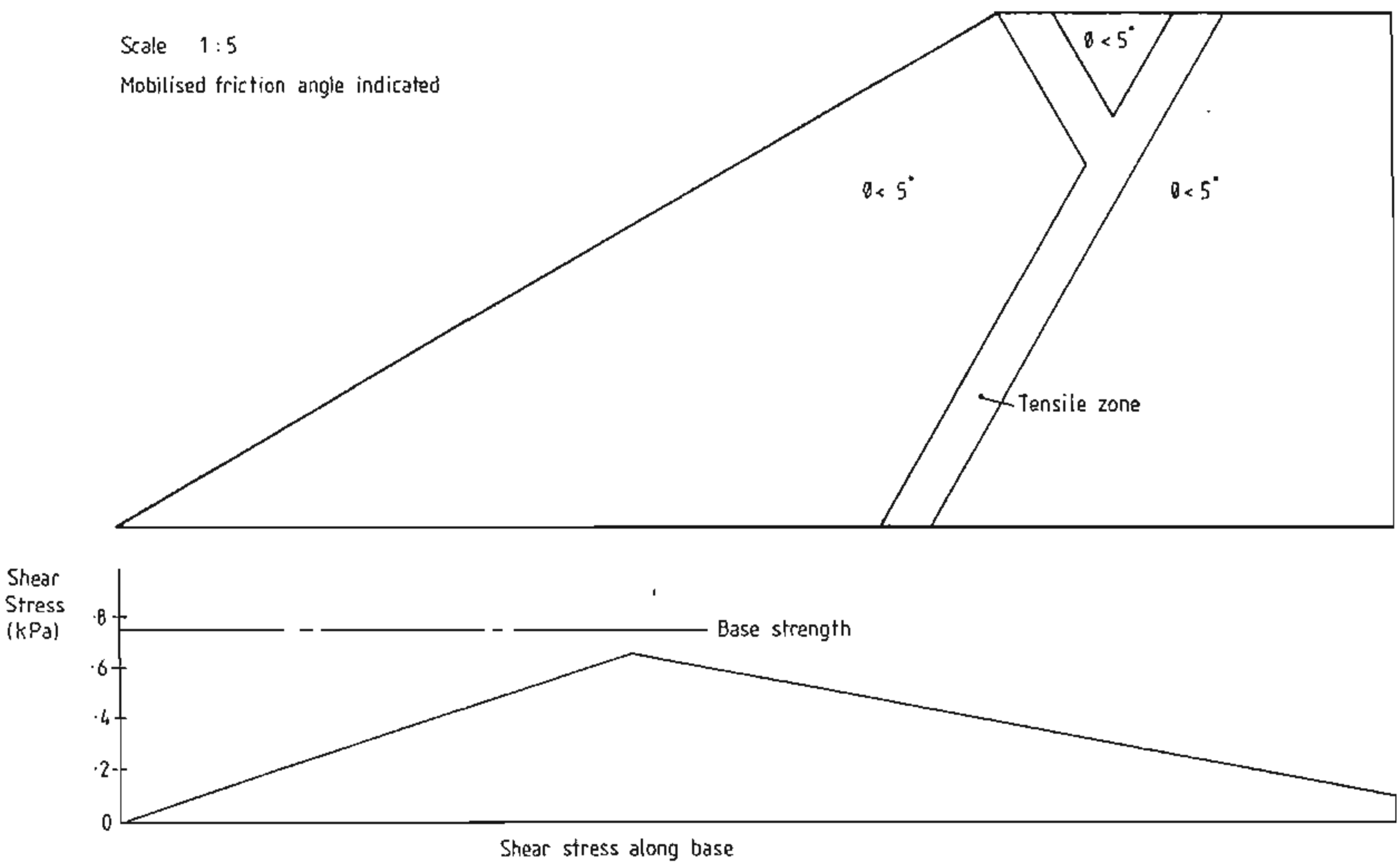

Figure 6.12 Discrete Stiffness Model Results:
Base Strength = .75 kPa

release cycles in the execution of the program; however, this was not practical. Thus, the main criterion for failure was the degree of mobilised shear along the base layer. Table 6.3 summarises the predictions of the clastic theory (cf. Section 6.2.3.4) and the results of the numerical model.

TABLE 6.3

Results from Clastic Theory and Numerical Model

Method	Arching Factor	$\frac{\tau}{\gamma H}$
Clastic Theory:		
Slip at max. shear	0	.289
stress:	1	.081
Slip at max. energy	0	.347
dissipation point	1	.097
Numerical Model:		
Failure	-	.085
Stable	-	.127

For both cases of full arching (k = 0), failure should be observed for both base strengths used in the numerical model; and both cases should be stable for no arching (k = 1) if the slip plane started from the point of maximum shear stress along the base. The only analytical model which agreed with the results given by the numerical model was the no arching solution for which the slip plane was located for the maximum energy dissipation per unit length of the base. The examples of full arching distribution may be intuitively discounted because of the ability of the base layer to deform and thus maintain the lower potential no arching stress state.

Overall displacements in the discrete stiffness model results were small because the centroids of the blocks were fixed and all displacement was limited to the joint-elements; therefore, the failure indicated in the results for the .5 kPa base strength was assumed to be indicative of the first stage in the sequence of failure. The observations from the physical model of the appearance of two slip planes in the initial stages of the failure sequence was supported by the base and tension zone in Figure 6.11. This evidence suggested that the virtual work approach, using the elastic theory, should be extended to include the slip plane which was indicated by the tension (n.b. numerically unresolved tension) zone in the slope. The inclusion of the second slip plane should lead to a predicted critical slip mechanism which is closer to reality.

6.3.3 The dynamic relaxation model

Cundall (op. cit.) developed a finite difference model which used a dynamic relaxation technique to simulate the load-deformation response for an assembly of blocks. The writer was mainly concerned with the modelling of a situation in which the rock blocks were represented individually or the investigation of an elastic continuum. However, the development of Cundall's major program resulted in a program which considered a pile of cylinders (Cundall's "Ball" program, ibid., p.115 ff.), on which a numerical model resembling the physical model slope was based.

In contrast with the discrete stiffness model (Burman, 1971a), Cundall's model concentrated on the kinematic aspects of discontinua, with contact points between moving blocks rather than fixed blocks separated by deformable joints. The results from the program were a series of diagrams showing the positions of all the blocks over a number of time steps. The stresses within the numerical slope could not be assessed from the results, therefore, the two numerical models could not be compared with each other. The program was based on the iterative application of Newton's fundamental equation relating force, mass, and acceleration. The displacements of the blocks were calculated from the integration of the acceleration over the time step between iterations. The origin of the disturbing forces in the model was the self-weight of the blocks, and forces were transmitted between blocks by a spring which was damped in the unloading (tensile) direction (as a means of keeping the assembly mechanically stable). A no tension condition applied for the examples used. Slip between blocks was allowed to occur once the joint yield criterion was satisfied; frictional contacts ($\phi = 35^0$) existed in the granular material, and the lower horizontal boundary had a constant yield stress which was expressed as a force effective on the horizontal repeated unit cross-section. Some trial studies were conducted to determine the effect of varying spring stiffness between units, however, it appeared that an arbitrary value which allowed little overlapping of units gave the most reasonable results.

In a similar manner to the discrete stiffness model, it was not feasible to consider individual grains in this model; however, a suggestion made by Cundall (op. cit.) which would reduce processor time and storage required was included in the program so that a larger number of units could be considered for the same computer usage. A problem which required attention in the dynamic relaxation method was numerical stability. Cundall (op. cit.) gave a formula for the maximum allowable size of time step, however, this was found to be inadequate for this particular problem. Although the time step for numerical stability was correctly given by the formula mentioned previously, an estimate of the mechanical (physical) stability of the spring-mass system was one eighth of the value needed for numerical stability. Thus, the author recommends that the following formula be adopted for the critical time step when the dynamic relaxation model is used with cylinders as the basic unit:

$$\Delta t \leqslant .2 \sqrt{\frac{m}{s}} \qquad (6.14);$$

where Δt is the time step, m is the mass of a cylinder of unit length, and s is the spring stiffness between units. Because meaningful relationships for interparticle spring stiffness and damping ratio were not established, the results of this numerical modelling method were considered qualitatively.

Unfortunately, the response of the numerical model with a cylinder as the basic unit had not been calculated; hence, the reliability of the author's results could not be determined, as they were in the use of the discrete stiffness model. Two examples of model slopes are given in Figures 6.13 and 6.14. The former figure more clearly illustrates the formation of a two-wedge failure mechanism displaying many characteristics seen in the physical models: e.g. an intact toe region and

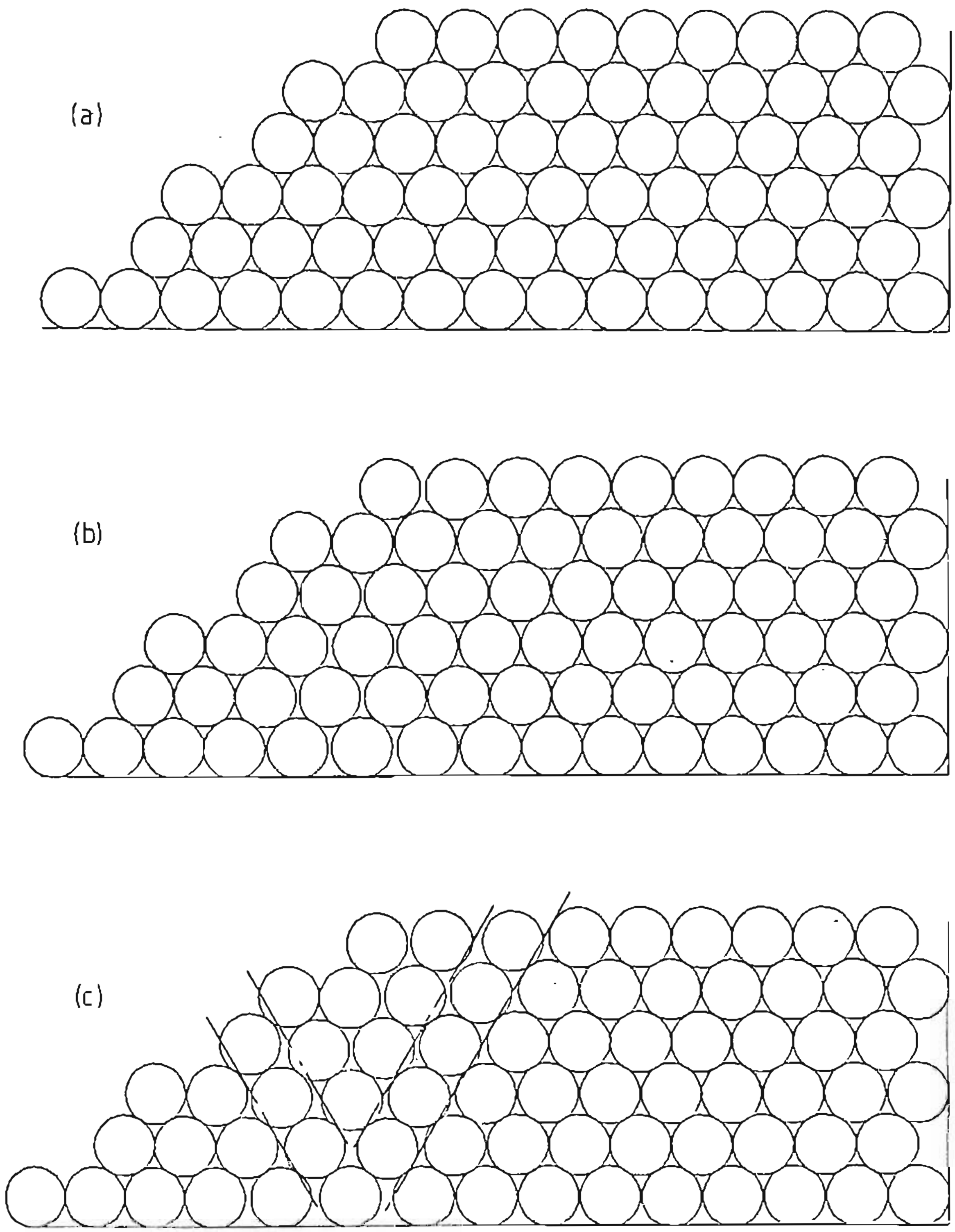

Figure 6.13 Dynamic Relaxation Model - Example 1

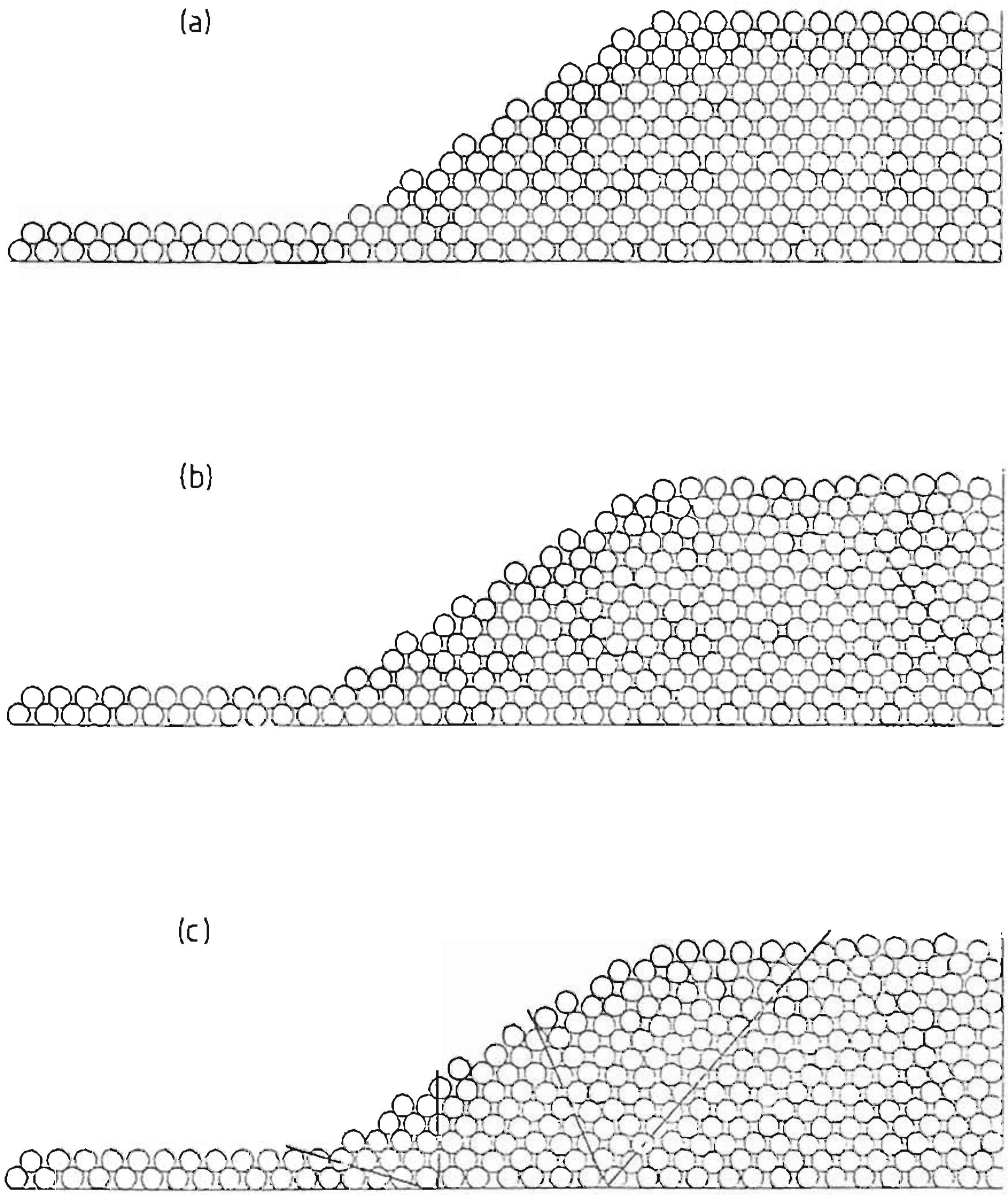

Figure 6.14 Dynamic Relaxation Model - Example 2

a back slip plane emerging slightly behind the crest; however, the rigid units in this example were large compared with the slope dimensions. Figure 6.14 illustrates a model with much smaller rigid units in which the interaction between units was not as easily recognised as in the previous figure, but the wedge form of failure was still evident.

6.4 Analogy to Silo Discharge

In the early stages of this study, the flow characteristics seen in slope experiments were compared with those of granular materials discharging from silos or slotted bins. There were properties observed during the discharge of a bin which made this line of approach interesting: a sudden increase in lateral thrust when flow was initiated (cf. Turitzin, 1963) may have been able to be linked with a change in arching state in Trollope's arching theory (cf. Trollope, 1968), which may have given the reason for the development of the flow slides in the early experiments; and the sequential development of flow regimes (McCabe, 1974). Further investigation into the topic showed that most solutions to granular flow were applicable only to the steady flow situation. Many researchers (e.g. Brown and Richards, 1965, and Giunta, 1969) relied on the use of a radial stress distribution for flow towards the silo opening, and this was based on the free fall state of particles at the opening. A radial stress distribution may exist when there is a back-pressure at the silo opening, however, the determination of this pressure to make the analysis relevant to the model slope would have been very difficult. A number of records of the inclination of the flow boundary (cf. Brown and Richards, op. cit.) showed that the characteristics of flow from bins were divergent from those observed in the model slope.

6.5 Summary

This study of the sequential failure of granular slopes was centred around the results of a Class II physical model. Once the sequence of failure had been defined, the investigation turned to the stability analysis of the slope as a small prototype, with the aim of establishing a relevant method which may be proposed for use in the field situation. The form of the failure mechanism precluded a slip-circle analysis, and the sequential development of the mechanism together with the difficulty in defining an adequate material yield function made the consideration of a plasticity solution impractical. Several force equilibrium methods and a generalised limit equilibrium approach were considered and compared with the observed results. These methods gave reasonable agreement with two of the three slip plane characteristics observed in the physical model tests.

Trollope (1975) used a virtual work approach to estimate stability of slopes using stresses calculated from the systematic arching theory (Trollope, 1968). The author extended this concept and applied it to the fully developed two-wedge mechanism. Because the virtual work approach was based on energy, the criterion for defining the critical failure mechanism had to be in the form of a dissipation function to maintain the continuity of the use of energy as a comparative base. Thus, the critical slip mechanism was defined to exist for the two-wedge mechanism when the energy dissipated per unit length of the base slip plane (i.e. through the dominant slip plane) was a maximum. The predicted and observed characteristics for the mechanism were in close accord. Because the two-wedge mechanism was statically determinate, the virtual work approach and a generalised force equilibrium method gave the same results; however, the author considers that the energy concept using virtual work gave a more realistic appreciation of the stability problem. An estimate of the stability of a slope using a virtual work approach was given by the energy quotient, Q, which expressed the energy surplus or deficit as a fraction of the energy input (see equation 6.13), and also indicated the severity of this imbalance.

Two numerical models based on discontinuum mechanics were used to qualitiatively examine the model slope. The discrete stiffness model gave results which supported the observed sequence of failure and the basis of the energy dissipation function. The second model concentrated on the kinematics of granular materials and demonstrated that the basic form of the critical failure mechanism could be predicted, however, the parameters for this mechanism would have to be calculated by other means (e.g. the virtual work approach).

CHAPTER 7

SUMMARY AND CONCLUSIONS

7.1 Field Evidence of Two-Wedge Mechanisms

A characteristic two-wedge planar failure mechanism was identified in a number of reports on landslips (e.g. Blight, 1969, and Bromhead, 1978). The formation of this failure mechanism was associated with a discontinuity in the strength and composition of the foundation material which was often in a thin, nearly horizontal layer positioned close to the base of the slope. The cause of the lower strength in the foundation layer was traced to several sources of which the main ones were: a naturally weak material (e.g. highly plastic clay); a change in material properties to lower values due to consolidation pressures; and a loss in effective strength due to increased pore water pressures from a rise in ground water level or dynamic loading. The slopes were constructed as part of an embankment or as landfill, and in one case the slope was cut by coastal erosion.

The low strength and position of the layer dictated the location of one of the planes in the failure mechanism. Earlier physical model studies of this phenomenon showed that a two-wedge mechanism developed clearly when the slope was a dry cohesionless material. The landslips reviewed in this study were all deep-seated failures. Wilson (1970) described the characteristics observed for some landslips and identified the different nature of displacements between progressive failures and those relevant to this study. It was shown that progressive failures exhibited movement which decreased linearly from the toe of the slope to the end of the slip plane; however, deep-seated two-wedge failures showed base movement which tended to be uniform.

Figure 7.1 shows a general profile of a landslip which formed a two-wedge mechanism. Some features associated with this mechanism are:

i) a relatively thin, weak base layer;

ii) uniform movement along the base slip plane;

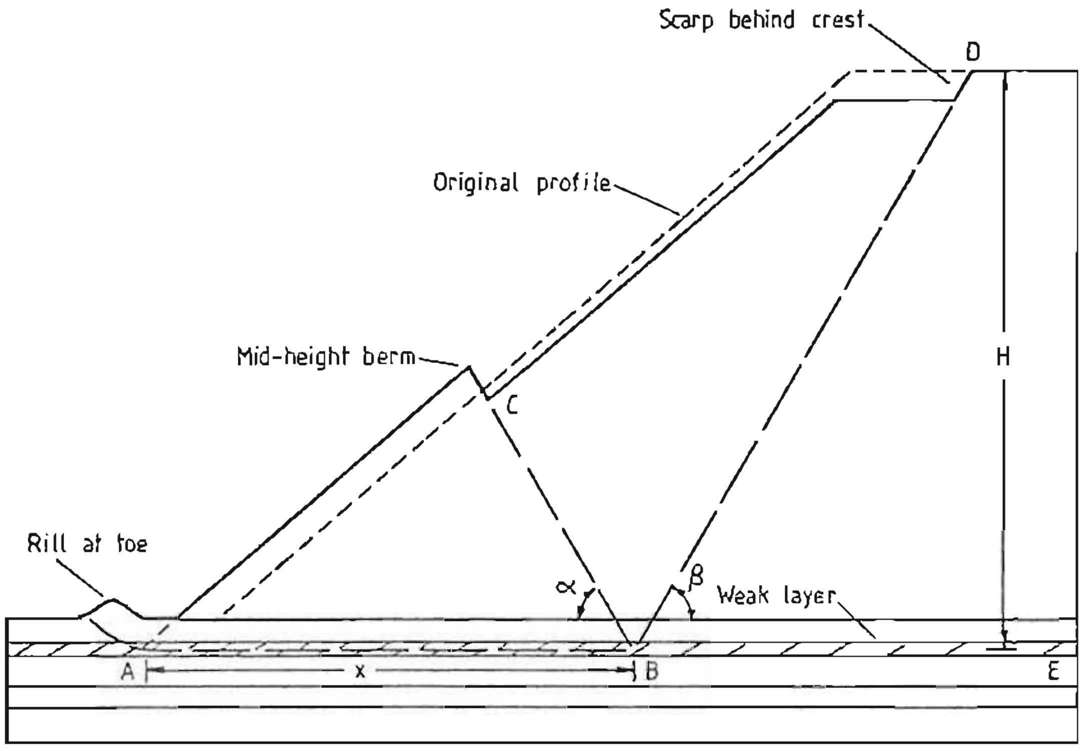

Figure 7.1 General Profile of Two-wedge Mechanism

iii) intact condition of the toe block and a rill of foundation material pushed up by the toe block;

iv) the appearance of a mid-height berm or a gentle S-shape of the slope face; and

v) formation of a slip scarp just behind the crest of the slope.

The physical model used in this study was designed to reproduce many of these characteristics, and allow a detailed record of the formation of the slip mechanism to be made.

7.2 Physical Modelling

Blight (op. cit.) and Holland (1977) used physical models to study the formation of a two-wedge mechanism for a cohesionless slope underlain by a weak layer. The former used a viscous bitumen compound to simulate the weak layer, while the latter used a thin metal shim withdrawn horizontally from the base of the slope. The aspect ratios of the apparatus used by both researchers were below the suggested values at which plane strain conditions were probable; therefore, the results achieved from those experiments were not considered to give more than a qualitative demonstration of the formation of a two-wedge failure mechanism. The level at which this study was undertaken required reliable results so that a definite sequence of failure could be established; therefore, the design of the modelling apparatus and the selection of materials was carried out to achieve that end.

Some physical restrictions were placed on the type of model which could be designed; hence, a small scale slope (less than 1 m high) of cohesionless material, acting under its natural self-weight, was the fundamental component around which further design was made. The details of the sample container and materials are given in Chapter 3, and only the principal points are included in this section. All components of the sample container were designed to limit the maximum deflections to less than 1% of the values commonly accepted to induce an active state in the soil. The effect of side wall friction was minimised by using plate glass walls which were thoroughly cleaned with acetone before each test; however, the remaining frictional effect was significant and further comment is made on this point later. The materials used were a well-graded silica sand for the slope and bentonite slurry (moisture content = 900%) for the base layer. The strength of the bentonite was too low to support the sand slope (at a height of 400 mm); therefore, a mechanical stiffening device was used to support the slope temporarily. Failure of the slope was initiated by the retraction of the mechanism to the base of the bentonite layer. Although this action did influence the rate of displacement in the first stage of failure, a test which was performed independently of the mechanism gave similar results to the other tests using the mechanism.

There were two basic methods for recording information from the modelling tests, and both were based on photography of the slope cross-section through the glass side wall. Qualitative results were obtained using a 16 mm movie camera, which gave a high exposure rate during the test but lacked the stability and range of lenses and film available for a 35 mm camera. The second device was a motor drive 35 mm Nikon data-back single lens reflex camera which was fitted with a large film magazine and a flat field lens. Reliable quantitative results were measured from the 35 mm film negatives through a digitised Zeiss Stecometer. The reliability of the results was assessed statistically from sets of control readings taken during the measurement of the film. Because the photographic results were recorded at the side wall, they also showed the greatest edge effects. A reasonable estimate of the correction needed to bring the viewed results to those in the plane strain condition in the centre of the slope was made from the post-failure characteristics of the free surface and the bentonite layer.

The purpose of the physical model was to provide a set of results which could be compared with a number of analytical and numerical approaches so that a method which adequately described the model performance might be found. The selected method would be applied to a prototype slope which was qualitiatively similar to the model, and the relevance of the method would finally be assessed from the response of the prototype.

7.3 Performance of Modelling Materials

Sultan and Seed (1967) commented on the importance of using material parameters which were assessed under conditions having similar stresses and deformation restrictions to those which existed in the model. Thus, the stress-deformation characteristics of the sand were determined in a plane strain device at confining pressures between 4 and 8 kPa. In all tests, the sample was isotropically consolidated and sheared in axial compression under drained conditions. These conditions did not match those in the model which were expected to be approximated by anisotropic consolidation and shearing at constant vertical load. Because the plane strain device was not easily modified to accommodate the latter conditions, a series of direct shear tests, which gave a rough approximation to the desired restrictions, was carried out. The results from the plane strain and direct shear tests concurred; hence, the data from the plane strain results was compared with some contemporary failure theories, but without success.

At the low confining pressures used, the sand deformed similarly to a medium dense sand at a confining pressure of about 250 kPa. The sand was found to conform to a Freudenthal failure criterion, and the author proposed a possible kinematic explanation of failure using this criterion (see Section 4.2.7). However, the stress-deformation characteristics of the sand were more readily interpreted by a criterion which described the sequence of failure in the sample according to the axial deformation or the deformation along the slip plane. The criterion, which was supported by both plane strain and direct shear tests, as well as model experiments, is summarised for deformation along the slip plane as follows:

i) initial compression up to 1.25 mm movement;

ii) onset of failure when the rate of volume change becomes zero, followed by growth of the shear zone at constant dilatancy to a deformation of 6.2 mm; and

iii) cessation of growth of the shear zone with further slip taking place within the zone at practically zero dilation.

The mechanistic approach to the failure criterion followed similar . descriptions given by Mandl, de Jong, and Maltha (1977) and Trollope's (1975) strong systone hypothesis.

The bentonite slurry was beyond its liquid limit of about 600% and fell in the region where it exhibited the properties of a non-Newtonian fluid. In the context of the model, the bentonite had a finite but low shear strength. This value could not be determined by conventional soil testing techniques, however, an extrusion rheometer was used to carry out the task. The shear strength was not determined reliably and the result was considered only as an order of magnitude estimate.

7.4 Results from Modelling Tests

Both qualitative and quantitative data was available from photographic records of the experiments. The main variable in the testing programme was the thickness of the bentonite layer; however, this did not alter the characteristics of the failure mechanism, although it was found that the total base displacement after failure increased non-linearly with increase in bentonite thickness (see Figure 5.21). The most likely relationship appeared to be one in which the total displacement was related to the base 2 logarithm of the layer thickness; however, the data was scattered and an approximate straight line fit was:

$$s = 40(t' - 2) \qquad (7.1),$$

where s = total displacement (mm),
$t' = \log_2 t$, and
t = layer thickness (mm).

For equation 7.1 to be meaningful, the layer thickness must be at least 4 mm, below which the displacement was assumed to be zero. At least two tests were carried out for each layer thickness to ensure repeatability of results.

The quantitative results were used to define the sequence of failure, which was confirmed from the qualitative results. The sequence of failure is illustrated in Figure 5.12 and is described from initiation as:

i) the simultaneous development of two slip planes - one through the weak layer and the second through the granular slope cutting the free surface just behind the crest; between the two planes was a broad shear zone dividing the front of the slope into toe and crest regions;

ii) movement of the two regions along their respective slip planes with the distortion in the shear zone tilting the lower half of the crest region away from the toe;

iii) formation of a third slip plane within the shear zone between the first two planes with no further shear distortion within that zone;

iv) movement along the three slip planes with negligible volume change within the toe and crest regions.

The formation described in the last stage of failure was called the two-wedge mechanism, and has been classified as a third order mechanism (i.e. three slip planes) by Trollope (op. cit.). A deformational failure criterion was defined from plane strain tests, and it was found that the displacement, at which the slip planes were first observed, corresponded reasonably well with the predictions made by the criterion. Thus, it was concluded that the failure of a granular material should be referred to an absolute deformation and not to a strain based on sample size. An extension of the deformational failure criterion would be to consider the variation of displacement to failure with stress level and sample particle size.

The formation of the two-wedge mechanism was important because it provided the means by which the large deformations in the slope occurred at residual strength conditions. The mechanism was located in the slope by defining three parameters:

i) $\frac{x}{H}$, where x is the distance AB and H is the slope height;

ii) α, the angle ABC; and

iii) β, the angle DBE.

The angles and length are shown in Figure 7.1. The average values, corrected to plane strain conditions, and an estimate of their variation measured from model tests were:

$$\frac{x}{H} = 1.15 \pm .1;$$

$$\alpha = 75^0 \pm 10^0;$$

$$\beta = 56^0 \pm 5^0.$$

Thus, the sequence of failure in the model slope was defined clearly in a number of stages and observations showed that the sequence could be described in terms of the deformational failure criterion of the granular material. At the end of failure, the total displacements were generally an order of magnitude higher than those required to bring about the residual state in the material. The dominance of the weak base layer in the development of the failure sequence was shown by the restriction of the sequence to its initial stages when the layer did not allow sufficient displacement along the slip planes for the residual conditions to occur. Therefore, in the prototype situation, attention would have to be given to the deformability of both the weak layer and the slope material so that the possibility of the development of the failure sequence could be assessed.

7.5 Analysis of Model Performance

There were two main influences which affected the methods of analysis considered for a numerical approach to the model results: the discontinuous nature of the slope material and the dominance of the weak layer in the determination of the failure mechanism. A detailed comparison of the stress-deformation response of the silica sand at low confining pressures revealed that the failure criterion was not adequately described by any of the continuum or discontinuum theories considered. Therefore, the methods of soil plasticity, critical state soil mechanics, and stress-dilatancy were discounted as feasible approaches to this modelling situation. Attention was given to limit equilibrium, simple wedge, and some earth pressure analyses where these procedures were suitable for use with a two-wedge failure mechanism. All of the methods, except one, required the failure mechanism to be fully developed, which limited these approaches to the case of ultimate stability. However, Trollope (op. cit.) used a virtual work approach combined with the writer's systematic arching theory to estimate the factor of safety in the base layer for initiation of the failure sequence. Trollope (ibid.) defined the slip plane as extending from the toe to the point of maximum shear stress along the weak layer.

Although many of the methods considered gave reasonable estimates for two of the three parameters used to define the failure mechanism, the generalised two-wedge method gave close agreement for all three parameters when the critical failure mechanism was defined so that the average shear stress along the base was a maximum. The author could not find any specific reason for the use of the average shear stress to define the mechanism in preference to the maximum shear stress or the maximum acceleration of the toe block; thus, a new approach to the definition of the critical mechanism was sought. Owing to the lack of energy dissipation by dilation at residual soil conditions and the static determinacy of the two-wedge mechanism, the results of a force equilibrium and virtual work analysis for the mechanism were exactly the same. The virtual work approach offered a significant advantage over the force equilibrium approach because the author found only one energy based criterion for the definition of the critical failure mechanism - the mechanism formed so that the energy dissipated per unit length of the base plane was a maximum. The use of the virtual work approach made the assessment of stability by a factor of safety based on strength parameters inappropriate. Thus, the author proposed an energy quotient, Q, which expressed the energy imbalance as a fraction of the energy dissipated so that a negative value of Q indicates instability; and the larger the magnitude of negative Q, the more severe would be the consequence of failure. The dissipation function was also applied to the initiation of failure using the systematic arching theory to give the stress distribution, and results from the discrete stiffness model (Burman, 1971a) showed that the author's analysis for the no arching (k = 1) case came close to the numerical results.

Both types of numerical model used to study the slope concurred with the findings of the physical model study. Unfortunately, the reliability of the numerical results was not high, and results were used qualitatively.

7.6 A Prototype Example

The ultimate test of the analysis recommended from this type of model study is its application to a prototype situation. The first landslip at the Vlakfontein site reported by Blight (op. cit.) had features similar to the model used in this study; hence, the author's virtual work approach for Q = 0 was applied under those field conditions.

The angle of repose of the rock dumps was assumed to be 38^0, and their height at 45.7 m (150 ft). The two sets of material parameters used by Blight (ibid.) were also used in these calculations:

Rock 1 - $\phi_1 = 39^0$, $\gamma_1 = 17.3$ kN/m^3 (110 pcf); and

Rock 2 - $\phi_2 = 41^0$, $\gamma_2 = 16.5$ kN/m^3 (105 pcf).

For initiation of failure the required foundation strength, τ_0, was estimated to be:

$$\frac{\tau_0}{\gamma H} = .127,$$

which occurred for a slip plane length of $\frac{x}{H} = 1.14$. Results for the critical two-wedge mechanism, as well as those for initiation, are given in Table 7.1.

Blight (ibid.) reported that unconsolidated, undrained triaxial and unconsolidated quick shear box tests gave foundation strength values in the range 44.8 to 93.1 kPa (6.5 to 13.5 psi). The predicted slip mechanism gave a reasonable estimation of that reported by Blight, because the prediction was for the first formation of the mechanism, while Blight has shown the final slope position (see Figure 7.2). Therefore, it was concluded that the virtual work approach was the appropriate analysis for a granular slope underlain by a weak layer.

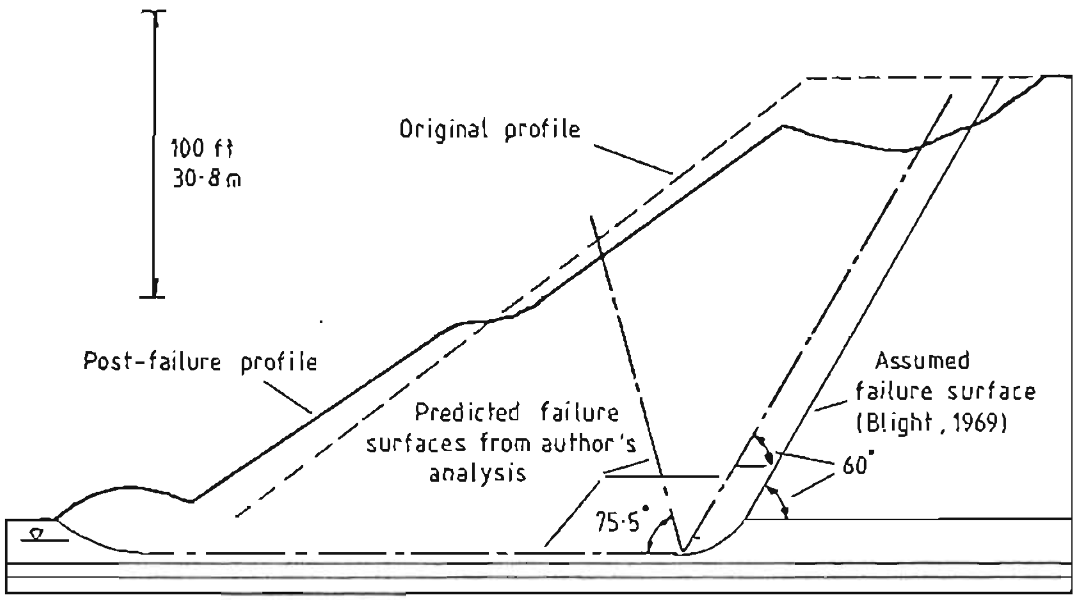

Figure 7.2 Comparison of Predicted and Observed Failure Mechanisms

TABLE 7.1

Prototype Results

Parameter	Units	Rock 1	Rock 2
Initiation			
τ_0	kPa	100.3	95.6
	psi	14.5	13.9
$\dot{x}$	m	52.2	52.2
	ft	171	171
Two-wedge			
α	deg	75½	75
β	deg	60	61½
$\frac{x}{H}$	-	1.04	1.07
x	m	47.5	48.9
	ft	156	160
$\frac{\tau}{\gamma H}$	-	.082	.075
τ	kPa	64.8	56.6
	psi	9.4	8.2

7.7 Implications and Suggestions for Future Projects

The unexpected response of loose sand sheared at low confining pressures showed that the understanding of the nature of deformation under self-weight loads in small scale models was not well established. Therefore, the interpretation of model performance will become reliable only when the stress-deformation response of the material has been investigated under similar stress and deformation conditions as exist in the modelling situation. For further conclusions to be drawn about the sequence of failure, the sand will need to be considered in simple shear so that the response of the large shear zone will be more clearly understood. Similarly, a more detailed and accurate investigation of the flow properties of the bentonite may allow improvements in the stability analysis to be made. Section 7.3 includes some comments on the development of deformational failure criteria for granular materials, which not only affects laboratory studies but also may be extended to the field.

The numerical dynamic relaxation model (Cundall, 1971) showed potential for the identification of the relevant failure mechanism; however, the current state of development of the program only considers mono-size units. A more realistic result may be achieved with the use of a mixture of unit sizes, and this modification might be considered as a future research topic. The discrete stiffness model (Burman, op. cit.) may be used to produce more reliable results if realistic values are provided for the joint properties. Both of these numerical techniques may be capable of replacing the physical modelling which was carried out in this study; however, much detailed research is required to bridge the gap between the numerical model and the real situation.

A different approach to physical modelling may be made through the use of a geotechnical centrifuge. The technique enables real materials to be used under loads similar to those experienced in the prototype, but still with a physically small model. In this way, soils which have a cohesive component of strength may be used without resorting to special techniques or the use of unusual materials (e.g. bentonite slurries). A model study which used a centrifuge would provide a means by which the kinematics of slope failure in the real material could be compared with that proposed by the virtual work analysis.

The identification of the most likely failure mechanism would help in the choice of location of any field measuring devices. This would not only help in field oriented research into slope kinematics, but would also assist in the efficient monitoring of any slope which created a hazard to the public or in industry.

REFERENCES

ANDRAWES, K.Z. (1976)
The Use of Stereo-photogrammetry for Measuring Displacement Fields
Report submitted to Science Research Council (UK), February, 1976; 38 pp.

ANON (1970)
Wedge Analysis
Appendix VII in "Engineering and Design: Stability of Earth and Rockfill Dams", U.S. Army Corps of Engineers, EM 1110-2-1902.

ANON (1977)
Methods of Testing Soils for Engineering Purposes
Australian Standard AS1289; Standards Association of Australia, Sydney.

ARTHUR, J.R.F. and ROSCOE, K.H. (1965)
An Examination of the Edge Effects in Plane-Strain Model Earth Pressure Tests
Proceedings, 6th International Conference on Soil Mechanics and Foundation Engineering, Montreal; Volume II, pp. 363-367.

BAKER, R. and GARBER, M. (1978)
Theoretical Analysis of the Stability of Slopes
Geotechnique; Volume 28, No. 4, pp. 395-411.

BISHOP, A.W. (1966)
The Strength of Soils as Engineering Materials
6th Rankine Lecture, *Geotechnique*; Volume 16, No. 2, pp. 91-128.

BISHOP, A.W. (1967)
Progressive Failure with Special Reference to the Mechanism Causing It
Proceedings of the Geotechnical Conference, Oslo; Volume 2, pp. 142-150.

BISHOP, A.W. (1971)
Shear Strength Parameters for Undisturbed and Remoulded Soil Specimens
Proceedings of the Roscoe Memorial Symposium, Cambridge, March 1971; pp. 3-58.

BISHOP, A.W. and GREEN, G.E. (1965)
The Influence of End Restraint on the Compression Strength of a Cohesionless Soil
Geotechnique; Volume 15, No. 3, pp. 243-266.

BISHOP, A.W., HUTCHINSON, J.N., PENMAN, A.D.M. and EVANS, H.E. (1969)
Geotechnical Investigations into the Causes and Circumstances of the Disaster of 21st October 1966
A Selection of Technical *Reports* submitted to the Aberfan Tribunal, Welsh Office; London HMSO, 80 pp.

BJERRUM, L. (1967)
Progressive Failure in Slopes of Over-consolidated Plastic Clay and Clay Shales
Journal of the Soil Mechanics and Foundations Division, *Proceedings* ASCE; Volume 93, No. SM5, pp. 1-49.

BLIGHT, G.E. (1969)
Foundation Failures of Four Rockfill Slopes
Journal of the Soil Mechanics and Foundations Division, *Proceedings* ASCE; Volume 95, No. SM3, pp. 743-767.

BOYD, G.L., KOMDEUR, W. and RICHARDS, B.G. (1978)
Open Strip Pitwall Instability at Goonyella Mine - Causes and Effects
Proceedings 1978 Australian Institute of Mining and Metallurgy Conference, North Queensland.

BRANSBY, P.L. (1971)
Discussion, Session 2
Proceedings of the Roscoe Memorial Symposium, Cambridge, March 1971; pp. 255-258.

BRANSBY, P.L. and SMITH, I.A.A. (1975)
Side Friction in Model Retaining-wall Experiments
Journal of the Geotechnical Engineering Division, *Proceedings* ASCE; Volume 101, No. GT7, pp. 615-632.

BROMHEAD, E.N. (1978)
Large Landslides in London Clay at Herne Bay, Kent
Quarterly Journal of Engineering Geology; Volume 11, No. 4, pp. 291-304.

BROWN, R.L. and RICHARDS, J.C. (1965)
Kinematics of the Flow of Dry Powders and Bulk Solids
Rheologica Acta; Band 4 Heft 3, pp. 153-165.

BURMAN, B.C. (1971a)
A Numerical Approach to the Mechanics of Discontinua
Thesis submitted for Ph.D.; Department of Civil Engineering, James Cook University of North Queensland, November, 1971.

BURMAN, B.C. (1971b)
Discussion on "Stresses beneath Granular Embankments" - Lee and Herington
Proceedings 1st Australia-New Zealand Conference on Geomechanics, Melbourne; pp. 551-553.

BURMAN, B.C. (1974)
Development of a Numerical Model for Discontinua
Australian Geomechanics Journal; Volume G4, No. 1, pp. 13-22.

BUTTERFIELD, R. and ANDRAWES, K.Z. (1972)
On the Angles of Friction between Sand and Plane Surfaces
Journal of Terramechanics; Volume 8, No. 4, pp. 15-23.

BUTTERFIELD, R., HARKNESS, R.M., and ANDRAWES, K.Z. (1970)
A Stereophotogrammetric Method for Measuring Displacement Fields
Geotechnique; Volume 20, No. 3, pp. 308-314.

CHEN, W-F. (1975)
Limit Analysis and Soil Plasticity
Developments in Geotechnical Engineering 7, Elsevier Scientific Publishing Co., Amsterdam, 638 pp.

CHUGAEV, R.R. (1964)
Stability Analysis of Earth Slopes
Izdatel 'stvo "Energiya" Maskva - Lenningrad, Israel Program for Scientific Translations, Jerusalem, 1966, 147 pp.

COLLIN, A. (1846)
Landslides in Clays
trans. W.R. Schriever, University of Toronto Press, 1956.

CORNFORTH, D.H. (1964)
Some Experiments on the Influence of Strain Conditions on the Strength of Sand
Geotechnique; Volume 14, pp. 143-167.

COXON, R.E. and BASSETT, R.H. (1976)
Centrifugal Modelling Methods in the Assessment of the Performance and Economics of Embankments Constructed on Soft Foundations
Proceedings 12th Congress, International Commission on Large Dams, Mexico; Volume I, pp. 463-484.

CUNDALL, P.A. (1971)
The Measurement and Analysis of Accelerations in Rock Slopes
Thesis submitted for Ph.D.; Imperial College of Science and Technology, University of London, February, 1971.

ENGINEERING NEWS RECORD (1929)
Reconstruction of Lafayette Dam Advised
Volume 102, January 31, 1929; pp. 190-192.

ENGINEERING NEWS RECORD (1937)
WPA Dam Fails at Kansas City
Volume 119, September 23, 1937; p. 495.

ENGINEERING NEWS RECORD (1941)
Foundation Failure Causes Slump in Big Dike at Hartford, Conn.
Volume 123, July 31, 1941; p. 142.

FORD, D.S. (1970)
Characteristics of the Plane Strain Behaviour of a Compacted Soil
Thesis submitted for M.Eng.Sc.; Department of Civil Engineering, James Cook University of North Queensland, October, 1970.

FULTON, M.J. (1979)
The Discrete Stiffness Model - Users Guide
Department of Civil and Systems Engineering, James Cook University of North Queensland (unpublished).

FUMAGALLI, E. (1968)
Model Simulation of Rock Mechanics Problems
Chapter 11 in "*Rock Mechanics in Engineering Practice*", ed. Stagg and Zienkiewicz; John Wiley and Sons, New York.

GIUNTA, J.S. (1969)
Flow Patterns of Granular Materials in Flat-bottom Bins
Journal of Engineering for Industry, *Transactions* of ASME; Volume 91, pp. 406-413.

GREEN, G.E. (1969)
Strength and Compressibility of Granular Materials under Generalised Strain Conditions
Thesis submitted for Ph.D.; University of London.

GREEN, G.E. (1971)
Strength and Deformation of Sand Measured in an Independent Stress Control Cell
Proceedings of the Roscoe Memorial Symposium, Cambridge, March 1971; pp. 285-323.

GREEN, G.E. and READES, D.W. (1975)
Boundary Conditions, Anisotropy and Sample Shape Effects on the Stress-strain Behaviour of Sand in Triaxial Compression and Plane Strain
Geotechnique; Volume 25, No. 2, pp. 333-356.

HAMMOND, R. (1956)
Dams
Chapter 2 in *'Engineering Structural Failures"*; Odhams Press Ltd., London.

HARLEY, I.A. (1967)
The Non-topographical Uses of Photogrammetry
The Australian Surveyor; September, 1967, pp. 237-263.

HOLLAND, H. (1977)
Prediction of Failure Mechanisms for a Clastic Slope
Thesis submitted for M.Eng.Sc.; Department of Civil and Systems Engineering, James Cook University of North Queensland.

JAMES, R.G. (1971)
Some Aspects of Soil Mechanics Model Testing
Proceedings of the Roscoe Memorial Symposium, Cambridge, March, 1971; pp. 417-440.

JANBU, N. (1957)
Earth Pressure and Bearing Capacity Calculations by Generalised Procedure of Slices
Proceedings 4th International Conference on Soil Mechanics and Foundation Engineering, London; Volume II, pp. 207-212.

JONES, G.K. (1963)
Chemistry and Flow Properties of Bentonite Grouts
Paper 4, Grouts and Drilling Muds in Engineering Practice; Butterworths, London.

KARAAL, K. (1977a)
Application of Energy Method
Journal of the Geotechnical Engineering Division, *Proceedings* ASCE; Volume 103, No. GT5, pp. 381-397.

KARAAL, K. (1977b)
Energy Method for Soil Stability Analyses
Journal of the Geotechnical Engineering Division, *Proceedings* ASCE; Volume 103, No. GT5, pp. 431-445.

KERISEL, J. (1972)
The Language of Models in Soil Mechanics
Proceedings 5th European Conference of Soil Mechanics, Madrid;
English translation.

KING, G.J.W. and DICKIN, E.A. (1970)
Comparison of Stress-dilatancy Theories
Journal of the Soil Mechanics and Foundations Division,
Proceedings ASCE; Volume 96, No. SM5, pp. 1697-1714.

KUESTER, J.L. and MIZE, J.H. (1973)
Optimization Techniques with FORTRAN;
McGraw-Hill Book Co., New York.

LEE, I.K. and HERINGTON, J.R. (1971)
Stresses Beneath Granular Embankments
Proceedings 1st Australia-New Zealand Conference on Geomechanics,
Melbourne; Volume 1, pp. 291-297.

LEE, K.L. (1970)
Comparison of Plane Strain and Triaxial Tests on Sand
Journal of the Soil Mechanics and Foundations Division,
Proceedings ASCE; Volume 96, No. SM3, pp. 901-923.

McCABE, R.P. (1974)
Flow Patterns in Granular Material in Circular Silos
Geotechnique; Volume 24, No. 1, pp. 45-62.

MANDL, G., de JONG, L.N.J. and MALTHA, A. (1977)
Shear Zones in Granular Material
Rock Mechanics; Volume 9, pp. 95-144.

MARSLAND, A. and LOUDON, A.G. (1963)
The Flow Properties and Yield Gradients of Bentonite Grouts in
Sands and Capillaries
Paper 3, Grouts and Drilling Muds in Engineering Practice;
Butterworths, London.

MARSLAND, A. and POWELL, J.J.M. (1977)
The Behaviour of a Trial Bank Constructed to Failure on Soft
Alluvium of the River Thames
Proceedings International Symposium on Soft Clay, Bangkok,
Thailand, 5-6 July 1977.

MORGENSTERN, N.R. and PRICE, V.E. (1965)
The Analysis of the Stability of General Slip Surfaces
Geotechnique; Volume 15, pp. 79-93.

PARCHER, J.V. and MEANS, R.E. (1968)
Slope Stability
Chapter 8 in *"Soil Mechanics and Foundations"*; Charles E. Merrill
Publishing Co., Columbus Ohio.

PASKIN, A.K. (1965)
The Application of Discrete Unit Models to Studies of the Shear
Strength of Granular Materials
Thesis submitted for Ph.D.; Department of Civil Engineering,
University of Melbourne.

PARRY, R.H.G. (1971)
Stability Analysis for Low Embankments on Soft Clays
Proceedings of the Roscoe Memorial Symposium, Cambridge, March 1971; pp. 643-668.

REIMBERT, M.L. and REIMBERT, A.M. (1974)
Retaining Walls - Anchorages and Sheet Piling, Volume I; Trans Tech Publications, Ohio.

ROBERTSON, R.E. and STIFF, H.A. Jr. (1976)
An Improved Mathematical Model for Relating Shear Stress to Shear Rate in Drilling Fluids and Cement Slurries
Society of Petroleum Engineers Journal; Volume 16, No. 1, pp. 31-36.

ROSCOE, K.H. (1970)
The Influence of Strains in Soil Mechanics
10th Rankine Lecture, *Geotechnique*; Volume 20, No. 2, pp. 129-170.

ROSCOE, K.H., ARTHUR, J.R.F. and JAMES, R.G. (1963)
The Determination of Strains in Soils by an X-Ray Method, Parts 1 and 2
Civil Engineering and Public Works Review; Volume 58, pp. 873-876, 1009-1012.

ROWE, P.W. (1962)
The Stress-dilatancy Relation for Static Equilibrium of an Assembly of Particles in Contact
Proceedings of the Royal Society, London; Series A, Volume 269, pp. 500-527.

ROWE, P.W. (1963)
Stress-dilatancy, Earth Pressures, and Slopes
Journal of the Soil Mechanics and Foundations Division, *Proceedings* ASCE; Volume 89, No. SM3, pp. 37-61.

ROWE, P.W. (1971)
Large Scale Laboratory Model Retaining Wall Apparatus
Proceedings of the Roscoe Memorial Symposium, Cambridge, March 1971; pp. 441-449.

SCHOFIELD, A. and WROTH, P. (1968)
Critical State Soil Mechanics;
McGraw-Hill, London.

SEED, H.B. and GOODMAN, R.E. (1964)
Earthquake Stability of Slopes of Cohesionless Soils
Journal of the Soil Mechanics and Foundations Division, *Proceedings* ASCE; Volume 90, No. SM6, pp. 43-73.

SEED, H.B. and SULTAN, H.A. (1967)
Stability Analyses for a Sloping Core Embankment
Journal of the Soil Mechanics and Foundations Division, *Proceedings* ASCE; Volume 93, No. SM4, pp. 69-83.

SKELLAND, A.H.P. (1967)
Non-Newtonian Flow and Heat Transfer;
John Wiley and Sons, Inc., New York.

SOKOLOVSKI, V.V. (1960)
Statics of Granular Media;
translated D.H. Jones and A.N. Schofield, Butterworths, London.

SULTAN, H.A. and SEED, H.B. (1967)
Stability of Sloping Core Earth Dams
Journal of the Soil Mechanics and Foundations Division,
Proceedings ASCE; Volume 93, No. SM4, pp. 45-67.

SUTHERLAND, H.B. and MESDARY, M.S. (1969)
The Influence of the Intermediate Principal Stress on the Strength of Sand
Proceedings 7th International Conference on Soil Mechanics and Foundation Engineering, Mexico; Volume I, pp. 391-399.

TERZAGHI, K. and PECK, R.B. (1948)
Stability of Base of Embankments
Article 52 in *"Soil Mechanics in Engineering Practice"*;
John Wiley and Sons, New York, pp. 395-406.

TROLLOPE, D.H. (1956)
The Stability of Wedges of Granular Materials
Thesis submitted for Ph.D.; University of Melbourne.

TROLLOPE, D.H. (1957)
The Systematic Arching Theory Applied to the Stability Analysis of Embankments
Proceedings 4th International Conference on Soil Mechanics and Foundation Engineering, London; Volume II, pp. 382-388.

TROLLOPE, D.H. (1968)
The Mechanics of Discontinua or Clastic Mechanics in Rock Problems
Chapter 9 in *"Rock Mechanics in Engineering Practice"*, ed. Stagg and Zienkiewicz; John Wiley and Sons, London.

TROLLOPE, D.H. (1971)
The Collapse of Clastic Aggregates
Proceedings 1st Australia-New Zealand Conference on Geomechanics, Melbourne; pp. 204-210.

TROLLOPE, D.H. (1973a)
Engineering - The Makings of Man
Inaugural Hawken Address presented to Queensland Division, Institution of Engineers Australia, October 9, 1973 (unpublished).

TROLLOPE, D.H. (1973b)
Sequential Failure in Strain-softening Soils
Proceedings 8th International Conference on Soil Mechanics and Foundation Engineering, Moscow; Volume I, pp. 227-232.

TROLLOPE, D.H. (1975)
An Approximate Design Method for Slopes in Strain-softening Materials
Proceedings 16th Symposium on Rock Mechanics: Design in Rock Mechanics, Minneapolis; pp. 40-46.

TROLLOPE, D.H. (1978)
Failure Criteria for Brittle Rock
Chapter 5 in *"An Introduction to Rock Mechanics"*, ed. H. Bock; Department of Civil and Systems Engineering, James Cook University of North Queensland.

TROLLOPE, D.H. (1979)
The Collapse of Slopes
Research Bulletin No. CS17; Department of Civil and Systems Engineering, James Cook University of North Queensland.

TURITZIN, A.M. (1963)
Dynamic Pressure of Granular Material in Deep Bins
Journal of the Structural Division, *Proceedings* ASCE; Volume 89, No. ST2, pp. 49-73.

VANMARCKE, E.H. (1977)
Reliability of Earth Slopes
Journal of the Geotechnical Engineering Division, *Proceedings* ASCE; Volume 103, No. GT11, pp. 1247-1265.

WHITMAN, R.V. and BAILEY, W.A. (1967)
Use of Computers for Slope Stability Analysis
Journal of the Soil Mechanics and Foundations Division, *Proceedings* ASCE; Volume 93, No. SM4, pp. 475-498.

WILSON, S.D. (1970)
Observational Data on Ground Movements Related to Slope Instability
Terzaghi Lecture, Journal of the Soil Mechanics and Foundations Division, *Proceedings* ASCE; Volume 96, No. SM5, pp. 1521-1544.

WU, T.H. (1976)
Soil Mechanics, 2nd ed.;
Allyn and Bacon Inc., Boston.

ZELIKSON, A. (1969)
Geotechnical Models Using the Hydraulic Gradient Similarity Method
Geotechnique; Volume 19, No. 4, pp. 495-508.

ZIENKIEWICZ, O.C. and NAYLOR, D.J. (1971)
The Adaptation of Critical State Soil Mechanics Theory for Use in Finite Elements
Proceedings of the Roscoe Memorial Symposium, Cambridge, March 1971; pp. 537-547.